APPLICATION OF GAS HYDRATES IN COLD STORAGE TECHNOLOGY: EXPERIMENTAL STUDY AND THERMODYNAMIC MODELING

By

Hamed Hashemi

(B.Sc, Chemical Engineering, Sharif University of Technology)

(M.Sc, Chemical Engineering, Shiraz University of Technology)

University of KwaZulu-Natal

This dissertation is submitted in fulfilment of the academic requirements for the degree of Doctor of Philosophy (PhD) in Chemical Engineering at the School of Engineering, University of KwaZulu-Natal

Supervisor: Prof. Deresh Ramjugernath

Co-Supervisors: Prof. Amir H. Mohammadi, and Prof. Paramespri Naidoo

September 2015

DECLARATION 1 - PLAGIARISM

I, Hamed Hashemi, declare that:

(i) The research presented in this thesis, except where otherwise indicated, is my original work.

(ii) This thesis has not been submitted for any degree or examination at any other university.

(iii) This thesis does not contain other persons' data, pictures, graphs or other information, unless specifically acknowledged as being sourced from other persons.

(iv) This thesis does not contain other persons' writing, unless specifically acknowledged as being sourced from other researchers. Where other written sources have been quoted, then: a) their words have been re-written but the general information attributed to them has been referenced; b) where their exact words have been used, their writing has been placed inside quotation marks, and referenced.

(v) Where I have reproduced a publication of which I am an author, co-author or editor, I have indicated in detail which part of the publication was actually written by myself alone and have fully referenced such publications.

(vi) This thesis does not contain text, graphics or tables copied and pasted from the internet, unless specifically acknowledged, and the source being detailed in the thesis and in the References sections.

_________________ ____________

Hamed Hashemi Date

As the candidate's supervisor I agree/do not agree to the submission of this thesis.

_________________ ____________

Prof. Deresh Ramjugernath Date

_________________ ____________

Prof. Amir H. Mohammadi Date

_________________ ____________

Prof. Paramespri Naidoo Date

DECLARATION 2 – PUBLICATIONS

DETAILS OF CONTRIBUTION TO PUBLICATIONS that form part and/or include research presented in this thesis (include publications in preparation, submitted, *in press* and published and give details of the contributions of each author to the experimental work and writing of each publication).

Publication 1: The Journal of Chemical Thermodynamics, 90, 2015, 193-198.
Journal Title: Clathrate Hydrate Dissociation Conditions of Refrigerants R404A, R406A, R408A and R427A: Experimental Measurements and Thermodynamic Modeling.
Authors: Hamed Hashemi, Saeedeh Babaee, Paramespri Naidoo, Amir H. Mohammadi, and Deresh Ramjugernath

Publication 2: The Journal of Chemical Thermodynamics, 80, 2015, 30-40
Journal Title: Experimental measurements and thermodynamic modeling of refrigerant hydrates dissociation conditions
Authors: Hamed Hashemi, Saeedeh Babaee, Paramespri Naidoo, Amir H. Mohammadi, and Deresh Ramjugernath

Publication 3: The Journal of Chemical Thermodynamics, 82, 2015, 47-52
Journal Title: Experimental study and Modeling of the Kinetics of Refrigerant Hydrate Formation
Authors: Hamed Hashemi, Saeedeh Babaee, Paramespri Naidoo, Amir H. Mohammadi, and Deresh Ramjugernath

Publication 4: Journal of Chemical and Engineering Data, 59, 2014, 3907–3911
Journal Title: Experimental Measurements and Thermodynamic Modeling of Clathrate Hydrate Dissociation Conditions for Refrigerants R116, R23, and Their Mixture R508B.
Authors: Hamed Hashemi, Saeedeh Babaee, Paramespri Naidoo, Amir H. Mohammadi, and Deresh Ramjugernath

Publication 5: The Journal of Chemical Thermodynamics, 81, 2015, 52-59.
Journal Title: Kinetic and thermodynamic behaviour of CF4 clathrate hydrates

Authors: Saeedeh Babaee, Hamed Hashemi, Paramespri Naidoo, Amir H. Mohammadi, and Deresh Ramjugernath

Publication 6: The Journal of Chemical Thermodynamics, (to be submitted)
Journal Title: Application of clathrate hydrate in energy systems: A review

Authors: Hamed Hashemi, Saeedeh Babaee, Paramespri Naidoo, Amir H. Mohammadi, and Deresh Ramjugernath

Publication 7: The Journal of Chemical Thermodynamics, (to be submitted)
Journal Title: Kinetics of the hydrate formation of the refrigerants R404A, R406A, R408A and R427A
Authors: Hamed Hashemi, Saeedeh Babaee, Paramespri Naidoo, Amir H. Mohammadi, and Deresh Ramjugernath

Additional works:
Journal papers:
Publication 1: The Journal of Supercritical Fluids, In Press, Corrected Proof.
Experimental measurement and thermodynamic modelling of hydrate phase equilibrium conditions for krypton + n-butyl ammonium bromide aqueous solution
Publication 2: Journal of Chemical Engineering Data, 60 (5), 2015, 1324–1330.
Journal Title: Experimental Measurements and Thermodynamic Modeling of Hydrate Dissociation Conditions for the Xenon + TBAB + Water System
Authors: Saeedeh Babaee, Hamed Hashemi, Paramespri Naidoo, Amir H. Mohammadi, and Deresh Ramjugernath

Publication 3: Journal of Chemical Engineering Data, 60, 2015, 217-221.
Journal Title: Phase Equilibria of Clathrate Hydrates of Ethyne + Propene
Authors: Kaniki Tumba, Hamed Hashemi, Paramespri Naidoo, Amir H. Mohammadi, and Deresh Ramjugernath

Publication 4: Fluid Phase Equilibria, 60 (5), 388, 2015, 182-187.
Journal Title: A Thermodynamic Consistency Test for Experimental Isobaric Data of Wax Solubility in Gaseous Systems
Authors: Javad Kondori, Hamed Hashemi, Saeedeh Babaee, Paramespri Naidoo, Amir H. Mohammadi, and Deresh Ramjugernath

Publication 5: Journal of Chemical Engineering Data, 59, 2014, 3900-3906.
Journal Title: Experimental Measurement and Thermodynamic Modeling of Hydrate Dissociation Conditions for the Argon + TBAB + Water System
Authors: Saeedeh Babaee, Hamed Hashemi, Paramespri Naidoo, Amir H. Mohammadi, and Deresh Ramjugernath

Publication 6: Journal of Chemical Engineering Data, 58, 2013, 3259-3264.

Journal Title: Dissociation Data and Thermodynamic Modeling of Clathrate Hydrates of Ethene, Ethyne, and Propene

Authors: Kaniki Tumba, Hamed Hashemi, Paramespri Naidoo, Amir H. Mohammadi, and Deresh Ramjugernath

Publication 7: Fluid Phase Equilibria, 360, 2013, 161-168.

Journal Title: Gas hydrate phase equilibrium in porous media: An assessment test for experimental data.

Authors: P. Ilani-Kashkouli, Hamed Hashemi, Farhad Gharagheizi, Saeedeh Babaee, Amir H. Mohammadi, and Deresh Ramjugernath

Publication 8: Fluid Phase Equilibria, 360, 2013; 68-76.

Journal Title: An assessment test for phase equilibrium data of water soluble and insoluble clathrate hydrate formers.

Authors: P. Ilani-Kashkouli, Saeedeh Babaee, Farhad Gharagheizi, Hamed Hashemi, Amir H. Mohammadi, and Deresh Ramjugernath

Publication 9: Journal of Chemical Engineering Data, (to be submitted)

Journal Title: Kinetics of the hydrate formation of Acethyene, Ethyne, Propene, propylene, ethane, ethylene.

Authors: Hamed Hashemi, Saeedeh Babaee, Paramespri Naidoo, Amir H. Mohammadi, and Deresh Ramjugernath

Book chapters:

Publication 1: Advances in Chemistry Research (Volume 25); Nova Science Publishers, Inc., NY, USA, Editors: James C. Taylor, pp.177-198.

Chapter Title: A Thermodynamic Consistency Test for Experimental Data of Salt Deposition in Saline Water.

Authors: Saeedeh Babaee, Hamed Hashemi, Javad Kondori, Amir H. Mohammadi, and Deresh Ramjugernath

Publication 2: Advances in Chemistry Research (Volume 24), 2014; Nova Science Publishers, Inc., NY, USA.

Chapter Title: Evaluation of the Experimental data for Gas Solubility in Liquid Water in Equilibrium with the Gas Hydrates.

Authors: Ilani-Kashkouli P., Saeedeh Babaee, Farhad Gharagheizi, Hamed Hashemi, Amir H. Mohammadi, and Deresh Ramjugernath

ABSTRACT

The ever-increasing demands for air conditioning technology especially in residential areas results in a severe imbalance between power generating utilities, especially during peak usage hours. To provide the required peak capacity, expensive peak-generators are compulsory. Hence, researchers are compelled to find an effective air conditioning system which can be utilized during peak-hours with the minimum of electrical consumption. One solution to this problem is to shift the electrical consumption from peak-hours to off-peak hours by a combination of a cold storage technology with the air conditioning system. In the cold storage system, the cold energy can be stored by a medium during off-peak hours (e.g. ice or water) and it can be released for use at peak hours. An air conditioning system which operates with cold storage technology usually consists of a storage medium, a storage tank, a coolant circulator, a pump and a condenser.

Due to the fundamental role of storage medium in cold storage systems, various investigations have been performed in order to design an applicable storage tank. Ice, eutectic salt, and water are the most common materials being used as storage materials in cold storage applications. However, the application of these conventional materials as storage medium is not practical, due to their formation at low temperatures, their low enthalpy of dissociation and their low density of cold storage. It was found that most refrigerant hydrates can be utilized as a suitable cold storage medium in air conditioning systems due to their significant properties such as high enthalpy of formation/dissociation close to that of ice, and temperatures of formation above the freezing point of water.

In this study an extended review on the application of clathrate/semiclathrate hydrates in cold storage systems is performed. The gas hydrate dissociation conditions of refrigerants R23, R134a, R125a, R22, R116, R410A, R407C, R408A, R508B, R404A, R406A, R427A and R507C have been measured experimentally using an isochoric pressure search method. From the measured experimental dissociation data, the enthalpies of hydrate dissociation are evaluated. Results indicate that R507C has the highest enthalpy of dissociation amongst the other refrigerant blends. R134a, R410A, R407C and R427A with low pressure of hydrate formation/dissociation, show the most suitable behaviour to be used in cold storage applications. A thermodynamic model with the ability to correlate dissociation conditions of refrigerant hydrates in the different phase equilibrium boundaries (Hydrate-Ice-Vapour, Hydrate-Aqueous solution-Vapour, Hydrate- Hydrate-Aqueous solution-Liquid refrigerant) has been proposed. The difference between model predictions and experimental data is reasonable. Furthermore, in order to examine the rate of the refrigerant hydrate formation, an experimental study has been performed on the kinetics of the hydrate formation of the refrigerant blends namely R407C, R410A, R507C, R404A, R406A, R408A and R427A. The induction time of hydrate formation, apparent rate constant of the hydrate reaction, water to hydrate conversion during hydrate nucleation and growth, storage capacity and the rate of hydrate formation of above mentioned refrigerants at different initial conditions (pressures and temperatures) have been calculated using a kinetic model. The results demonstrate that in the presence of pure water R407C has the maximum apparent rate constant, appropriate induction time, and highest storage capacity at temperate pressures and temperatures amongst the eight refrigerants studied. The effect of sodium dodecyl sulfate (SDS) with different concentrations of 400, 500 and 600 ppm on hydrate nucleation and growth rate was investigated. In contrast to the refrigerants R406A, R404A, R408A and R427A an inhibition effect of SDS on gas hydrate nucleation rate was found for the refrigerants R407C, R410A and R507C. The most relevant kinetic results were found for the system R406A + 400 ppm SDS solution.

ACKNOWLEDGEMENTS

First and above all, I cannot begin this acknowledgment without expressing my sincere respect to Almighty God for his incomparable grace, exceptional protection and support throughout the lows and highs of my PhD journey. Lord, I am very thankful for showing me your extreme love and care and giving me the power and patient that enabled me to finish this phase of my life.

I want to express my wholehearted appreciation to my parents, especially my mother. I am extremely indebted to their determined support and patient. I am grateful for anything they have done for me throughout my life.

My deepest gratitude goes to my supervisor **Prof. Deresh Ramjugernath** and co-supervisors **Prof. Amir H. Mohammadi** and **Prof. Paramespri Naidoo**. I would not have received a PhD scholarship without their unconditional trust and confidence in me. I highly appreciate their determined support, their passion for my research, and their patience in guiding this research to fruition. Thank you so much for being a wonderful supervisor and for your remarkable advice

My profound appreciation goes to my wife, **Saeedeh Babaee**, for her love and her support in my career and for standing with me during all difficulties which I have been through. Without her care and support I would not have been able to accomplish my PhD study successfully.

I am indeed indebted to **Prof. Giancarlo Contrafatto** and his lovely wife **Elaine Contrafatto** for their invaluable support, patience and care throughout our stay in South Africa. I highly appreciate their kindness for being such good friends and providing us with an environment to feel like home.

I would like to extend my sincere appreciation to the people working in the workshop, **Mr Leon Augustyn** for construction of the experimental equipment, **Dr Wayne Nelson** and **Mr Ayanda Khanyile** for their invaluable assistance during my experimental work.

List of Figures

List of Tables

Nomenclature

symbol	Description	unit
a,b	Parameters of EoS	Pa. (m^3 / mol)^2
f_j	Fugacity of the gas component j	Pa
h	Molar enthalpy	J / mol
C_{pw}	Heat capacity at constant pressure	J / (mol. K)
g	Gibbs free energy	J / mol
k	Boltzmann's constant	J / K
k_{app}	Rate constant of hydrate reaction	mol /(min. Pa)
$K_{v\text{-}s,i}$	Distribution coefficient	-
N	Number of experimental data	--
n	Mole number	mol
n_{w_0}	Initial number of moles of water in the liquid phase	mol
P	Pressure	Pa
Q_k	UNIFAC surface area parameter (Eq. (26))	-
Q_1	Lower quadruple point	-
Q_2	upper quadruple point	-
R	Universal ideal gas constant (Eqs. (19),(20))	m^3.Pa / (mol.K)
R_k	UNIFAC volume parameter	-
$\overline{R}$	Average radius of the cavity	m
r	Radial coordinate	m
s	Structure of gas hydrate	--
T	Temperature	K
t	Time	s
V_{cell}	Volume of the cell	m^3
V_H	Volume of hydrate during	m^3
V_{W_0}	Initial volume of water	m^3
v_i'	Number of cavities of type I per water molecule in a unit hydrate	--
v	Partial molar volume	m^3 / mol
y_i	Composition in the vapour phase	-
Y_i	Composition in the hydrate phase	-
Z	Compressibility factor	-
z	Mole fraction	-

Greek symbols

Symbol	Description	Units
Δ	Change in a property	--
μ	Chemical potential	J / mol
$\omega(r)$	Spherically symmetric cell potential in the cavity	J / mol
ω	Acentric factor	--
ε	Characteristic energy	J / mol
σ	Collision diameter	m
a	Radius of spherical molecular core	m
α	Attractive parameter of a cubic EoS	--
β	Empty hydrate phase	--
γ_i	Activity coefficient of component *i*	--
ϕ	Fugacity coefficient	--
θ_i	area function	--
θ_{ki}	Hydrate cage occupancy	--
Φ_i	Segment function	--
$\bar{v}_m$	Number of cavities of type m per water molecule in the unit hydrate cell	--
v_w	volume of the empty hydrate lattice	m^3 / mol
ν_{ki}	Number of groups of kind *k* in molecule *i*	--
Γ_k	Residual activity coefficient of group *k* in a solution	--

Superscripts

β	Empty hydrate phase
I	Ice phase
L	Liquid water phase
H	Hydrate phase
EOS	Equation of state
MT	Empty hydrate
EL	Effect of the electrolytes
Cal	Calculated
Exp	Experimental
sat	Saturation

Subscripts

m	Cavity type *m*
w	Water
I	Ice
R	Refrigerant
i,j	Component

ABBREVIATIONS

CFC	chlorofluorocarbons
CHS	clathrate hydrate slurries
CoP	Coefficient of performance
CP	Cyclopentane
DPG	Dodecyl polysaccharide glycoside
DSC	Differential scanning calorimeter
DSLM	Demand side load-management
EOS	Equation of state
GC	Gas chromatograph
GH	Gas hydrate
HCFC	Hydrochlorofluorocarbons

HFCs	Hydrofluorocarbons
HP-DSC	High pressure differential scanning calorimetry
L_w-H-V	Hydrate – liquid water –vapour
H-I-V	Hydrate – ice –vapour
H-L_w-L_R	Hydrate – liquid water –liquid refrigerant
IT	Induction time
LABS	Linear alkyl benzene sulfonate
MCH	Methylcyclohexane
MPCMS	Microencapsulated PCM slurries
ODP	Ozone Depletion Potentials
GWP	Global Warming Potentials
PCME	PCM emulsions
PCS	Phase change slurries
PEG	Poly-ethylene glycols
PPG	Propylene glycol
PR	Peng-Robinson
QCM	Quartz Crystal Microbalance
QS	Quaternary salts
RO	Reverse osmosis
PCM	Phase change material
SC	Storage capacity
SDS	Sodium dodecyl sulfate
SPCMS	Shape-stabilized PCM slurries
SHS	Sodium hexadecyl sulfate
STS	Sodium tetradecyl sulfate
STP	Standard temperature and pressure
TBAB	Tetra-n-butylammonium bromide
TBAC	Tetra-n-butylammonium chloride
TBAF	Tetra-n-butylammonium fluoride
TBPB	Tetra-n-phosphonium bromide
TCD	Thermal conductivity detector
THF	Tetrahydrofuran
TME	Trimethylolethane
VLE	Vapour-liquid equilibrium
vdWP	van der Waals and Platteeuw

1

Introduction

The application of air conditioning for cooling is increasing all over the world. However, the large consumption of electrical energy by such technology imposes a severe peak load on the power generating utilities during peak hours. As the result, expensive peaking generators are needed to fulfil this peak loads. Consequently, the strategy of demand side load-management (DSLM) has attracted an immense deal of interest and numerous studies have been performed in an attempt to try to discover practicable solutions to this issue. It was found that it is possible to shift the electric consumption from peak hours to off-peak hours using a technology called "cold storage". The ability to store the cold energy using a medium during off-peak periods and releasing the stored cold energy from that medium during peak demand periods using small electrical energy consumption was achieved by incorporating cold storage technology in air conditioning systems.

In the early 1980s, gas hydrates attracted considerable attention as the phase change materials for cold storage purposes (Tomlinson, 1982). Their distinguished properties have been used favourably to replace conventional cold storage materials. Gas hydrates have also been looked upon recently as a power generator in gas engines (Obara, 2010, Obara et al., 2011a) and a coolant in refrigeration systems. The pressure produced from the dissociation of the gas hydrate could be utilized as a source of mechanical energy in compression engines.

Water and ice are the most common cold storage materials which have been used since the innovation of the cold storage technology (Akbari and Mertol, 1989). However both suffer from some drawbacks which are described briefly as follows:

1.1. Cold storage using sensible heat of chilled water

In air conditioning, chilled water with the temperature range of 5 to 7 ºC is stored in the cold storage tank. Due to the low specific heat of water (4.184 kJ/kg ºC) the maximum cooling potential is only 29.288 kJ per 1 kg of chilled water when the functional temperature difference is 7° C. Hence, the small amount of the cold storage is the shortcoming in using chilled water (Akbari and Mertol, 1989).

1.2. Cold storage using fusion heat of Ice

A greater amount of cold storage would be achieved by using partial conversion of chilled water to ice due to the large heat of fusion of ice (335 kJ/kg). For instance, the cold storage amount of about 117.15 kJ/kg can be stored using chilled water containing 20 percent of ice by volume when the functional temperature difference is 7° C. However, in this method the refrigeration unit should be working at the temperatures close to that of the freezing point of water. Hence, a larger amount of power will be used by this method compared to the scenario described above using chilled water (Akbari and Mertol, 1989).

1.3. Cold storage using hydrates

In the 1980s, important research studies led to the consideration of gas hydrates and salt hydrates as a medium for the storage of cold energy in air conditioning systems (Tomlinson, 1982, Akbari and Mertol, 1989). Salt hydrates or *eutectic salts* (e.g. $Na_2B_4O_7.10H_2O$, $Na_2SO_4.10H_2O$, NaCl, NH_4Cl) are comprised of a mixture of water and salt with the freezing temperature range of 8-16°C. However, they have several limitations such as (Akbari and Mertol, 1989, Guo et al., 1996):

- Low enthalpy of phase change
- Reduction of recharge capacity due to the melting incongruently, in which the heavier particles settle out during melting, consequently during freezing the settled salts does not recombine with the saturate solution
- Low heat transfer rate
- High corrosion

Clathrate hydrates are recognized to be an ideal cold storage medium due to their unique properties such as (Tomlinson, 1982, Carbajo, 1983, Mori and Mori, 1989a, Mori and Mori, 1989b, Oowa et al., 1990, Akiya et al., 1999, Xie et al., 2004, Yingming et al., 2004, Li et al., 2012, Wang et al., 2014, Hashemi et al., 2015b):

- The formation temperatures are within a practical operating temperature range of conventional air conditioning systems (278-285) K.
- The large enthalpy of phase change resulting in the high density of cold storage

- The direct use of chilled water as the circulation medium instead of antifreeze coolant or brine
- The use of conventional water chillers rather than a costly ice-maker

Since the first application of gas hydrates as a cold storage medium in 1982, it has attracted a great deal of attention in energy conservation engineering and initiated a significant interest in the use of applicable gases or refrigerants for cold storage technology. The characterization of several gases and refrigerants as clathrate hydrates in cold storage systems has been studied and different ways of charging and discharging cold energy has been proposed and developed (Tomlinson, 1982, Carbajo, 1983, Mori and Mori, 1989a, Mori and Mori, 1989b, Oowa et al., 1990, Isobe and Mori, 1992, Tanii et al., 1997, Yingming et al., 2004, Bi et al., 2010).

1.4. Gas hydrates

The interaction between water molecules and molecules of appropriate size and shape such as nitrogen, methane, hydrogen sulphide etc. at suitable conditions such as low temperatures (or high pressures) results in the formation of a crystalline inclusion compound which is known as gas/clathrate hydrate (Sloan and Koh, 2008). The hydrogen bonded water molecules (host) in the gas hydrate structure produce cavities which can be occupied by the guest molecule(s). Depending on the size and shape of the guest molecule three types of gas hydrate structures of sI, sII, and sH would form. Each structure has its own characteristics which will be described in the proceeding sections. It has been discovered that not only small molecules such as methane, ethane, propane, and carbon dioxide form gas hydrates but large molecules such as heavy hydrocarbons namely cyclohexane, cycloheptene, dimethylbutane, and methylcyclohexane can form structure H of gas hydrate (Sloan and Koh, 2008).

Studies on natural gas hydrates can be categorised into the following:

- Research since the discovery of gas hydrates in 1810 to date focussing on gas hydrates as a scientific phenomenon in which gas and water are converted into a solid.
- Investigations from 1934 to date into gas hydrates as an obstruction in the transportation of natural gas in gas processing industry. It is essential to study the details of the gas hydrate formation conditions in order to find an effective way to prevent their formation in gas pipelines.

- Investigations from 1963 until the present, discovery of natural gas hydrates in deep oceans and permafrost regions as well as in celestial environments. Estimates of the quantity of world gas hydrates deposits are uncertain, however comparing to all other fossil fuel reserves, the energy in these hydrate deposits is significant.The study of gas hydrates became more interesting after the increase in energy price in the 1970s and over 7000 papers on natural gas hydrates have been published since then (Makogon et al., 2007).

1.4.1. Gas hydrate structures

As depicted in Figure 1.1, according to the arrangement of water molecules in the crystal, gas hydrates are classified into three common structures of cubic sI, cubic sII and hexagonal sH (Sloan and Koh, 2008). The two former structures, (sI and sII) were first detected using x-ray diffraction experiments of the hydrate crystal by von Stackelberg et al. (1940s-1950s)(Sloan and Koh, 2008). The less common structure H (sH) which forms with a small molecule (e.g. methane) and a large molecule (e.g. cycloheptane), was detected by (Kvenvolden, 1988). There are other types of structures such as sIII, sT, etc., however their formation in the natural gas industry has not been detected.

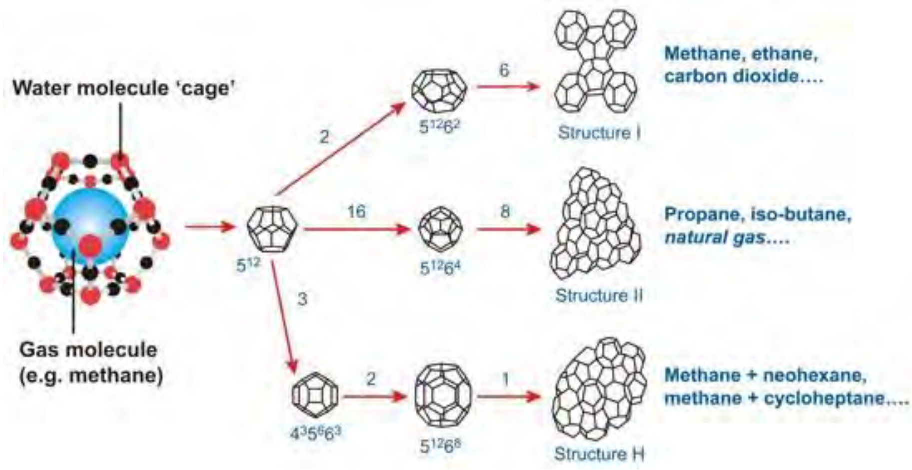

Figure 1.1. The cage arrangements of three types of hydrate structures (Makogon, 1988)

1.4.1.1. Structure I

Structure I is known as the simplest gas hydrate structure comprising pentagonal dodecahedron and tetrakaidecahedron cages. The arrangement used by Jeffry (1984) (Lee et al., 2003) is applied for identifying the hydrate cages. For example, a 12-sided cage (pentagonal dodecahedron) is presented by 5^{12} where 5 is the number of edges in a face type and superscript 12 is the number of faces with 5 edges. The 14-sided cavity (tetrakaidecahedron) is identified by $5^{12}6^{2}$ with 12 pentagonal and 2 hexagonal faces. Methane, carbon dioxide, ethane and hydrogen sulphide are examples of some compounds which form sI hydrates. Unlike ethane which can only occupy large cavities ($5^{12}6^{2}$) of sI hydrates the other three gases can fit in both large and small (5^{12}) cavities (Sloan and Koh, 2008).

1.4.1.2. Structure II

Structure II (sII) of gas hydrates comprises two types of cavities in a unit cell. Small cavities of (5^{12}) as in sI, and large cavities of hexakaidecahedron which are consisted of 16-sided polyhedron with 12 pentagonal faces and 4 hexagonal faces ($5^{12}6^{4}$). Propane and iso-butane are the examples of sII hydrate formers which are occupying the large cavities ($5^{12}6^{4}$) of hydrate. Under suitable conditions, nitrogen can form sII by occupying both large and small cavities (Sloan and Koh, 2008).

1.4.1.3. Structure H

Structure H (sH) hydrate which is less common than sI and sII, consists of three types of cavities namely, regular dodecahedron as in sI and sII (5^{12}), the irregular dodecahedron ($4^{3}5^{6}6^{3}$) and icosahedron ($5^{12}6^{8}$). Ripmeester et al. (1987) described structure H for the first time using NMR spectroscopy and x-ray powder diffraction. One significant feature of sH is that two molecules with different sizes are necessary to stabilize the structure. Small molecules, for example methane or hydrogen sulphide (known as help gas), enter both small cavities (5^{12} and $4^{3}5^{6}6^{3}$) and large molecules (larger than 7.3 Å), such as iso-butane, which enters the large cavity of $5^{12}6^{8}$. Unlike sI and sII, which normally form hydrates with single occupants of either the small and/or large cavity, no exclusion to the necessity of a double hydrate (help gas) has been discovered for sH. The characteristics of different gas hydrate structures are shown in Table 1.1.

Each cavity in all three hydrate structures can be occupied by at most one molecule at moderate pressures. Multiple occupancy of the large cavities of structure II, can be obtained at very high pressures, by small molecules such as nitrogen, hydrogen, methane, and argon. Figure 1.2, a modification of a figure originally proposed by von Stackelberg (1949), shows a relationship between the guest molecule size (or the largest van der Waals diameter) and the size of each cavity (Sloan and Koh, 2008).

Table 1.1. The crystal cell of hydrate structures (Sloan and Koh, 2008).

Hydrate Structure	Structure (I)		Structure (II)		Structure (H)		
Crystal system	Cubic		Cubic		Hexagonal		
Ideal unit cell formula	Small 5^{21}	Large $5^{21}6^{1}$	Small 5^{21}	Large $5^{21}6^{4}$	Small 5^{21}	Medium $4^{3}5^{6}6^{3}$	Large $5^{21}6^{8}$
Cavities number per unit cell	2	6	16	8	3	2	1
Cavity diameter (Å)	7.9	8.6	7.8	9.5	7.8	8.1	11.2
Coordination number	20	24	20	28	20	20	36
Cavity number per water molecule number	1/23	3/23	2/17	1/17	3/34	2/34	1/34
Water molecules per unit cell	46		136		34		
Volume of unit cell (m^3)	1.728×10^{-27}		5.1787×10^{-27}		---		
Typical former	CH_4, C_2H_4, H_2S, CO_2		N_2, C_3H_8, i-C_4H_{10}		Methylcyclohexane, cyclopentane, etc.		

The following details should be mentioned about Figure 1.2:

- At relatively high pressures (i.e., less than 30 MPa at about 260–290 K), molecules with diameters less than 3.5 Å turn out to be too small to occupy any cavity, whereas those above 7.5 Å molecules are too large to stabilize any cavity.
- When the small cavities of a structure have been occupied by a molecule, the large cavities will be occupied by that molecule too.
- Since 1983, it has been known that the smallest guests (argon, krypton, nitrogen, and oxygen) form sII rather than sI.

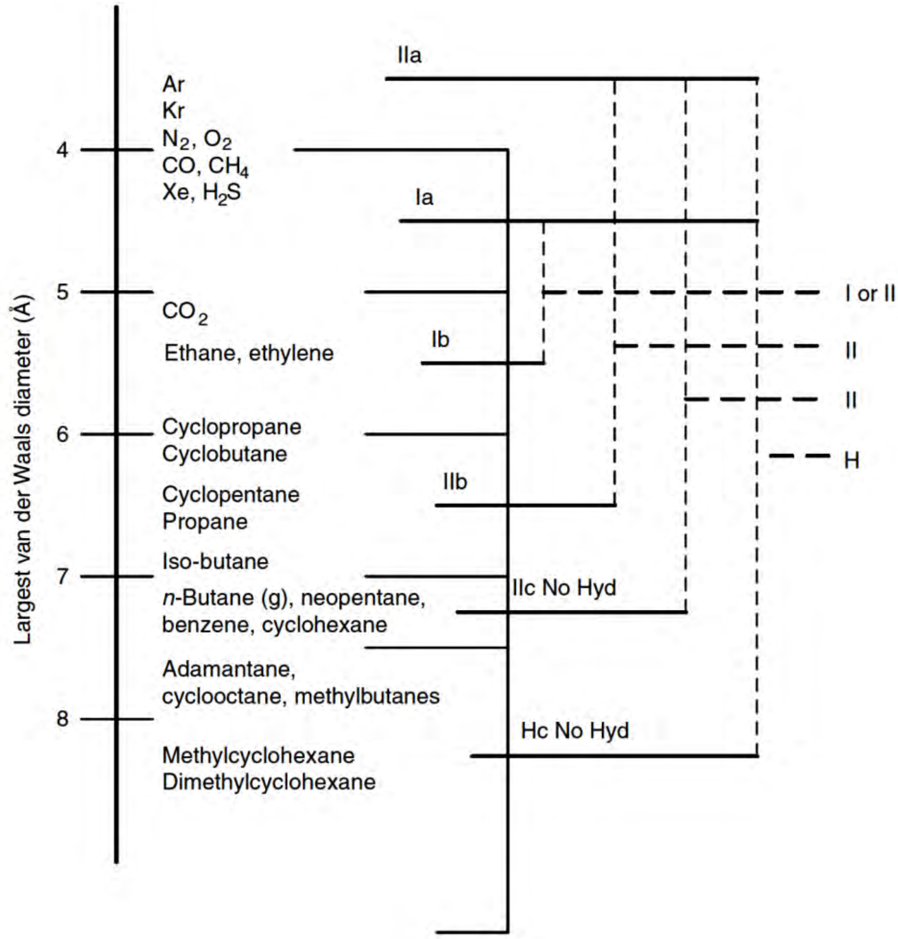

Figure 1.2. Associations between the molecular sizes of various typical hydrate formers and the equivalent hydrate structures (Sloan and Koh, 2008)

1.4.2. Semi-clathrate hydrates

Additional unusual hydrate structures which can be formed by quaternary ammonium salts, originally detected by Fowler et al. The hydrate which is produced by these molecules called "semiclathrate" in which part of the hydrate cavity is broken to accommodate the large salt molecule (Fowler et al., 1940, Sloan and Koh, 2008). In the semiclathrate hydrates formed by alkylamines, the amin groups participate in the attached water networks and the alkyl may inhabit the cavities and stabilize the hydrate structure (Sloan and Koh, 2008). The semiclathrate hydrate produced by tetra-*n*-butyl ammonium bromide (TBAB), the TBA^+ ion is enclosed in a cavity formed by bonded water networks and the halogen anion (Br^-). A usual three dimensional outlook of TBAB semi-clathrate hydrate is depicted in Figure 1.3.

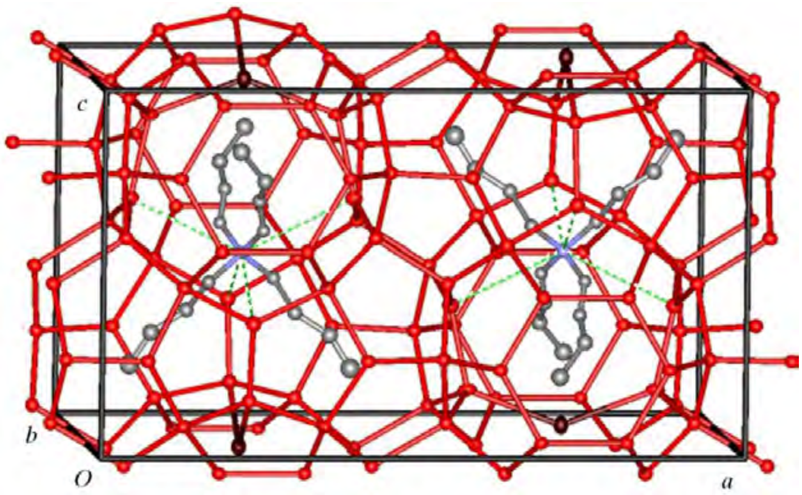

Figure 1.3. Three dimensional view of TBAB semiclathrate hydrate unit cell with 38 molecules of water and one molecule of TBAB $(C_4H_9)_4N^+.Br^-.38H_2O$ (Shimada et al., 2005).

1.4.3. Gas hydrate applications

Despite the fact that gas hydrates can cause significant damage to the oil and gas industry due to their formation in numerous hydrocarbon production and processing operations, it has been well studied that they can also be utilized in numerous positive applications. The outstanding properties of gas hydrates such as their high concentration (containing 184 volume of gas per one volume of hydrate at STP), large heat of fusion, formation temperature above ice point etc. have been used in the following processes positively: gas storage and transportation, gas separation (especially for the gasses with close boiling point in which conventional distillation is no longer applicable) (Englezos, 1993), carbon dioxide sequestration (Lee et al., 2003), cold storage systems (Hashemi et al., 2015b), desalination of sea water (Briggs et al., 1962), concentration of fluids in food industry (Glew, 1962), hydrate actuator in a hybrid power system (Obara, 2010, Obara et al., 2011b), refrigeration systems (Ogawa et al., 2006) The reader is referred to the references cited for further details on the applications which is discussed in Appendix A.

In the current topic area of energy conservation, it has been found that gas hydrates can also be utilized in refrigeration processes as a circulator coolant, a means in compression gas engine as hydrate actuator (gas hydrate engine) for producing of energy and also a media for storage of cold energy in cold storage systems due to their remarkable properties such as high concentration of gas, high enthalpy of dissociation and suitable temperature of formation.

1.4.3.1. Gas hydrates in refrigeration systems

Gas hydrates can be utilized as media for refrigeration purposes efficiently in order to decrease the electrical consumption. Three different ways of clathrate hydrate application in the refrigeration systems have been proposed to date: (1) Gas hydrates as a media for storing the cold energy which is explained in detail in the next section (Carbajo, 1983, Ternes, 1984, Akbari and Mertol, 1989, Mori and Mori, 1989a, Mori and Mori, 1989b, Oowa et al., 1990, Isobe and Mori, 1992, Guo et al., 1996, Tanii et al., 1997, Akiya et al., 1999, Liang et al., 2001, Yingming et al., 2004, Bi et al., 2010, Li et al., 2012, Wang et al., 2014, Hashemi et al., 2015b) (2) gas hydrates as a slurry for conveying the cold energy in secondary refrigeration loop (refer to section 2.2.6) (Darbouret et al., 2005, Zhang et al., 2010, Zhang and Ma, 2012, Youssef et al., 2013) (3) gas hydrates as a working fluid which is explained in section 2.2.7 (Ogawa et al., 2006).

1.4.3.2. Cold storage technology

Many studies have been undertaken in order to manage the load of the utilities by shifting some of the power demands from peak hours to off-peak hours, reasons for which have been explained earlier. Cold storage technology with the ability to be charged during off-peak hours and discharged during the peak hours using little on-peak electricity is a technique for achieving more economical air conditioning systems (Tomlinson, 1982, Carbajo, 1983). With the application of such technology the electricity is used for charging a storage tank when it is less expensive. The stored cold energy is used afterwards to cool the medium during the time when electricity is most expensive. (Tomlinson, 1982, Carbajo, 1983, Kubota et al., 1984, Ternes, 1984, Akbari and Mertol, 1989, Mori and Mori, 1989a, Mori and Mori, 1989b, Oowa et al., 1990, Isobe and Mori, 1992, Guo et al., 1996, Tanii et al., 1997, Akiya et al., 1999, Liang et al., 2001, Yingming et al., 2004, Fournaison et al., 2004, Darbouret et al., 2005, Delahaye et al., 2006, Zhang et al., 2010, Bi et al., 2010, Hashimoto et al., 2010a, Hashimoto et al., 2010b, Kumano et al., 2011, Zhang and Ma, 2012, Youssef et al., 2013, Li et al., 2012, Wang et al., 2014, Hashemi et al., 2015b). According to the type of the storage medium and the approach it is utilized, cold storage technologies in air conditioning systems are categorized into two types: (1) sensible heat storage (2) latent heat storage. Latent heat storage can be achieved by means of phase change materials (PCMs). Li et al. reviewed various PCMs which can be used as the cold storage medium in air conditioning systems (Li et al., 2012). Figure 1.4 shows a classification of various PCMs suggested by Abhat et al. (Abhat, 1983).

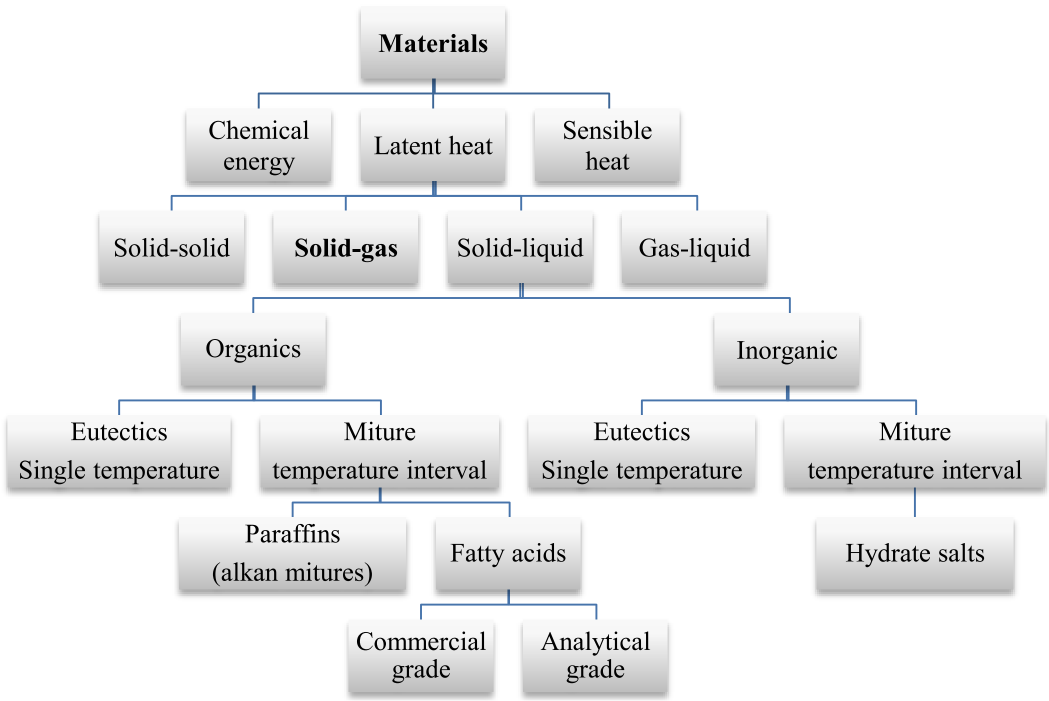

Figure 1.4. Classification of various PCM (Abhat, 1983).

Generally a PCM which is used in cold storage applications is considered as "promising" when it meets the following characteristics:

1. Melting temperature and pressure positioned in the practical range of operation: (278 to 281) K and pressures close to atmospheric pressure.
2. Large heat of fusions which results in a more compact cold storage tank and high cold storage capacity.
3. High thermal conductivity and low degree of subcooling.
4. Low in cost, nontoxic, environmentally friendly and be chemically stable.
5. The ability to be reproduced or cyclic stability, which can allow the storage materials to be used many times in cold storage and release processes.

1.4.3.3. Gas hydrates as promising PCMs

It is difficult to find a PCM which can fulfil all the aforementioned requirements. Figure 1.5 shows a comparison between the cold storage characteristics of various PCMs, including refrigerant hydrates.

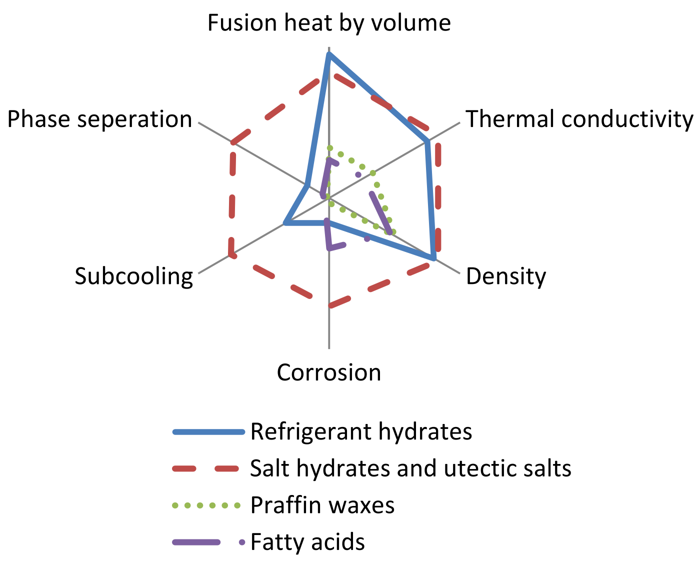

Figure 1.5. Comparison of characteristics of various PCMs

Gas hydrates are among the most promising PCMs used in cold storage applications with the properties such as melting temperature within the practical rang of operation (278-285) K, large heat of fusion (270-430 kJ/kg) resulting in the high storage capacity and high thermal conductivity as it can be observed in Figures 1.5 and 1.6. Furthermore, the application of gas hydrates improves the heat transfer efficiency. Table 1.2 shows the performance parameters of the cold storage systems using water, ice, eutectic salts and clathrate hydrates such as coefficient of performance (CoP) of the refrigerator which represents the overall efficiency of the refrigerator and economical characteristics such as investment for the construction of the corresponding refrigerator.

Table 1.2. Performance and characteristics of various cold storage materials (Wang et al., 2014)

Storage medium	water	Ice	Eutectic salts	Clathrate hydrates
Phase change temperature range/°C	0-10	0	8-12	5-12
Heat transfer performance	Superior	Medium	Inferior	Superior
[a]CoP of refrigerator	1	0.6-0.7	0.92–0.95	0.89–1
[b]Investment	<0.6	1	1.3-2	1.2-1.5

[a]Coefficient of performance

[b]Capital cost for the refrigeration system

After the application of gas hydrates as a PCM in cool storage processes in 1980s, when the gas hydrate was found in refrigeration systems during their crystallization in the expansion valves (Tomlinson, 1982), many studies have been performed which can be classified into three groups : (1) the studies which are aimed at measurement of phase equilibrium conditions of the gas hydrates (thermodynamic studies) (2) studies with the aim of characterization of the cold storage process (3) the studies which have considered the hydrate formation characteristics (kinetic studies).

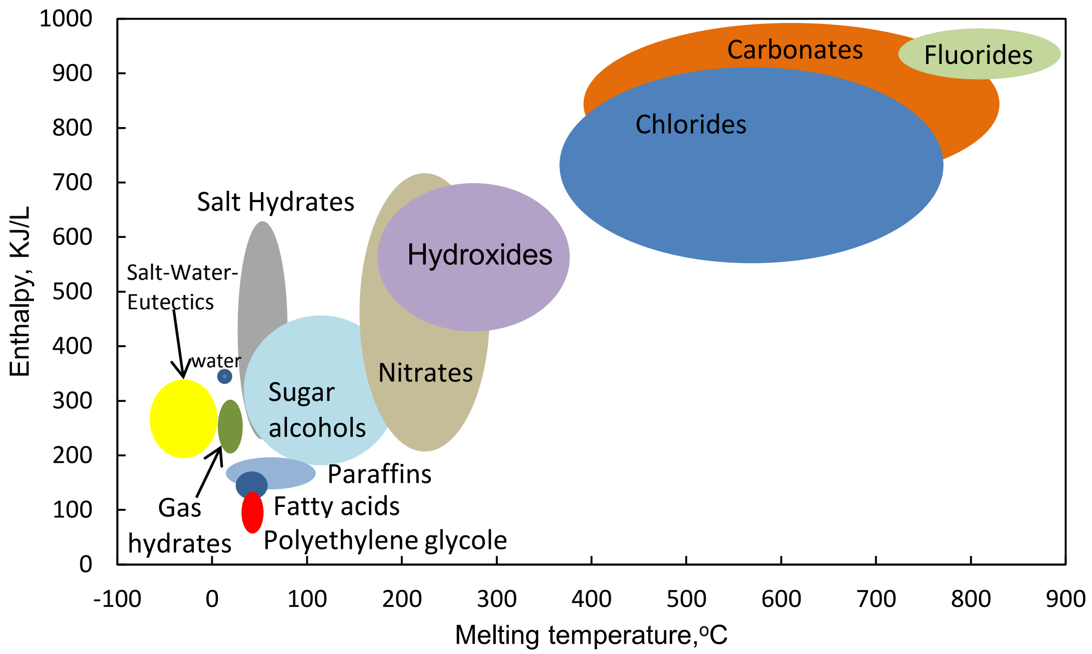

Figure 1.6. The enthalpy of fusion and melting temperature of various PCMs.

As discussed earlier, refrigerant hydrates have brilliant prospects for use as a media in cold storage systems. The conceptual design of a cold storage system based on the gas hydrate crystallization requires precise phase equilibrium data of refrigerant hydrates as well as an accurate knowledge on the kinetics of the refrigerant hydrates formation. Most refrigerants used for cold storage applications are phased out due to the environmental restrictions. Furthermore, it has been established that mixed clathrate hydrates provide more compatible cold storage medium than single clathrate hydrates. The main objective of this thesis is to introduce new refrigerant blends for application in cold storage systems. For this purpose, cold storage technology using hydrates has been studied with the two main areas focussing on (1) experimental measurements for new refrigerant blends R410A, R407C, R408A, R404A, R508B, R406A, R427A and R507C as well as pure refrigerant R116, (2) thermodynamic modelling involving prediction of the hydrate dissociation conditions. The experimental work consisted of a thermodynamic study and kinetic study. In the thermodynamic study equilibrium dissociation conditions (pressure-temperature) and the enthalpy of dissociation of refrigerant hydrates are measured. The hydrate nucleation and formation rate of the abovementioned refrigerants is analysed through the kinetic study.

This thesis consists of eight chapters. This introductive chapter delivers the industrial context and motivations behind clathrate hydrates cold storage research. The advantages of the application of the clathrate hydrates over conventional materials are discussed briefly. As this thesis is concerned with the phase equilibria of refrigerant hydrate-forming systems from experimental point of view, a general overview to their potential application in air conditioning systems is given. In the 2nd chapter an extended review of hydrates (clathrates/semi-clathrates) application in cold storage systems has been presented. The phase equilibrium studies of various clathrate/semi-clathrate hydrates as well as their kinetics of formation are reviewed. The different procedures to enhance the cold storage characteristics of the clathrate hydrates are discussed. Different aspects of the charge and discharge process of the cold storage systems are presented and the advantages and disadvantages of each procedure are presented. The theoretical models for describing the hydrate equilibrium conditions are discussed briefly in the 3rd chapter. The historical background of the theory of the model developed in this study is discussed. The correlation and equations for presenting the different phases are specified and the criterion for the hydrate equilibrium is identified. In the 4th chapter a conceptual formalisms related to the experimental illustration of thermodynamic properties of systems including gas hydrates are delivered. Experimental procedures at pressures ranging from moderate to considerably high pressures are highlighted. The advantages as well as limitations of each procedure are discussed. The most usual equipment and experimental techniques employed are described. The principles of the applied techniques and the criteria for determining equilibrium conditions are explained. The main part of the experimental study performed in this thesis is presented in chapters 5 and 6. A combination of new and implemented aspects from the literature was applied in the construction of the experimental apparatus. The development and preparation of the preferred isochoric apparatus is presented in chapter 5. The purity of the material used in this study, calibration of the measuring devices as well as their uncertainty of measurement, different parts of the experimental apparatus, and the procedures used in phase equilibrium and kinetics measurements are presented in the 5th chapter. The phase equilibrium of the refrigerants studied as well as their kinetics of hydrate formation is presented in this chapter. The effect of the temperature, pressure and surfactants on the rate of the hydrate formation is studied. The refrigerants considered in the 5th chapter include pure refrigerants viz. R134a, R23, R32, R125a and R116 as well as refrigerant blends namely R407C (HFC-32/HFC-125/HFC-134a, 23/25/52 wt%,), R410A (HFC-32/HFC-125, 50/50 wt%), R507C (HFC-125/HFC-143a, 50/50 wt%), R404A (HFC-143a/ HFC-125/ HFC-134a, 44/4/52 wt%), R406A (HCFC-R22/HFC-R142b/HC-600a, 54/41/4 wt%)), R408A (HFC-143a/ HFC-125/ HCFC-22, 46/7/47 wt%), R427A (HFC-134a/ HFC-125/ HFC-32/ HFC-143a, 50/25/15/10 wt%), R508B (R23/R116, 46/54 wt%).

The results obtained from experimental study as well as thermodynamic modelling are presented and discussed in the 6^{th} chapter. The measured experimental data are plotted against the modelling results and the accuracy of the model in correlating the experimental data is examined. In addition to the abovementioned refrigerants in chapter 5, pure refrigerants R134a, R143a, R142b, R141b and R32 are also modelled using the developed model in this thesis. Finally the general concluding remarks as well as some directions for the future work on the clathrate/semiclathrate hydrate cold storage systems are presented in the 7^{th} and the 8^{th} chapters respectively.

2

Application of Hydrates in Cold Storage Systems: Review of Experimental Studies

In this chapter an extended review of hydrates (clathrates/semi-clathrates) application in cold storage systems is presented. The phase equilibrium studies of various clathrate/semi-clathrate hydrates as well as their kinetics of formation are reviewed.

2.1. Phase equilibrium studies

The main part of a cold storage system is the storage tank. An economic study reveals that the total cost of a storage system is determined by the cost of the storage tank (Tomlinson et al., 1984). Consequently, in order to obtain a cost-efficient storage system a more compact storage tank is necessary. Low pressure refrigerant hydrates have clear prospects as cold storage materials in air conditioning technologies. Hence, the main objective of many studies has been devoted to the measurement of gas hydrates phase equilibrium conditions. Continued studies led to the consideration of refrigerant hydrates (Tomlinson, 1982). It has been well established that most refrigerants can form hydrates at low pressures (close the atmospheric pressure) and medium temperatures (278-290 ºC). Characterization of various refrigerant hydrates including CFCs and HCFCs such as CFC-11 and CFC-12, HCFC-22, HCFC-21 and HCFC-141b were first investigated (Tomlinson, 1982, Carbajo, 1983, Isobe and Mori, 1992). Even though the applications of such refrigerants have shown to be quite promising, however at the very beginning of development, they have encountered the main challenge of CFC and HCFC restrictions. Consequently, the study of CFC alternatives was persistently pursued since the end of 1980s (Mori and Mori, 1989b, Oowa et al., 1990, Isobe and Mori, 1992, Guo et al., 1996). Table 2.1 presents the hydrate dissociation pressure and temperature ranges of some pure CFC, HCFC, HFC as well as their Ozone Depletion Potentials (ODP) and their Global Warming Potentials (GWP). HFC-134a shows the lowest dissociation pressures among all pure HFC hydrates. The enthalpy of hydrate dissociation which reflects the capacity of the cold storage can be estimated using the Clapeyron equation from equilibrium dissociation data.

Table 2.2 shows the upper quadruple points (Hydrate -Liquid refrigerant-aqueous solution - Vapour) for various halogenated carbon.

Mixed refrigerant gas hydrates have been shown to be a significant cold storage medium. The mixture of low and high pressure refrigerants can provide mixed hydrates with the pressure and temperature ranges of decomposition lying between practical ranges of cold storage applications (temperature range of (278-285) K and at atmospheric pressure) (Guo et al., 1996). Furthermore, the hydrate formation characteristics can be improved by mixing of the different refrigerants. Table 2.3 presents the hydrate equilibrium dissociation data as well as enthalpy of dissociations of various refrigerant blends.

2.2. Kinetic studies

The hydrate formation rate is another key factor which should be considered before designing a cold storage system. In developing a cost-effective cold storage system, fast nucleation is necessary. Gas hydrates occur at water and gas interface and their growth rate depends on the diffusion of the gas and water molecules through the hydrate phase. Generally gas hydrate formation consists of the following steps (Sloan and Koh, 2008):

- Hydrate nucleation which is an intrinsically random (unpredictable) process.
- Hydrate growth which may be controlled by kinetic, heat and mass transfer limitations.

Table 2.1. Pressure and temperature ranges of pure refrigerant hydrates.

Refrigerant	*T* range ,K	*P* range, MPa	[a]ΔH, kJ/kg	[b]ODP	[c]GWP	Ref.
R11(CCl_3F)	273.2-281.8 266.6-281.5	0.0082-0.059 0.0055-0.0624	189.0	1	4000	(Carbajo, 1983) (Wittstruck et al., 1961)
R12(CCl_2F_2)	273.1-284.2 264.9-285.0	0.0399-0.0449 0.023-0.43	185.0	1	2400	(Carbajo, 1983) (Wittstruck et al., 1961)
R23(CHF_3)	266.2-292.4 282.5-292.3 275.4-285.8	0.241-4.45 0.92-3.85 0.45-1.566	89.7	1	3000	(Kubota et al., 1984) (Mooijer-van den Heuvel et al., 2006) (Hashemi et al., 2015)
R13($CClF_3$)	273.3-281.6	0.324-3.92	90.1	1	4200	(Kubota et al., 1984)
R22($CHClF_2$)	267.7-289.5 277.8-289.4 276.3-287.4 274.9-285.9	0.067-0.774 0.154-0.773 0.141-0.587 0.506-0.113	87.6	0.055	1700	(Wittstruck et al., 1961) (Javanmardi et al., 2004) (Chun et al., 1996) (Hashemi et al., 2015)
R32(CH_2F_2)	275.5-294.2 274.6-292.5 278.1-291.3	0.2-10.4 0.19-1.34 0.27-1.133	54.2	0	650	(Hashimoto et al., 2010b) (Akiya et al., 1999) (Mohammadi and Richon, 2010)
R134a($C_2H_2F_4$)	279.4-282.9 265.3-283.1	0.178-0.379 0.0393-0.4144	124.1	0	1300	(Mohammadi and Richon, 2010) (Liang et al., 2001)

Table 2.1 continued

	275-283.8 274.1-283.1 274.4-282.2	0.062-9.68 0.055-0.415 0.065-0.345				(Hashimoto et al., 2010a) (Akiya et al., 1999) (Hashemi et al., 2015)
R143a($C_2H_3F_3$)	275.9-283.6	0.15-9.2	101.7	0	1000	(Hashimoto et al., 2010a)
R141b(C_2H2F_4)	268.4-282.5 273.6-289.6	0.0062-0.0402 0.0081-0.0526	285	0.086	700	(Liang et al., 2001) (Tanii et al., 1997)
R125a(C_2HF_5)	274.9-283.6 274.9-284.3 274.6-284.6	0.127-0.86 0.117-7.87 0.117- 5.986	108.2	0	3400	(Akiya et al., 1999) (Hashimoto et al., 2010a) (Hashemi et al., 2015)
R152a($C_2H_4F_2$)	279.7-287.7 264.7-288.1 265.6-288.1	0.153-0.416 0.0495-0.4437 0.04-0.823	102.5	0	120	(Mohammadi and Richon, 2010) (Liang et al., 2001) (Kubota et al., 1984)

[a]At upper quadruple point

[b]Ozone Depletion Potential

[c]Global Warming Potential

Hence, it is expected that gas hydrate formation is a time-consuming phenomenon. Several elements can promote the abovementioned steps and as the result increase the hydrate formation rate; such factors are the mechanical agitation, magnetic interference, gas solubility, and surfactants additives.

Table 2.2. Clathrate hydrate upper quadruple points (Q_2) of various halogenated carbons

Refrigerant	T_{Q2} ,K	P_{Q2}, MPa	ΔH, kJ/kg	ODP	GWP	Ref
R11(CCl_3F)	281.8	0.059	289	1	4000	(Carbajo, 1983)
R12(CCl_2F_2)	285.3	0.0449	270.4	1	2400	(Carbajo, 1983)
R21($CHCl_2F$)	281.8	0.101	276.6	0.04	151	(Carbajo, 1983)
R21(CHCl2F)	281.9	0.101	267	0.04	151	(Tanii et al., 1997)
R30 (CH_2Cl_2)	274.9	0.021	230	0	8.7	(Tanii et al., 1997)
CBr_2F_2	278.2	0.052	-	-	-	(Tanii et al., 1997)
R-140(C_2H_3C1)	274.3	0.182	-	0.03	770	(Carbajo, 1983)
R-160Bl (C_2H_5Br)	274.6	0.022	-	-	-	(Carbajo, 1983)
R-150 (CH_3CHCl_2)	274.7	0.009	-	-	-	(Carbajo, 1983)
R-20 ($CHC1_3$)	274.9	0.009	-	-	-	(Carbajo, 1983)
R-40I1(CH_3I)	277.5	0.023	-	-	-	(Carbajo, 1983)
R-160 (C_2H_5C1)	278.0	0.078	-	-	-	(Carbajo, 1983)
R-12B2 (C Br_2F_2)	278.1	0.051	-	1.7	-	(Carbajo, 1983)
R-22B1($CHBrF_2$)	283.1	0.268	-	0.74	-	(Carbajo, 1983)
R-12B1 ($CBrC1F_2$)	283.2	0.169	-	3	-	(Carbajo, 1983)
R-13B1 ($CBrF_3$)	284.2	1.141	-	10	5600	(Carbajo, 1983)
R-142b ($CH_3CC1\ _2F_2$)	286.3	0.231	-	0.055	2000	(Carbajo, 1983)
R-40B1 (CH_3Br)	287.9	0.152	-	-	-	(Carbajo, 1983)
R-31(CH_2ClF)	291.1	0.286	-	0.02	-	(Carbajo, 1983)

Table 2.2 continued

R-41(CH_3F)	292.0	3.232	-	0	92	(Carbajo, 1983)
R-40(CH_3C1)	293.7	0.495	-	0.02	13	(Carbajo, 1983)
R-161(C_2H_5F)	296.0	0.808	-	0	-	(Carbajo, 1983)

2.2.1. Effect of additives

It has been proven that surfactants can increase the hydrate formation rate significantly and as a result decrease the energy costs of the hydrate formation. Generally surfactants are divided into two groups: anionic (e.g. Sodium dodecyl sulphunate (SDS), sodium tetradecyl sulfate (STS) and sodium hexadecyl sulfate (SHS)) and non-ionic (e.g. dodecyl polysaccharide glycoside (DPG)).

Table 2.3. Pressure and temperature ranges of hydrate refrigerant blends.

Refrigerant	composition	Mass percent%	*T*,range, K	*P*range, MPa	[a]*ΔH, kJ/mol.K*	[b]ODP	[c]GWP	Ref.
R410A	R32/R125	50/50	278.2-292.1	0.2569-1.3073	73.7	0	1725	(Akiya et al., 1999)
R407C	R32/R125/R134a	23/25/52	274.4-286.1	0.0804-0.6335	103.4	0	1525	(Akiya et al., 1999)
-	R11+R12	(0-100)/(0-100)	281.9-285.3	0.059-0.449	-	-	-	(Carbajo, 1983)
-	R11+R114	(0-100)/(0-100)	273.2-281.8	0.065-0.08	-	-	-	(Carbajo, 1983)
-	R12+R114	(0-100)/(0-100)	273.8-282.1	0.124-0.196	-	-	-	(Carbajo, 1983)

The effect of the addition of SDS, DPG and their mixtures as well as liquid hydrocarbons such as cyclopentane (CP) and methylcyclohexane (MCH) on gas hydrate formation rate was studied by Sun et al. (Sun et al., 2003). The effect of some additives such as powder alumina or zinc on the HFC134a and HCFC-123 hydrate formation in a direct contact cold storage system which was incorporated into a vapour compression refrigerator loop was studied by Isob and Mori (Isobe and Mori, 1992). They found that in the presence of surfactants, a more porous hydrate-foam layer would form resulting in the reduction of the supercooling of the system. An even larger reduction in the supercooling was obtained by the addition of a non-ionic surfactant. Tanii et al. conducted an experiment on HCFC-141b hydrate in the presence of 0.05 wt% surfactant. They found that adding 0.05 wt% surfactant brought the tank temperature close to the critical decomposition temperature of HCFC- 141b gas hydrate, decreasing the supercooling extent, and bringing the clathrate formation and decomposition up to 40 wt% of clathrate (Tanii et al., 1997).

Li et al. proposed an effective way for fast nucleation and growth of clathrate hydrate of HCFC-141b using a static water column by addition of the surfactant (sodium dodecylbenzenesulfonate-6) and a metal rod, which was placed in centre of the column (Li et al., 2004). It was found that, for example, when the temperature is within the range of 274.15–279.15 K, the hydrate nucleation began within 3–30 min and the hydrate formation can be accomplished in 1.5–8 h. The major disadvantage of using surfactants is that they increase the space for storing a specified mass of gas hydrate by increasing the gas hydrate effective specific volume (Isobe and Mori, 1992). The effects of calcium hypochlorite or benzenesulfonic acid sodium salt solutions with various concentrations on the crystallization process of HFC-141b were studied Bi et al. (Bi et al., 2006). They found that the degree of subcooling of the hydrate formation decreases to 0.78 ^{o}C by using benzenesulfonic acid sodium salt with a concentration of 0.03 wt %, and the rate of the formation of the hydrate increases 0.2 g/s by addition of calcium hypochlorite with the concentration of 0.08 wt%. Bi et al. investigated the effects of calcium hypochlorite or benzenesulfonic acid sodium salt with different concentrations on the dissolution process of gas hydrate crystallization (Bi et al., 2009). It was found that calcium hypochlorite with a concentration of 0.08 wt % increases the dissolution rate of HCFC-141b hydrate significantly. Xie et al. developed new small scale gas hydrate cold storage equipment. They found that the cold storage performance improves with the addition of 0.04 wt % of sodium dodecyl benzene sulfonate (SDS) to the system. They also utilized HCFC-141b as the hydrate former in their experiments (Xie et al., 2010). Wu and Wang used n-butanol as the additive in a HCFC-134a hydrate formation process. They found a significant increase in the cold storage rate by adding n-butanol solution at a concentration of 1.34 wt %. It was demonstrated that adding alcohol would result in a smooth cold storage operation which is industrially applicable (Wu and Wang, 2012).

2.2.2. *Effect of gas solubility*

Gas solubility is another factor which has a significant influence on the hydrate equilibrium pressure and hydrate formation rate (Sloan and Koh, 2008). The solubilities of some refrigerants are presented in Table 2.4. It can be seen that the solubility of these refrigerants is comparable to that of CO_2 which is a highly soluble gas. Temperature and pressure are two main elements which influence gas solubility. It has been established that in the existence of a hydrate with an increase in the temperature of the system the gas solubility increases whereas in the absence of hydrate, the gas solubility increases with decreasing temperature. At a pressure of 6 MPa the amount of gas dissolved in liquid in equilibrium with gas hydrates is reported to be 0.0163 mol% and 0.0281 mol% at the temperatures of 274.25 K and 282.95 K respectively (Servio and Englezos, 2001). One way to increase the gas solubility is the application of the co-solvents for instance dissolved propylene glycol (PPG) and poly-ethylene glycols (PEG) (King Jr, 2001). However, their effect on the gas hydrate crystallization process is unknown.

Table 2.4. Refrigerant solubilities in pure water

Refrigerant	Formula	T_{range}, K	P_{range}, bar	Solubility range (mole/mole)	Ref.
HCHC-22	CHF_2Cl	278.24-338.11	0.4574-0.8852	0.000589-0.000148	(Zheng et al., 1997)
HFC-23	CHF_3	278.20-338.21	0.6875-0.9147	0.000287-0.000712	(Zheng et al., 1997)
HFC-32	CH2F2	289.16-302.26	1.013	0.000758-0.000446	(Miguel et al., 2000)
HFC-134a	$CH2FCF_3$	275.16-338.12	0.6377-0.9306	0.0004080-0.000801	(Zheng et al., 1997)
HFC-152a	CHF_2CH_3	278.19-338.19	0.3667-0.7992	0.000660-0.000197	(Zheng et al., 1997)
HFC-125	CHF_2CF_3	289.16-303.03	1.013	0.000769-0.000470	(Miguel et al., 2000)
R744	CO_2	278.15-338.15	0.4906-0.8417	0.000551-0.000168	(Zheng et al., 1997)

2.2.3. Effect of mechanical stirring, ultrasound and magnetic fields

Three different approaches for the hydrate formation promotion were applied by Xie et al. (Xie et al., 2010). The methods consist of (1) non-stop mechanical blending, in which the blender operates until the complete formation of the hydrate (2) 5 minutes of mechanical blending with the mechanical agitator working for 5 minutes after the stabilization of the temperature (3) gas hydrate formation under inducement of melting ice, in which the hydrate crystallization can be induced using freezing of the water in the cold storage tank and melting it by increasing the temperature to 2 ºC. It was found that among all the above-mentioned methods continuous mechanic blending was more effective resulting in an overall cold storage quantity of 27.2 MJ and an average hydrate growth velocity of 0.5876 kg/min. However, prolonged mechanical agitation is energy intensive and the fittings can become loose. Linga et al. suggested that working in the quiescent conditions throughout clathrate hydrate formation would result in the cost effective and safer process. They proposed the application of ultrasound for enhancement of the gas-liquid mass transfer specifically below gas induction speed (Linga et al., 2010). Liu et al. specified an ultrasound wave power range of 58~1000 W which is beneficial to accelerate the hydrate crystallization process (Kai-Hua and Shuan-Shi, 2003). Liu et al. studied the influence of the magnetic field on HCFC-141b gas hydrate formation. They concluded that in the presence of a specific magnetic field (Liu et al., 2003):

- Hydrate growth can be extended into both water and refrigerant phases.
- The hydrate nucleation induction time can be decreased from 9 hr to 40 min depending on the magnetic pole, magnetic intensity and the number of iron wires
- The final water to hydrate conversion can be improved to 100% in some cases.

2.2.4. Effect of crystallizer flow rate

Bi et al. studied the effect of volumetric flow rate in the crystallizer on gas hydrate formation rate using an experimental cold storage apparatus. They obtained the optimum range of 150–450 l/h for a crystallizer flow rate in which the extent of supercooling decreased to a minimum of 1.97 °C rapidly with increasing the flow rate (Bi et al., 2004). Even though a higher flow rate can improve the convection heat transfer between the gas hydrate and the refrigerant, it can also produce a small temperature rise of the gas hydrate resulting in an increase in the degree of supercooling. It should be mentioned that the optimum values obtained for the flow rate are highly dependent on the crystallizer dimensions and for different crystallizers new values should be obtained.

2.2.5. Different configurations of cold storage process

For a better insight into the cold storage process and the heat transfer methods between the coolant and cool storage media it is essential to investigate the design of the hydrate storage apparatus. Xie et al. summarized various configurations of cold storage systems (Xie et al., 2004). Generally gas hydrate cold storage systems according to the heat transfer method between circulator fluid (which is usually water) and the cold storage medium (gas hydrate) can be classified as four types: (a) direct-charged/direct- discharged (b) direct-charged/indirect-discharged (c) indirect-charged/direct-discharged (d) indirect-charged/indirect-discharged. Schematic diagrams of these configurations are shown in Figure 2.1. In direct contact charge or discharge, the coolant and the cold storage medium (gas hydrate) are in direct contact during heat transfer whereas in indirect contact charge or discharge a coil or heat exchanger is used for the heat transfer between coolant and the gas hydrate. A number of researchers studied direct contact-charged/direct-contact discharged type of cold storage (Mori and Mori, 1989a, Carbajo, 1985, Najafi and Schaetzle, 1991, Ternes, 1984, Schaetzle et al., 1987). Researchers (Tanii et al., 1997, Carbajo, 1983) conducted their experimental work on direct contact-charged/indirect-contact discharged system. Some researchers used the indirect-contact charged/indirect-contact discharged methods in their measurements (Bi et al., 2009, Bi et al., 2004, Bi et al., 2006, Wu and Wang, 2012). The advantages and drawbacks of different types of charging and discharging processes are presented in Table 2.5 (Carbajo, 1983, Carbajo, 1985, Guo et al., 1996, Wang et al., 2014).

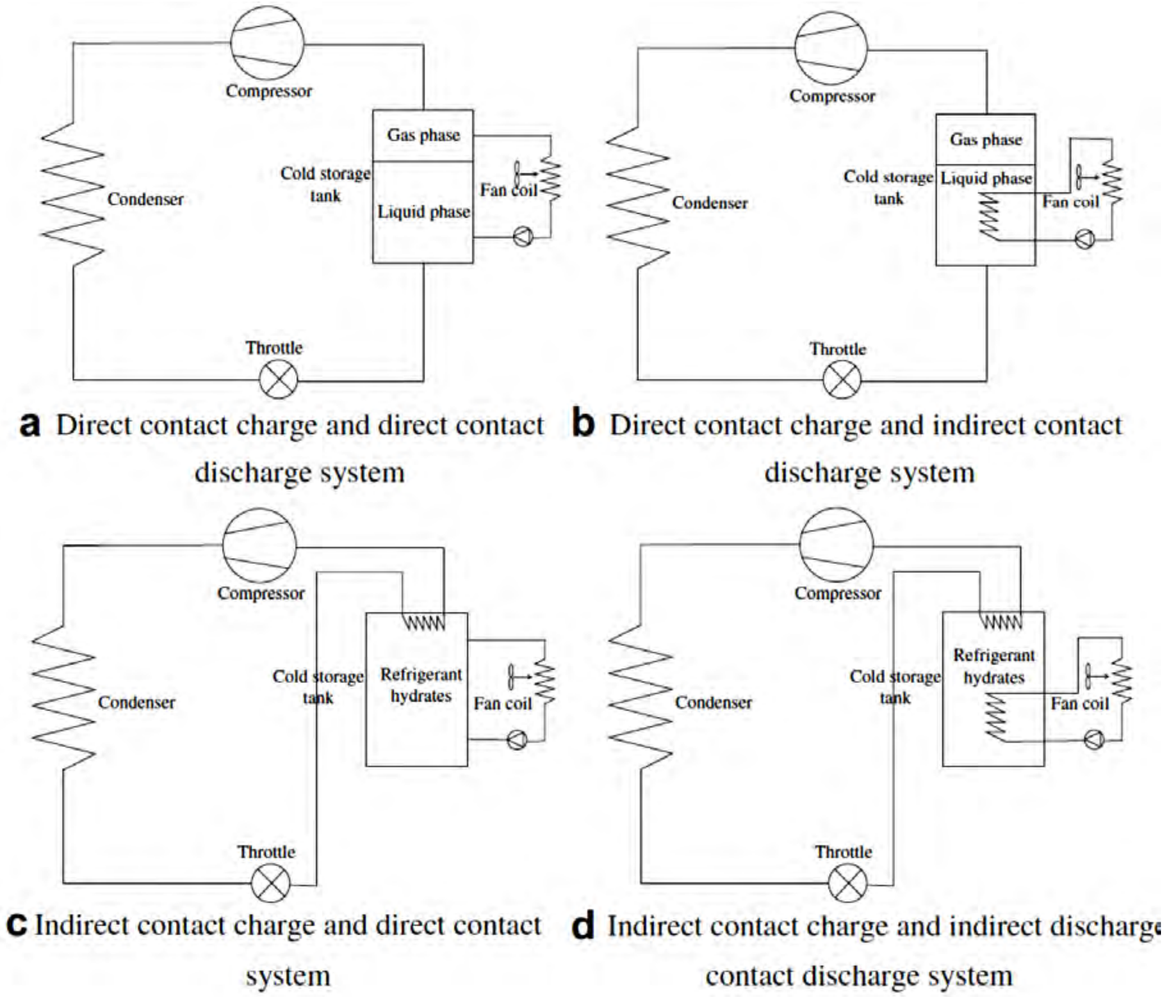

Figure 2.1. Different designs of gas hydrate cold storage systems (Xie et al., 2004).

Table 2.5. Different configurations of charge and discharge processes.

Process type	advantages	Disadvantages
Direct contact charge	No need of evaporator heat exchanger; effective heat transfer; efficient dispersion of refrigerant into the water; high rate of hydrate formation; refrigerants returning to compressor with high temperatures; no need of defrosting equipment ;low energy consumption	Expensive oil-free compressor , water separator and receiver are required; high investment
Indirect contact charge	Ordinary compressor can be utilized; application of conventional refrigeration cycle; low cost	Evaporator heat exchanger is required; comparatively low heat transfer performance during formation of hydrate around the coils; mechanical agitator is needed; low temperature in the evaporator and reduced compressor performance; defrosting equipment is necessary; high energy consumption
Direct contact discharge	No need for a heat exchanger; low temperature difference between cold storage medium and circulator; low energy consumption	The need for an expensive pump to liquefy the refrigerant for pump without cavitation; leaks at the seals
Indirect contact discharge	Application of ordinary pump	Heat exchanger is required; high temperature difference between cold storage medium and circulator; high energy consumption

2.2.6. Gas hydrates as slurries in secondary refrigeration

The application of a secondary loop for cold supply is an effective approach to decrease the amount of conventional greenhouse refrigerants in primary refrigeration circuits. However, their application involves using heat exchangers and extra circulating pumps resulting in energy losses in the system. One solution to this problem is the application of two-phase (solid-liquid) secondary refrigerants (known as phase change slurries (PCSs)), which consists of solid particles suspended in a aqueous solution (Jerbi et al., 2013). In addition to being used as a cold storage medium in a static cold storage tank which was described earlier, phase change materials (PCMs) have also been utilized recently as slurries for conveying the cold energy in secondary refrigeration systems (Youssef et al., 2013, Jerbi et al., 2013). A PCS which is used as two phase (solid-liquid) secondary refrigerant in refrigeration systems should fulfil the following requirements: (1) suitable rheological characteristics so it can easily flow through the pipes, (2) formation in the practical temperature and pressure range of air conditioning systems, (3) having high enthalpy of fusion. PCSs comprise a carrier fluid (e.g. water) as the continuous phase and a phase change material (PCM) as the distributed phase. Hence, they can use both latent heat of the PCMs and sensible heat of the carrier fluid and that of the PCM simultaneously. Various classes of PCSs have been investigated for secondary refrigeration applications including clathrate hydrate slurries (CHSs), Microencapsulated PCM slurries (MPCMS), Shape-stabilized PCM slurries (SPCMS) and PCM emulsions (PCME) (Youssef et al., 2013). Ice slurries are the most common PCSs. However, their generation involves using power consuming mechanical processes (Guilpart et al., 2006). Currently, only clathrate hydrate slurries (CHSs) and ice slurries have been utilized in practical applications and other slurries are of interest in laboratory studies. Two major concerns of PCM slurries application are their stability and degree of subcooling. The application of CHSs as a secondary fluid in refrigeration systems have been considered by numerous researchers (Fournaison et al., 2004, Delahaye et al., 2006, Martinez et al., 2008, Zhang and Ma, 2012, Youssef et al., 2013). Two types of CHSs have been known including clathrate hydrate of CO_2 and semi-clathrate hydrate of quaternary salts. In the next sections a literature survey has been carried out on the cold storage and transportation characteristics.

2.2.6.1. CO_2 clathrate and semi-clathrate hydrate slurries

CO_2 can form a two phase hydrate slurry which is a mixture of solid hydrate particles and aqueous solution. One way of increasing of the phase change enthalpy of CO_2 hydrate slurry, is increasing the amount of the solid hydrate particles. However, their flowing characteristics should be considered before increasing of the hydrate particles. Fournaison et al., Marinhas et al. and Delahaye et al. studied the formation and flow characteristics of CO_2 clathrate hydrate in a secondary refrigeration during its high phase change enthalpy state (500 kJ/kg_{water}) (Fournaison et al., 2004, Marinhas et al., 2006, Delahaye et al., 2008). Unlike conventional gas hydrates and ice slurries, CHSs have the advantage of being formed without application of mechanical processes resulting in low power consumption. Marinhas et al. proposed an approach for CO_2 hydrate slurry production by injection of CO_2 in cold water without using the mechanical processes (Marinhas et al., 2006). A conceptual design of a hydrate based refrigeration system proposed by Jerbi et al. is presented in Figure 2.2 in which CO_2 hydrate slurry has been used as a secondary two phase refrigerant (Jerbi et al., 2013). The system consists of two parts, (a) a tank reactor with the capacity of 26.47 L which can withstand pressures up to 4.5 MPa and provide a heat flux of 1-5 kW for the hydrate slurry fraction between 0 to 22%, (b) the circulation loop in which the CO_2 hydrate slurry goes through the heat exchanger to be dissociated and thereby cool the medium. One major problem with application of CO_2 clathrate hydrate is its high pressure of formation/dissociation. One solution to this concern is the application of different thermodynamic hydrate promoters such as THF, TBAB, and TBPB. It has been well established that these promoters can reduce the hydrate equilibrium dissociation/formation conditions considerably (Delahaye et al., 2006, Lin et al., 2008, Martinez et al., 2008, Mayoufi et al., 2011, Mayoufi et al., 2010). Furthermore, Delahaye et al. showed that the CO_2 + THF semi-clathrate hydrate dissociation enthalpy is twice that of the pure CO_2 (Delahaye et al., 2006).

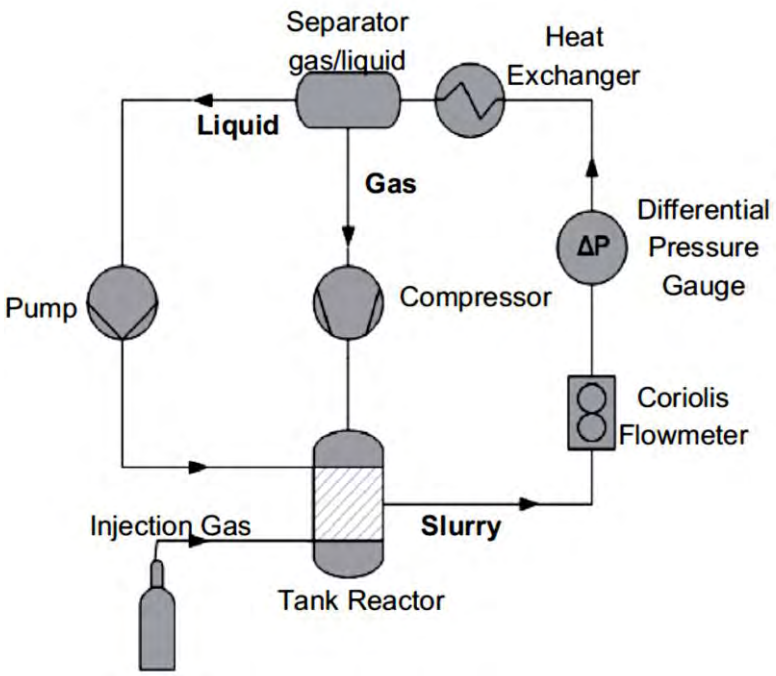

Figure 2.2. Conceptual design of a refrigeration unit using CO_2 hydrate slurry (Jerbi et al., 2013)

Among the abovementioned promoters TBAB has been studied intensively. Figure 2.3 shows phase equilibrium conditions of clathrate/semi-clathrate hydrate of CO_2 in the presence of different TBAB aqueous solutions (Eslamimanesh, 2012). CO_2 is able to form semi-clathrate hydrate in the presence of TBAB which is more stable than the ordinary clathrate hydrate. A comprehensive review of CO_2 clathrate/semi-clathrate hydrate have been performed by Eslamimanesh et al. (Eslamimanesh et al., 2012). THF decreases the equilibrium pressure by changing the hydrate structure from sI to sII (Martinez et al., 2008). The application of heavy hydrocarbons such as cyclopentane (CP), neopentane, cyclohexane, and benzene is a different way for changing the hydrate structure and lowering the hydrate equilibrium pressure. It was found that the promotion effect of CP on CO_2 gas hydrate formation/dissociation is higher than that of THF and TBAB (Zhang and Lee, 2008). In the hydrate crystal formed by CP, CO_2 molecules occupy small cavities while large cavities are occupied by CP molecules. A summary of experimental investigations on clathrate and semi-clathrate hydrates for the systems containing carbon dioxide + gas/gases in the presence of hydrate promoters have been depicted in Table 2.6 (Eslamimanesh et al., 2012).

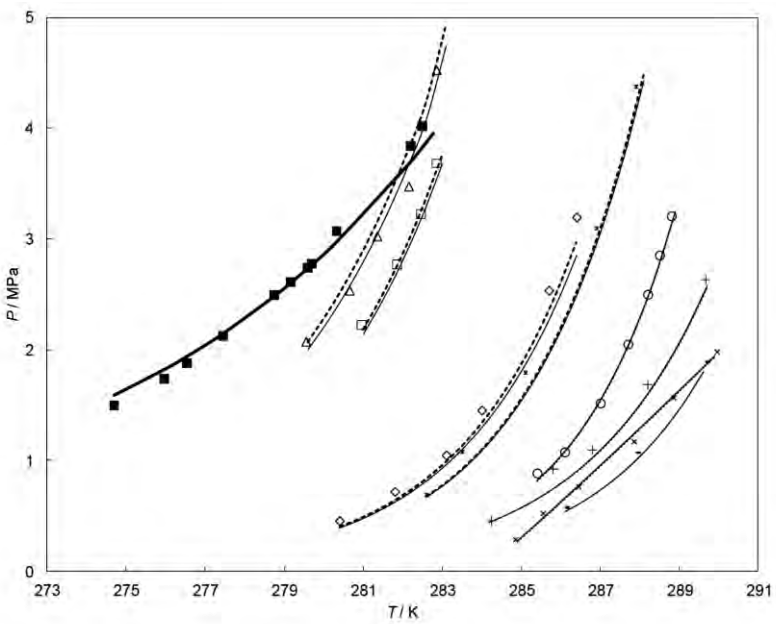

Figure 2.3. Dissociation conditions of CO_2 semi-clathrate hydrate in the presence of TBAB aqueous solutions with various TBAB mass fractions (taken from (Eslamimanesh, 2012)): ■, 0.0% (pure water)(Ohgaki et al., 1993, Fan and Guo, 1999, Mohammadi et al., 2005); Δ, 0.01% (Oyama et al., 2008); □, 0.02%(Oyama et al., 2008); ◊, 0.05% (Mohammadi et al., 2011); *, 0.5%; ○, 0.1%(Mohammadi et al., 2011); +, 0.167% (Mohammadi et al., 2011); ×, 0.25 (Mohammadi et al., 2005); -, 0.35 (Mohammadi et al., 2005); solid and dash lines, thermodynamic models from (Eslamimanesh, 2012).

2.2.6.2. Semi-clathrates of quaternary salts (QS)

Semi-clathrate hydrates of quaternary salts (QS) such as TBAB have a brilliant prospect as a media for storage and transportation of cold energy due to their outstanding properties such formation conditions around atmospheric pressure and 12°C which is beneficial to the air conditioning systems. There are two different types of TBAB semi-clathrate hydrate including type A with the columnar shape and hydration number of 26 and type B with undefined form of crystals and hydration number of 38 (Oyama et al., 2005).

Table 2.6. A review of experimental investigations on clathrate/semi-clathrate hydrates for the systems of carbon dioxide + gas/gases + hydrate promoters (Eslamimanesh et al., 2012).

System	Objective	Ref.
CO_2 + CH_4 + water/neohexane emulsion	PVT studies	(Beltrán and Servio, 2010)
CO_2 + N_2 + THF aqueous solution	PVT and kinetic studies	(Linga et al., 2007)
CO_2 + CH_4 + water/aqueous sodium chloride solution	PVT studies	(Fan et al., 2000)
CO_2 + N_2 + TBAB/THF aqueous solutions	PVT studies	(Lu et al., 2009)
CO_2 + N_2 + TBAB aqueous solution and CO_2 + CH_4 + TBAB aqueous solution	Measurements of enthalpy of dissociations	(Deschamps and Dalmazzone, 2010)
CO_2 + H_2 + TBAB aqueous solution and CO_2 + H_2 + THF aqueous solution	study of semi-clathrate hydrate dissociation conditions and the effects of various additives through using equilibrium cell	(Fan et al., 2009)
CO_2 + N_2 + TBAB aqueous solution in the presence of dodecyl trimethyl ammonium chloride (DTAC)	Kinetic study, pressure drop, split fraction via a crystallizer cell	(Li et al., 2010c)
CO_2 + N_2 + TBAB/TBAF aqueous solution	PVT studies	(Fan et al., 2009)
CO_2 + N_2 + TBAB aqueous solution	PVT studies	(Meysel et al., 2011)
CO_2 + H_2 + TBAB aqueous solution	PVT and kinetic study	(Li et al., 2010b)
CO_2 + H_2 + TBAB aqueous solution	PVT and kinetic studies	(Kim et al., 2011)
CO_2 + H_2 + TBAB aqueous solution/Cyclopentane	Kinetic studies	(Li et al., 2010c)
CO2 +H_2+cyclopentane	PVT study	
CO_2 + H_2S + TBAB aqueous solution	Manufacturing of a high pressure equilibrium cell for the gas separation of various gas mixtures by means of hydrate formation techniques.	(Kamata et al., 2004)
CO_2 + N_2+cyclopentane/water emulsion	Kinetic study	(Li et al., 2010a)
CO_2 + N_2 + TBAB aqueous solution	PVT studies	(Mohammadi et al., 2012)
CO_2 + N_2 + TBAB aqueous solution	PVT studies	(Belandria et al., 2012)

After the first application of TBAB as the secondary refrigerant for storage and transportation of cold energy by Fukushima et al. (Fukushima et al., 1999) several studies have been performed on TBAB hydrate characteristics (Lipkowski et al., 2002, Darbouret et al., 2005, Oyama et al., 2008, Wenji et al., 2009). There are also numerous investigations on the thermophysical and rheological properties of semi-clathrate hydrate slurries of TBAB (Takao et al., 2001, Fukushima et al., 2002, Ogoshi and Takao, 2004). Takao et el. found out that the application of fine nucleating particles would decrease the subcooling degree of TBAB semi-clathrate formation (Takao et al., 2001). The hydrate nucleation and growth on heat exchanger coils in a refrigeration system is an anticipated phenomenon. Daitoku et al. studied various scraper shapes in order to detach and suspend these particles (Daitoku and Utaka, 2007). The influence of brushed surface heat exchangers on the formation of TBAB clathrate hydrate slurry was studied by Darbouret et al. (Darbouret et al., 2005). Generally various crystallization processes have been proposed for the clathrate/semi-clathrate hydrate formation: gas injection, cooling and heat exchanger surface scraping or brushing. The semi-clathrate hydrate formation of TBAC, TBAF, TBPB and TBMAC has also been studied by many researchers (Dyadin and Udachin, 1984, Nakayama, 1987, Mayoufi et al., 2010, Mayoufi et al., 2011, Clain et al., 2012, Mayoufi et al., 2012, Suginaka et al., 2012).

Semi-clathrate hydrates of Trimethylolethane (TME) can also be used as cold storage and transport materials (Yamazaki et al., 2002, Kakiuchi et al., 2003). The structure of TME is different from conventional clathrate hydrates (I, II, H). Yamazaki et al. showed that the clathrate hydrate formed by TME consists of three water molecules (trihydrate) (Yamazaki et al., 2002). A comprehensive review of thermophisycal properties of TBAB, TBAC, TBAF, and TME semi-clathrate hydrates can be found in literature (Zhang and Ma, 2012). Table 2.7 presents characteristics of different clathrate/semiclathrate hydrate slurries. As observed from Table 2.8, unlike ice slurry (Ayel et al., 2003), most of clathrate/semi-clathrate hydrate slurries seem to be non-Newtonian even at low solid fractions. Nevertheless, rheological behaviour types (Bingham, Ostwald-de-Waele, Herschel-Bulkey, Shear thinning, Shear thickening, thixotropic etc.) of these slurries still remain controversial between researchers.

Table 2.7. Characteristics of clathrate/semi-clathrate hydrate slurries

Hydrate former	Hydration number	Hydrate structure	Dissociation temperature (°C)	Enthalpy of fusion (kJ/kg)	Hydrate density (kg/m^3)
CO_2	^{a}7.23	sI	0–10	^{a}374	1062
TBAB	^{b}24–38	Semi-clathrate	^{b}9.5–12.4	^{c}193.2–205	^{d}1030–1082
TBAC	^{e}29.7–32.1	Semi-clathrate	^{e}14.7–15	^{f}200.7	^{g}1029–1034
TBAF	^{e}28.6–32.3	Semi–clathrate	^{e}27.2–28.3	^{f}229.7	^{g}1035–1057
TBPB	^{h}32–36.6	Semi–clathrate	^{i}281.1–282.4	^{j}203.8	^{k}1140

Table 2.7 continued

TME	[l]3	Trihydrate	[l]30	[l]218	[l]1090–1120

[a](Kang et al., 2001); [b] (Lipkowski et al., 2002, Ogoshi and Takao, 2004, Darbouret et al., 2005, Oyama et al., 2005);[c] (Ogoshi and Takao, 2004, Oyama et al., 2005); [d] (Ogoshi and Takao, 2004, Darbouret et al., 2005); [e] (Dyadin and Udachin, 1984, Nakayama, 1987); [f](Nakayama, 1987);[g] (Dyadin and Udachin, 1984); [h] (Dyadin and Udachin, 1984, Mayoufi et al., 2010, Clain et al., 2012, Suginaka et al., 2012); [i] (Dyadin and Udachin, 1984, Mayoufi et al., 2010, Suginaka et al., 2012); [j] (Mayoufi et al., 2010); [k] (Clain et al., 2012); [l] (Yamazaki et al., 2002)

2.2.7. *Gas hydrates as a working fluid*

Ogawa et al. proposed a novel hydrate based refrigeration system in which the working medium (hydrate slurry) cyclically goes through compression, hydrate formation, decompression and hydrate dissociation (Ogawa et al., 2006). The working medium is desired to form hydrate at temperatures above 30°C and moderate pressure; therefore the heat produced by hydrate formation reaction can be released by an easy accessible environmental fluid (e.g. air, river water, ground water etc.). The application of exothermic as well as endothermic characteristics of hydrate formation and dissociation reactions in a refrigeration loop is advantageous over previous refrigeration systems such as clathrate hydrate cold storage systems (in which the formation and storage of the clathrate hydrate occur within the lower-pressure/lower-temperature segment of the traditional vapour-compression refrigeration cycle) and secondary hydrate refrigeration systems (in which a hydrate slurry is utilized only as the secondary refrigerant for conveying the cold energy) (see section 2.2.6).

Table 2.8. Rheological behaviour of clathrate/semi-clathrate hydrates.

Hydrate former	Liquid	[a]φ_s	Rheology	Ref.
CO_2	Aqueous+[b]TA	0.04–0.1	Newtonian: [c]μ_{app}:3.3–16.6 mPa s	(Delahaye et al., 2011)
CO_2	Aqueous	-	μ_{app} increases before nucleation and decreases after	(Oyama et al., 2002)
CO_2	Aqueous	0.04–0.1	[d]OdW [e]S-thicken	(Delahaye et al., 2008)
CO_2	Aqueous	0.1–0.2	[f]HB S-thin, μ_{app} : 4-42 mPa s (at 400 s^{-1})	(Delahaye et al., 2008)
HCFC-141b	Aqueous	0.1–0.68	OdW S-thicken: μ_{app}:1.1–1.7 mPa s (at 400 s^{-1})	(DQ and XG, 2008)
TBAB	Aqueous	0.22–0.31	OdW S-thin, μ_{app}: 30-2000 mPa s	(Fukushima et al., 1999)
TBAB	Aqueous	0.04–0.53	Bingham, μ_{app}: 8-170 mPa s	(Darbouret et al., 2005)
TBAB	Aqueous	0–0.16	OdW S-thin, μ_{app}: 4-42 mPa s	(Xiao et al., 2006)
TBAB	Aqueous	0.06–0.2	OdW S-thin, μ_{app}: 3-100 mPa s	(Ma et al., 2010)
TBAB	Aqueous	0.02–0.25	OdW S-thin, μ_{app}: 2-5 mPa s	(Kumano et al., 2011)
TBAB	Aqueous	0.12–0.7	OdW S-thin, μ_{app}: 3.5-1000 mPa s	(Hashimoto et al., 2011)

Table 2.8 continued

TBAF	Aqueous	0–0.42	OdW S-thin, μ_{app}: 10-750 mPa s	(Hashimoto et al., 2011)
TBPB	Aqueous	0–0.28	OdW S-thin, μ_{app}: 4-41 mPa s	(Clain et al., 2012)

[a]hydrate volume fraction=$V_{solid}/(V_{solid}+V_{liquid})$
[b]Surfactant
[c]apparent viscosity
[d] Ostwald-de-Waele
[e]Shear thickening
[f] Herschel-Bulkley

A conceptual design of a gas hydrate based refrigeration system which utilizes hydrates as the working fluid, is shown in Figure 2.4. The system principally contains (1) a compressor for mixing and pressurizing of water and hydrate former, (2) a reactor in which clathrate hydrate can be formed at temperatures greater than the environment so the heat generated can be easily released, (3) a water separator for the separation of water and clathrate hydrate which is formed in the hydrate reactor, (4) a slurry pump to send the concentrated hydrate slurry from the separator to a heat exchanger (dissociating reactor) to dissociate thereby refrigerate the medium to be cooled (5) pumps for water circulation through two circulation loops to enhance the flowing properties of hydrate slurry before flowing to the reactors. Ogawa et al. used a mixture of HFC-32 and cyclopentane (CP) as the working fluid in their refrigeration system (Ogawa et al., 2006). The maximum dissociation temperature of HFC-32/CP clathrate hydrate is reported to be 27 °C at 1.78 MPa which is lower than the anticipated heat release temperature.

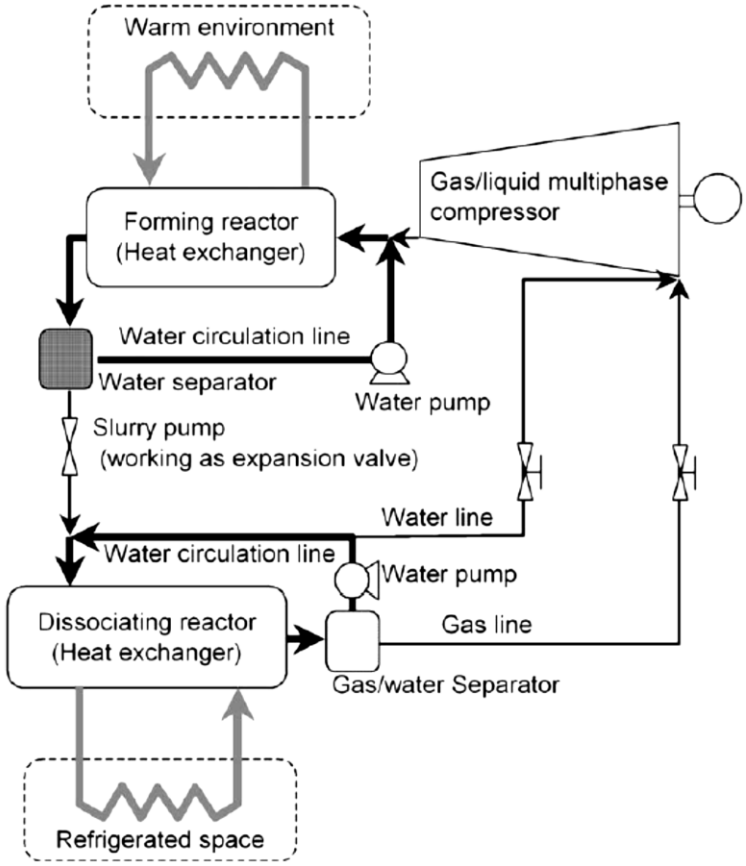

Figure 2.4. Schematic diagram of clathrate hydrate based refrigeration system (Ogawa et al., 2006).

The following requirements of the clathrate hydrates are essential for improving the system efficiency in the hydrate based refrigeration systems:

- High maximum hydrate formation temperature, in order to release the heat generated during hydrate formation process to the environmental fluids (air, river water, coastal water etc.) which is adjustable using hydrate promoters as stated earlier.
- Small temperature dependency of hydrate equilibrium pressure to provide a sufficient temperature difference between the two reactors (formation and dissociation reactors).
- Large heat of formation/dissociation
- Safety and environmentally friendly

3

Theoretical Models

During the past century, numerous theoretical studies and models have been presented on the prediction and correlation of phase equilibria data for gas hydrates systems. Early efforts for predicting gas hydrate equilibrium conditions were based mostly on experimental work performed during the 1940s and 1950s. These models have been reviewed extensively by Sloan and Koh (Sloan and Koh, 2008). Generally, the theoretical models of hydrate dissociation/formation conditions can be classified into three groups, viz., estimation techniques, thermodynamic models and kinetic models. It is beyond the scope of this thesis to present a comprehensive review of all models which have been used to estimate the hydrate dissociation/formation conditions (pressure, temperature and composition). Nevertheless, the descriptions of the most commonly used theoretical models are presented in this chapter.

3.1. Estimation techniques

Kamath proposed an exponential correlation in 1984 for estimation of the phase behaviour of simple hydrates. The proposed correlation can be employed for prediction of gas hydrate phase equilibria containing three phases liquid water (L_w)-hydrate (H)-Vapor (V) and Ice (I)-H-V for the hydrate formers such as methane, carbon dioxide, ethane, nitrogen and so forth.

The simplest method for prediction of the (L_W-H-V) equilibrium conditions is the "Gas Gravity Method" proposed by Katz. Since the method considered only hydrates of natural gases, it should be applied for systems of natural gases with low contents of non-combustible compounds such as nitrogen and carbon dioxide (Sloan and Koh, 2008). Application of the method is simple; Katz proposed the use of charts (Figure 3.1) presenting hydrate equilibrium pressures versus temperature and gas gravity (molecular mass of gas relative to the molecular mass of air). By calculation of the gas gravity and knowing the temperature, the gas hydrate equilibrium pressure can be obtained from the charts. However, the prediction of the formation pressures were approximate at best, due to the restricted amount of experimental data existing at that time (Sloan and Koh, 2008).

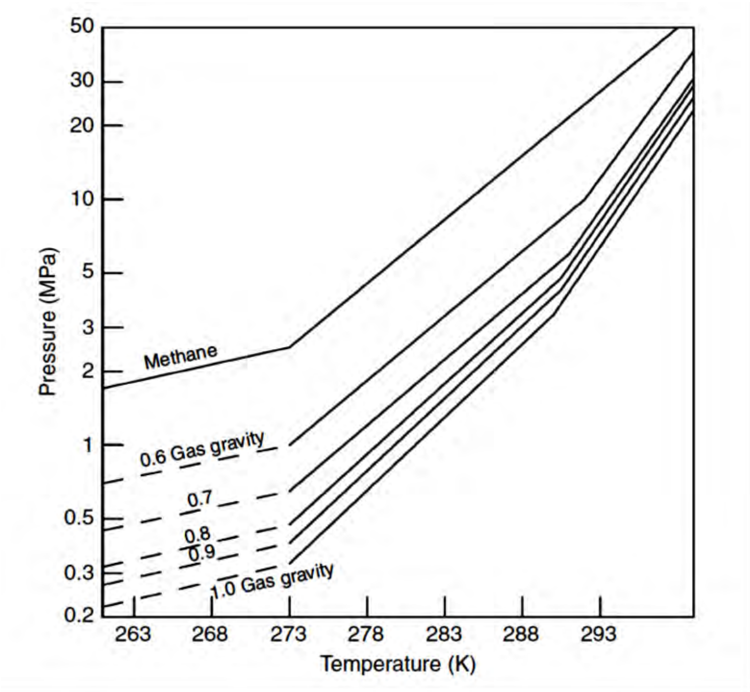

Figure 3.1. The Katz gas gravity charts (Sloan and Koh, 2008).

In another method known as the "distribution coefficient method" or the "*K*-value method" which was developed a few years earlier, an ideal solution of gas phase components in the hydrate phase is assumed. Considering this assumption, a distribution coefficient of each hydrate former is given by:

$$K_{v-s,i} = \frac{y_i}{Y_i} \tag{3.1}$$

where y_i and Y_i are the water-free mole fractions of component i in the vapour and hydrate phases respectively. K value charts for individual hydrate formers (e.g. methane, carbon dioxide, ethane, nitrogen) have been produced as a function of temperature and pressure. Figure 3.2 presents the *K*-values for methane. Hydrate equilibrium conditions can be obtained by an iterative approach combining readings from the chart and fulfilling the constraint:

$$\sum_{i=1}^{n} \frac{y_i}{K_{vs\,\mathrm{i}}} = 1 \tag{3.2}$$

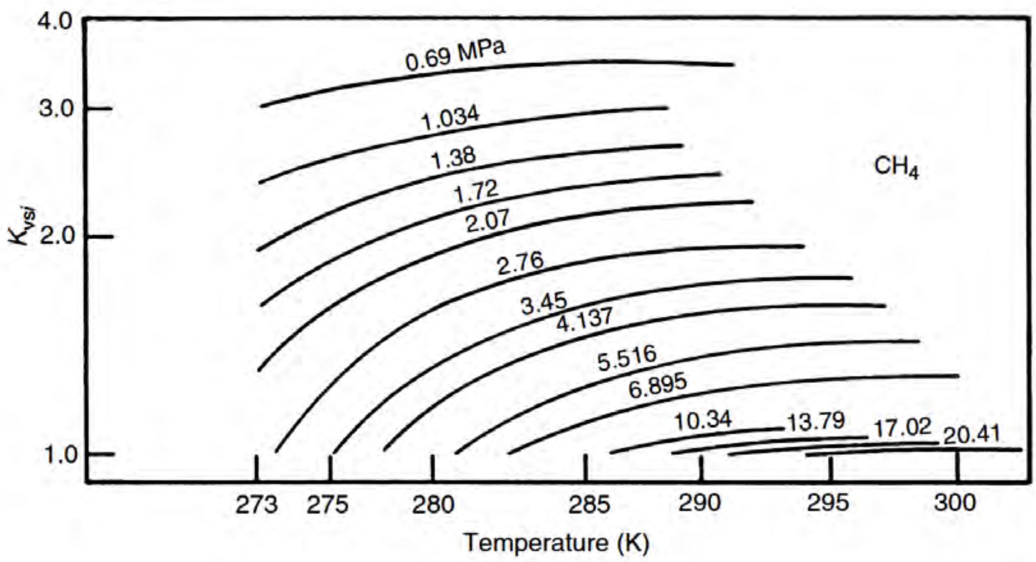

Figure 3.2. *K*-values diagram for methane (CH_4) (Sloan and Koh, 2008, Carroll, 2009)

The *K*-value method offers precise temperature/pressure conditions for usual light gases found in natural gases. Nevertheless, it has been confirmed to be less accurate for mixtures with high content of ethane, propane, or butane (Sloan and Koh, 2008). The constraints of the *K*-value method could be due to the fact that in its original form, the differences in hydrate structures were not taken into account.

3.2. Thermodynamic models

Thermodynamic models which are based on the thermodynamic equilibrium of the neighbouring phases are based on two criteria: (1) the equality of fugacities (fugacity approach), and (2) the equality of chemical potentials (activity approach). Depending on the pressure and temperature of the system the following phases may be present during gas hydrate equilibrium conditions (Sloan and Koh, 2008):

- Solid hydrate phase (H): This phase consists of crystalline hydrates which contains water molecules and gas molecules which can be trapped inside the hydrate crystal lattice. Different types of hydrate crystals may be formed simultaneously at certain conditions (such as crystals, type I and II).
- The aqueous phase (L_w): This phase contains mainly water. In addition, other components in the system which were dissolved in water can exist in this phase.
- Vapour phase (V): comprises mainly gases (or water depending on the equilibrium conditions) with the ability to form hydrate (it is possible that some of them are not able to form a hydrate).

- Liquid phase: containing mostly hydrocarbons (L_{HC}); a small amount of water can be dissolved in this phase.
- Ice-phase (I): This phase consists of water molecules which have been frozen.

It should be mentioned that depending on the system and the equilibrium conditions, some of the above-mentioned phases may not be formed. The existence of the different equilibrium phases can be determined using the Gibbs free energy theory (Sloan and Koh, 2008).

3.2.1. *Activity approach*

The solid solution theory of gas hydrates was proposed by van der Waals and Platteeuw (vdWP) in 1958 (Waals and Platteeuw, 2007). This model deals with the solid phase separately and is usually combined with an equation of state and an activity coefficient model for the description of co-existing fluid phases. In this theory the hydrate phase is considered as a solid solution of hydrate formers in a crystalline host lattice. The fundamental theory behind the vdWP model is claimed to come from statistical mechanics. A detailed derivation of the vdWP model equations using statistical mechanics can be found in the work of Sloan and Koh (Sloan and Koh, 2008). Nonetheless, Hendriks and Meijer showed that the model can also be developed by the application of chemical reaction theory and classical thermodynamic equations (Hendriks and Meijer, 2004).

In 1972, Parrish and Prausnitz developed a procedure that formulated the vdWP hydrate model for computer calculations (Parrish and Prausnitz, 1972). The vdWP model is based on the equality of chemical potential of water in all phases present at equilibrium. For example at H-L_w/I-V equilibrium it can be stated that:

$$\mu_w^H = \mu_w^{l/\alpha} = \mu_w^V \tag{3.3}$$

in which $\mu_w^{l/\alpha}$ presents the chemical potential of water in liquid or ice phase. Instead of calculating the absolute chemical potential of water in the hydrate phase, μ_w^H, van der Waals and Platteeuw described a meta-stable, crystal-like phase (known as β-phase) with the same structure as in the hydrate. The β-phase was identified as meta-stable, since it cannot form without the presence of guest molecules. The hydrate structure is stabilized using the interaction between the hydrate former and the water molecules inside hydrate cavities. For modelling purposes, it is more convenient to use this description of a metastable hydrate phase.

Subtracting the chemical potential of the unoccupied hydrate lattice (μ_w^{β}) from the both sides of equation (3.3) yields:

$$\Delta\mu_w^{\beta-H} = \Delta\mu_w^{\beta-I/\alpha} \tag{3.4}$$

Using the following assumptions concerning the presence of the hydrate former molecules in the hydrate cavities, it is possible to apply a method such as the Langmuir adsorption theory for describing the guest-host interactions (Sloan and Koh, 2008):

- Hydrate cavities are spherical.
- Each cavity can engage a maximum of one guest molecule.
- The interactions between guest-guest molecules are negligible.
- The structural properties of the water lattice are not deformed by guest molecules.
- Ideal gas partition function for the guest molecule is applicable
- Energy release distribution for water molecules is independent of the occupancy method of guest molecules.

Hence, the difference in the chemical potential of water between a hypothetical empty clathrate lattice and the actual clathrate can be demonstrated by the occupancy of the hydrate former in the water cavities, using the Langmuir monolayer adsorption theory:

$$\Delta\mu_w^{\beta-H} = RT \sum_{m=1}^{N.cavity} \nu_m \ln\left(1+\sum_{i=1}^{nc} C_{mi} f_i\right) \tag{3.5}$$

where R and T are the universal gas constant and temperature respectively. *N.cavity* and *nc* denote the number of cavity and the number of components respectively. v_m is the number of cavities of type *m* per water molecule in a unit cell of hydrate crystal lattice, f_i, is the fugacity of the guest molecule in the gas phase which can be obtained using an appropriate Equation of State (EoS), C_{mi} indicates the Langmuir constant of the guest molecule *i* in the cavity type *m*.

Van der Waals and Platteeuw suggested that the Langmuir adsorption constants can be predicted using the cell theory of Lennard-Jones-Devonshire as follows (Waals and Platteeuw, 2007):

$$C_{mi} = \frac{4\pi}{kT}\int_0^{\infty} \exp\left[-\frac{\omega(r)}{kT}\right] r^2\, dr \tag{3.6}$$

in which k and T are the Boltzmann's constant and temperature respectively, $w(r)$ presents the spherical core cell potential function to define the interaction between the water and guest molecule and r defines the distance between the cavity centre and guest molecule.

McKoy and Sinanoğlu studied three different cell potential functions in order to predict the hydrate equilibrium pressure (McKoy and Sinanoğlu, 1963). They established that the use of the Kihara cell potential is the most appropriate approach in such calculations, and suggested a procedure for incorporating it in the hydrate equilibrium predictions. Later, Parrish and Prausnitz proposed an ultimate equation for the cell potential of the gas component j in cavity type m, in a slightly improved form (Parrish and Prausnitz, 1972):

$$w(r) = 2z\varepsilon\left[\frac{(\sigma^*)^{12}}{\bar{R}^{11}r}\left(\delta^{10} + \frac{\alpha}{\bar{R}}\delta^{11}\right) - \frac{(\sigma^*)^6}{\bar{R}r}\left(\delta^4 + \frac{\alpha}{\bar{R}}\delta^5\right)\right] \tag{3.7}$$

where z specifies the coordination number for each cavity (the number of oxygen molecules around the cavity), ε shows the hard core radius and depth of the energy well, σ presents the collision diameter, and $\bar{R}$ is the average radius of the cavity. Furthermore, $\sigma^* = \sigma - 2\alpha$ and the values for δ^N can be obtained using:

$$\delta^N = \frac{1}{N}\left[\left(1 - \frac{r}{\bar{R}} - \frac{a}{\bar{R}}\right)^{-N} - \left(1 + \frac{r}{\bar{R}} - \frac{a}{\bar{R}}\right)^{-N}\right] \tag{3.8}$$

where N is an integer equal to 4, 5, 10 or 11.

From equation (3.7) it can be observed that at r=0 (centre of the cavity) the Kihara potential function is undefined. Nevertheless, when approaching the limiting value of the cell potential from the positive side, it can be shown that this point is a removable singularity (Herslund, 2013). Additionally, there is a discontinuity with a change of sign at the distance from the centre of the cavity equal to $r = R_m - a_j$. Furthermore, approaching $r = R_m - a_j$ with larger r values, the cell potential approaches minus infinity, resulting in the divergence of the Langmuir adsorption coefficient. Hence, great attention should be taken while integrating the Kihara cell potential.

In this work, the Kihara cell potential function was estimated from the centre of the cavity to the singularity point at $r = R_m - a_j$. Therefore, equation (3.6) can be rewritten as:

$$C_{mi} = \frac{4\pi}{kT} \int_0^{R_m - a_j} \exp\left[-\frac{\omega(r)}{kT} \right] r^2 \, dr \tag{3.9}$$

As the application of equation (3.9) is rather complicated, a simple empirical equation of the Langmuir constant was proposed by Parrish and Prausnitz for simplicity in calculations, as shown below (Parrish and Prausnitz, 1972):

$$C_{ij} = \frac{A_{ij}}{T} \exp\left[\frac{B_{ij}}{T} \right] \tag{3.10}$$

in which A_{ij} and B_{ij} are adjustable parameters which can be found for different hydrate formers in the open literature.

Parrish and Prausnitz proposed an expression for evaluation of the difference between chemical potential of the empty hydrate lattice and ice or liquid phase, $\Delta\mu_w^{\beta-l/\alpha}$, which included the reference pressure P_R (Parrish and Prausnitz, 1972). Subsequently, Holder et al. developed a simplified version of the Parrish and Prausnitz model in which the application of P_R was excluded as shown below (Holder et al., 1995):

$$\frac{\Delta\mu_w^{\beta-l/\alpha}}{RT} = \frac{\Delta\mu_w^0}{RT} - \int_{T_0}^{T} \frac{\Delta h_w^{\beta-l/\alpha}}{RT} dT + \int_{P_0}^{P} \frac{\Delta v_w^{\beta-l/\alpha}}{RT} dP - \ln(a_w) \tag{3.11}$$

where the reference temperature and pressure (T_0 and P_0) are set equal to 273.15 K and the vapour pressure of the ice, respectively. Since P_0 is small compared to the hydrate equilibrium pressure, it is usually set equal to zero. $\Delta\mu_w^0$ defines the difference in the chemical potential of water in the empty hydrate lattice and liquid phase at T_0. $\Delta h_w^{\beta-l/\alpha}$ presents the molecular enthalpy difference between the meta-stable β-phase and liquid water or ice, $\Delta v_w^{\beta-l/\alpha}$ is the molecular volume difference between the meta-stable β-phase and liquid water or ice. It should be mentioned that ln (a_w) in equation (3.11) for the ice phase is zero. $\Delta h_w^{\beta-l/\alpha}$ contains two parts, including the enthalpy of phase change from ice to liquid water at T_0, and a heat capacity contribution due to the heating of the liquid from T_0 to the corresponding temperature, T:

$$\Delta h_w^{\beta-l/\alpha} = \Delta h_w^0 + \int_{T_0}^{T} \Delta C_{pw} dT \tag{3.12}$$

where Δh_w^0 presents the enthalpy differences between the meta-stable β-phase and liquid water or ice at T_0. In order to calculate the specific heat capacity difference, ΔC_{pw}, in equation (3.12), the following empirical equation can be used:

$$\Delta C_{pw} = -38.12 + 0.141\left(T - T_0\right) \tag{3.13}$$

Therefore, by evaluating equations (3.4), (3.5) and (3.11), at either a specified pressure or temperature, the corresponding equilibrium temperature or pressure can be determined.

For temperatures below the freezing point of water, the specific heat capacity difference is equal to zero.

3.2.2. Fugacity approach

Using an alternate thermodynamic approach, the fugacity of each component in all phases present at equilibrium conditions must be equal, which can be stated as:

$$f_w^L(P,T) = f_w^V(P,T) = f_w^H(P,T) \tag{3.14}$$

where f_w is the fugacity of water in the vapour (V), liquid (L), and hydrate (H) phases.

3.2.2.1. Hydrate phase

In this study the fugacity of water in the hydrate phase (H) is calculated using the vdWP model as follows:

$$f_w^H = f_w^\beta \exp\left(\frac{-\Delta\mu_w^{\beta-H}}{RT}\right) \tag{3.15}$$

in which $\Delta\mu_w^{\beta-H}$ shows the difference between the chemical potential of the meta-stable β-phase and the actual hydrate phase, as explained in section 3.2.1. The fugacity of the meta-stable β-phase, f_w^β, can be obtained using the following equation (Waals and Platteeuw, 2007):

$$f_w^\beta = f_w^{lo} \exp\left(\frac{-\Delta\mu_w^{\beta-l}}{RT}\right) \tag{3.16}$$

in which, $f_w^{l o}$ presents the fugacity of pure water in the liquid phase. The following equation is used to calculate the chemical potential difference between the empty hydrate lattice and the liquid phase, $\Delta\mu_w^{\beta-l}$, as indicated below:

$$\frac{\Delta\mu_w^{\beta-l}}{RT} = \frac{\Delta\mu_w^0}{RT} - \int_{T_0}^{T} \frac{\Delta h_w^{\beta-l}}{RT} dT + \int_{P_0}^{P} \frac{\Delta v_w^{\beta-l}}{RT} dP \tag{3.17}$$

The parameters in equation (3.17) were introduced in section (3.2.1).

3.2.2.2. Fluid phases

The fugacity in the vapour and liquid phases can be determined by means of a suitable equation of state (EoS) and mixing rule. In this study, the Peng-Robinson equation of state modified by Stryjek and Vera (PRSV) (Stryjek and Vera, 1986) together with modified Huron Vidal second order mixing rule (MHV2) EoS-G^E (Dahl and Michelsen, 1990, Dahl et al., 1991) and UNIFAC activity model (Magnussen et al., 1981) was used for estimating water fugacity in the vapour and liquid phases as explained in Appendix B. The following equation was obtained for the estimation of the fugacity of water in the fluid phases, f_i (Stryjek and Vera, 1986, Proust and Vera, 1989, Hashemi et al., 2015b):

$$\ln\frac{f_i}{z_i P} = \frac{b_i}{b_m}(Z-1) - \ln(Z-B) - \frac{\alpha}{2\sqrt{2}}\left(\frac{1}{n}\frac{\partial n^2 a}{\partial n_i} - \frac{b_i}{b_m}\right)\ln\left(\frac{Z+2.414B)}{Z-0.414B}\right) \tag{3.18}$$

where

$$\frac{1}{n}\frac{\partial(n^2 a)}{\partial ni} = \alpha b_i RT + \frac{\partial(n\alpha)}{\partial(n_i)} b_m RT \tag{3.19}$$

$$\frac{\partial(n\alpha)}{\partial n_i} = \frac{1}{(q_1+\alpha q_2)}\left(q_1\alpha_i + \ln\gamma_i + q_2(\alpha_i^{\ 2}+\alpha^2) + \ln\frac{b_m}{b_i} + \frac{b_i}{b_m} - 1\right) \tag{3.20}$$

$$B = \frac{b_m P}{RT} \tag{3.21}$$

$$z_i = \frac{n_i}{\sum n_j} = \frac{n_i}{n} \tag{3.22}$$

$$\frac{\partial(nb_m)}{\partial n_i} = b_i \tag{3.23}$$

in which n stands for the number of molecules and z_i stands for the mole fraction of component i and Z presents the compressibility factor. For the evaluation of the activity coefficient of refrigerants and water in equation (3.20), γ_i, the UNIFAC activity model was applied as explained in Appendix B (Magnussen et al., 1981, Hashemi et al., 2015a, Hashemi et al., 2015b).

3.3. Kinetic model

A brief overview of the kinetic models has been presented by Sloan and Koh (Sloan and Koh, 2008). A kinetic model for methane, ethane, and their mixtures was developed by Englezos et al. (Englezos et al., 1987). The model was based on this assumption that clathrate hydrate nucleation and growth happen in the liquid layer at the gas-liquid boundary. Englezos et al. showed that the rate of hydrate formation can be formulated as (Englezos et al., 1987, Zhang et al., 2007):

$$r(t) = \frac{dn}{dt} = k_{app}(f - f_{eq}) \tag{3.24}$$

where k_{app} presents the rate constant of hydrate reaction, f is the fugacity of the hydrate former at instantaneous pressure and temperature; and f_{eq} shows the fugacity of the hydrate former at the equilibrium pressure and initial temperature. Additional clarifications regarding the estimation of the equilibrium pressure and fugacities have been described earlier (see section 3.2). Using the kinetic model presented in this thesis, the quantity and rate of gas consumption, storage capacity of gas hydrate, water to hydrate conversion, and rate constant during hydrate formation of several refrigerants can be evaluated.

3.3.1. Apparent rate constant during hydrate growth

The hydrate growth rate can be presented using the following equation (Englezos et al., 1987, Zhang et al., 2007, Mohammadi et al., 2014):

$$r(t_i) = -\left.\frac{dn_R}{dt}\right|_{ti} = \left.\frac{\Delta n_R}{\Delta t}\right|_{ti} = \frac{n_{R,i-1} - n_{R,i+1}}{(t_{i+1} - t_{i-1})n_{w_0}} \tag{3.25}$$

where $n_{R,i-1}$ and $n_{R,i+1}$ present the number of moles of hydrate former in the gas phase at t_{i-1} and t_{i+1} respectively. n_{w_0} is the initial number of moles of water in the liquid phase. The apparent rate constant at a specific time t_i, is estimated by the following expression:

$$k_{app} = \frac{\left(\dfrac{n_{R,i-1} - n_{R,i+1}}{(t_{i+1} - t_{i-1})n_{w_0}}\right)}{(f - f_{eq})_{ti}} \tag{3.26}$$

3.3.2. Water to hydrate conversion

The hydrate formation can be expressed as a reaction between the refrigerant (R) and water molecules as follows (Sloan and Koh, 2008):

$$R + MH_2O \longrightarrow R.MH_2O + \Delta H \tag{3.27}$$

where M signifies the hydrate number (number of water molecules per guest molecules) which can be calculated by the succeeding equation for Structure II (Sloan and Koh, 2008):

$$M = \frac{136}{8\theta_L + 16\theta_S} \tag{3.28}$$

where:

$$\theta_{ki} = \frac{C_{ki} f_k}{1 + \sum_j C_{ji} f_j} \tag{3.29}$$

where f_k is the fugacity of hydrate former in the gas phase and C_k is the Langmuir constant. Further details concerning the calculation of the Langmuir constants and the fugacities of the studied hydrate former are delivered in section 3.1. The number of moles of the hydrate former consumed throughout hydrate formation is obtained using the real gas law as follows (Englezos et al., 1987, Mohammadi et al., 2014):

$$\Delta n_R = \frac{P_0 V_0}{Z_0 R T_0} - \frac{P_t V_t}{Z_t R T_t} \tag{3.30}$$

where P and T are the pressure and temperature of the cell respectively, and R stands for the Universal Gas constant. Z signifies the compressibility factor for the hydrate former which can be evaluated by the PRSV EoS combined with the MHV2 mixing rule and UNIFAC activity model (see section 3.2). Subscripts "0" and "*t*" in equation (3.30) denote the initial conditions and conditions at time, *t,* of the system respectively. For the calculation of the volume of the hydrate former inside the cell at time *t* (V_t) the following equation has been used (Mohammadi et al., 2014):

$$V_t = V_{cell} - V_{W_0} + V_{RW_t} - V_{H_t} \tag{3.31}$$

where V_{cell} and V_{W_0} are the cell volume (approximately 40 cm^3) and initial volume of water (16 cm^3) respectively. The subsequent expression has been applied for estimation of the volume of water reacted, V_{RW_t}, at time *t*:

$$V_{RW_t} = M \times \Delta n_R \times v_w^L \tag{3.32}$$

where v_w^L shows the molar volume of water which can be calculated by the following expression (Mohammadi et al., 2014):

$$v_w^L = 18.015 \times \begin{bmatrix} 1 - 1.0001\times10^{-2} + 1.33391\times10^{-4}\left(1.8(T-273.15)+32\right) + \\ 5.50654\times10^{-7}\left(1.8(T-273.15)+32\right)^2 \end{bmatrix} \times 10^{-3} \tag{3.33}$$

The molar volume, V_{H_t}, of the hydrate at time t, can be estimated by following equation (Mohammadi et al., 2014):

$$V_{H_t} = M \times \Delta n_R \times v_w^{MT} \tag{3.34}$$

in which that v_w^{MT} is the volume of the empty hydrate lattice which can be evaluated using the following expression (Klauda and Sandler, 2000):

$$v_w^{MT} = \left(17.13 + 2.249\times10^{-5}T + 2.013\times10^{-6}T^2\right)^3 \frac{10^{-30}N_A}{136}$$
$$-8.006\times10^{-9}P + 5.448\times10^{-12}P \tag{3.35}$$

in which temperatures are in K and the pressures are in MPa. Water to hydrate conversion which is known as the number of moles of water converted to hydrate per mole of feed water can be calculated as follows:

$$\text{water to hydrate conversion} = \frac{\mathrm{M}\times\Delta n_R}{n_{W_0}} \tag{3.36}$$

3.3.3. Storage Capacity of gas hydrate

The storage capacity (SC) of the gas hydrate is defined as the volume of the gas stored in a volume of the hydrate at standard pressures and temperatures. The storage capacity of the hydrate former during hydrate formation is calculated using the following equation (Ganji et al., 2007b, Ganji et al., 2007a, Manteghian et al., 2013, Mohammadi et al., 2014):

$$SC = \frac{V_{STP}}{V_H} = \frac{\Delta n_R RT_{STP}/P_{STP}}{V_H} \tag{3.37}$$

where subscript *STP* indicates standard conditions and V_H shows the volume of hydrate formed at time *t* which can be evaluated by equation (3.34).

4

Experimental Procedures and Equipment for Gas Hydrate Phase Equilibrium Measurement: A review

The experimental procedures and equipment used for hydrate phase equilibrium studies are highlighted in this chapter. The principles of the applied techniques and the criteria for establishing equilibrium are also explained.

The design, development and operation of chemical processes include a cyclic and communicating approach comprising experimental, theoretical, modeling and simulation stages (Richon, 2009). As illustrated in Figure 4.1, suitable design process should pursue the progression from conception of ideas through literature review, selection, design and manufacture of equipment, procedures, measurements, data reliability and consistency tests to the ultimate achievement.

The development of gas hydrates based technologies involves particular temperature and pressure conditions and the application of complicated systems with many components that are beyond typical operations and current databases. Furthermore, an industrial design depends on precise modelling which requires consistent experimental data. Consequently, experimental thermodynamic data are of industrial importance.

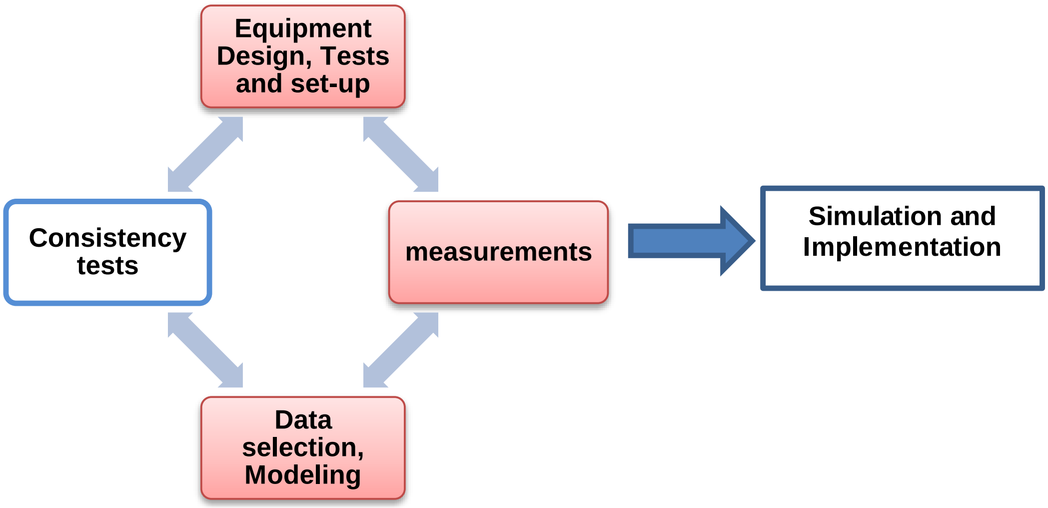

Figure 4.1. Strategy of process design, the highlighted blocks designate the stages undertaken in this thesis (Richon, 2009).

Hydrate formation typically involves an appropriate combination of temperature and pressures above the gas-hydrate-liquid phase boundary. Hence, phase behaviour studies for systems containing gas hydrates are principally involved with pressures ranging from moderate to comparatively high pressures, therefore methods applicable at these conditions only are reviewed.

Different procedures have been developed concerning measurement of high-pressure fluid phase equilibrium. Nevertheless, their capability relies on the properties to be measured the desired accuracy the use and the system under analysis. A comprehensive review on thermodynamic measurement techniques for multicomponent mixtures can be found in the International Union of Pure and Applied Chemistry (IUPAC) (Measurement of the Thermodynamic Properties of Multiple Phases Volume VII). Over the past three decades a number of reviews published which cover a collection of high-pressure phase-equilibrium systems as well as a classification scheme of experimental methods investigated (Dohrn and Brunner, 1995, Christov and Dohrn, 2002, Dohrn et al., 2010, Fonseca et al., 2011). Furthermore, Richon (1996) and Richon and de Loos (2005) studied the enhancements on accurate and operational experimental equipment for phase equilibrium measurements (Richon, 1996, Richon and de Loos, 2005) and an extended review was performed by Raal and Mühlbauer on the static and dynamic equipment (Raal and Mühlbauer, 1997).

Researchers classify the methods for measuring phase equilibrium into two main categories: (1) dynamic (open circuit) methods involve forced circulation of one or more phases, while (2) with static methods (closed circuits) equilibrium can be achieved with or without recirculation of fluid phases, generally using an internal stirring mechanism to reduce the time required to reach equilibrium (Richon, 1996, Richon and de Loos, 2005).

Based on the above classification, a static high pressure apparatus was used to perform hydrate phase equilibrium measurements. Special attention is given to the precision and accuracy of the results obtained. The criteria, the choice of the technique applied and the principles for equilibrium are presented in this chapter. Furthermore, the calibration of measuring sensors and the experimental uncertainties are discussed.

4.1. Visual and non-visual techniques

The most commonly used experimental methods for determining hydrate equilibrium conditions can also be classified into visual and non-visual techniques. Visual technique which is based on the visual observation of the formation and dissociation of hydrate crystals was successfully achieved in a pyrex tube flow apparatus by Hammerschmidt in 1934 and in a windowed cell by Deaton and Frost in 1937 (Hammerschmidt, 1934, Sloan and Koh, 2008).

Since in the visual method the observation of hydrate crystals (at constant temperature or pressure) is required it can only be used at temperatures above the freezing point of water to avoid any confusion with ice crystals (Schroeter et al., 1983). Furthermore, it may take several hours for the system to reach equilibrium conditions, hence the procedure may become somewhat time consuming. Alternatively, hydrate phase equilibrium measurements at high and low pressures can also be carried out in an isochoric (constant volume) cell without the need for visual observation. In the isochoric method the intersection point of the cooling and heating curves is established as the equilibrium dissociation point; this is explained in further detail in section 4.5.

Three procedures have been developed for functioning a hydrate formation/dissociation apparatus including: isobaric, isothermal and isochoric (Sloan and Koh, 2008). The characteristics of each method have been summarized in Table 4.1. Since the hydrate dissociation point in which the last crystal of hydrate dissociates completely, is a repeatable point, in all procedures the hydrate dissociation is used to determine the pressure and temperature of the hydrate equilibrium conditions. In the isothermal and isobaric procedures, the equilibrium condition is determined by visual observation of a phase change (the disappearance of the hydrate crystals). In the isochoric method, a corresponding change in pressure as a function of temperature (due to density changes) in a constant volume cell confirms hydrate formation and/or dissociation. It should be mentioned that when the equilibrium cell is a visual cell it is possible to detect the hydrate dissociation point visually in the isochoric pressure search method.

Table 4.1. Commonly used experimental procedures for measuring hydrate dissociation conditions (Sloan and Koh, 2008)

Method	Principle	Hydrate formation	Hydrate dissociation
Isothermal	Constant temperature	Temperature increase	Visual observation of hydrate crystal disappearance, trial and error procedure
Isobaric	Constant pressure	Exchange of gas or liquid from an external tank	
Isochoric	Constant volume	Pressure decrease	the intersection point of the cooling and heating curves, visual observation

4.2. Visual isothermal method

The viability of application of the isothermal method for determination of the hydrate dissociation pressure of CO_2 was investigated in a sapphire tube variable volume cell developed in University of KwaZulu-Natal (Ngema et al., 2014a) with accurate results. Since equilibrium conditions can be achieved within few minutes, a considerable amount of time is saved using this technique for measuring hydrate dissociation data. Figure 4.2 presents the schematic diagram of an isothermal equipment developed by Richon which utilizes a variable volume cell (Ngema et al., 2014a). The main part of the equipment is comprised of a high pressure variable volume cell (part C in Figure 4.2) which is made of sapphire tube. As observed in Figure 4.2, the pressure of the cell can be increased or decreased at a constant temperature to a desire value by a hydraulic piston driven by a hand pump (L) (WIKA, model HD 250). The pressure of the cell is monitored as function of system volume at constant temperature (AA). For the formation of the gas hydrate the pressure of the cell is increased stepwise by 100 kPa per 2 minutes. After the formation of hydrate, the pressure of the cell decreased using the hand pump (L) until complete dissociation of the hydrate is accomplished and the corresponding pressure is recorded as the hydrate dissociation pressure. The measurements are repeated three times in order to evaluate their accuracy (Ngema et al., 2014a). Even though the procedure has shown to be quite promising however it suffers from disadvantages of the visual techniques which are explained earlier in section 4.1.

4.3. Non visual isothermal method

Figure 4.3 shows a nonvisual isothermal equipment used by Makagon et al. for measuring the hydrate dissociation conditions (Makogon et al., 1996). In nonvisual isothermal method the hydrate dissociation point is indicated using a trial and error procedure. As shown in Figure 4.4 after pressurizing the cell to a desire value at a constant temperature the hydrate formation is indicated by a significant drop in the pressure. After stabilization of the pressure of the cell it is partially vented. Consequently, the increase in the pressure due to hydrate decomposition confirms that the system is below equilibrium conditions. However, if the pressure decreased, the system is above equilibrium pressure. Supposing the system is bellow equilibrium pressure and the pressure of the system increased. In the following cycle the system is loaded slightly above the primary stabilized value. Consequently, a drop of the pressure shows the pressure is above equilibrium conditions and the hydrate formation is restarted. This trial and error method is repeated until the difference between formation and dissociation pressure is about ±7 kPa (Makogon et al., 1996).

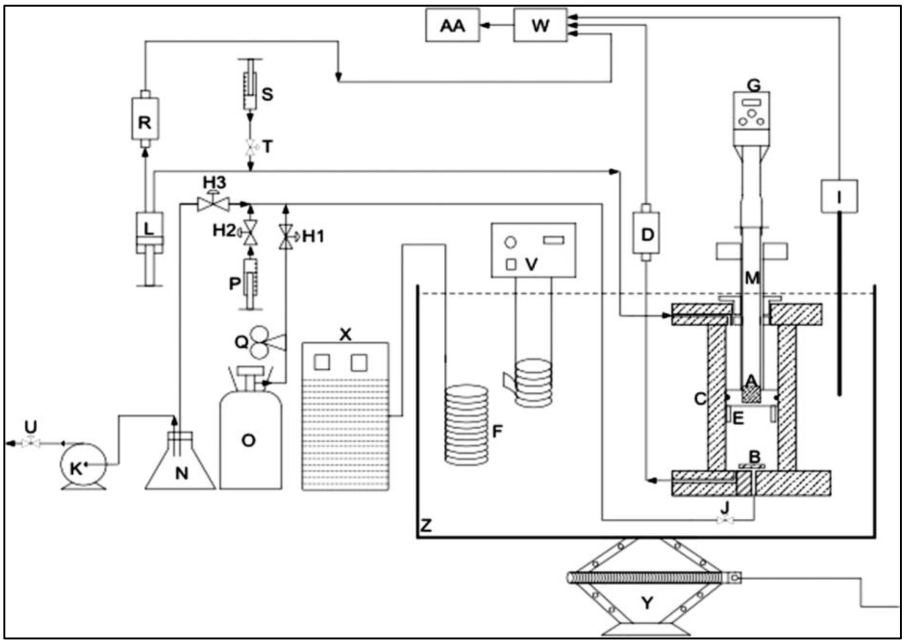

Figure 4.2. Schematic flow diagram of the isothermal method using variable volume equilibrium cell (Ngema et al., 2014a): A, Neodymium magnet; B, magnetic stirrer bar; C, variable volume cell; D, pressure transducer for the cell; E, impeller; F, cooling coil; G, overhead mechanical stirrer; Hi, shut-off valve i; I, Pt-100; J, drain or loading valve; K, vacuum pump; L, hydraulic cylinder; M, mechanical shaft; N, vacuum flask; O, refrigerant gas cylinder; P, liquid syringe with aqueous solution; Q, pressure regulator; R, pressure transducer for the hydraulic cylinder; S, hydraulic liquid; T, inlet valve for the

hydraulic liquid; U, vent valve to atmosphere; V, temperature programmable circulator; W, data acquisition unit; X, cold finger; Y, mechanical jack; Z, water bath; AA, computer.

4.4. Isobaric method

In isobaric method, the pressure of the cell remains constant throughout the experiment using exchanging the liquid or gas with an external gas or liquid supply. The temperature of the cell is decreased for the hydrate formation which is confirmed by a significant charge of the gas or liquid from the supply. After the formation of hydrate the temperature is increased gradually until the dissociation of the last crystal observed which is taken as the equilibrium hydrate dissociation condition (Sloan and Koh, 2008). The isobaric temperature search method is based on the visual observation of the hydrate dissociation.

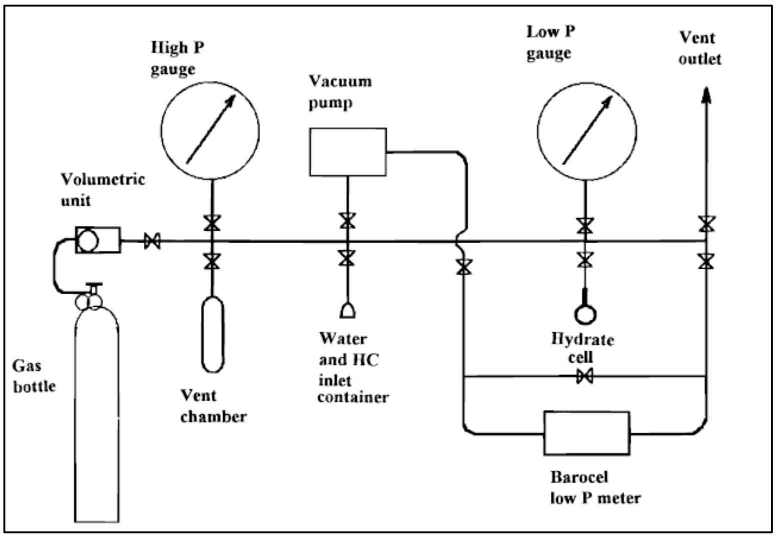

Figure 4.3. Nonvisual isothermal equipment taken from (Makogon et al., 1996)

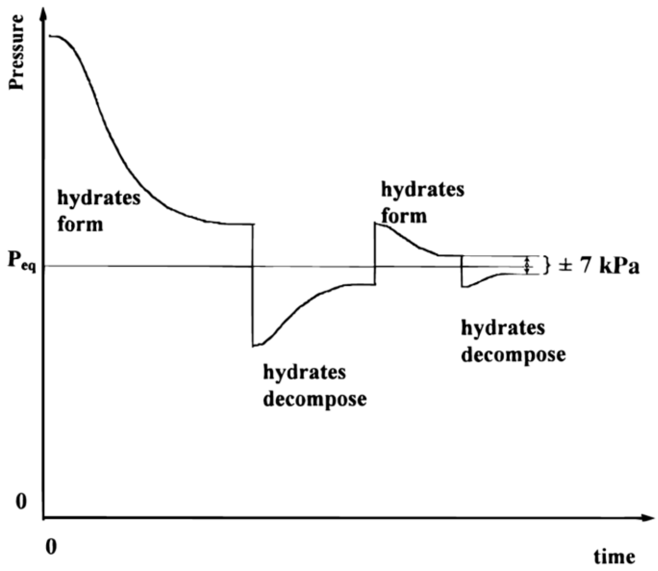

Figure 4.4. Hydrate pressure search procedure in nonvisual isothermal method (Makogon et al., 1996).

4.5. Isochoric method

The isochoric technique is based on the classical procedure developed in Professor Kobayashi's laboratory (Marshall et al., 1964). Usually, in the isochoric method, hydrates are formed by decreasing the temperature of the system. The differential pressure change is measured with respect to the accompanying differential temperature change in a constant volume cell. For each cell loading, pressure is monitored as a function of temperature thereby making possible to determine the *P-T* curve. Therefore, the slope of the isochoric *P-T* curve can be presented by $(\partial P/\partial T)_V$. Hydrate crystals are dissociated afterwards using stepwise heating. The hydrate dissociation point is determined using the intersection of the cooling and heating curves which presents a phase transition, thus indicating the hydrate dissociation point (Ohmura et al., 2004). A graphical illustration for the determination of the hydrate dissociation point is depicted in Figure 4.5. Consequently, the hydrate phase boundary of a system can be determined by plotting several experimental dissociation data at different pressures for a specific load.

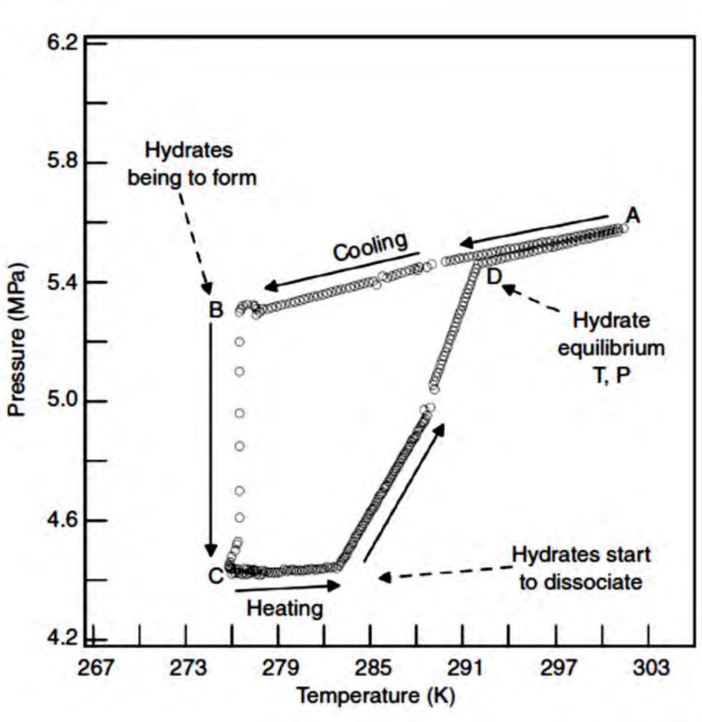

Figure 4.5. Primary cooling and heating curve for formation and dissociation of simple hydrates using the isochoric method (Sloan and Koh, 2008).

In the isochoric method, the equilibrium conditions are determined using temperature and pressure measurements. No visual observation or complicated calculations are involved, resulting in a reliable determination of the hydrate dissociation data. Furthermore, the technique is applicable over a wide range of temperatures and pressures, and small amounts of fluids are used, since no volume changes are required. In addition, the technique is suited to automated control of experiments (Sloan and Koh, 2008). Therefore, the isochoric method is regarded comparatively beneficial for phase behaviour measurements of multicomponent mixtures, compared to the isobaric and isothermal methods with visual observation. Based on the above reasons, the isochoric method incorporating stepwise heating and efficient mixing was utilized in this investigation.

4.6. Hydrate Phase Equilibrium apparatus

The main characteristics of the apparatus and experimental procedures are reviewed in this section which have been mainly derived from the comprehensive review by Sloan and Koh with the addition of illustrative examples from the literature in order to present their main advantages and also some of the experimental problems usually experienced (Sloan and Koh, 2008). Three established experimental techniques representative of recent developments are discussed in the following paragraphs.

The static technique can be regarded as one of the classical procedures for measuring hydrate phase equilibrium data, especially at high pressures. Deaton and Frost are known as the first developers of static apparatus (Deaton and Frost, 1937). In their apparatus, a glass windowed equilibrium cell (refer to Figure 4.6) was placed in a thermo-regulated bath. The cell was equipped with a valve system to allow for inlet and outlet gas flow regulation. The temperature and pressure of the system were measured using the thermocouple and pressure transducer. The phase equilibrium data were measured using visual observation of hydrate formation and disappearance. There are no significant changes in the above-mentioned principles of the equilibrium cell of Deaton and Frost over the past decades. Recent improvements in the design of hydrate phase equilibrium static equipment incorporate modern measuring devices that enhance experimental uncertainties, designs and materials that extend the operating ranges, precise construction and operation to study unusual conditions and systems, enhancements in the data acquisition and minimization of monotony.

Even though accurate and thermodynamically consistent data can be obtained using static and dynamic procedures, the static method is generally preferred for the measurement of phase equilibrium data due to their main advantages such as (Oellrich, 2004):

- Simplicity of the technique and experimental apparatus
- Applicability at high pressures and different temperatures
- Applicability for single and multiple component systems, enabling reliable evaluation of industrial systems
- Easy modification of total compositions and quantities of fluid samples
- Small amount of materials are required
- Ability to be an automated process enables the measurements to be performed overnight

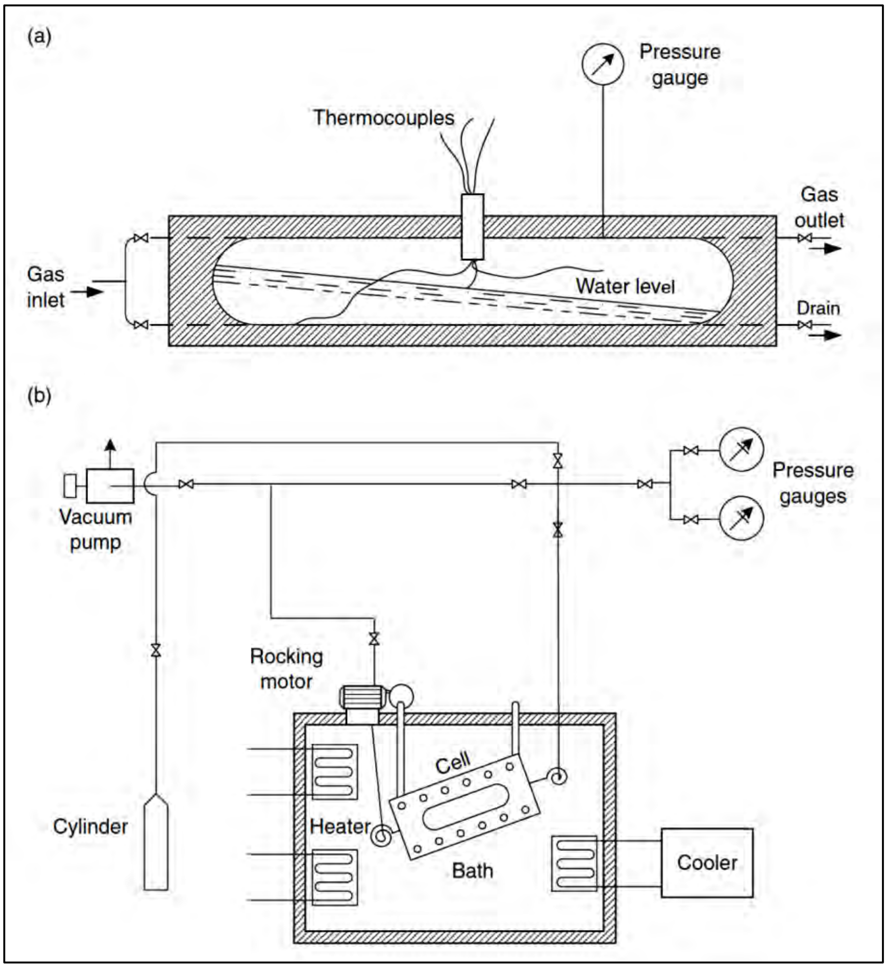

Figure 4.6. Static hydrate equilibrium cell used by Deaton and Frost (Deaton and Frost, 1937) as cited in (Sloan and Koh, 2008).

The requirement of a large amount of time to ensure that the system has reached equilibrium conditions (especially when long metastable periods occur) remains a major disadvantage of the static procedure for hydrate phase equilibrium measurement.

The Quartz Crystal Microbalance (QCM) is an example of an alternative experimental technique appropriate for gas hydrate phase equilibrium measurements (Mohammadi et al., 2003). As depicted in Figure 4.7, the QCM includes a thin disk of quartz placed between two electrodes. Crystal oscillation at a certain resonant frequency is activated when an electric current passes through the electrodes. Hydrate formation is then detected by a change in the resonance frequency once the hydrate is attached to the surface of the quartz crystal. The pressure and temperature of the system are measured using a pressure transducer and a thermocouple in a high pressure cell (Sloan and Koh, 2008).

The application of small amounts of samples (approximately one droplet of water) in the QCM method enables a significant reduction in the time required for each experiment

(Mohammadi et al., 2003). Even though the QCM method has been considered impractical due to the good contact constraint between the surface of the quartz crystal and hydrates, it has been well established that by modifying the droplet size, this method gives reasonable results, especially for rapid and practical gas hydrate application purposes, i.e. selecting a hydrate promoter from among various candidates (Sloan and Koh, 2008).

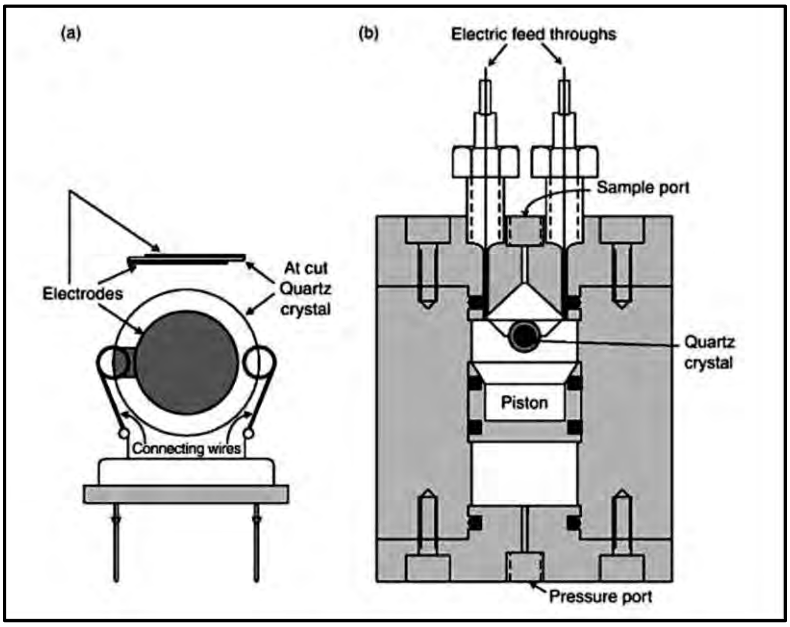

Figure 4.7. (a) Schematic diagram of the QCM, and (b) the QCM placed within a high pressure cell (Mohammadi et al., 2003, Sloan and Koh, 2008).

Recently, calorimetric approaches such as Differential Scanning Calorimetry (DSC) have also been applied for the measurement of hydrate phase equilibrium and thermal property data for gas hydrates. Dalmazzone et al. developed a micro-DSC analyzer incorporated with special high-pressure vessels. The High Pressure Differential Scanning Calorimetry (HP-DSC) apparatus was used to specify the thermodynamic stability boundaries of methane and natural gas hydrates in solutions of inhibitors (Dalmazzone et al., 2002). Deschamps and Dalmazzone used the same procedure to investigate dissociation enthalpies and phase equilibria of TBAB semi-clathrates with gases (Deschamps and Dalmazzone, 2010). As it is presented in Figure 4.8, the equipment comprises a micro DSC VII, to measure the difference in heat flow between the sample and the reference material. The system can operate between a temperature range of 228.15 to 393.15 K and pressures up to 40 MPa coupled to a pressure multiplicator.

Simultaneous measurement of thermodynamic and thermal data is the main advantage of the micro-DSC technique. This method is also relatively faster than the PVT techniques and requires a smaller amount of sample (~ 5mg) (Le Parlouër et al., 2004). However, discrepancies in the measured thermodynamic properties using similar calorimetric techniques can be somewhat greater than the specified experimental uncertainties. For example, different equilibrium temperatures of TBPB semi-clathrates measured using the DSC have been reported by different laboratories (Suginaka et al., 2012).

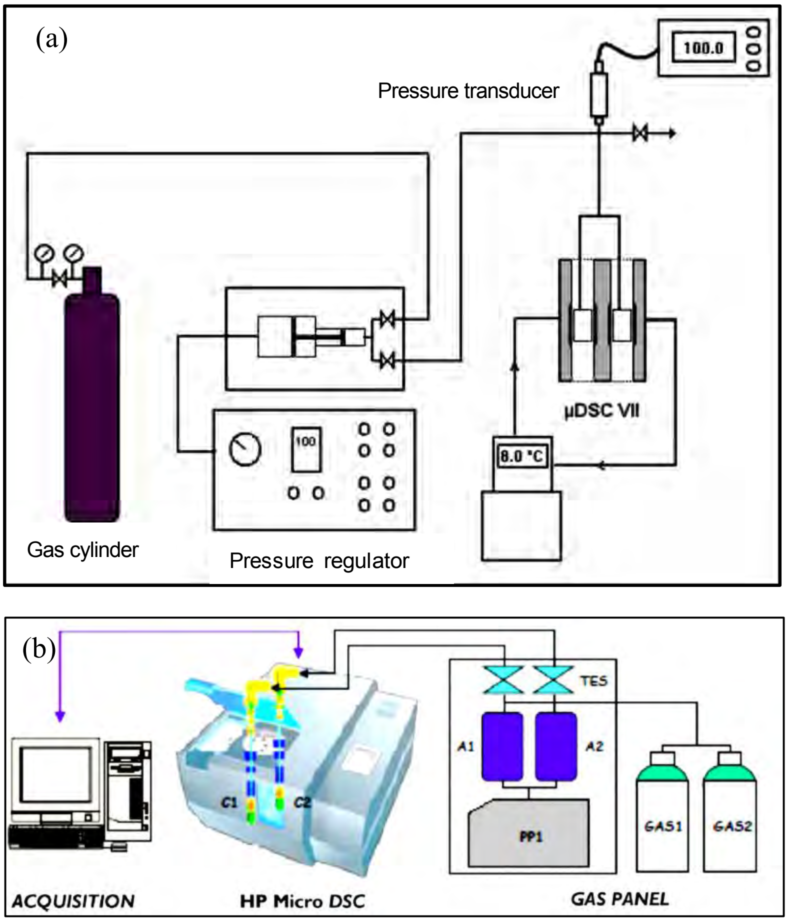

Figure 4.8. Schematic diagram of a high-pressure micro DSC VII device (a) (Deschamps and Dalmazzone, 2010) (b) (Sfaxi et al., 2014).

5

Experimental Apparatus and Procedure Used in This Study

The equipment design and the operating procedure is presented in this chapter along with the calibration of the measuring instruments, calculation of their uncertainties, and the preparation of the apparatus for measurements. Furthermore, the kinetic measurements and kinetic data analysis are also discussed in detail.

5. Description of the experimental apparatus and procedure

5.1. Materials

Table 5.1 presents details of the suppliers of the chemicals used in this thesis as well as their purities. Ultrapure Millipore Q water with an electrical resistivity of 18 MΩ.cm was used in all measurements.

Table 5.1. Purities and suppliers of the chemicals used in the experiments

Chemical	Formula	[b]Purity	Supplier
Distilled water	[a]H_2O	-	UKZN
SDS	$C_{12}H_{25}NaO_4S$	0.990	Sigma-Aldrich
HFPO	C_3F_6O	0.980	Sigma-Aldrich
R22	$CHClF_2$	0.997	Afrox
R23	CHF_3	0.998	A-gas
R134a	CF_3CH_2F	0.999	Afrox
R125a	CF_3CHF_2	0.999	Afrox
R116	C_2F_6	0.998	A-gas
R407C	[c]$0.23CH_2F_2/0.52CH_2FCF_3/0.25CHF_2CF_3$	0.998	Afrox
R507C	[c] $0.5CH_3CF_3/$ $0.5CHF_2CF_3$	0.998	Afrox
R410A	[c] $0.5CH_2F_2/05.CHF_2CF_3$	0.998	Afrox
R404A	[c] 0.52 $C_2H_3F_3/0.44$ $C_2HF_5/$ 0.4 $C_2H_2F_4$	0.998	Afrox
R406A	[c]0.55 $CHClF_2/$ 0.41 $C_2H_3ClF_2/0.4$ C_4H_{10}	0.998	Afrox

R408A	[c] 0.46 $C_2H_3F_3$/ 0.07 C_2HF_5/ 0.47 $CHClF_2$	0.997	Afrox
R427A	[c] 0.5$C_2H_2F_4$/ 0.25 C_2HF_5/ [c] 0.15 CH_2F_2/ 0.1$C_2H_3F_3$	0.995	Afrox
R508B	[c] 0.46 CHF_3+0.54 C_2F_6	0.998	A-gas

[a] Ultrapure Millipore Q water with an electrical conductivity of 18 MΩ.cm .

[b] mole fraction as stated by supplier.

[c] mass fraction as stated by supplier.

5.2. Experimental apparatus

The schematic diagram of a non-visual isochoric apparatus used in this study is depicted in Figure 5.1. A photograph of the experimental set-up is shown in Figure 5.2. In the following section, the specifications of each item are presented.

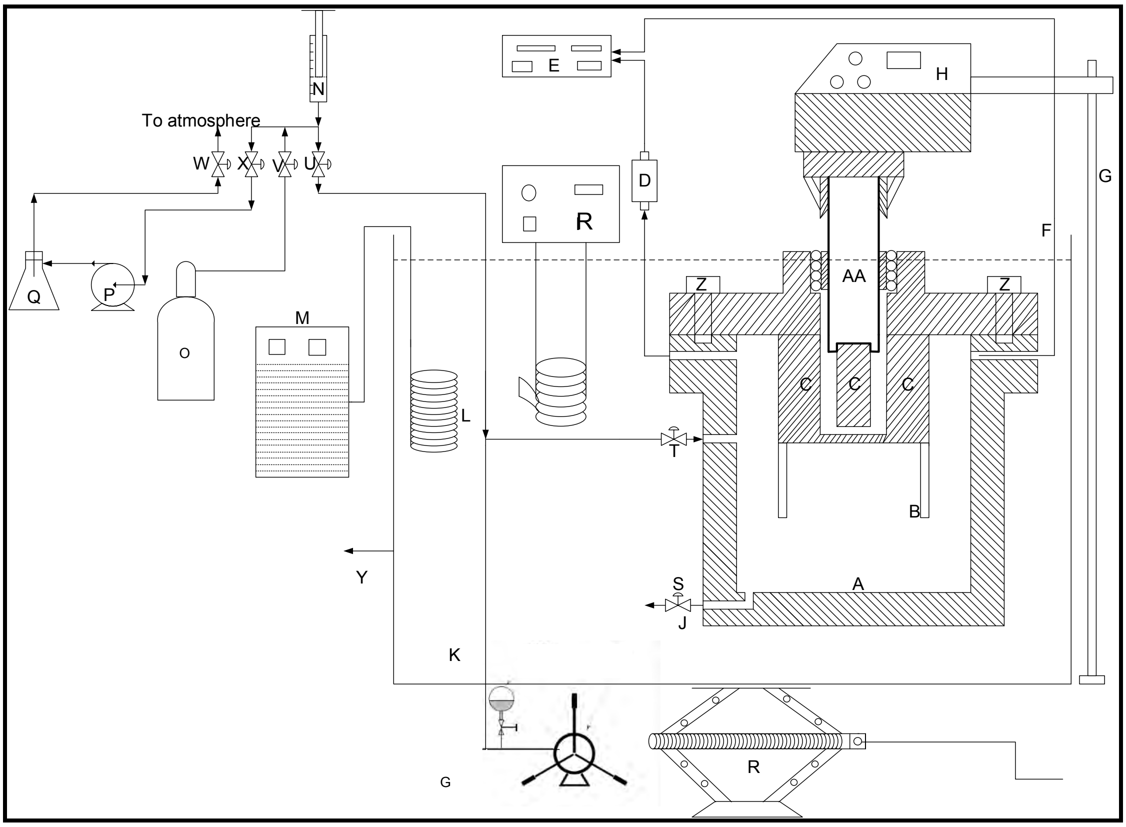

Figure 5.1. A schematic diagram of the static high pressure apparatus used in this study. AA, mixer shaft; A, high pressure equilibrium cell; B, stirrer; D, pressure transducer; E, data acquisition system; F, temperature probe; H, stirrer motor; HP; hydraulic hand pump; J, drain line; K, thermos-statted bath; M, cold finger; N, syringe for injecting solution; O, gas cylinder; P, vacuum pump; R, mechanical jack; PT, pressure transmitter; R, regulator; S, drain valve; Z, bolts.

5.2.1. The high pressure equilibrium cell

The main part of the experimental apparatus is a stainless steel high pressure equilibrium cell with the internal volume of approximately 40 cm^3 which can withstand pressures up to 20 MPa. A magnetic stirrer ensures agitation to facilitate good mixing in order to reach equilibrium quickly. Different parts of the high pressure equilibrium cell are illustrated in Figures 5.3 and 5.4. The equilibrium cell can be loaded/ evacuated through a hole placed at the top-left of its body with a diameter of 1/8'. The pressure of the cell was measured using a pressure transducer which is connected to the cell via a 1/16' nut located at the top-right of the cell. The drainage and liquid injection were performed via an1/8'connnection located at the bottom of the equilibrium cell. The input/output of the gas and liquid were controlled using two ball valves supplied by Swagelok. The cell temperature was measured using a Pt-100 platinum resistance temperature probe located at the top of the cell.

Sealing between the cylinder flange and the cell body was accomplished using an O-ring inserted into the flange and the flange was bolted to the cell body using 6×10 mm stainless steel bolts. The O-ring use must be compatible with the chemicals (refrigerants and SDS) used in the measurements. In this study the most suitable O-ring material was Viton. A schematic diagram of the equilibrium cell is depicted in Figure 5.3. A photograph of the cell body and a schematic diagram of the top view of the cell are presented in Figure 5.4.

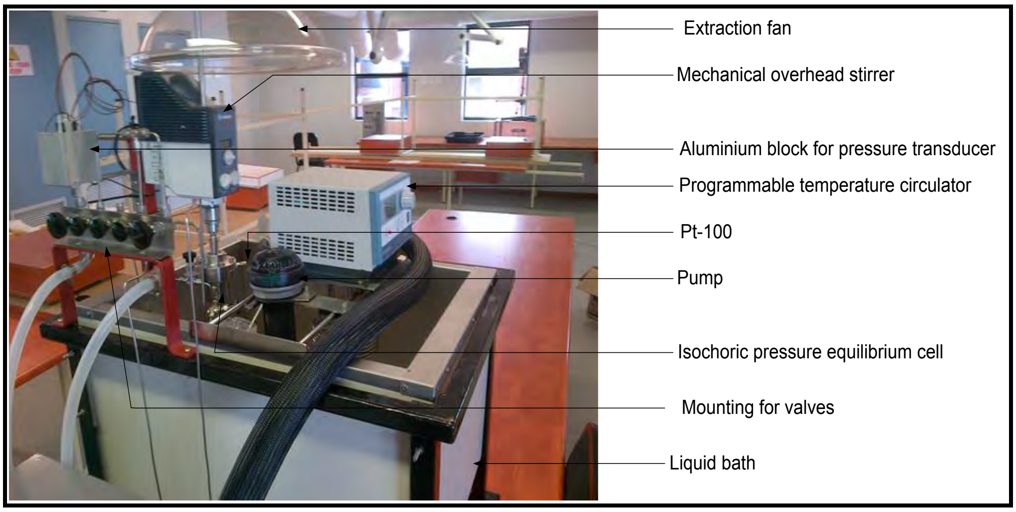

Figure 5.2. Photograph of the experimental apparatus

5.2.2. *Hydraulic hand pump*

As depicted in Figure 5.1, in this study in order to pressurize the gas inside the high pressure equilibrium cell, distilled deionized water was injected to the cell using a WIKA HD-250 hydraulic hand pump.

5.2.3. *Agitation of the cell contents*

As mentioned in chapter 2, agitation of the system increases the rate for gas hydrate formation significantly. Hence, in this study strong agitation of the system was provided. The agitation system consisted of a Heidolph RZR 2041 motor (mechanical overhead stirrer in Figure 5.2), a shaft with a strong magnet and a stirrer device with four blades and a gold coated magnet. The mechanical overhead stirrer motor was placed at the top of the cell in order to rotate the shaft. This motor is equipped with two gear speeds of 40 - 400 rpm and 200 - 2000 rpm. A stirrer speed of 600 rpm was used for all experiments.

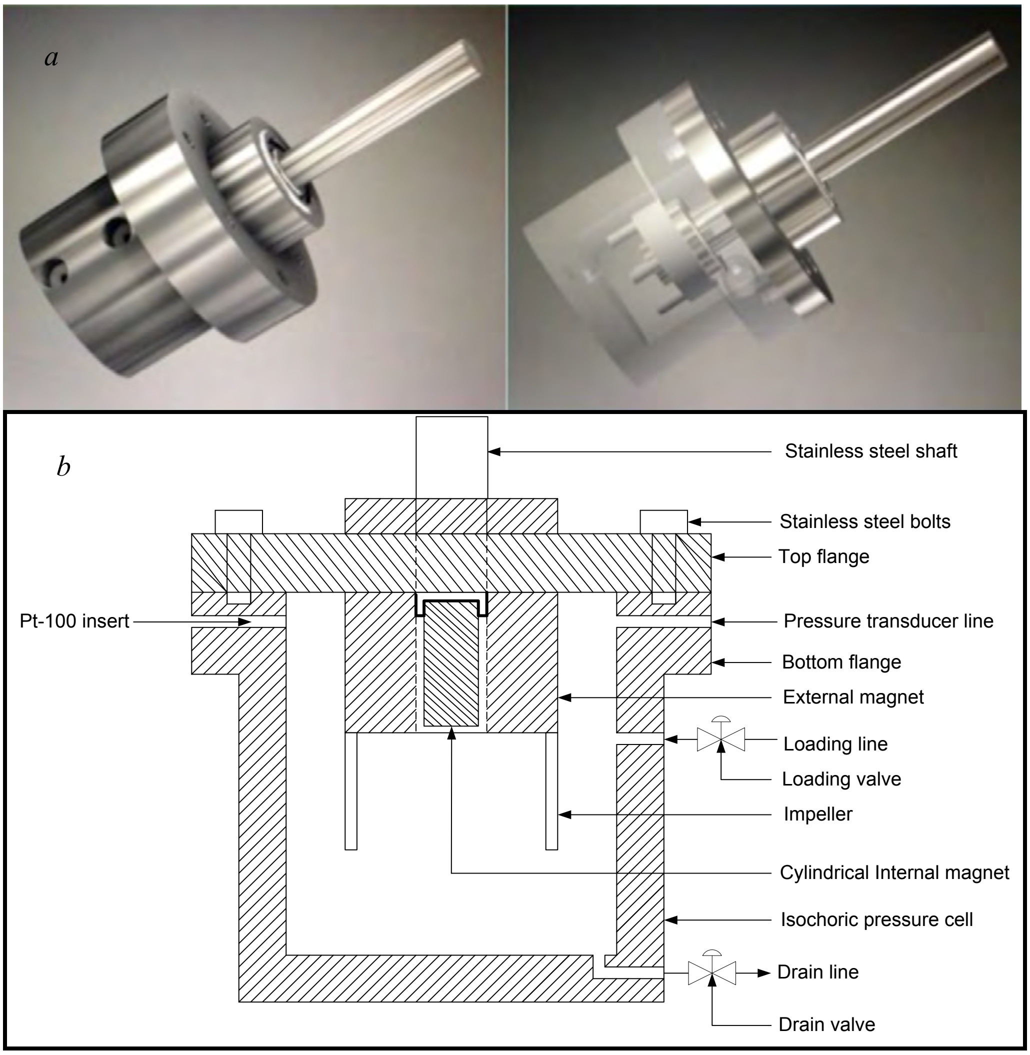

Figure5.3. Isometric view and schematic of the used equilibrium cell in this study, Dominique Richon (personal communication).

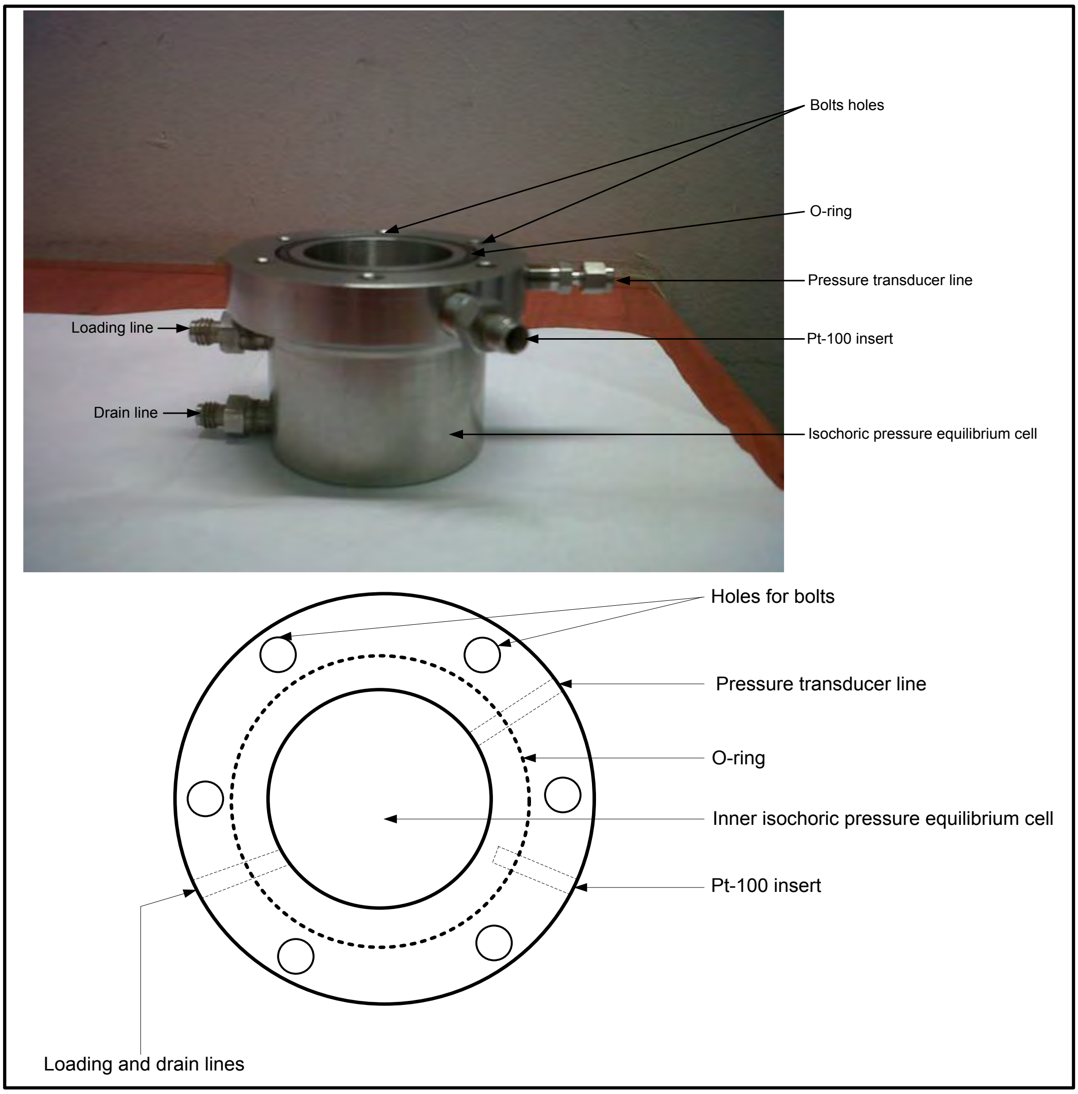

Figure 5.4. Side and top view of the high pressure equilibrium cell used in this study.

Figure 5.5 shows a photograph of the stirrer device as well as a schematic diagram of the stirring mechanism used in this study. The magnets inside the stirrer device and shaft were made from Neodymium to provide a strong magnetic field. As observed from Figure 5.5, the stirring device consists of four detachable blades to agitate the cell contents. The length, height and width of each blade were 4, 23, and 1 mm, respectively. The agitation system employed in this study is one of the most efficient agitation systems which can provide complete mixing of the gas, liquid and hydrate phases inside the cell resulting in the reduction of the gas hydrate formation /dissociation time compared to the use of a magnetic bar stirring device.

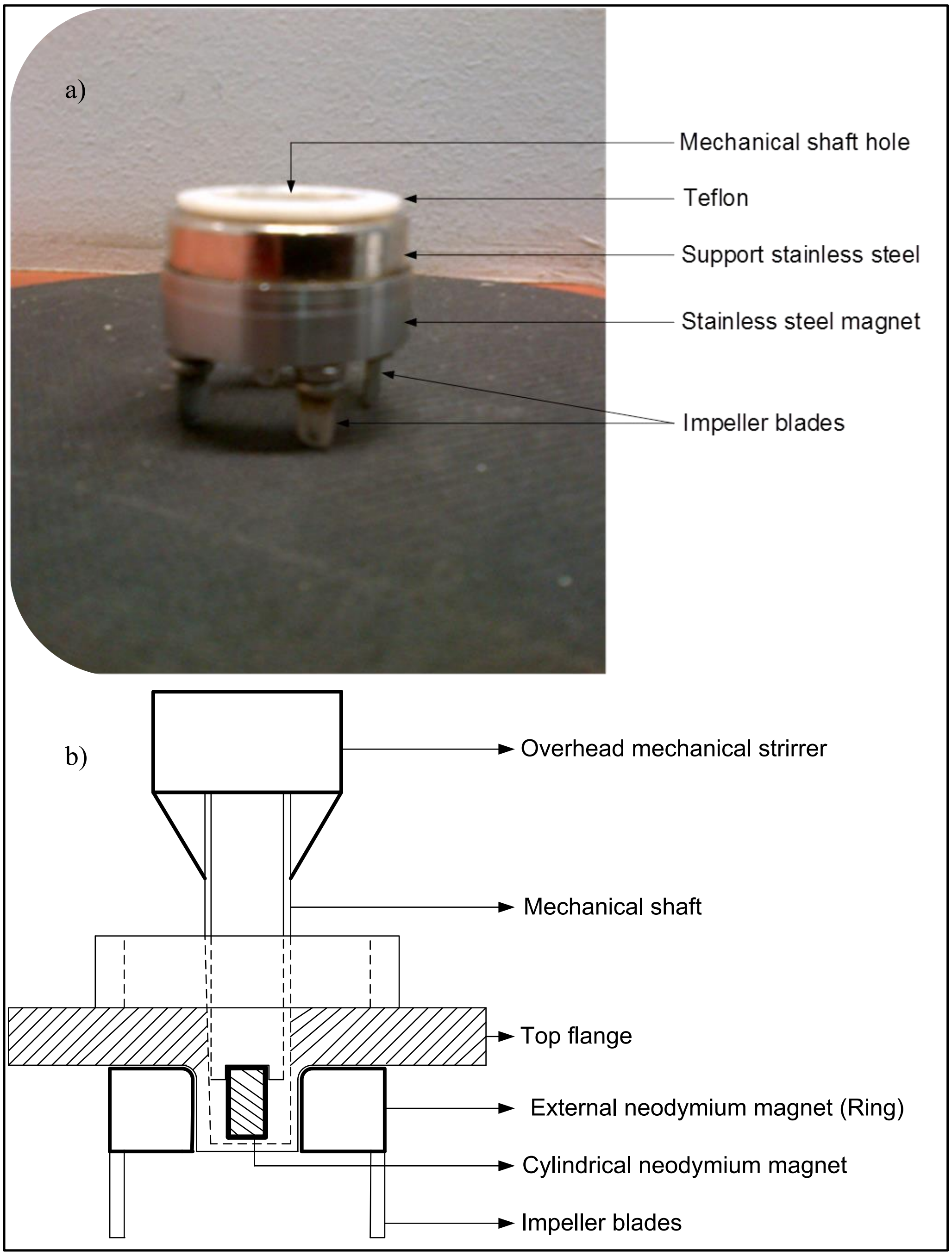

Figure 5.5. (a) A photograph of the stirrer device used in this study (b) schematic diagram of the stirring mechanism

5.2.4. The liquid thermostatted bath

A thermostatted bath was employed to keep the cell temperature at a constant value (see Figure 5.2). It was constructed from 316 stainless steel with the dimensions of 43×35×26 cm. The bath was filled with 50 mass percent of ethylene glycol aqueous solution which was suitable to operate in the temperature ranges of 263.15 to 323.15 K. The cell was immersed in the bath to prevent heat transfer from the environment to the cell.

5.2.5. Temperature controllers

A TXF200 programmable temperature controller supplied by PolyScience® was used to control the temperature of the bath which was equipped with an immersion circulator pump and an internal temperature probe. It can operate in the temperature range of 243.15 K to 323.15 K. The programmable temperature controller provides an adjustable rate of cooling/heating during hydrate formation/dissociation.

An immersion cooler or cold finger supplied by PolyScience® was used in order to decrease the bath temperature. The cooler consisted of an evaporator, condenser, compressor and throttling valve for cooling of the liquid bath down to 173.15 K.

5.2.6. Temperature Probe

A Pt100 (platinum temperature probe) with ± 0.03 K uncertainty was connected to the cell in order to measure the temperature of the cell. The temperature probe was connected electrically to a 34972A LX Agilent data acquisition system. The temperature was monitored and recorded along the time during the experiment using the data acquisition system.

5.2.7. Pressure Transducer

A WIKA pressure transducer with an accuracy of 0.05% of full scale was utilized to measure the pressure of the cell. The pressure transducer was connected to the body of the cell to measure the pressure of the cell. Using the 34972A LXI Agilent data acquisition system, the cell pressure was electronically recorded and displayed along with time. In order to avoid any possible vapour condensation inside the pressure transmitter, it is housed in an aluminium block with a constant temperature of 313.2 K. This constant temperature is provided by two heating cartridges which are inserted at the top of the aluminium block. Each heating cartridge has an 8 mm outside diameter and 40 mm length. The temperature of the aluminium block was measured with a calibrated 3 mm diameter and 20 mm length class A, 3-wire Pt-100 and controlled by a Shinko ACS-13A digital indicating controller.

5.3. Leak test

Prior to calibrating the various instruments and performing measurements, it is crucial to ensure that there is no leak in the system. Hence, in this study a leak test was performed after assembling the apparatus. For this purpose, nitrogen at a pressure of 10 MPa was introduced to the equilibrium cell at a constant temperature (298.15 K) to eliminate the influence of temperature fluctuations on the gas pressure. Any possible leakage was determined by a decrease in the pressure reading over a period of 15 hours or if left overnight. To find the leak, a leak detecting fluid “(SNOOP®)” was used on all connections and fittings. The existence of the bubbles around a fitting confirms the existence of the leak. The fitting was tightened and covered with thread tape or sealed using Loctite to eliminate the problem. If using Loctite on the fitting, the equilibrium cell and all fittings were evacuated to allow for better sealing and for the sealant to dry.

5.4. Calibration of Measuring Devices and determining Experimental Accuracies

In order to develop reliable thermodynamic predictive tools and hydrate-based industrial processes it is vital to measure the hydrate phase equilibrium data with the highest possible accuracy. The accuracy of the results depends on the accuracy of the measuring instruments. Therefore, in this study before performing the experimental work, close attention was paid to the calibration of the measuring devices and careful calibration of all measuring instruments, i.e., temperature probes, pressure transducers, was performed against reference instruments. These calibrations were checked periodically to determine possible changes.

5.4.1. Calibration of Temperature probe

The equilibrium temperature is measured using Pt-100 Platinum resistance thermometer probes, which were calibrated against a standard temperature unit, model "CTH 6500" supplied by WIKA with the accuracy of ±0.03 K for the temperature range of 73.15 K to 473.15 K. The Pt-100 sensors and the reference probe were submerged in a thermos-statted bath filled with a mixture of ethylene glycol and water. The temperature of the bath was increased and decreased at uniform intervals from (258 to 315) K three times in order to account for any hysteresis during calibration. At each temperature step the temperatures of the two probes (standard probe and temperature probe) were allowed to stabilize and recorded within 10 seconds for two minutes. The resultant temperature readings were then averaged. The actual temperature measurements were plotted against the standard temperature measurements, resulting in a second order polynomial relation (Figure 5.6). The equation of this line is subsequently used to determine the true temperature value. The maximum uncertainty on the temperature measurement obtained from this calibration is within ± 0.02 K.

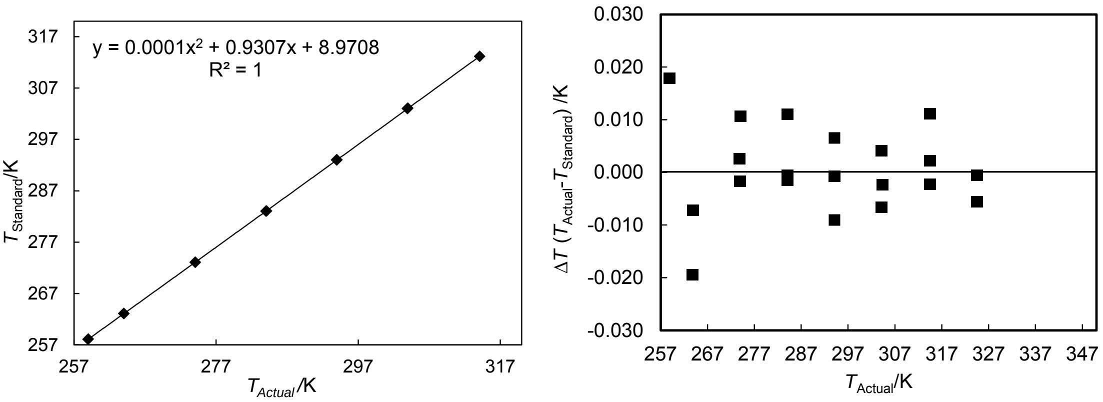

Figure 5.6. Calibration of the Pt-100 temperature probe used in this study. A second order relation between standard and actual probe was obtained with a maximum error in repeatability of 0.02 K. These results were verified on 26 Aug 2014.

5.4.2. Calibration of Pressure transducer

The calibration of the pressure transducer was performed by connecting the standard pressure transducer to a source of pressure (often nitrogen which was used to fill the equilibrium cell). The standard pressure transducer is suitable to measure pressures in the ranges of 0 to 1 MPa with an accuracy of ±0.006 MPa. The standard pressure transducer was calibrated at a temperature of 298.15 K. Therefore during the pressure calibration, the temperature of the equilibrium cell was kept at the constant temperature of 298.15 K. The pressure calibration was performed in the pressure range of 0.9 to 10 MPa. For this purpose, first the temperature of the cell was set to the constant value of 298.15 K. Thereafter, nitrogen was introduced to the system in order to pressurize the cell to a desire pressure. Subsequently, the system was allowed to reach a constant pressure. The pressure readings from the pressure transducer and the standard pressure transducer were recorded 10 times during a 2 minute interval and values were then averaged. The pressure calibration was performed step by step from low to high pressures and vice versa. Pressures read through the instrument and from the reference were fitted to a second order polynomial correlation, allowing the actual or true pressure values to be calculated. Figure 5.7 shows a second order relation between the standard transducer and the cell pressure transducer as well as deviations of the actual pressures from the standard pressures. As observed in Figure 5.7, the maximum pressure deviation between the standard and actual pressure is approximately 0.0008 MPa.

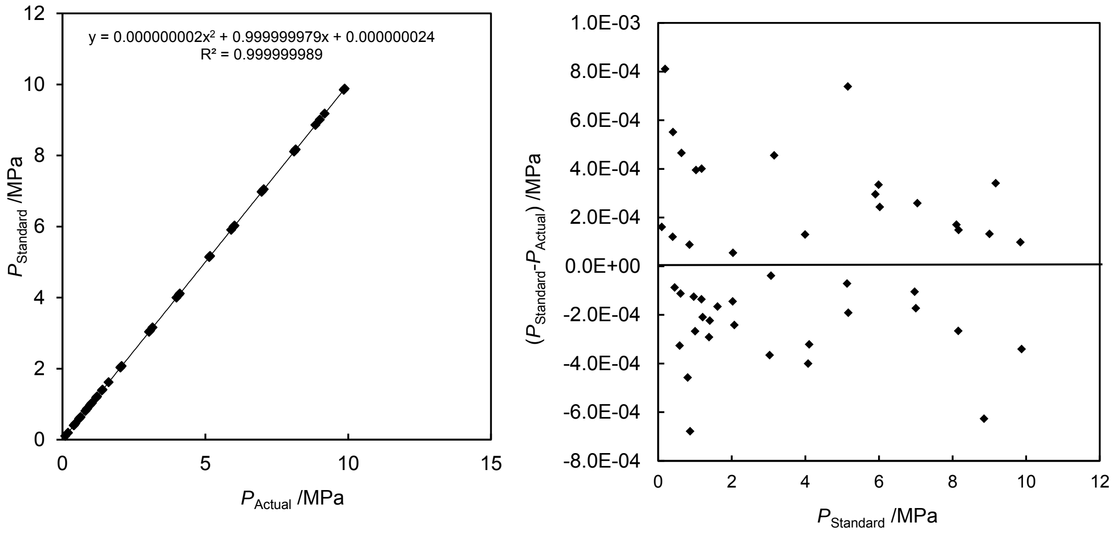

Figure 5.7. Calibration of the WIKA pressure transducer used in this study. A second order relation between standard and transducer pressure was achieved (left), deviations from the standard pressure with the maximum value of ±0.0008 MPa (right), these results were verified on 15 September 2014.

5.5. Vapour pressure test

To examine the accuracy of the experimental measurements, the vapour pressure of refrigerant R134a was measured and compared to available experimental data from literature. At the beginning of the experiments the cell was evacuated to approximately 0.00002 MPa using a vacuum pump for nearly 30 minutes to remove air and any possible impurities inside the cell. After the cell was immersed in a thermo-statted bath the temperature was set to a desired value. Subsequently, the cell was pressurized to a desired value by introducing R134a into the cell. The stirrer speed was set to the speed of 600 rpm to agitate the equilibrium phases inside the cell. In order to specify that the vapour-liquid equilibrium is reached inside the cell at the corresponding temperature, the pressure of the system was decreased by releasing some of the R134a gas. The pressure of the cell rose back to its initial value during the R134a liquid vaporization and hereby the existence of the liquid R134a inside the cell was confirmed. The equilibrium vapour pressure conditions were achieved when the pressure stabilized at the constant temperature. The results of the R134a vapour pressure measurements are shown in Figure 5.8. As seen in this figure there is reasonable agreement between the measured data and those from literature.

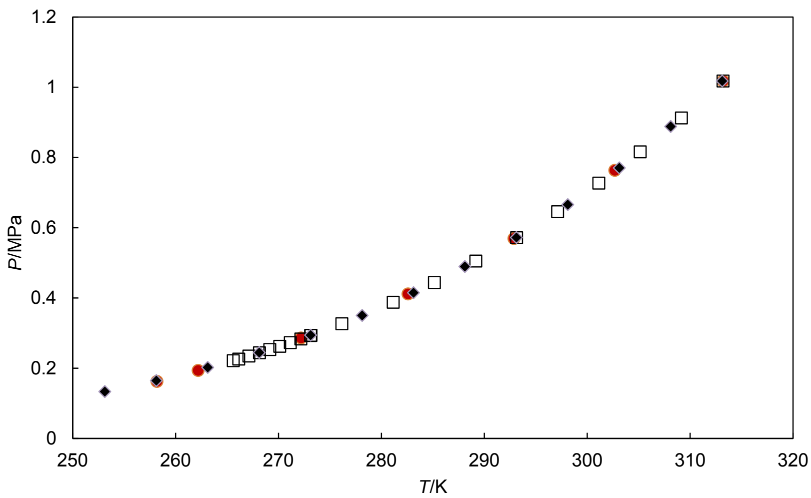

Figure 5.8. Experimental data of vapour pressure of R134a, ●, this study; □, (Goodwin et al., 1992); ♦, (Kubota et al., 1989).

5.6. Experimental procedures

The formation and dissociation of the gas hydrate for refrigerant systems was the focus of this study. In the following sections the procedures which were employed in the thermodynamic and kinetic measurements are explained.

5.6.1. Gas hydrate dissociation measurement

The experimental procedure for the measurement of gas hydrate dissociation conditions commences with the cleaning and washing of the equilibrium cell (see Figure 5.1). This was performed using deionized water. After initial evacuation of the cell (through the valve X) to a pressure of approximately 0.00002 MPa, for 30 minutes using an Edwards vacuum pump P, approximately 16 cm^3 of distilled deionized water was loaded into the cell through the water injection valve U (see Figure 5.1). Afterwards, the cell was evacuated again to remove any traces of air. The cell was then submerged in the temperature controlled bath (K) in which the temperature was set to a temperature above hydrate stability zone. The pressure of the cell was thereafter increased to a desire value by introducing the corresponding gas through the valve V in Figure 5.1.

After stabilization of the temperature and pressure of the cell, the stirrer (H) was switched on and set at a speed of 620 rpm for all measurements to agitate the phases inside the cell. After the stabilization of the pressure which decreased due to gas solubility in water, the temperature controller (R) was set to 6-7 K below the anticipated hydrate dissociation temperature. This process is known as the cooling step. Hydrate formation was established by a sudden drop in the pressure due to the gas encapsulation inside the hydrate cavities. Further subcooling was performed in the case of no formation of the gas hydrate. After formation of the gas hydrate and stabilization of the pressure, the temperature of the equilibrium cell was then increased in a step-wise manner. The resultant *P-T* curve is known as the heating curve. During the heating process, the pressure of the system increases due to the gas hydrate dissociation. At the beginning of the heating process, large temperature steps of 0.5 K/h were chosen until the temperature approached the conditions close to the final dissociation point in which heating steps of 0.1 K/h were used. Figure 5.9 shows an example of a primary cooling and heating curve obtained in this study for the R508B hydrate. As observed in Figure 5.9, the intersection between the cooling and heating curves indicates the equilibrium transition from (hydrate + liquid + gas) to (liquid + gas) and was therefore reported as the hydrate dissociation point. The procedure was repeated at different pressures in order to determine the hydrate phase boundaries over a wide temperature range.

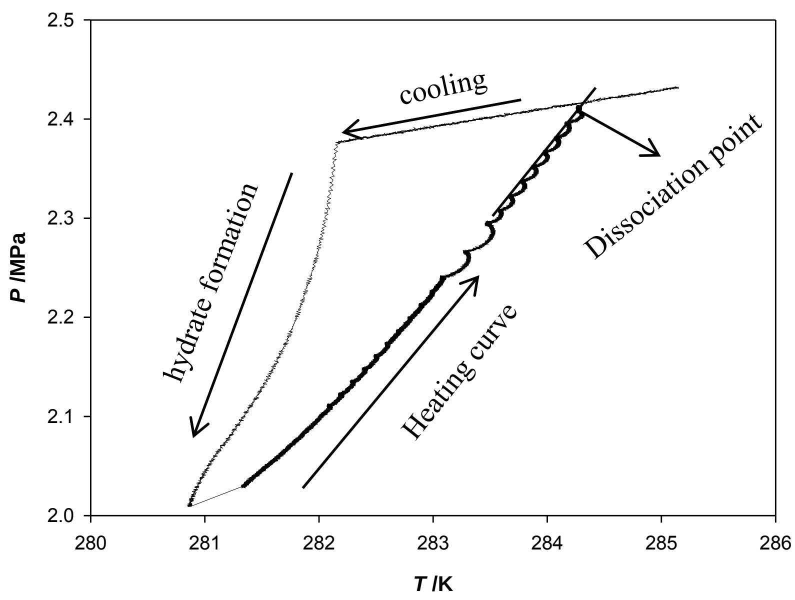

Figure 5.9. Primary heating and cooling curve for R508B hydrate obtained in this study.

5.6.2. Kinetic measurements

The main objective of the kinetic measurements is to specify the hydrate formation rate and evaluate the influence of different parameters such as pressure, temperature and surfactant additives on this rate. In this procedure the preparation of the cell is similar to that of the thermodynamic procedure, described earlier in which the cell was first washed using distilled deionized water and then evacuated for a period of at least 30 minutes. Subsequently, approximately 16 cm^3 of water was introduced to the cell which was then place under vacuum (0.00002 MPa) for at least 30 minutes to remove any trace of air. Subsequently, the cell was immersed into the temperature controlled bath with the temperature adjusted to a desired value. After stabilization of the temperature of the system, the considered hydrate former (refrigerant) was introduced into the cell until the pressure of the cell reached to the desired value. It should be mentioned that the pressure and the temperature of the system should be within the hydrate stability zone. After pressurizing the cell, the stirrer was turned on with a constant speed of 620 rpm throughout all measurements. Figure 5.10 shows a typical curve obtained for R407C during a kinetic study. As it is clear in Figure 5.10, the formation of the gas hydrate can be detected by either increasing the temperature (due to the exothermic nature of gas hydrate reaction) or decreasing the pressure of the cell. Subsequently, the induction time is defined as the period over which the temperature (or the pressure) remains at the constant value before onset of a significant change in the temperature (or the pressure) of system. After the nucleation of hydrate, the temperature of the cell decreases back to its initial value and the pressure of the cell decreases constantly until a steady state condition was achieved, at which the pressure of the cell remains constant.

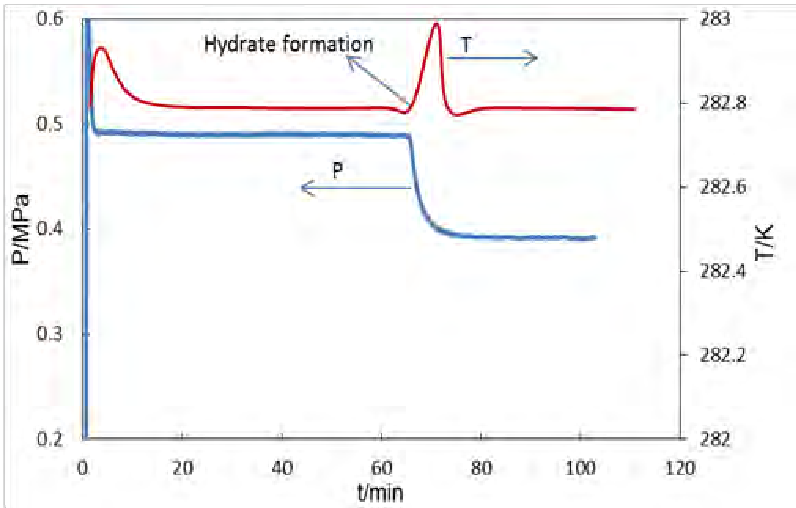

Figure 5.10. Pressure and temperature changes during R407C hydrate nucleation and growth at a constant temperature and pressure of 282.8 K and 0.71 MPa, respectively, stirring speed of 620 rpm with 40% (volume percent) distilled water of the equilibrium cell.

5.7. NIST uncertainty analysis of the experimental hydrate dissociation data.

Any experimental measurement suffers from uncertainty which is caused by two factors of the limitation of the measuring instrument (systematic error) and the skill of the person(s) performing the measurements (random error). The uncertainty of the experimental measurement is defined as the interval around an experimental data point which is related to the accuracy of that point (Taylor, 2009). Therefore, if the measurement of the data point was repeated at the same condition, the result should lie within the stated interval. Stating the uncertainties in the experimental/measured data enables a good comparison between the results obtained from different researchers and laboratories in the same area of measurements. As a result, users are able to judge the accuracy of the experimental data and select those with higher accuracy to provide more accurate models and avoid repetition in uncertainties of experiments if differences are not significant. (Birch, 2003). The difference between the experimental test result and the stated value for a specific property is not important, if this difference lies within the uncertainty range (Birch, 2003).

5.7.1. Uncertainties estimation

Prior to reporting the results of an experimental measurement, it is vital to specify and report the influence of all sources of uncertainties on the measurements. When more than one source of uncertainty is present, the overall uncertainty is defined as the combined standard uncertainty. In this study, the uncertainty is expressed based on NIST guidelines for reporting uncertainty:

$$u_c(x) = \pm\sqrt{\sum_i u_i(x)^2} \tag{5.1}$$

According to the NIST guidelines, for evaluation of the uncertainty of the measurements which includes various components, two procedures of type A and type B should be followed. Type A uncertainties for temperature and pressure is related to the numerous transducer readings for a stable system (repeatability) and the difference between readings from two different conditions (reproducibility) which can be calculated using:

$$u_c(x) = \pm\frac{\sigma}{\sqrt{N_{rp}}} \tag{5.2}$$

in which that σ stands for the standard deviation of the data and N_{rp} is the number of data points (or number of data pairs in the case of reproducibility).

Type B uncertainties comes from the polynomial fitted to the calibrations as well as any specifications stated by manufacturers. This type of uncertainty is evaluated as follows:

$$u_{calibration}(x) = \frac{\mathrm{b}}{\sqrt{3}} \tag{5.3}$$

$$u_{instrument}(x) = \frac{\mathrm{b}}{\sqrt{3}} \tag{5.4}$$

where b is the half width of the interval,

$$\mathrm{b} = \left(\frac{\mathrm{a}_+ \pm \mathrm{a}_-}{2} \right) \tag{5.5}$$

Therefore, the combined standard uncertainty for a specific variable, *x*, which may be temperature or pressure, is defined by the following equation:

$$u_c(x) = \pm\sqrt{u_{instrument}(x)^2 + u_{calib}(x)^2 + u_{repeatibilty}(x)^2 + u_{reproducibility}(x)^2} \tag{5.6}$$

in which $u_{intrument}$ is the standard uncertainty of the instrument (temperature probe or pressure transmitter), u_{calib} is the standard uncertainty due to the temperature or pressure calibration correlation and $u_{repeatibility}$ and $u_{reproducibility}$ are the standard uncertainty come from repeatability and reproducibility respectively (type A). The upper and lower uncertainty limits from the pressure and temperature calibrations were determined from the second order polynomial. As can be observed in Figure 5.6, the uncertainty for temperature calibration is ± 0.02 K. Similarly, in Figure 5.7 the uncertainty for pressure calibration is ± 0.0008 MPa. The combined uncertainties for temperature and pressure in this study are reported in Table 5.2.

Table 5.2. Temperature and pressure combined uncertainties

Calibration	a	b	$u_{calibration}$	u_c *(x)*
Pressure transducer (0-10 MPa)	0.0008	0.0007	0.0004 MPa	±0.01 MPa
Temperature probe	0.02	0.02	0.01 K	±0.03 K

Temperature fluctuation is inevitable during an experiment which is due to the various sources such as inefficient liquid circulation in the bath, heat exchange with the environment and instrument manufacturer error. Based on this fact, the repeatability uncertainty can be obtained using the following expressions:

$$u\ (x_i) = \left(\frac{1}{n(n-1)} \sum_{k=1}^{n} \left(X_{i,k} - \overline{X}_i \right)^2 \right)^{1/2} \tag{5.7}$$

where,

$$\overline{X}_i = \frac{1}{n} \sum_{k=1}^{n} \left(X_{i,k} \right) \tag{5.8}$$

5.7.2. Reporting uncertainty

The uncertainty can be reported as either the combined standard uncertainty or by the inclusion of a coverage factor. Depending on the application of experimental data, it is normally required to expand the combined standard uncertainty, $u_c(x)$, using a coverage factor, k, to obtain the expended uncertainty, $U(x)$, as the follows: (Birch, 2003)

$$U(x) = ku_c(x) \tag{5.9}$$

A larger interval for the result of an experimental measurement is provided using the expanded uncertainty rather than the combined standard uncertainty. In this study, a coverage factor equals to unity (k=2) was applied to provide precise experimental data.

6

Results and Discussion

This chapter provides the results obtained from the experimental work, as well as from the modelling of the measured data. Dissociation conditions of different refrigerants have been studied using experimental investigations. The rate of the hydrate formation of these refrigerants was obtained from kinetic measurements. Dissociation data was also regressed using a thermodynamic model and the accuracy of the model is presented. The rate of the hydrate formation, storage capacity, and apparent rate constant of the hydrate formation and the effect of the SDS solution on these parameters are discussed through the results of the kinetic model. From the experimental results the potential of refrigerants studied to be used as a cold storage medium is discussed.

6.1. Experimental results

6.1.1. Thermodynamic study

Clathrate hydrate dissociation pressure as the function of temperature for different refrigerants was obtained in this study using the isochoric pressure search method (refer to chapters 4, 5) at the pressure and temperature range of (0.065-9.99) MPa and (272.2-293.2) K. The refrigerants used in the thermodynamic study were pure refrigerants, viz. HFC-23, HFC-125a, HFC-R134a, HCFC-22, CF-116 and refrigerant blends with ASHRAE numbers of R407C (HFC-32/HFC-125/HFC-134a, 23/25/52 wt%), R410A (HFC-32/HFC-125, 50/50 wt%), R507C (HFC-125/HFC-143a, 50/50 wt%), R404A (HFC-143a/ HFC-125/ HFC-134a, 52/4/44 wt%), R406A (HCFC-R22/HFC-R142b/HC-600a, 54/41/4 wt%), R408A (HFC-143a/ HFC-125/ HCFC-22, 46/7/47 wt%), R427A (HFC-134a/ HFC-125/ HFC-32/ HFC-143a, 50/25/15/10 wt%) and R508B (CF-116/HFC-23, 54/46 wt%).

In this study the hydrate phase equilibrium measurements for the pure refrigerants were performed through two different phase boundaries, viz. L_w-H-V in which three phases: hydrate (H), liquid water (L_w) and vapor are present and H-L_w-L_R in which three phases: hydrate (H), liquid water (L_w), and liquid refrigerants (L_R) are in equilibrium. In the case of refrigerant blends, since there is more than one quadruple point in the system, depending on the number of pure constituents, it is difficult to specify the coexisting phases at the pressures in which the liquid refrigerant (L_R) is present in the system. Hence, in this study the point at which the slope of the hydrate dissociation curve changes is addressed as critical decomposition point and at the pressures lower than this point three phases of L_w-H-V are in equilibrium.

It should be mentioned that the relevant hydrate phase region for cold storage applications is L_w-H-V. Further hydrate phase equilibrium conditions are studied in order to investigate the refrigerant hydrate behavior.

In this study the test system comprising of pure refrigerants R125a, R23, R22 and R134a were measured to verify the accuracy and reproducibility of the measured data. As depicted in Figures 6.1 to 6.4 there is a reasonable agreement between the experimental data obtained in this study and those of the literature which confirms the calibration and the experimental technique. The measured data for pure refrigerants investigated in this study are presented in the Tables 6.1. It should be mentioned that in Tables 6.1 for the refrigerant R116 these data are newly reported and there is no experimental data in the open literature for this refrigerant.

Table 6.2 shows the hydrate dissociation conditions for the refrigerant blends viz. R404A, R406A, R408A, R410A, R407C, R507C, R508B and R427A. Figures 6.5 to 6.12 illustrate the plots of the dissociation conditions for the pure refrigerants along with the blends comprising the specific pure component in order to study the effect of mixing of pure refrigerants on the gas hydrate dissociation conditions. The vapor pressure of refrigerant blends were also obtained in this study and depicted along with the hydrate dissociation data in Figures 6.5 to 6.12. For the refrigerants R404A, R406A, R408A, R508B and R427A the measurements are also performed above the critical decompositions point as shown in in Figures 6.5 to 6.12 and Table 6.2. However, for the cold storage applications the hydrate dissociation when three phases H-L_w-W are in equilibrium is of interest.

Table 6.1. Experimental equilibrium hydrate dissociation data (L_w-H-V and L_w -H-L_R) obtained in this study for pure refrigerants[a].

R116 (L_w-H-V)		**R125a (L_w-H-V)**		**R23 (L_w-H-V)**		**R22 (L_w-H-V)**		**R134a(L_w-H-V)**	
P/ MPa	*T*/ K	*P*/ MPa	*T*/ K	*P*/MPa	*T*/ K	*P*/MPa	*T*/ K	*P*/ MPa	*T*/ K
0.521	273.6	0.117	274.6	0.450	275.4	0.113	274.9	0.065	274.4
0.595	274.3	0.155	276.0	0.647	278.3	0.150	277.0	0.071	274.8
0.811	275.9	0.206	277.4	0.713	279.2	0.194	279.0	0.143	278.1
0.944	276.5	0.250	278.1	0.956	281.7	0.210	279.6	0.200	279.8
1.225	277.9	0.272	278.5	1.010	282.1	0.390	284.3	0.300	281.5
1.784	278.7	0.316	279.6	1.133	283.3	0.506	285.9	0.345	282.2
L_w -H- -L_R		0.366	280.2	1.350	284.6			**L_w -H- L_R**	
2.600	279.2	0.399	280.7	1.566	285.8			1.450	283.3
3.906	279.6	0.495	281.6	1.819	286.9			4.420	283.5
7.371	280.1	0.637	282.5	1.988	287.8			9.680	283.9
		0.745	283.2	2.544	289.3				
		0.850	283.7	2.727	290.1				
		0.969	284.0	3.440	292.0				
		1.030	284.3	**L_w -H- L_R**					
		L_w -H -L_R		4.49	292.3				
		1.852	284.4	6.49	292.8				
		2.961	284.4	9.15	293.2				
		4.601	284.5						
		5.986	284.6						

[a]u(T) = ±0.03 K; u(P) = ±0.01 MPa

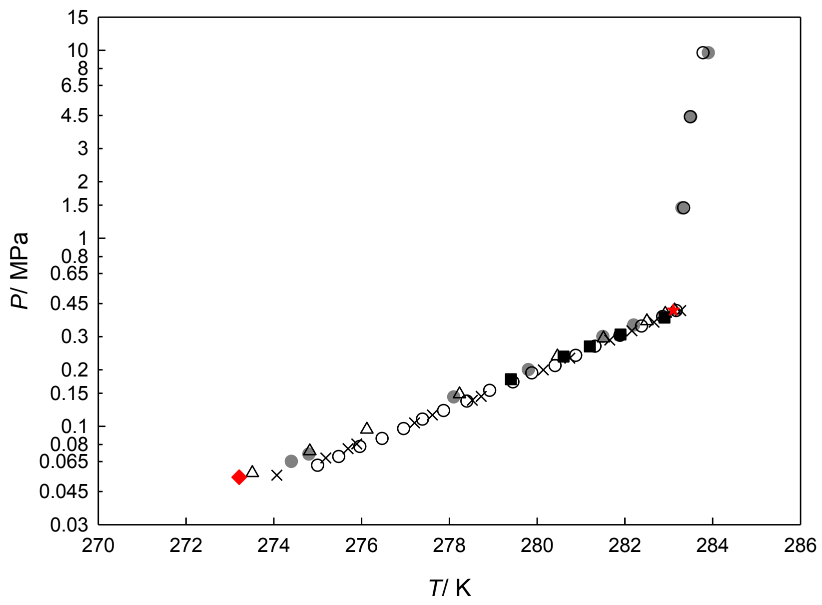

Figure 6.1. Hydrate phase diagram of R134a ($C_2H_2F_4$); Experimental data:●, this work; ■, (Mohammadi and Richon, 2010); Δ, (Liang et al., 2001);○, (Hashimoto et al., 2010a); ×, (Akiya et al., 1999); ★, upper quadruple point, (Liang et al., 2001); ♦, lower quadruple point (Mori and Mori, 1989b).

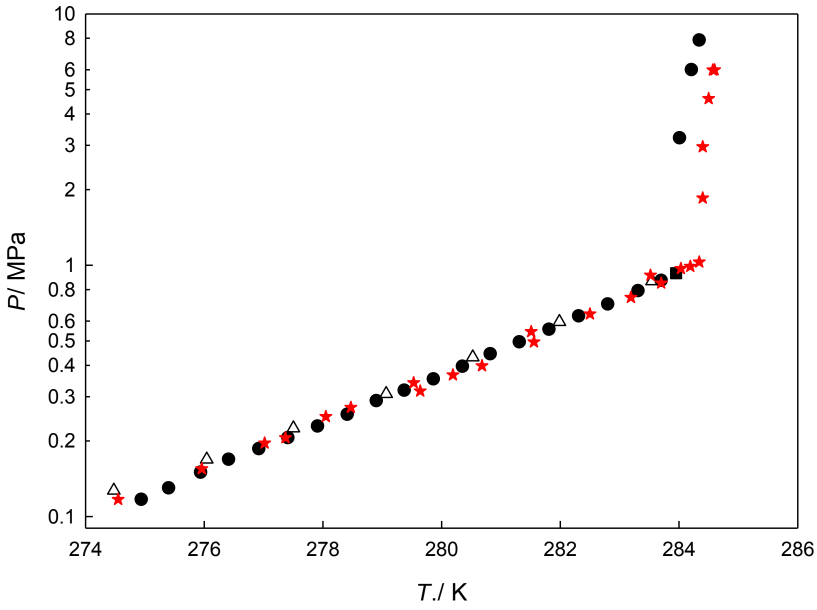

Figure 6.2. Hydrate phase diagram of R125a (C_2HF_5); Experimental data: ★, this work; ●, (Hashimoto et al., 2010a); Δ, (Akiya et al., 1999); ■, upper quadruple point, (Hashimoto et al., 2010a).

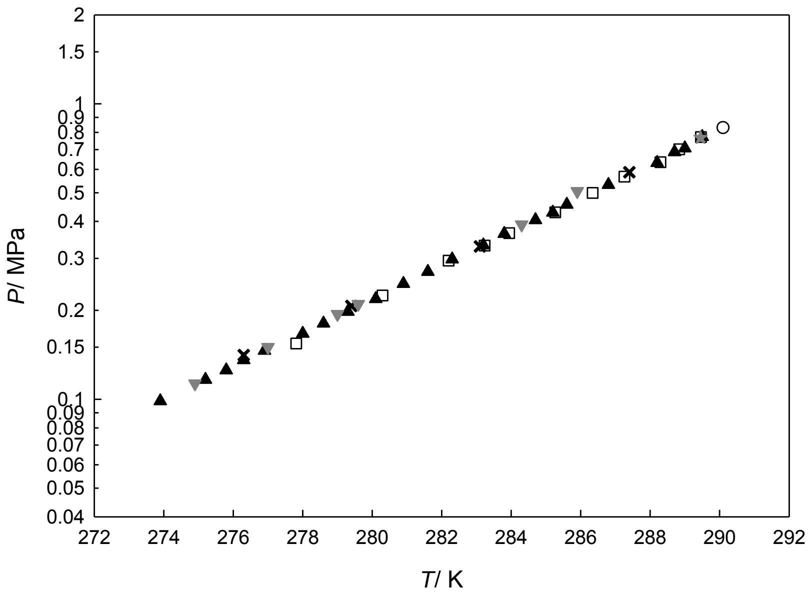

Figure 6.3. Hydrate phase diagram of R22 ($CHClF_2$); Experimental data: ▼, this work; ▲,(Wittstruck et al., 1961); □, (Javanmardi et al., 2004); ×, (Chun et al., 1996); ○, ★, upper quadruple points, (Carbajo, 1983), (Chun et al., 1996).

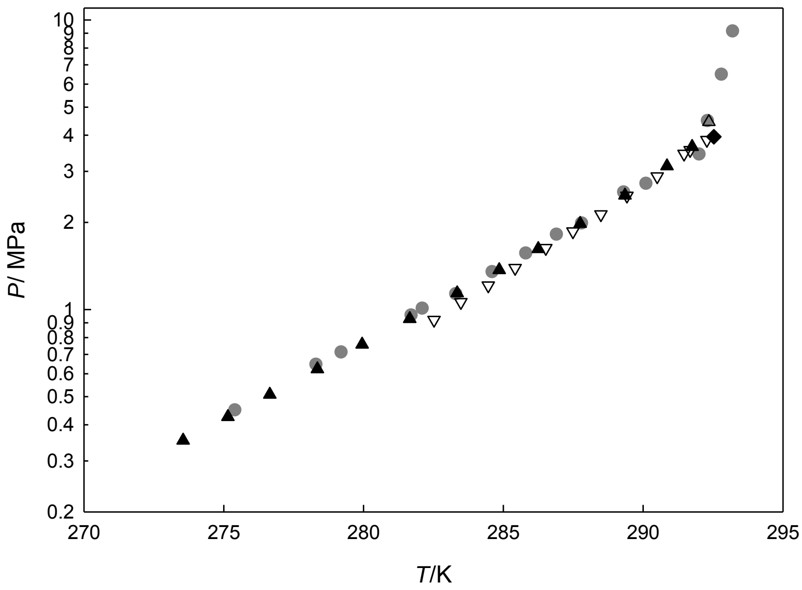

Figure 6.4. Hydrate phase diagram of R23(CHF_3); Experimental data: ●, this work; ▲, (Kubota et al., 1984); ▽, (Mooijer-van den Heuvel et al., 2006) ; ◆, upper quadruple point, (Mooijer-van den Heuvel et al., 2006); △, upper quadruple point, (Kubota et al., 1984);

Table 6.2. Experimental equilibrium hydrate dissociation data obtained in this study for refrigerant blends

P,MPa	*T*, K	*P*,MPa	*T*, K	*P*,MPa	*T*, K	*P*, MPa	*T*, K	*P*, MPa	*T*, K
R 410A		R507C		R508B		R407C		R427A	
0.178	277.0	0.184	276.7	0.527	272.2	0.106	275.8	0.0791	272.7
0.270	280.0	0.231	277.7	0.830	276.5	0.153	278.4	0.0950	274.6
0.383	283.2	0.252	278.1	1.090	278.5	0.187	279.1	0.1503	277.2
0.589	286.1	0.302	279.0	1.458	280.8	0.240	280.9	0.2859	281.2
0.568	286.2	0.353	279.7	1.744	281.9	0.265	281.6	0.4419	283.9
0.904	289.4	0.396	280.2	2.082	283.3	0.335	282.7	0.6388	286.3
0.969	290.0	0.420	280.5	2.415	284.3	0.364	283.8	[b]*0.8298*	*287.6*
[b]*1.365*	*292.5*	0.530	281.4	2.923	285.7	0.445	284.6	1.4216	287.9
		0.627	282.3	[b]*3.360*	*286.5*	0.500	285.4	2.7023	288.1
		0.791	282.9	4.890	286.4	0.580	286.6	7.6234	288.7
		[b]*0.849*	*283.3*	7.164	286.5	0.830	288.2		
				8.957	286.6	0.917	289.1		
						1.027	289.9		
						[b]*1.270*	*291.4*		
R406A		R404A		R408A					
0.112	275.8	0.128	274.7	0.148	274.9				
0.140	276.9	0.165	275.8	0.182	275.6				
0.199	278.8	0.188	276.6	0.301	278.1				
0.203	279.5	0.214	277.3	0.393	279.8				
0.310	281.1	0.314	279.0	0.555	281.3				
0.439	282.7	0.492	280.9	0.711	282.1				
[b]*0.536*	*283.7*	0.692	282.4	[b]*0.787*	*282.6*				
1.301	285.0	0.849	283.3	1.577	284.2				
2.098	285.2	0.946	283.7	2.666	284.6				
3.512	285.4	[b]*1.136*	*284.3*	6.010	285.0				
9.081	286.2	2.003	285.3						
		2.83	285.6						
		9.995	286.5						

[a]$u(T)$ = ±0.03 K; $u(P)$ = ±0.01 MPa

[b]critical decomposition point in which three phase L_w-H-V coexist

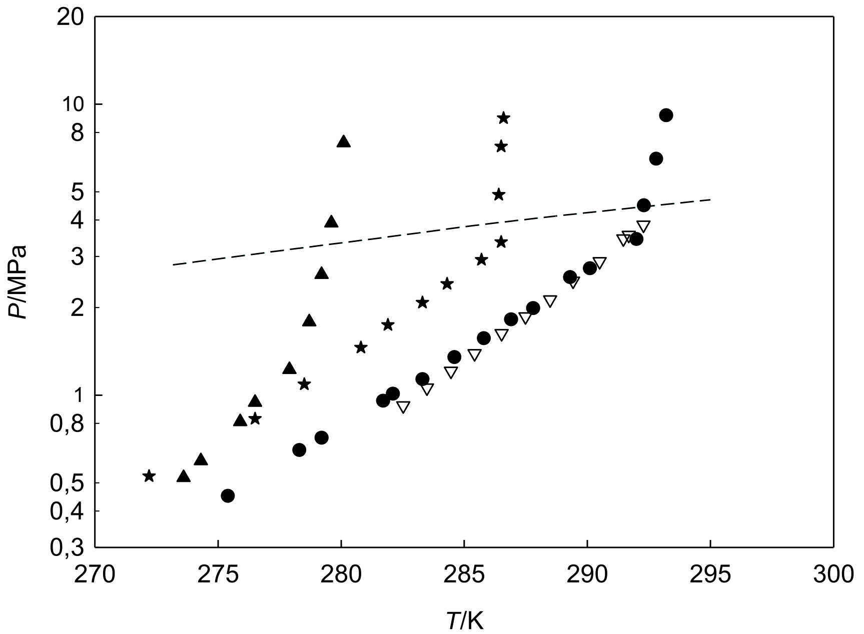

Figure 6.5. Plot of Equilibrium hydrate dissociation data for refrigerants blends investigated in this study: ★, R508B (R23/R116) (this work); ●, R23 (this work); ▽, R23 (Mooijer-van den Heuvel et al., 2006); ▲, R116 (this work); dash line, vapour pressure of R508B (this work).

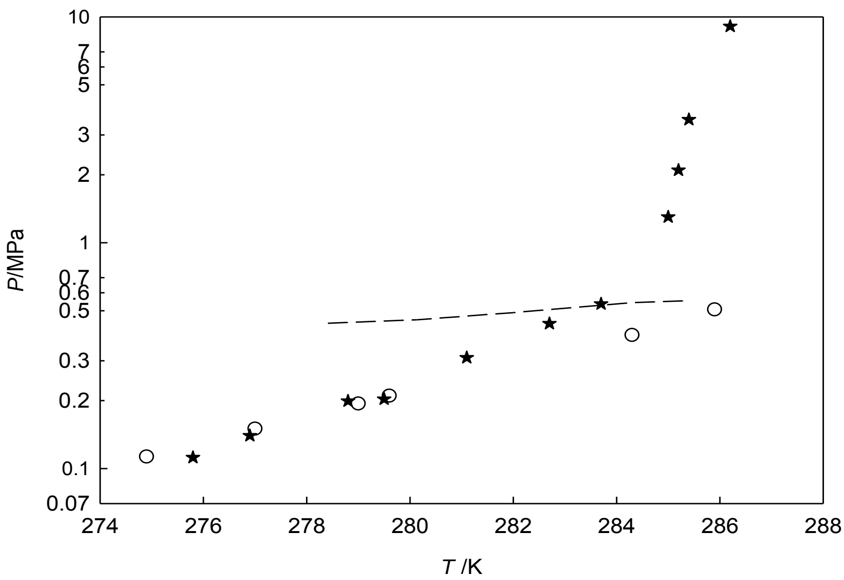

Figure 6.6. Hydrate dissociation conditions for refrigerants:★ , R406A (R22/ R142b/R600a) (this work); ○, R22 (this work); dash line, vapour pressure of R406A (this work).

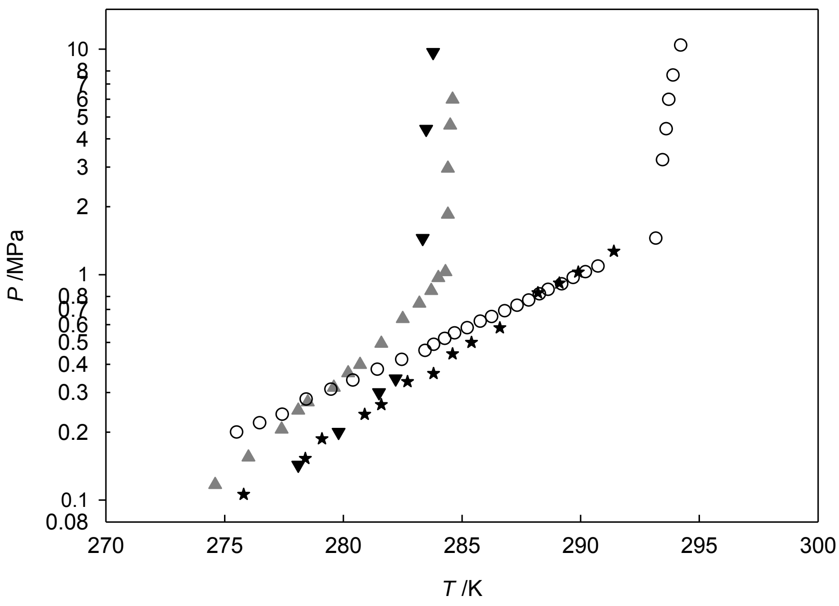

Figure 6.7. Hydrate dissociation conditions for refrigerants: ★, R407C (R32/ R125/R134a) (this work);○, R32 (Hashimoto et al., 2010b); ▲, R125a (this work), ▼, R134a (this work); dash line, vapour pressure of R407C.

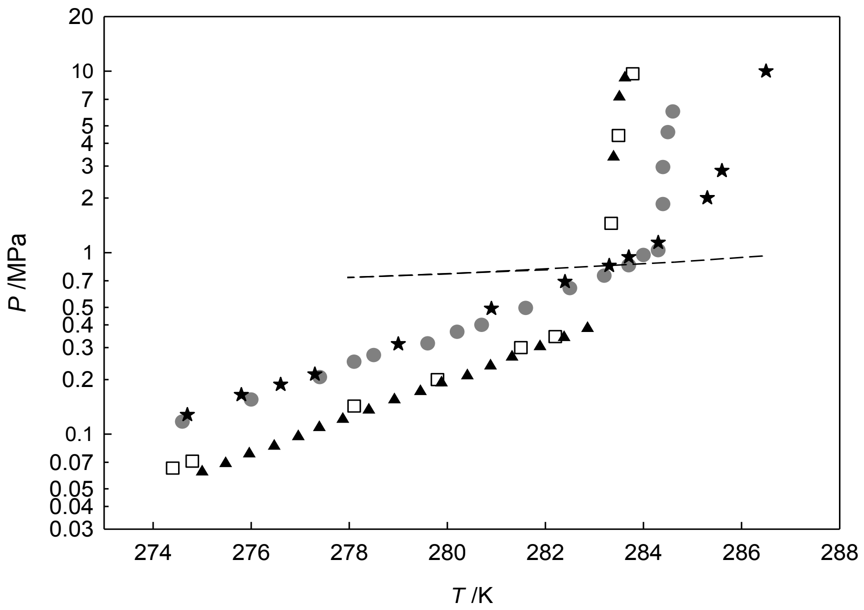

Figure 6.8. Hydrate dissociation conditions for refrigerants: ★ , R404A (R143a/ R125a/R134a) (this work);●,R125a (this work); ▲, R143a (Hashimoto et al., 2010a); □, R134, (this work); dash line, vapour pressure of R404A (this work).

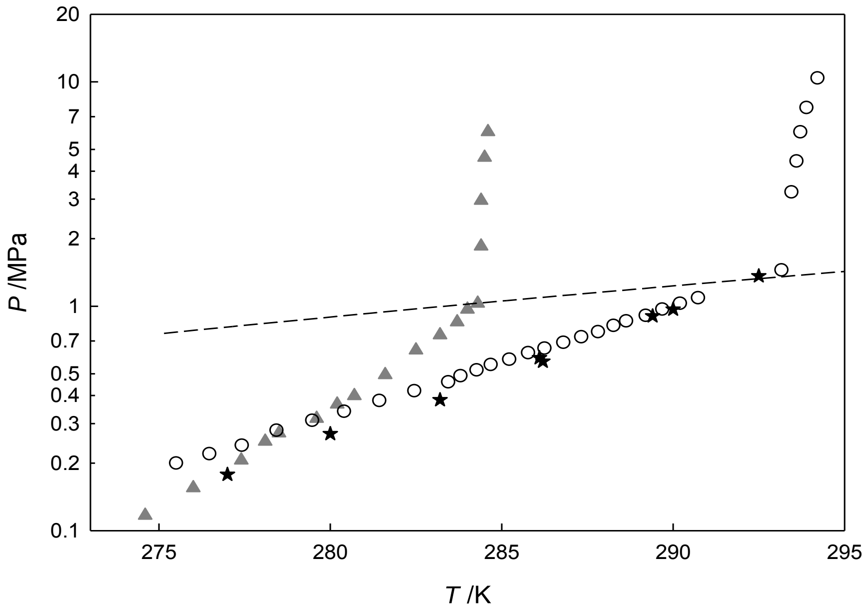

Figure 6.9. Hydrate dissociation conditions for refrigerants: ★, R410A (R32/ R125) (this work);○, R32 (Hashimoto et al., 2010b); ▲, R125a (this work); dash line, vapour pressure of R410A (this work) .

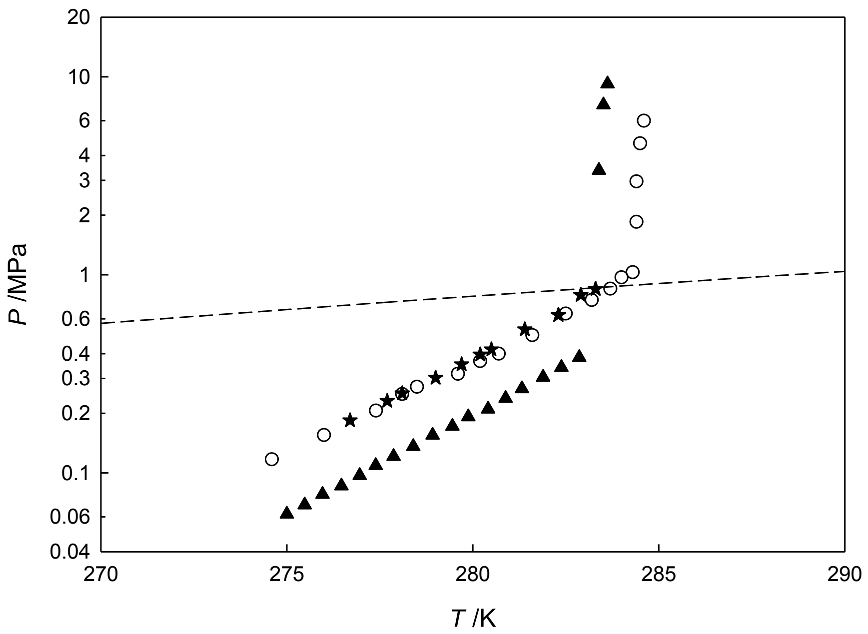

Figure 6.10. Hydrate dissociation conditions for refrigerants: ★ , R507C (R125a/R134a) (this work); ○, R125a; ▲, R143a (Hashimoto et al., 2010a); dash line, vapour pressure of R507C (this work).

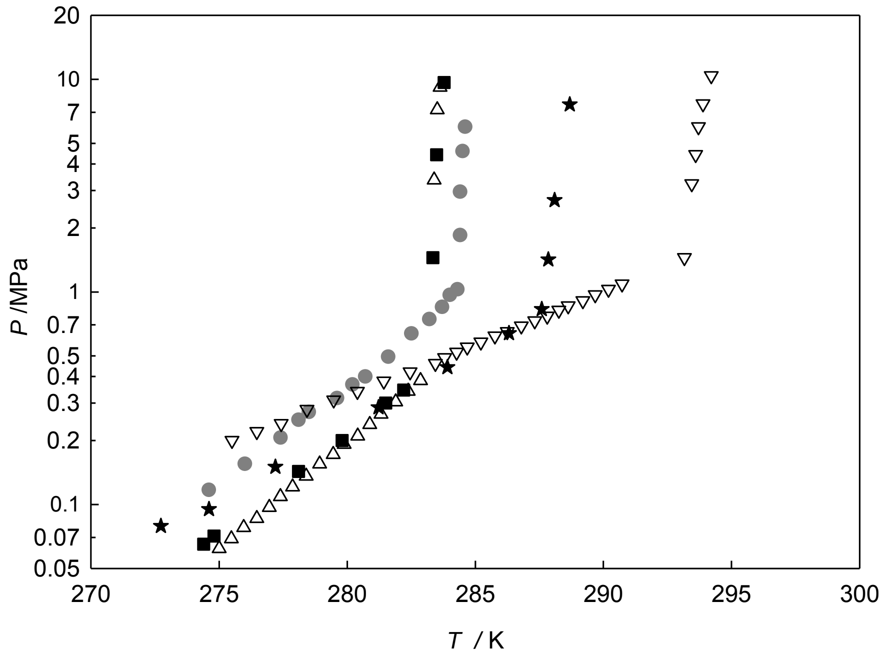

Figure6.11. Hydrate dissociation conditions for refrigerants: ★, R427A (R125a/R134a/R143a/R32) (this work); ●, R125a (this work); Δ, R143a (Hashimoto et al., 2010a); ▽, R32 (Hashimoto et al., 2010b); ■, R134a (this work); dash line, vapour pressure of R427A (this work).

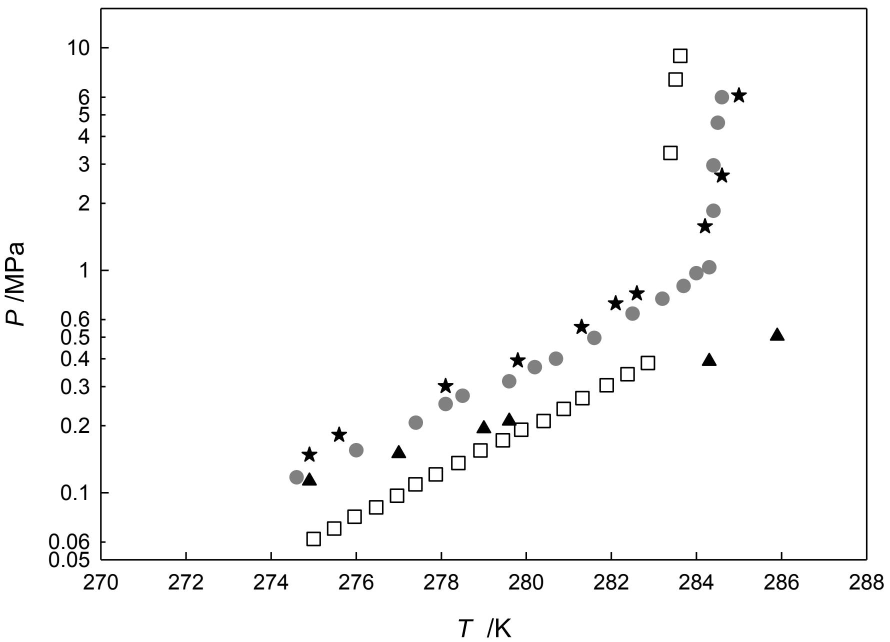

Figure 6.12. Hydrate dissociation conditions for refrigerants: ★, R408A (R125a/R22/R143a) (this work); ●, R125a (this work); □, R143a (Hashimoto et al., 2010a); ▲, R22 (this work); dash line, vapour pressure of R408A (this work).

Clathrate hydrate dissociation conditions were obtained for eight new refrigerant blends. According to the experimental results most refrigerants used in this study form hydrate in the temperature range of (278-285) K which is suitable for cold storage applications. The effect of mixing of pure refrigerants on gas hydrate dissociation conditions can be observed from Figures 6.5 to 6.12. For the refrigerant blend namely R508B with the certified composition of R23/R116, 46/54 wt%, the hydrate dissociation curve is placed between that of the pure refrigerants R116 and R23 (Figure 6.5). The pressure and temperature ranges of (0.527-3.360) MPa and (272.2-286.5) K were obtained for R508B at L_w-H –V phase boundary. It was found that the refrigerant R406A (R22/R142b/R600a, 54/41/4%) can form a hydrate at the pressures slightly lower than that for R22. The hydrate dissociation conditions for R142b are still unknown. A mixture of refrigerants R32/R125/R134a namely R407C with the composition of 23/25/52 wt%, also forms a hydrate at pressures lower than that of its pure constituents. The hydrate dissociation (L_w-H-V) pressure and temperature range of (0.106-1.27) MPa and (275.8-291.4) K was found for R407C. For R404A (R125a/R134a/ R143a, 44/4/52 wt%), the hydrate dissociation pressure was higher than that of R134a and R143a. The dissociation pressure and temperature ranges of (0.128-1.136) MPa and (274.7-284.3) K was obtained for R404A hydrate (H-L_w -V). The hydrate dissociation pressure range of (1.365-0.178) MPa at the corresponding temperature range of (277.0-292.5) K was obtained for R410A (R32/ R125, 50/50 wt%) which was lower than that for R32 and R125a. The hydrate dissociation pressure of R427A (R134a/ R125a/R32/R143a, 50/25/15/10 wt%) was lower than that for R125a and R32 and slightly higher than that for R134a and R143a. The dissociation pressure and temperature range of (0.0791-0.8298) MPa and (272.7-287.6) K was obtained for R427A at L_w-H-V phase equilibrium conditions. For R408A (R143a /R125a/R22/, 46/7/47 wt%) the hydrate dissociation curve was at pressures higher than that for its pure constituents with the pressure and temperature range of (0.148-0.711) MPa and (274.9-282.1) K. The same result was obtained for R507C (R125a/R143a, 50/50 wt%) with the temperature and pressure ranges of (276.7-283.3) K and (0.184-0.849) MPa. For the refrigerant blend namely R508B with certified composition of R23/R116, 46/54 wt% the pressure and temperature ranges were (0.527-8.957) MPa and (272.2-286.6) K respectively. One can observe from mixed gas hydrate dissociation conditions that the pressure and temperature ranges can be changed by adjusting the composition of the mixtures. According to the experimental hydrate dissociation conditions, R427A showed the minimum pressure of dissociation which is particularly suitable in cold storage applications. Hence, the hydrate dissociation conditions of high pressure refrigerants can be decreased by addition of low pressure refrigerants.

6.1.1.1. Enthalpy of hydrate dissociation

For the estimation of the enthalpy of dissociation of the refrigerant hydrates which is a critical property of a cold storage medium, the Clausius-Clapeyron equation was used as follows:

$$\Delta H = -RZ\frac{d\ln(P)}{d(1/T)} \tag{6.1}$$

in which *Z* is the compressibility factor obtained using the PRSV equation of state (Proust and Vera, 1989) and *R* is the gas constant. In equation (6.1), *d*ln*(P)/dT* was calculated using the three phase (L_w-H-V) experimental hydrate dissociation data reported in Table 6.2 and Figures 6.5 to 6.12. The enthalpy of hydrate dissociation for four new refrigerants R427A, R404A, R406A, R408A, R410A, R507C and R407C at different temperatures was obtained and is reported in Table 6.3. The enthalpies of hydrate dissociation at the critical temperature of decompositions are reported in Table 6.3. The temperature dependency of the hydrate dissociation enthalpy is depicted in Figure 6.13 for the refrigerants investigated in this study and some pure refrigerants in literature.

Table 6.3. Enthalpy of hydrate dissociation obtained in this study[a].

T_{exp}/K	P_{exp}/MPa	ΔH/(kJ/mol)	T_{exp}/K	P_{exp}/MPa	ΔH/(kJ/mol)	T_{exp}/K	P_{exp}/MPa	ΔH/(kJ/mol)	T_{exp}/K	P_{exp}/MPa	ΔH/(kJ/mol)
	R507C			R404A			R410A			R407C	
276.7	0.184	146.20	274.7	0.128	142.7	0.178	277.0	79.668	275.8	0.106	112.843
277.7	0.231	145.16	275.8	0.165	141.6	0.270	280.0	78.580	278.4	0.153	111.872
278.1	0.252	144.70	276.6	0.188	141.0	0.383	283.2	77.256	279.1	0.187	111.171
279	0.302	143.59	277.3	0.214	140.2	0.589	286.1	74.841	280.9	0.240	110.079
279.7	0.353	142.46	279.0	0.314	137.3	0.568	286.2	75.095	281.6	0.265	109.561
280.2	0.396	141.50	280.9	0.492	132.0	0.904	289.4	71.044	282.7	0.335	108.108
280.5	0.420	140.97	282.4	0.692	125.7	0.969	290.0	70.233	283.8	0.364	107.502
281.4	0.530	138.48	283.3	0.849	120.4	[b]*1.365*	*292.5*	*65.023*	284.6	0.445	105.792
282.3	0.627	136.25	283.7	0.946	116.9				285.4	0.500	104.616
282.9	0.791	132.39	284.3	1.136	109.6				286.6	0.580	102.874
[b]*283.3*	*0.849*	*130.96*	[b]*285.3*	*1.531*	*89.2*				288.2	0.830	97.160
	R406A			R408A					289.9	1.027	92.260
275.8	0.112	124.6	274.9	0.148	142.1		R427A		[b]*291.4*	*1.270*	85.465
276.9	0.140	123.8	275.6	0.182	141.1	0.079	272.7	102.5			
278.8	0.199	122.3	278.1	0.301	137.7	0.095	274.6	102.2			
279.5	0.203	122.2	279.8	0.393	134.9	0.150	277.2	101.1			
281.1	0.310	119.4	281.3	0.555	130.0	0.286	281.2	98.5			
282.7	0.439	115.9	282.1	0.711	125.0	0.442	283.9	95.4			
283.7	0.536	113.3	282.6	0.787	122.5	0.639	286.3	91.4			
[b]*284.8*	*0.626*	*110.7*	[b]*283.7*	*0.926*	*117.7*	[b]*0.830*	*287.6*	*87.3*			

[a] u(T) = ±0.03 K, u(P) = ±0.01 MPa

[b] Critical decomposition point

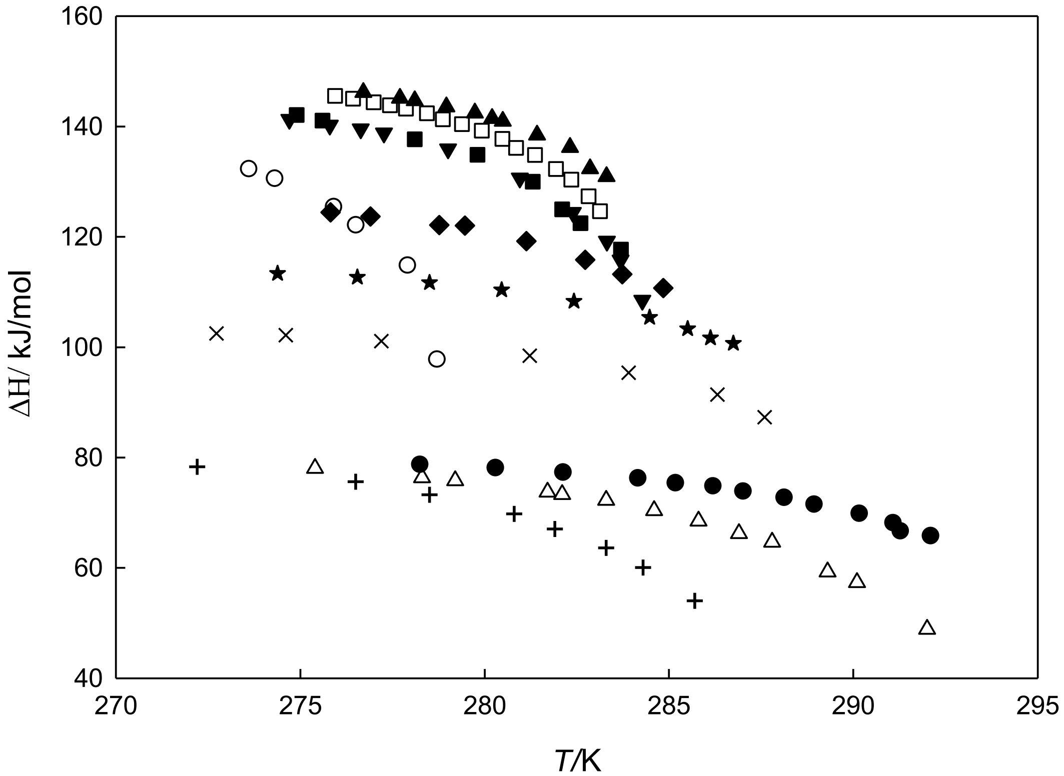

Figure 6.13. Temperature dependency of the hydrate dissociation enthalpies of: ★, R407C; ●, ×, R427A; ▲, R507C; ●, R410A; ♦, R406A;▼, R404A; ■, R408A;+, R508B;○, R116; □, R143a; Δ, R23; obtained in this study.

The enthalpy of hydrate dissociation decreases slowly with an increase in temperature as observed in Figure 6.13. Table 6.4 lists the enthalpy of hydrate dissociation for refrigerants measured in this study and that obtained from literature.

As observed from Table 6.4 comparing the values of enthalpy of hydrate dissociation, from the refrigerants proposed in this study R507C has the maximum value of 130.96 kJ/mol at its critical temperature of decomposition of 283.3 K. Hence, it is expected that R507C provides a cold storage medium with a larger storage capacity. The lowest enthalpy of hydrate dissociation of 54.2 kJ/mol was found for R32 at the corresponding critical temperature of decomposition of 294.1 K. Most of the refrigerants studied in this work show a comparable enthalpy of hydrate dissociation to those in literature.

Table 6.4. Comparison between hydrate dissociation enthalpy of proposed refrigerants in this study and those of the literature.

Refrigerant	^aT_C/K	^aP_C/MPa	ΔH/(kJ/mol)	Ref
R404A	285.3	1.531	89.20	This work
R406A	284.8	0.626	110.70	
R408A	283.7	0.926	117.70	
R410A	1.365	292.5	65.02	
R427A	272.7	0.079	87.30	
R407C	291.4	1.270	85.47	
R507C	283.3	0.849	130.96	
R23	292.0	3.440	48.89	(Mooijer-van den Heuvel et al., 2006)
R32	294.1	1.489	54.20	(Akiya et al., 1999)
R125a	284.4	0.944	108.20	
R134a	283.5	0.417	124.10	
R143a	283.1	0.81	117.14	(Hashimoto et al., 2010a)

^{a}critical decomposition point

6.1.2. Kinetic results

In this section the kinetics of hydrate formation rates were studied. Prior to the application of gas hydrates as a cold storage medium it is essential to be aware of their kinetics of hydrate formation. Therefore, in this study, the rate of the hydrate formation of the refrigerants studied was evaluated and the effect of some parameters such as initial pressure, initial temperature, degree of subcooling and addition of surfactants such as SDS on the hydrate nucleation and growth rate were investigated. The refrigerants studied in the kinetic experiments are R407C, R507C, R410A, R404A, R406A, R408A and R427A.

6.1.2.1. Initial conditions and degree of subcooling

Table 6.5 shows the initial conditions and the degree of subcooling (also known as driving force, $\Delta T = T\text{-}T_{equilibrium}$) for refrigerants investigated in this study. Figure 6.14 demonstrate the degree of subcooling for R407C. The graphs depicting the initial conditions for the remaining refrigerants are presented in Figures C.1 and C.2 included in Appendix C. Some figures are included in this section to illustrate the conclusions and observations.

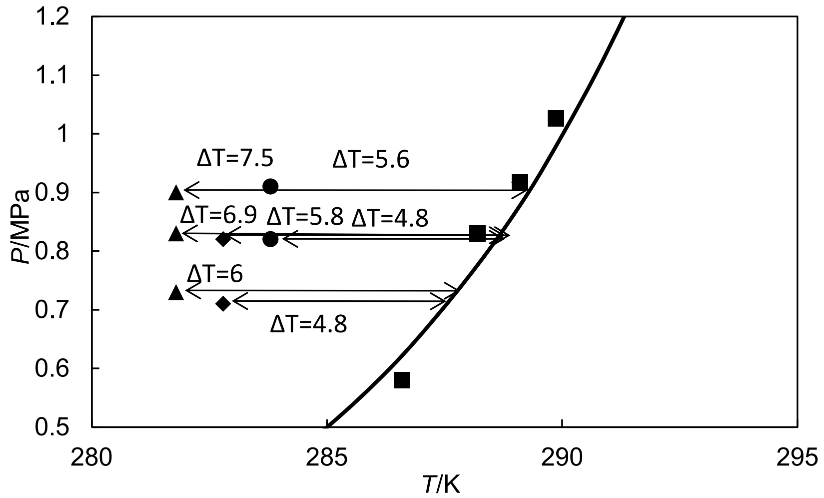

Figure 6.14. Initial conditions and degree of subcooling for R407C, ▲, 281.8K; ♦, 282.8K; ●, 283.8K; gas hydrate equilibrium conditions: ■, this work; Solid lines, model correlations.

In this study the initial conditions were selected in the hydrate stability zone to ensure the formation of the clathrate hydrate.

6.1.2.2. Induction time

As mentioned previously, after stabilization of the pressure during the solubility of the gas, the clathrate hydrate formation is confirmed by a dramatic drop in the pressure of the system. As depicted in Figure 6.15 the induction time is defined as the time elapsed before this pressure drop. Further graphical illustration of the pressure change before and during gas hydrate formation for the refrigerants studied at different initial condition is given in Figures C.3 to C.16 in Appendix C.

Table 6.5 shows the values of induction time obtained for the abovementioned refrigerants from Figures 6.15 and C.3 to C.16 at different initial pressures and temperatures. It is clear from Figure 6.15 as well as Figures C.3 to C.12 in Appendix C for the refrigerants R407C, R410A, R507C and R404A the induction time depends on the initial temperature and pressure (degree of subcooling) and it decreases with increasing driving force (ΔT). For instance, for the hydrate formation of R410A, with the driving force equal to ΔT = 4.8 K (temperature of 284.8 K and a pressure of 1 MPa) the induction time is more than one day while it decreases dramatically to the value of seven minutes with the driving force of ΔT = 5.53 K (pressure of 1.1 MPa). It should be mentioned that the energy consumption in a practical application increases with the high degree of subcooling. Therefore, an ideal value of the degree of subcooling should consider economic aspects.

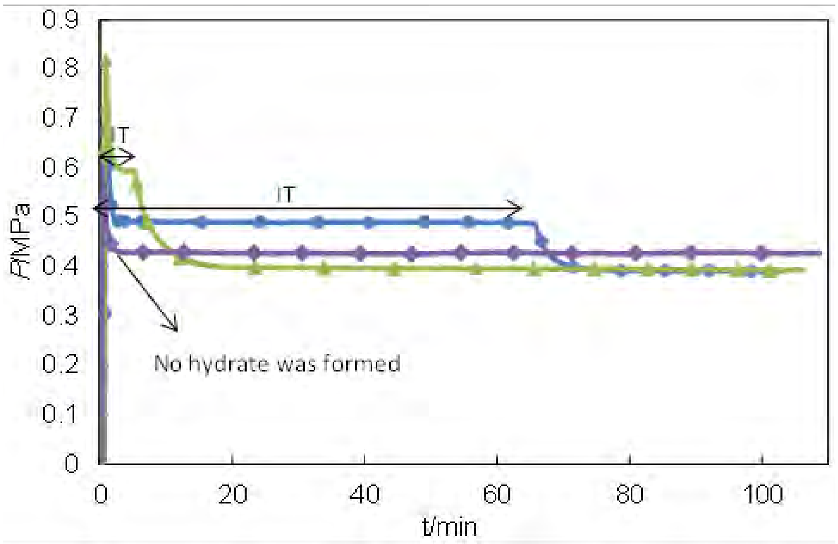

Figure 6.15. Pressure change during R407C hydrate formation at a constant temperature of 282.8 K and varying pressures with a stirrer speed at 620 rpm. ♦, 0.6 MPa; ●, 0.72 MPa; ▲, 0.82 MPa. IT, induction time.

Table 6.5. Induction time of hydrate formation for refrigerants used in this study in the presence of pure water[a].

Refrigerant	[b]T_0/K	[c]P_0 /MPa	ΔT/K	[d]IT /min
R410A	282.8	0.81	5.1	335
		0.93	6.3	0
		1.0	6.8	0
	283.8	0.92	5.2	39
		1.0	5.8	4
		1.1	6.5	2
	284.8	1.0	4.8	1673
		1.1	5.5	7
R407C	281.8	0.73	6.0	5
		0.83	6.9	4
		0.90	7.5	0
	282.8	0.71	4.8	65
		0.82	5.8	5
	283.8	0.82	4.8	9
		0.91	5.6	1
R507C	279.9	0.64	2.4	5
		0.71	2.9	4
		0.75	3.1	3
	280.9	0.81	2.2	5

Table 6.5 continued

R404A	281.0	1.170	3.3	2
	282.0	1.147	2.3	12
	283.0	1.220	1.5	[g]n.f.
R406A	282.0	0.651	2.2	0
	283.0	0.651	1.2	[g]n.f.
R408A	281.0	0.864	2.5	165
R427A	283.1	1.052	6	40

[a] u(T) = ±0.03 K, u(P) = ±0.01 MPa,

[b] Initial temperature; [c] Initial pressure; [d]Induction time;

As shown in Table 6.5 the highest temperature (with degree of subcooling equal to 4.8) with an appropriate induction time equal to 7 min was obtained using R410A. Nevertheless, the resultant pressure was relatively high (1.1 MPa). The lowest degree of subcooling equal to 2.2 was obtained for R406 A with an induction time equal to zero. The results obtained with R507C are also favourable with a temperature of 279.9 K, which is the lowest value found in all the measurements. The highest induction times with a high degree of subcooling equal to 6 is obtained for the refrigerants R427A in the presence of pure water which makes it less interesting for cold storage applications.

6.1.2.3. Gas hydrate formation and growth rate

The properties of Storage Capacity (SC), final water to hydrate conversion, final moles of gas consumed and the apparent rate constant at induction time were also obtained in this study for the refrigerants viz. R407C, R410A, R507C, R404A an R427A and are reported in Table 6.6 and Figures C.17 to C35 in Appendix C. Figures 6.16 and 6.17 show the effect of initial pressure at a constant temperature on storage capacity and apparent rate constant during R407C hydrate formation respectively.

Table 6.6. Final storage capacity, final water to hydrate conversion, final moles of gas consumed, apparent rate constant at induction time for refrigerants used in this study[a].

Refrigerant	[b]T_0/K	[c]P_0 /MPa	ΔT/ K	[d]IT /min	[e]SC/ (V/V)	Final water to hydrate conversion (mole %)	Final moles of gas consumed per moles of water	[f]$K_{app}\times10^9$ $\left(\frac{mole\,G}{(\text{mole W}).\text{min. Pa}}\right)$
R410A	282.8	0.81	5.1	335	1.9	1.2	0.002	2.1
		0.93	6.3	0	3.8	2.4	0.003	4.8
		1.0	6.8	0	4.5	2.8	0.003	5.2
	283.8	0.92	5.2	39	2.9	1.7	0.002	3.2
		1.0	5.8	4	3.5	2.1	0.003	4.4
		1.1	6.5	2	5.1	3.3	0.004	8.5
	284.8	1.0	4.8	1673	2.3	1.3	0.002	2.1
		1.1	5.5	7	4.2	1.6	0.002	4.2
R407C	281.8	0.73	6.0	5	3.1	3.8	0.002	16.5
		0.83	6.9	4	4.6	5.8	0.004	18.5
		0.90	7.5	0	9.1	11.5	0.007	29.3
	282.8	0.71	4.8	65	1.8	2.6	0.001	12.9
		0.82	5.8	5	3.8	4.7	0.003	16.2
	283.8	0.82	4.8	9	2.3	2.8	0.002	12.8
		0.91	5.6	1	5.1	6.4	0.004	28.1
R507C	279.9	0.64	2.4	5	3.5	4.2	0.003	3.1
		0.71	2.9	4	5.2	6.3	0.004	3.5
		0.75	3.1	3	5.5	6.5	0.004	5.0
	280.9	0.81	2.2	5	5.5	6.8	0.004	5.3
R404A	281.0	1.170	3.3	2	9.7	1.2	0.007	5.2
	282.0	1.147	2.3	12	7.9	1.0	0.006	4.8
	283.0	1.220	1.5	[g]n.f.	-	-	-	-
R406A	282.0	0.651	2.2	0	2.3	1.2	0.002	25
	283.0	0.651	1.2	[g]n.f.	-	-	-	-
R408A	281.0	0.864	2.5	165	2.7	3.1	0.003	0.6
R427A	283.1	1.052	6	40	3.0	2.2	0.002	0.4

[a] u(T) = ±0.03 K, u(P) = ±0.01 MPa,

[b] Initial temperature; [c] Initial pressure; [d]Induction time; [e] Storage Capacity; [f]Apparent rate constant; [g]no hydrate was formed

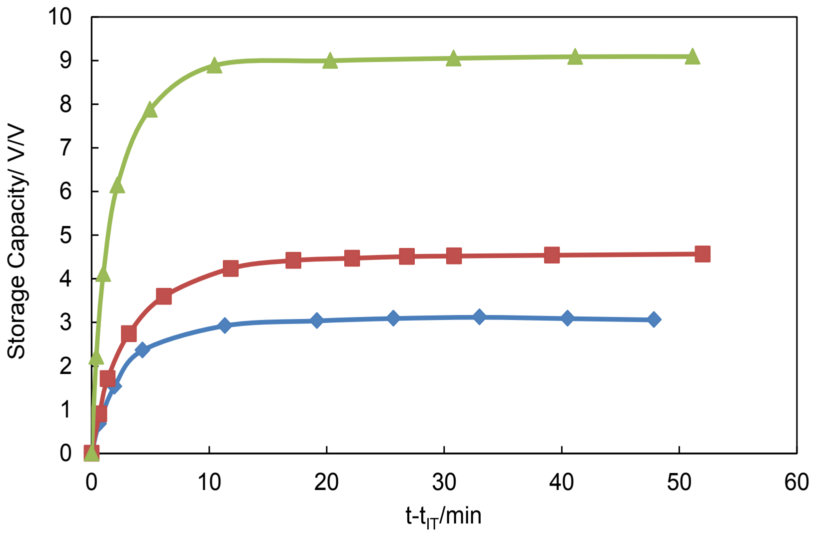

Figure 6.16. Storage Capacity during R407C hydrate growth at an initial temperature of 281.8 K and the initial pressures of: ♦, 0.73 MPa; ■, 0.81 MPa; ▲, 0.9 MPa in the presence of pure water, solid lines; trend lines.

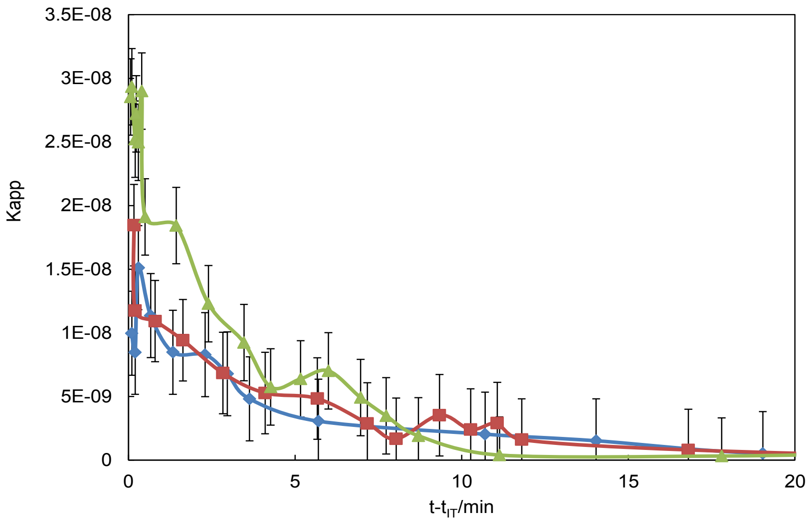

Figure 6.17. Apparent rate constant as a function of time during R407C hydrate growth at an initial temperature of 281.8 K and initial pressures of ♦,0.73; ■, 0.83; ▲, 0.9MPa; solid lines, trend lines.

During hydrate nucleation and growth, the storage capacity increases and the apparent rate constant decreases quickly to a constant value at which the hydrate formation is completed. One can observe from Figures 6.16 and 6.17 that the storage capacity and apparent rate constant increases with an increase in the initial pressure, at a particular temperature. According to the results obtained, the hydrate of R407C showed the maximum values of final storage capacity, final water to hydrate conversion, final moles of gas consumed and apparent rate constant at induction time with the degree of subcooling equal to 7.5 (initial temperature and pressure of 281.8 K and 0.9 MPa respectively). A comparatively high apparent rate constant was also obtained for R406A at initial temperature and pressure of 282 K and 0.651 MPa respectively with a low degree of subcooling equal to 2.2 compared to that of R407C. The lowest values of apparent rate constant was obtained for the refrigerants R408A and R427A. Figure 6.18 presents the apparent rate constant of the hydrate formation for the different refrigerants at different degree of subcooling. As observed from Figure 6.18 the maximum apparent rate constant at the lowest degree of subcooling is for R406A.

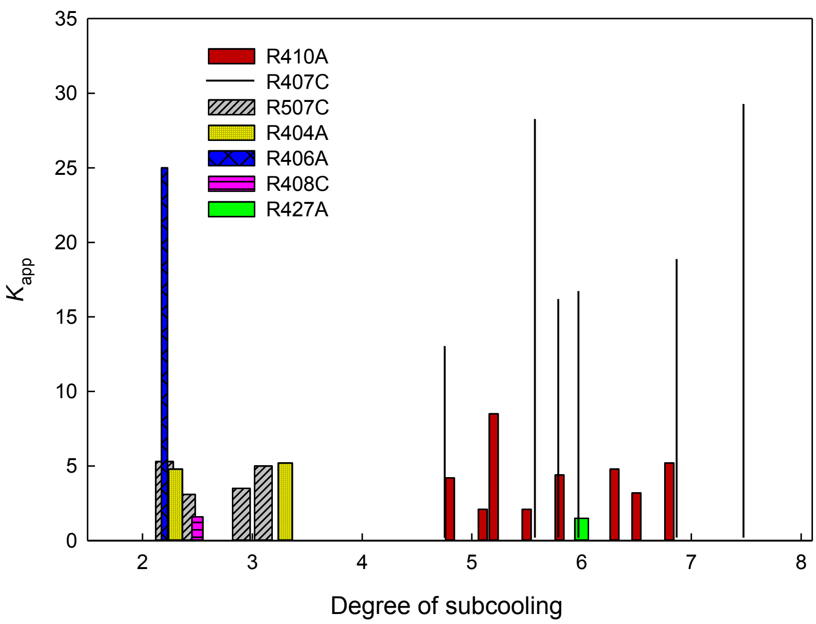

Figure 6.18. Apparent rate constant of refrigerant hydrates studied in the presence of pure water

6.1.2.4. Effect of liquefaction of refrigerant on hydrate nucleation

As was mentioned earlier, the hydrate nucleation and growth rate increase considerably with an increase in pressure. Nevertheless, as depicted in Figure 6.19 for the hydrate formation of R507C, with an increasing of the pressure the rate of the hydrate nucleation increases up to a particular pressure and at the higher pressures no hydrate formation was observed even after a significant period of time. The main reason for such behaviour is related to the formation of the liquid refrigerant (liquefaction of the refrigerant). With the formation of liquid phase the dispersion of the gas molecules into water decreases significantly resulting in the slow nucleation of hydrate. Therefore, before gas hydrate formation takes place it is essential to ensure that no liquid refrigerant has formed inside the cell.

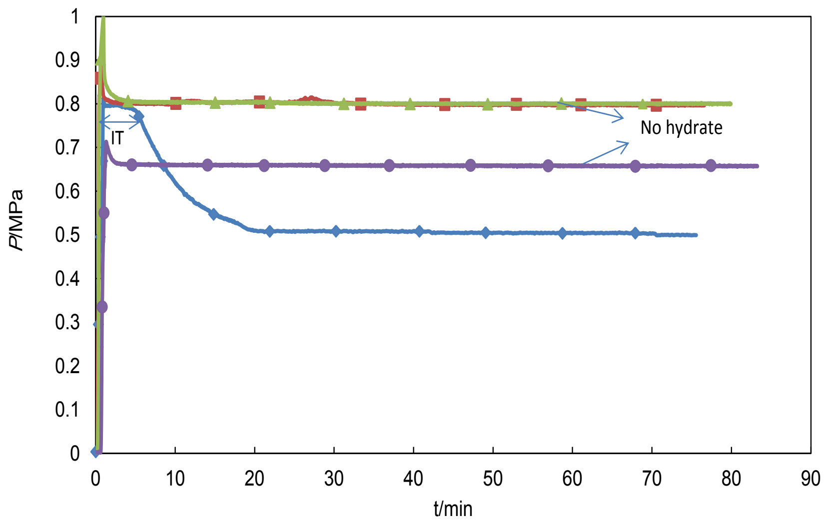

Figure 6.19. Pressure change during R507C hydrate formation at a constant temperature of 280.9 K and varying pressures, and 620 rpm stirrer speed: ●, 0.71 MPa; ♦, 0.81 MPa; ■, 0.91MPa; ▲, 1 MPa; IT, induction time; solid lines, trend lines.

6.1.2.5. Effect of SDS aqueous solution on the kinetics of gas hydrates

It has already been established that SDS has a promotion effect in methane hydrate nucleation (Zhang et al., 2007).This has been confirmed in this study by measuring the induction time of methane hydrates in the presence of SDS solution. As observed in Figure 6.20, the SDS solution increases the methane hydrate nucleation rate significantly. Hence the effect of the addition of a SDS solution on refrigerant hydrate nucleation at concentrations of 100 ppm, 400 ppm and 600 ppm was also considered in this study. The results are summarized in Table 6.7.

For some of the refrigerants considered in this thesis, an inhibition effect of SDS solution was observed on the gas hydrate formation rate and the hydrate nucleation was not initiated even after a considerable period of time. It has been established that, with the increasing of the SDS concentration the rate of the hydrate formation increases until a specific concentration of the SDS, after which the rate of the hydrate formation decreases (Zhang et al., 2007). Since for some refrigerants in this study SDS concentrations equal to or less than 100 ppm showed an inhibition effect on gas hydrate formation the effect of a higher concentration (e.g. 400 ppm) was also evaluated to confirm the measurements. Figure 6.21 shows the pressure change of R410A in the presence of pure water and 100 ppm SDS solution at the temperature and pressure equal to 283.8 K and 0.93 MPA respectively. The pressure change of R410 A in the presence of 400 ppm SDS solution is depicted in Figure C.11 in Appendix C. It is clear from Figures 6.21 and C.11 that the SDS solution with concentrations of 100 and 400 ppm SDS inhibited the hydrate formation of R410A. The pressure change before and during R507C hydrate formation in the presence of 100 and 400 ppm SDS aqueous solution is depicted in Figures C.9 and C.10 in Appendix C. As can be observed from Table 6.7 for R507C in the presence of 400 ppm SDS solution the induction time is about ten times greater than that of pure water and the apparent rate constant decreased significantly (Figures C.30 in Appendix C). However, there was no any significant change in the final storage capacity and only the slope of the storage capacity curve as the function of time decreased (Figures C.23 in Appendix C). For R407C no hydrate formation was detected at different SDS concentrations of 100 and 400 ppm.

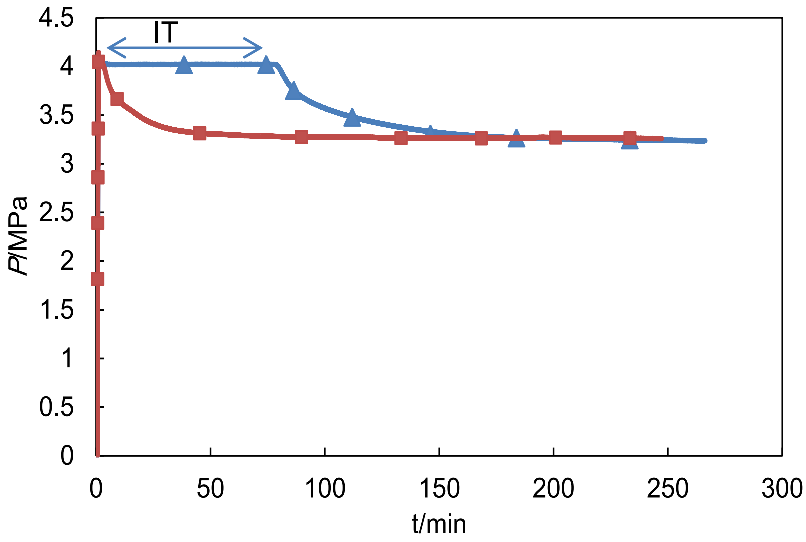

Figure 6.20. Pressure change during methane hydrate formation at a constant temperature of 275 K and 620 rpm stirrer speed, ▲, pure water, ■, 400 ppm SDS, IT, induction time; solid lines, trend lines.

Table 6.7. Induction time, final storage capacity, final water to hydrate conversion, final moles of gas consumed, apparent rate constant at induction time and the effect of SDS for refrigerants used in this study[a].

Refrigerant	[b]T_0/K	[c]P_0 /MPa	ΔT/ K	[d]IT /min	[e]SC/ (V/V)	Final water to hydrate conversion (mole %)	Final moles of gas consumed per moles of water	[f]$K_{app}\times 10^9$ $\left(\frac{mole\, G}{(\text{mole W}).\,\text{min. Pa}}\right)$
R410A	282.8	0.81	5.1	335	1.9	1.2	0.002	2.1
		0.93	6.3	0	3.8	2.4	0.003	4.8
		1.0	6.8	0	4.5	2.8	0.003	5.2
	283.8	0.92	6.5	39	2.9	1.7	0.002	3.2
		1.0	5.8	4	3.5	2.1	0.003	4.4
		1.1	5.2	2	5.1	3.3	0.004	8.5
	284.8	1.0	5.5	1673	2.3	1.3	0.002	2.1
		1.1	4.8	7	4.2	1.6	0.002	4.2
R407C	281.8	0.73	6.0	5	3.1	3.8	0.002	16.5
		0.83	6.9	4	4.6	5.8	0.004	18.5
		0.90	7.5	0	9.1	11.5	0.007	29.3
	282.8	0.71	4.8	65	1.8	2.6	0.001	12.9
		0.82	5.8	5	3.8	4.7	0.003	16.2
	283.8	0.82	4.8	9	2.3	2.8	0.002	12.8
		0.91	5.6	1	5.1	6.4	0.004	28.1
R507C	279.9	0.64	2.4	5	3.5	4.2	0.003	3.1
		0.71	2.9	4	5.2	6.3	0.004	3.5
		0.75	3.1	3	5.5	6.5	0.004	5.0
	280.9	0.81	2.2	5	5.5	6.8	0.004	5.3
R507C+400 ppm SDS	280.9	0.81	2.2	53	5.7	6.9	0.004	3.9
R404A	281.0	1.170	3.3	2	9.7	1.2	0.007	5.2
	282.0	1.147	2.3	12	7.9	1.0	0.006	4.8
	283.0	1.220	1.5	[g]n.f.	-	-	-	-
R404A+400 ppm SDS	282.0	1.147	2.3	5	8.9	11.4	0.007	4.9
R406A	282.0	0.651	2.2	0	2.3	1.2	0.002	15.6
	283.0	0.651	1.2	[g]n.f.	-	-	-	-
R406A+400 ppm SDS	282.0	0.651	2.2	0	3.2	1.7	0.002	41
R406A+400 ppm SDS	283.0	0.651	1.2	108	0.9	0.5	0.001	7.5
R406A+500 ppm SDS	283.0	0.651	1.2	54	1.2	0.6	0.002	8.1

Table 6.7 continued

R406A+600 ppm SDS	282.0	0.651	2.2	14	1.5	0.8	0.001	4.3
R408A	281.0	0.864	2.5	165	2.7	3.1	0.003	0.6
R408A+400 ppm SDS	281.0	0.864	2.5	170	4.0	4.7	0.003	1.6
R408A+600 ppm SDS	281.0	0.864	2.5	36	2.0	2.7	0.002	1.2
R427A	283.1	1.052	6	40	1.5	2.1	0.004	1.5
R427A+400 ppm SDS	283.1	1.019	6	3.5	2.4	3.1	0.005	1.9

[a] u(T) = 0.1 K, u(P) = 0.005 MPa,

[b] Initial temperature; [c] Initial pressure; [d]Induction time; [e] Storage Capacity; [f]Apparent rate constant; [g]no hydrate was formed

A different behaviour of hydrate formation in the presence of SDS solutions was observed for 404A, R406A, R408A and R427A. It is clear from Table 6.7 for the refrigerant R406A at the initial temperature and pressure of 283 K and 0.651 MPa respectively, in the presence of 400 ppm SDS solution the hydrate formation was promoted and as the result the induction time decreased and storage capacity as well as apparent rate constants increased (see Figures C.14, C25 and C.34 in Appendix C). However, a large value of induction time equal to 108 min was obtained. Hence, the effect of SDS solution with the concentration equal to 500 ppm was also investigated. The results showed that the promotion effect of 500 ppm SDS solution is larger than that of the 400 ppm (see Figures C.14 in Appendix C). Conversely, for R406A gas hydrate in the presence of SDS solution with the concentration of 600 ppm at the initial temperature and pressure of 282 K and 0.651 MPa respectively, the induction time increased significantly comparing to that of pure water and 400 ppm SDS solutions (Figure C.13 in Appendix C) and storage capacity as well as apparent rate constant decreased dramatically (refer to Appendix C, Figures C.25 and C.34). For R408A, as shown in Table 6.7 and Figure C.15 of Appendix C, SDS solution with the concentration of 400 ppm did not have a significant influence on the gas hydrate nucleation whereas a promotion effect was observed at a concentration of 600 ppm. The storage capacity and apparent rate constant as the function of time for R408A in the presence of pure water, 400 and 600 ppm SDS aqueous solutions are depicted in Figures C.26 and C.35 respectively. The hydrate formation rate of the refrigerants R404A and R427A are promoted using 400 ppm SDS solution (Figures C.12 and C.16 in Appendix C). Figures C.24 and C.33 in Appendix C show the change of the storage capacity and apparent rate constant as a function of time for R404A hydrate in the presence of pure water and 400 ppm SDS aqueous solution.

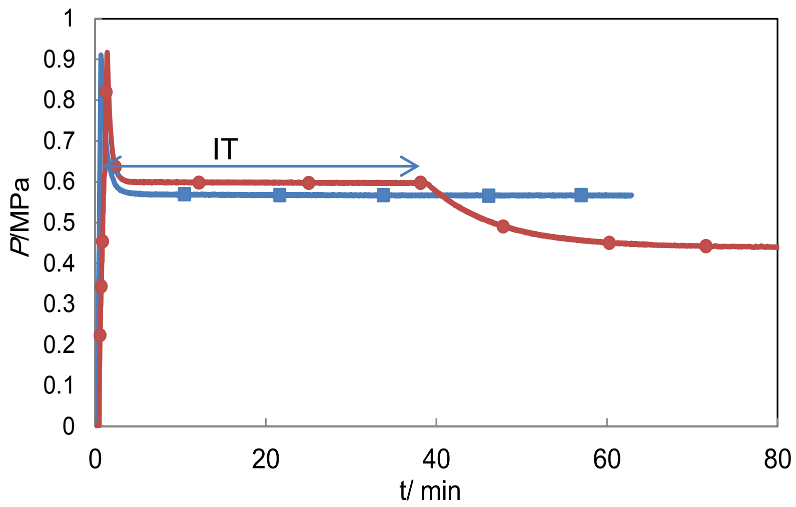

Figure 6.21. Pressure change during R410A hydrate formation at a constant temperature of 283.8 K and pressure of 0.92 MPa and 620 rpm stirrer speed; ■, 100 ppm SDS; ●, pure water; IT, induction time; solid lines, trend lines.

6.1.2.6. Summary of Kinetic results

Table 6.7 summarizes the results obtained in the kinetic study for all refrigerant blends in the presence of pure water as well as SDS solutions. According to the kinetic results, most of the refrigerants studied in this work show an appropriate behaviour suitable for use as a media in cold storage systems. The degree of subcooling, induction time, storage capacity and apparent rate constant are crucial parameters in selecting a refrigerant as a cold storage media. The SDS solution inhibited the hydrate formation for three refrigerants R410A, R407C and R507C and promoted the hydrate formation for the refrigerants R404A, R406 A, R408A and R427A. In the presence of pure water R406A is able to form a hydrate with a small degree of subcooling and high apparent rate constant. The highest apparent rate constant at a very low degree of subcooling is obtained for R406A hydrate in the presence of 400 ppm SDS solution. It was found that SDS solution increases the rate of the hydrate formation of R406A until 500 ppm concentration. The minimum degree of subcooling (driving force) needed for the formation of gas hydrate of R427Awas equal to 6 which is a highest value found of all the refrigerants studied. It should be noted that, the hydrate formation/dissociation pressure is a more attractive parameter for the selection of a refrigerant for the cold storage purposes. From the thermodynamic studies it was found that the hydrate dissociation pressure of R427A is lower than that of R406A.

6.2. Modelling results

A graphical illustration of the algorithm used in this study is shown in Figure 6.21. The algorithm of the model developed is able to estimate the phase equilibrium conditions from the incorporating of the PRSV EoS (Stryjek and Vera, 1986) with the van der Waals-Platteeuw hydrate model. The EoS parameters were calculated using MHV2-G^E (Michelsen, 1990, Dahl and Michelsen, 1990) mixing rule coupled with the UNIFAC activity model (Hashemi et al., 2015a, Hashemi et al., 2015b, Hashemi et al., 2014). Themodel used enabled an accurate calculation of the equilibrium conditions in systems with both hydrate forming and non-hydrate forming components. The interaction between water and gas molecules inside the hydrate cavities was taken to account using two approaches: Kiahara potential function and the correlation proposed by Parrish and Prautsnitz. (Parrish and Prausnitz, 1972) which were optimized for different pure refrigerants in this study. The model proposed by van der Waals-Platteeuw (vdWP) (Waals and Platteeuw, 2007) includes a number of parameters which are mostly model specific, for the some of which have been reported extensively in the literature such as structural parameters of the hydrate lattice (refer to chapter 3). The thermodynamic properties of the reference hydrate are also among such parameters which are included in Table C.1 in Appendix C. The PRSV EoS (Stryjek and Vera, 1986) requires four pure component parameters (T_C, P_C, ω and k_1). These parameters have been reported in Appendix C (Table C.2) for various components considered in this study. The UNIFAC group contribution activity model (Magnussen et al., 1981) contains two model specific parameters including volume and surface area parameters (see Appendix C). These parameters are given in Table C.3 . Depending on the structural composition of the molecules, the UNIFAC model also needs a number of temperature-independent group interaction parameters (see equation (B. 22)) which can be found in Appendix C (Table C.4) for various refrigerant main groups and water. In the algorithm shown in Figure 6.22 the weight function equal to 0.001 was chosen in the calculations.

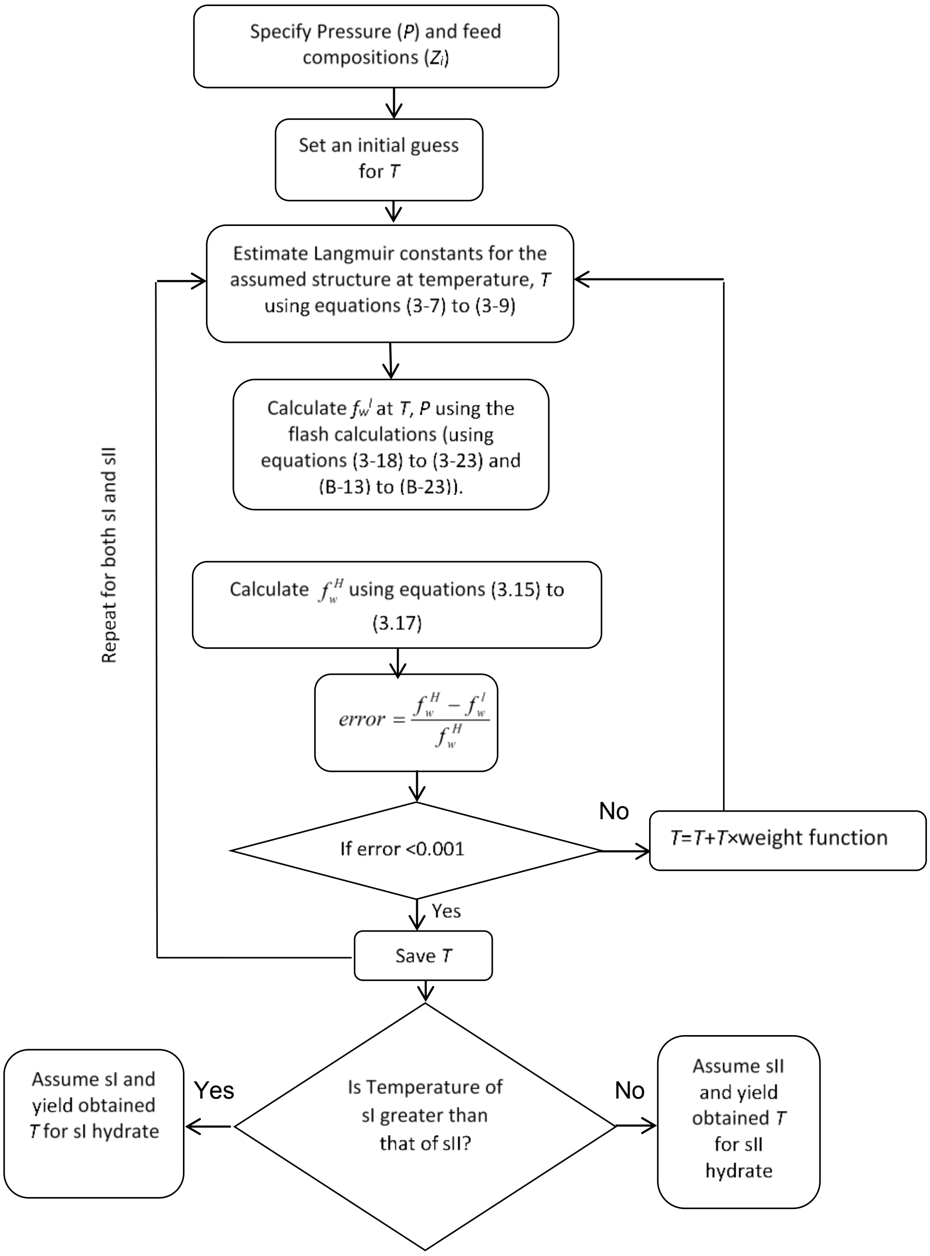

Figure 6.22. Flow chart of the algorithm used in fugacity approach using Newton Raphson method (Smith et al., 1996).

The hydrate dissociation conditions of different refrigerant hydrates in the following phase equilibrium boundary were estimated using an existing thermodynamic model from the literature : H-I-V, L_w-H-V and L_w-H-L_R. Generally (for both fluid phase modeling and hydrate modeling), in cases, where correlation of parameters is needed, optimisation is done by minimising the sum of absolute relative deviations between model regressions and experimental data. The objective function is defined as in the following equation:

$$F_{obj} = \left(\frac{1}{NDP}\right)\sum_{k=1}^{NDP}\left(\frac{|T_{\exp} - T_{cal}|}{T_{\exp}}\right)_k \tag{6.2}$$

Where T_{exp} and T_{cal} are defined as the experimental and calculated hydrate dissociation temperatures respectively and *NDP* stands for the number of data points. Optimisation of the parameters in this study is performed by application of an optimisation procedure based on MATLAB® genetic algorithm.

As mentioned previously, in this study, two approaches including the Kihara potential function and the empirical equation (3.10) was employed for the estimation of the interaction parameters between the gas and water molecules (Langmuir constant) in the hydrate structure.

Tables 6.8 and 6.9 show the Kihara parameters as well as the parameters of equation (3.10) which are obtained using the minimisation of equation (6.2) for different refrigerants. The experimental data reported in Table 6.10 as well as those obtained in this study are used for the optimization of the parameters reported in Tables 6.8 and 6.9. These pure parameters are also applied for the modelling of the hydrate dissociation conditions for the mixed refrigerant hydrates (Hashemi et al., 2014, Hashemi et al., 2015b).

Table 6.8. Kihara parameters optimized in this study

Refrigerant	*a*/ Å	σ/ Å	ε/k/ K
R11(CCl_3F)	0.922	3.622	310.60
R12(CCl_2F_2)	0.910	3.614	277.80
R13($CClF_3$)	0.917	3.660	309.30
R22($CHClF_2$)	0.913	2.840	256.41
R23(CHF_3)	0.910	3.100	200.00
R32(CH_2F_2)	0.790	2.890	198.60
R134a($C_2H_2F_4$)	1.311	2.722	241.32
R143a($C_2H_3F_3$)	1.220	3.100	202.30
R141b($C_2H_2F_4$)	0.870	3.172	232.70
R125a(C_2HF_5)	1.321	2.574	270.12
R152a($C_2H_4F_2$)	0.952	2.958	205.98
R116(C2F6)	1.080	2.79	230.00
R600a(C4H10)	0.910	3.590	215.98
R142b($C_2H_3ClF_2$)	1.430	3.172	232.70

Table 6.9. Optimized parameters of equation (3.10)[a].

Refrigerants	Small cavities		Large cavities/ K	
	A_{ml}/ K/MPa	B_{ml}/K	A_{ml}/ K/MPa	B_{ml}/K
		Structure I cavities		
R23(CHF_3)	8.18×10^{-4}	5.20×10^{-4}	2.21×10^{-10}	5.29×10^{3}
R32(CH_2F_2)	3.71×10^{-4}	4.11×10^{3}	3.92×10^{-4}	2.54×10^{-3}
R152a($C_2H_4F_2$)	0	0	3.00×10^{-10}	5.70×10^{-3}
		Structure II cavities		
R11(CCl3F)	0	0	8.20×10^{-10}	6.60×10^{3}
R12(CCl_2F_2)	0	0	2.17×10^{-6}	4.10×10^{3}
R13($CClF_3$)	0	0	4.17×10^{-6}	5.80×10^{3}
R32(CH_2F_2)	4.1×10^{-6}	1.4×10^{3}	3.80×10^{-7}	3.90×10^{3}
R22($CHClF_2$)	7.18×10^{-4}	3.2×10^{-4}	3.21×10^{-10}	6.12×10^{3}
R134a($C_2H_2F_4$)	0	0	7.4×10^{-8}	4.98×10^{3}
R143a($C_2H_3F_3$)	0	1.51×10^{3}	1.14×10^{-7}	4.77×10^{3}
R141b($C_2H_2F_4$)	0	0	1.33×10^{-7}	5.33×10^{3}
R125a(C_2HF_5)	0	0	2.37×10^{-7}	4.45×10^{3}

[a] $C_{ij} = \frac{A_{ij}}{T}\exp\left[\frac{B_{ij}}{T}\right]$

When comparing the model results to the experimental data, the term Average Absolute (relative) Deviation (AAD) is used where AAD is defined according to equation (6.3):

$$AAD\% = \left(\frac{100}{NDP}\right)\sum_{k=1}^{NDP}\left(\frac{\left|T_{\exp}-T_{cal}\right|}{T_{\exp}}\right)_k \quad (6.3)$$

where T_{exp} and T_{cal} are defined as the experimental and calculated hydrate dissociation temperatures respectively and NDP stands for the number of data points.

The AAD%'s of the model using the Kihara approach and the empirical equation (3.10) as well as the structure of the hydrates are shown in Table 6.10 for pure refrigerants and Tables 6.11 and 6.12 for refrigerant blends at three abovementioned hydrate phase equilibrium boundaries. The model results for the remaining refrigerants are depicted graphically in Figures C.36 to C.51 in Appendix C for pure and mixed refrigerant hydrates. Figures 6.23 and 6.24 show a comparison between modelling results and experimental data for the pure refrigerant R134a as well as refrigerant blend R507C at different phase equilibrium regions (H-I-V), (L_W-H-V) and (H-L_W-L_R).

As presented in Figure 6.23, 6.24 as well as in Tables 6.10 to 6.12, there is a reasonable agreement between the modelling results and the experimental data for both pure and mixed refrigerants in the three abovementioned hydrate phase boundaries. As observed in Figure 6.23 for the H-I-V and L_w-H-V phase boundaries there is a slight difference between modelling results using Kihara approach and the empirical equation (3.10). However, one can observe from Tables 6.10 and 6.11 that at H-L_w-L_R hydrate phase boundary the Kihara potential function is giving more consistent results than those obtained using the empirical equation (3.10) in most cases. The maximum AAD% of 0.29 and 0.90 and the minimum values of 0.02 and 0.01 were obtained for Kihara and empirical approach respectively.

It should be noted that as long as the refrigerant is in the gaseous state the possible maximum hydrate dissociation temperature equals to the upper quadruple temperature of that refrigerant (T_{Q_2}). Hence, in order to release the heat produced by the gas hydrate formation in a cold storage system the temperature of the utilized reservoir fluid needs to be lower than T_{Q_2}. Consequently, the knowledge of the upper quadruple point is of great interest in cold storage systems. The upper and lower quadruple points Q_1 (L_w-H-I -V) and Q_2 (L_w -H- L_R-V) (see Figure 6.23) are also estimated in this study and compared to the experimental data for pure refrigerants. In this study the upper and lower quadruple points were estimated using the developed model. The upper quadruple was chosen as the intersection point between L_w-H-V and H-L_w-L_R curves and the lower quadruple point was selected as the intersection between H-I-V and L_w-H-V curves. The results are depicted in Tables 6.13 and 6.14 as well as Figures 6.23 and C.36 to C.47 (Appendix C) for pure refrigerants.

As can be observed from Tables 6.13 and 6.14 there is a reasonable agreement between values of Q_1 and Q_2 estimated using the model in this study and experimental data obtained in literature.

Table 6.10. AAD% of the model for different pure refrigerant hydrate dissociation conditions.

Refrigerant	*AAD%						Structure	Ref
	Based on Eq. (3.6)			Based on Eq. (3.10)				
	H-I-V	L_w-H-V	H- L_w-L_R	H-I-V	L_w-H-V	H- L_w-L_R		
R11	0.29	0.08	-	0.28	0.07	-	II	(Carbajo, 1983, Wittstruck et al., 1961)
R12	0.14	0.11	-	0.51	0.15	-	II	(Carbajo, 1983, Wittstruck et al., 1961)
R13	-	0.02	0.09	-	0.03	0.01	II	(Kubota et al., 1984)
R22	0.17	0.09	-	0.12	0.09	-	II	(Javanmardi et al., 2004, Wittstruck et al., 1961, Chun et al., 1996)
R32	-	0.09	0.12	-	0.15	0.04	I	(Mohammadi and Richon, 2010, Hashimoto et al., 2010b, Akiya et al., 1999)
R23	0.04	0.12	0.09	0.07	0.17	0.29	I	This work, (Kubota et al., 1984, Mooijer-van den Heuvel et al., 2006)
R134a	0.10	0.10	0.04	0.18	0.07	0.07	II	This work, (Mohammadi and Richon, 2010, Liang et al., 2001, Hashimoto et al., 2010a, Akiya et al., 1999)
R143a	-	0.05	0.06	-	0.02	0.03	II	(Hashimoto et al., 2010a)
R141b	0.13	0.02	-	0.13	0.07	-	II	(Liang et al., 2001)
R125a	-	0.14	0.18	-	0.09	0.22	II	This work, (Akiya et al., 1999, Hashimoto et al., 2010a)
R152a	0.14	0.17	0.04	0.90	0.08	0.22	I	(Kubota et al., 1984, Mohammadi and Richon, 2010, Liang et al., 2001)

Table 6.11. Comparison between the model results and experimental hydrate dissociation data obtained in this study for refrigerant blends.

Refrigerant	AAD%					Ref
	Based on Eq. (3.10)		Based on Eq. (3.6)			
	L_w-H-V	H-L_w-L_R-V	L_w-H-V	H-L_w-L_R-V	Structure	
R507C	0.03	-	0.05	-	II	This work
R410A	0.13	-	0.09	-	II	(Akiya et al., 1999); this work
R407C	0.19	-	0.10	-	II	(Akiya et al., 1999); this work
R11+R12	-	0.03	-	0.06	II	(Carbajo, 1983)
R11+R114	-	0.09	-	0.14	II	(Carbajo, 1983)
R12+R114	-	0.08	-	0.20	II	(Carbajo, 1983)

Table 6.12. Comparison between the model results and experimental hydrate dissociation data obtained in this study using the Kihara approach.

Refrigerant	T_{range}/K	P_{range}/MPa	Structure	AAD%
R427A	272.7-287.9	0.079-7.623	II	0.1
R404A	274.7-286.5	0.128-9.995	II	0.1
R406A	275.8-286.2	0.112-9.081	II	0.1
R408A	274.9-285	0.148-6.10	II	0.1
R508B	272.2-286.6	0.527-8.957	II	0.2
R116	273.6-280.1	0.521-7.371	II	0.1

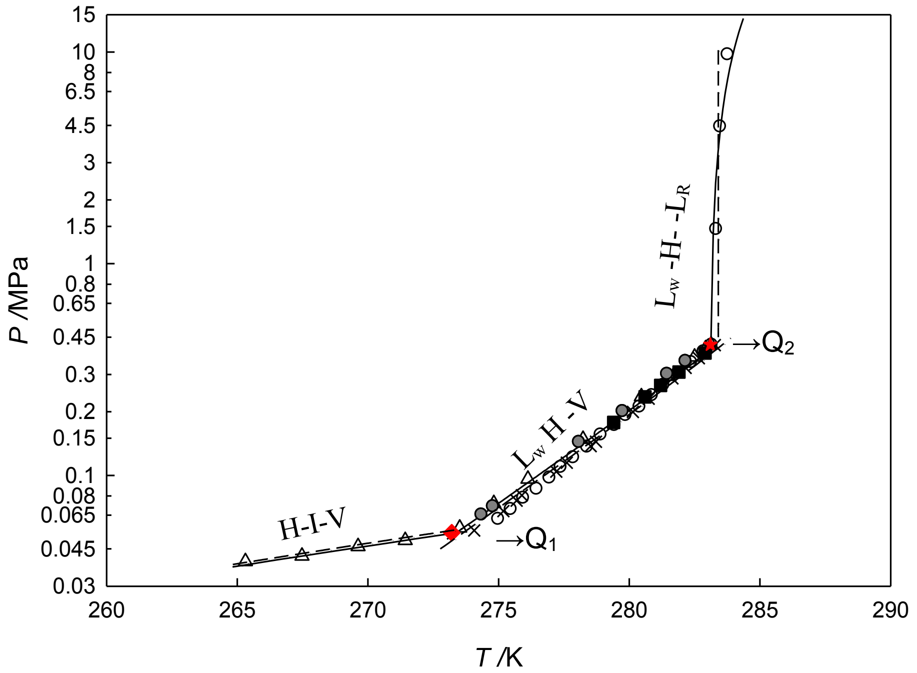

Figure 6.23. Hydrate phase diagram of R134a ($C_2H_2F_4$); Experimental data:●, this work; ■, (Mohammadi and Richon, 2010); Δ, (Liang et al., 2001);○, (Hashimoto et al., 2010a); ×, (Akiya et al., 1999); ★ , upper quadruple point, (Liang et al., 2001); ♦, lower quadruple point (Mori and Mori, 1989b); Solid lines, model predictions using the Kihara approach, dash lines model predictions using the Parrish and Prausnitz (1972) approach.

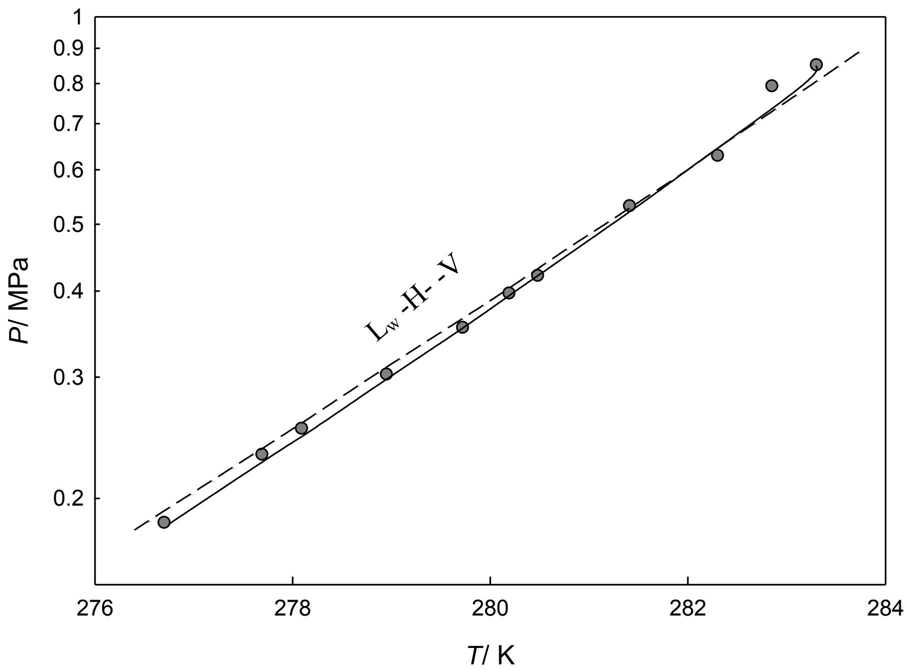

Figure 6.24. Hydrate phase diagram of R507C (mixture of R125a/R143A) with mole percent respectively:70/30); Experimental data:●, this work; solid lines, model predictions using the Kihara approach, dash lines model predictions using the Parrish and Prausnitz (1972) approach.

Table 6.13. Prediction of the upper quadruple point, Q_2, for various refrigerants used in this study.

Refrigerant	Q_2				Ref.
	P_{exp} /MPa	T_{exp}/K	P_{pred}/MPa	$T_{Pred.}$/K	
R134a	0.414	283.13	0.400	283.11	(Liang et al., 2001)
R143a	0.838	283.33	0.800	283.32	(Hashimoto et al., 2010a)
R125a	0.930	283.95	0.870	283.62	(Hashimoto et al., 2010a)
R152a	0.444	288.15	0.550	288.01	(Liang et al., 2001)
R141b	0.040	281.49	0.042	281.70	(Liang et al., 2001)
R11	0.059	281.85	0.058	281.60	(Carbajo, 1983)
R12	0.449	285.25	0.440	284.40	(Carbajo, 1983)
R13	-	-	2.500	281.70	-
R22	0.768	289.45	0.830	290.60	(Carbajo, 1983)
R32	1.450	293.16	1.500	292.68	(Hashimoto et al., 2010b)
R23	-	-	3.650	291.80	-

Table 6.14. Prediction of the lower quadruple point, Q_1, for various refrigerants and their mixtures used in this study.

Refrigerant	Q_1				
	P_{exp} /MPa	T_{exp}/K	P_{pred} /MPa	$T_{Pred.}$/K	Ref.
R32	-	-	0.1600	272.8	-
R134a	0.0537	273.21	0.0566	273.5	(Liang et al., 2001)
R141b	0.0075	273.14	0.0087	273.3	(Liang et al., 2001)
R143a	-	-	0.0900	273.3	-
R125a	-	-	0.0903	273.7	-
R152a	0.0739	273.16	0.0706	273.7	(Liang et al., 2001)
R11	-	-	0.0082	272.9	-
R12	-	-	0.0370	273.2	-
R13	-	-	0.1500	269.5	-
R22	0.0870	272.9	0.0840	272.7	(Wittstruck et al., 1961)
R23	-	-	0.3500	274.2	-
R407C	-	-	0.0520	273.0	-
R410A	-	-	0.1100	273.3	-

The Kihara potential function parameters as well as those of correlation (3.10) for 14 pure refrigerants were optimized in this study most of which are newly reported and cannot be found in the open literature. The parameters optimized for pure refrigerants were applied to estimate the hydrate dissociation conditions of their blends. There were slight differences between the results of the two models and a reasonable agreement was found between the modelling results and experimental dissociation data in different hydrate equilibrium phase boundaries. However, the application of correlation (3.10) is recommended because of the complexity of Kihara potential function approach. Using the developed model in this study the hydrate dissociation conditions of a new refrigerant blend for which there is no experimental data available in literature can be estimated. The upper and lower quadruple point for pure refrigerants was estimated and compared to the experimental data in literature. A good agreement was observed between the model results and experimental data. For some of the refrigerants considered in this study no quadruple points can be found in literature and only the modelling results are reported.

The structure of the gas hydrate was also predicted using the model developed in this study. It was found that except R23, R32 and R152a which are forming structure I of gas hydrate, all the refrigerants studied are forming structure II of gas hydrate.

6.3. Summary of the experimental results

Generally, the following properties of the refrigerants for use in cold storage systems are desired:

- Low pressure of hydrate formation/dissociation (which is the most relevant parameter)
- High temperature of critical decomposition point
- The large enthalpy of phase change resulting in the high density of cold storage
- High value of the hydrate formation rate (K_{app})
- Low induction time of hydrate formation (IT)
- Low degree of subcooling for the hydrate formation (ΔT)

In this study according to the thermodynamic and kinetic results three refrigerants viz. R407C, R427A and R406A showed an appropriate behaviour for use as a cold storage media considering the abovementioned parameters. Table 6.15 summarizes the advantage and disadvantages of the refrigerants considered in this study and those of the literature for use as a cold storage media.

Table 6.15. Advantages and disadvantages of the refrigerants studied in this work and those of the literature for the application as a cold storage media.

Refrigerant	advantage	disadvantage
R404A	High enthalpy of dissociation, Low induction time, promotion effect of SDS solution	high pressure of dissociation, high price, low K_{app},
R406A	Low pressure of dissociation, high enthalpy of dissociation, low induction time, high K_{app}, low price, promotion effect of SDS solution	Low temperature of critical decomposition
R408A	High enthalpy of dissociation, promotion effect of SDS solution	high pressure of dissociation, high induction time, low K_{app}
R427A	Low pressure of dissociation, high enthalpy of dissociation, high temperature of critical decomposition, promotion effect of SDS solution	high induction time, low K_{app}, high price,
R407C	Low pressure of dissociation, high enthalpy of dissociation, low induction time, high K_{app}, high temperature of critical decomposition,	inhibition effect of SDS solution, high price
R410A	high temperature of critical decomposition	low enthalpy of dissociation, high price, inhibition effect of SDS solution, high degree of subcooling,
R507C	high enthalpy of dissociation, low price, low induction time	high pressure of dissociation, low K_{app}, inhibition effect of SDS solution
R508B		high pressure of dissociation, low enthalpy of dissociation, high price,

Table 6.15 continued

R116		high pressure of dissociation, low enthalpy of dissociation, high price,
R134A	Low pressure of dissociation, high enthalpy of dissociation, promotion effect of alumina or zinc	low temperature of critical decomposition,
R143A	Low pressure of dissociation, high enthalpy of dissociation	low temperature of critical decomposition,
R32	high temperature of critical decomposition	High pressure of dissociation, Low enthalpy of dissociation, high price
R23	high temperature of critical decomposition	High pressure of dissociation, Low enthalpy of dissociation,

According to the thermodynamic results (section 6.1.1), R427A and R407C showed the minimum hydrate dissociation pressure between the refrigerants studied in this work and those used in the literature (such as R143a, R32, R23 and R125a) (Akiya et al., 1999, Mooijer-van den Heuvel et al., 2006, Hashimoto et al., 2010b, Hashimoto et al., 2010a) with a high temperatures of critical decomposition (287.6 K and 291.4 respectively) resulting in the high possible hydrate formation temperature. The temperature and pressure range of (272.7-287.6) K and (0.0791-0.830) MPa was found for R427A respectively at L_w-H-V phase equilibrium boundary. The hydrate dissociation pressure and temperature range of (0.106-1.27) MPa and (275.8-291.4) K was found for R407C. However, for R427A and R407C relatively low enthalpy of hydrate dissociation (87.3 and 85.5 kJ/mol respectively) were found which are still higher than that of R32 and R23 used in literature. Form a kinetic perspective, a comparatively high induction time with high degree of subcooling (equal to 6) resulting in a low apparent rate constant were found for R427A hydrate (section 6.1.2). The maximum apparent rate constant of the hydrate formation in the presence of pure water was obtained for R407C. An inhibition effect of the SDS solution was found for R407C gas hydrate.

It was found from the thermodynamic and kinetic results that R406A is an appropriate candidate for use in cold storage systems. The hydrate dissociation temperature and pressure range of (275.8-283.7) K and (0.112-0.536) were found for R406A. At a constant temperature, the pressure of the R406A hydrate dissociation is slightly higher than that of R427A and

R407C and lower than the refrigerants such as R143a, R32 and R23 used in the literature (Akiya et al., 1999, Mooijer-van den Heuvel et al., 2006, Hashimoto et al., 2010b, Hashimoto et al., 2010a). The relatively high enthalpy of hydrate dissociation equal to 110.75 kJ/mol was found for R406A at its critical decomposition temperature. The induction time and degree of subcooling are zero and 2.2 respectively for R406A which are amongst the lowest values obtained in this study for the refrigerants investigated. Furthermore, a promoting effect of SDS solution was found for R406A at the presence of the 400 and 500 ppm SDS solution. The hydrate formation R406A was observed after 54 minutes in the presence 500 ppm SDS solution with the degree of subcooling equal to 1.2 which is the lowest value obtained in this study. Furthermore, the highest apparent rate constant was related to the R406A+400 ppm SDS. Additionally, from an economical perspective R406A has a lower price than R427A, R407C and the refrigerants used in literature such as R125a, R134a and R32.

6.4. Conceptualized cold storage process: application of the equilibrium and kinetics data

A conceptual diagram of a cold storage process proposed in this study is depicted Figure 6.25. Gas hydrate storage systems can be considered as storage heat exchangers in which an amount of heat removed from a building is applied to dissociate the hydrate inside a tank and after a period this heat is removed from the tank (thereby forming the gas hydrate once again) and rejected to the outdoor environment using chiller. The process is comprised of three generic components: (1) the hydrate manufacturer (storage component) (2) the refrigerating component or cooling unit (3) the discharge component.

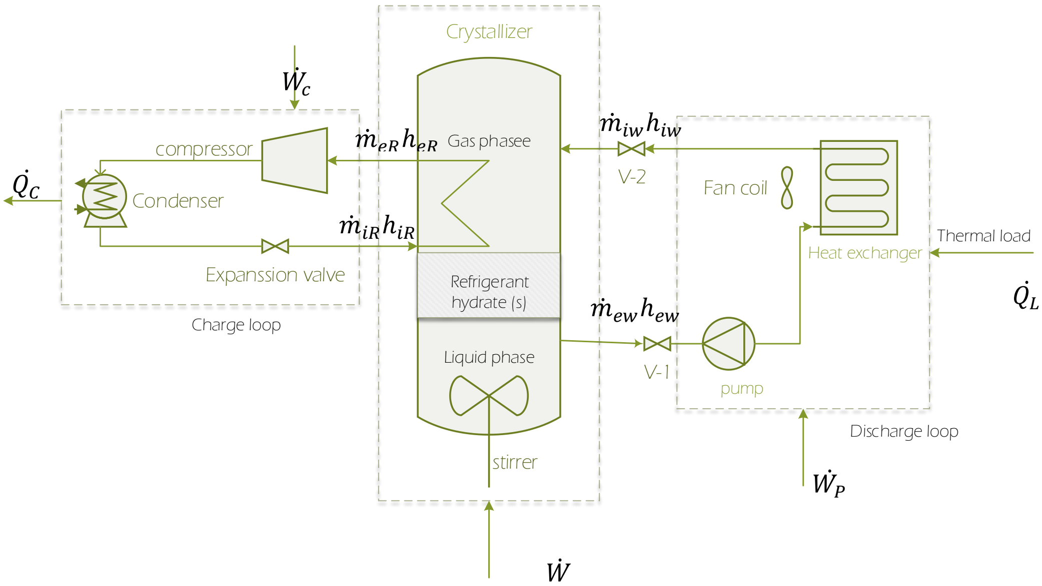

Figure 6.25. Conceptual design of a cold storage process using refrigerant hydrates

In the charge loop which is operating during off-peak hours the refrigerant or coolant and the contents of the cold storage tank are not in direct contact; this is to avoid the plugging of the equipment during gas hydrate formation. Even though the application of direct contact charge process would provide better heat transfer between cold storage medium and the coolant due to the effective dispersion of the phases, however an expensive water separation unit is required in this condition and also there is the possibility of plugging of the fitting due to the hydrate formation. The charge loop is a simple refrigeration cycle which carries the cold energy to the tank for the formation of gas hydrate. In this stage in order to improve the dispersion of the phases, a mechanical blender is utilized in the tank. According to the kinetic studies the agitation combined with addition of a sufficient amount of SDS (400 ppm in 16 cm^3 of pure water) would efficiently promote the diffusion of the phases and effectively increase the hydrate formation rate with the induction time equal to zero (see Tables 6.7 and 6.15). This system can operate effectively with low pressure refrigerants introduced in the thermodynamic study carried out in this thesis. According to the results obtained in this thesis, R406A combined with 400 ppm SDS in 16 cm^3 of pure water would provide enhanced cold storage medium.

The discharge loop operates at peak hours to provide the cold energy to the medium. In this loop the gas hydrate and the refrigerant are in direct contact in order to provide effective heat transfer. As observed in Figure 6.25 the refrigerant enters to the storage tank trough valve 2, loses the heat and dissociates the gas hydrate which is formed earlier in the charge loop. The refrigerant is then pumped to a heat exchanger to the air-conditioned unit.

6.4.1. Storage performance

A simple thermodynamic description of the gas hydrate cold storage process considers a control volume drawn around the storage tank of a direct expansion crystallizer with agitation as shown in Figure 2.1. An energy balance is sustained at all times for this process is specified by:

$$(\dot{m}_{iw}h_{iw} - \dot{m}_{ew}h_{ew}) + (\dot{m}_{iR}h_{iR} - \dot{m}_{eR}h_{eR}) + \dot{Q} + \dot{W} = \frac{dU}{dt} \qquad (6.4)$$

where,

$\frac{dU}{dt}$= rate of change of internal energy in the tank

i= inlet,

e= exit,

$\dot{m}$= mass flow rate

$\dot{Q}$= energy flow rate as heat gains through the tank,

$\dot{W}$= energy flow as mechanical agitation,

h=enthalpy,

R= refrigerant,

W= water

This energy balance is made based on the assumption that water and refrigerate are the only components that can enter or exit the storage vessel. One of the most important storage parameters are the system internal energy U and the rate of the change of this parameter during charging with the refrigeration loop and discharging using a heat load imposed on the system.

For a sensible heat storage system it is simple to determine the change in the internal energy dU/dt from the temperature changes. However, in the case of hydrate storage involving latent heat, storage temperatures alone are not enough to determine the thermodynamic state and internal energy at any time. Nonetheless, the instantaneous rate of the change of internal energy can be determined indirectly from Equation (6.4) which can be integrated over time to yield the internal energy of the system at any time, a parameter that indicates how much hydrate is present in the storage tank during charging and discharging processes.

7

Conclusions

Experimental thermodynamics plays an important role in the design of economical, sustainable and safe technologies. In this work the potential of the refrigerant hydrates as a medium in cold storage technology has been investigated by means of experimental and thermodynamic modelling studies. In order to encourage the application of the gas hydrates in cold storage refrigeration systems, a review of contemporary research advancement considering the properties of clathrate/semi-clathrate hydrates, enhancing of the clathrate/semi-clathrate hydrate characteristics, and cold storage technology based on the clathrate/semi-clathrate hydrates is presented. It was found that mixed clathrate hydrates are more useful in cold storage applications. Refrigerant clathrate hydrates, CO_2 clathrate/semi-clathrate hydrates as well as techniques to enhance their phase change characteristics are presented. Furthermore, different configurations of cold storage systems based on the formation/dissociation of clathrate/semi-clathrate hydrate as well as their advantages and drawbacks are presented.

As presented in the review chapter, cold storage based gas hydrate formation/dissociation, has a clear advantage over water in respect of cold storage density; over ice for the appropriate formation/dissociation temperature; and over eutectic salts for the outstanding phase change enthalpy and ageing resistance.

The hydrate dissociation conditions of pure refrigerants viz. R22 ($CHClF_2$), R23 (CHF_3), R134a ($C_2H_2F_4$), R125a (C_2HF_5) were measured experimentally based on two hydrate phase boundaries including L_w-H-V and H-L_w-L_R and compared to the literature data. Good agreement was observed between experimental data obtained in this study and those of literature which confirms the reliability of the experimental procedure and technique. The hydrate dissociation conditions for the new systems R410A (R32/R125a), R507C (R143a/R125a) and R407C (R32/R125a/R134a), R404A (R143a/ R125/ R134a), R406A (R22/ R142b/R600a), R408A (R143a/ R125/ R22), R427A (R134a/ R125/ R32/ R143a), R508B (R23/R116), R116 as well as HFPO were measured experimentally. It was found that HFPO cannot form hydrate due to its large molecular size. The kinetics of the hydrate formation of the refrigerants R410A (R32/R125a), R507C (R143a/R125a) and R407C (R32/R125a/R134a), R404A (R143a/ R125/ R134a), R406A (R22/ R142b/R600a), R408A (R143a/ R125/ R22), R427A (R134a/ R125/ R32/ R143a) were studied. To the best of our knowledge there is no kinetic study on refrigerant hydrate formation in the literature considering the parameters undertaken in this study.

The thermodynamic studies showed that the properties of the single clathrates can be improved by mixing pure refrigerants. The equilibrium pressure and temperature of the mixed hydrate can be enhanced by changing the composition of the pure refrigerants to a desire value. For example the pressure of the hydrate dissociation of R116 was decreased significantly by adding R23 to the system. The hydrates of R407C, R427A and R406A showed the lowest dissociation pressures at a constant temperature between refrigerants studied in this work and those of the literature. The critical decomposition point of refrigerants studied was obtained. Gas hydrate dissociation measurements were performed within L_w-H-V phase as well as pressures above critical decomposition point. R410A and R406A showed the highest and lowest temperature of the critical decomposition point respectively.

It was found that the enthalpy of hydrate dissociation decreases by increasing the temperature. A comparatively low enthalpy of hydrate dissociation at the critical temperature of decompositions was obtained for R407C and R427A whereas a high enthalpy of the hydrate dissociation was found for R406A. R507C showed the maximum enthalpy of hydrate dissociation at critical temperature and pressure of decomposition between refrigerants studied in this work and those of the literature. However, the hydrate dissociation pressure was higher than that of R427A, R407C and R406A.

The kinetics measurements revealed that the rate of the hydrate formation very much depends on the initial conditions and degree of subcooling. It was found that with increasing the pressure or decreasing the temperature the induction time decreases and storage capacity (SC), final water to hydrate conversion, final moles of gas consumed and apparent rate constant at induction time of the hydrate formation increase rapidly. The effect of the initial temperature at a constant pressure was larger than the effect of the initial pressure at a constant temperature on the gas hydrate formation rate. R427A showed the maximum possible degree of subcooling between refrigerants studied. The minimum possible degree of subcooling was obtained for R406A in the presence of pure water. The maximum values of the apparent rate constant in the presence of pure water were obtained for R407C. It was found that when the liquid refrigerant forms inside the system the induction time of the gas hydrate formation increases significantly. Hence, it is essential to avoid the formation of the liquid refrigerant inside the system.

The effect of SDS solutions with concentrations of 100, 400, 500 and 600 ppm was investigated on the kinetics of the gas hydrate formation. For three refrigerants viz. R402A, R407C and R507C an inhibiting effect on SDS was observed at concentrations of 100 and 400 ppm. For R410A and R407C hydrate formation was not detected even after a significant period of time. For the refrigerants R404A, R406A, R408A and R427A a promotion effect of the SDS solution was observed. The hydrate formation of R406A was promoted until 500ppm SDS solution and an inhibiting effect was observed at 600 ppm SDS solution. R406A in the presence of 500 ppm SDS solution showed the minimum degree of subcooling. The maximum apparent rate constant was obtained for the system R406A+400ppm SDS solution.

According to the experimental results three refrigerants R427A, R407C and R406A are suitable for use in cold storage systems.

A model was developed with the ability to estimate the gas hydrate dissociation conditions. The main advantage of the model developed is that there is no need of the refrigerants solubility data in water. Two approaches comprising Kihara potential function and Parrish and Prausnitz were used in order to consider the interaction between water and guest molecules inside the hydrate cavities. The Kihara potential parameters as well as the parameters of equation (3.10) for 14 pure refrigerants were optimized and reported which are mostly new and couldn't be found in the literature. The gas hydrate dissociation conditions of the refrigerant blends were estimated using the parameters obtained for the pure refrigerants. There was a slight difference between the modeling results using the abovementioned approaches. However, the application of empirical equation (3.10) is recommended because of the complexity of the Kihara potential function approach.

The upper and lower quadruple points of pure refrigerants were also obtained using the developed model. Good agreement was observed between the model predictions and experimental data. The hydrate structure of different refrigerants were estimated and reported. All the refrigerants studied formed structure II of gas hydrates except R32 and R152a which formed structure I. The hydrate stability zone in various phase equilibrium boundaries can be estimated using the results of this study.

8

Recommendations

Even though some interesting results were obtained throughout this study, further investigation is still necessary to achieve a good understanding of the thermodynamic and structural complexity of the refrigerants clathrate/semi-clathrate hydrates forming systems.

It was clear that low pressure refrigerant hydrates have a distinct advantage over other substances as a cold storage media. Hence, the study of the refrigerant hydrates formation in the presence of the thermodynamic promoters such as TBAB, TBAC, TBAF, TBPB, TBMAC, THF and $TBANO_3$ is of great interest.

The application of the additives in order to enhance the phase change properties of the refrigerant hydrates (e.g. the enthalpy of hydrate dissociation), and also to promote the gas hydrate formation rate still needs attention.

Nano particles are widely being used with the purpose of modification of the phase change properties of different PCMs. However their effect on the cold storage properties as well as hydrate dissociation condition of the refrigerants is still unknown.

Although the clathrate/semiclathrate hydrates applications in cold storage systems are studied widely, the investigations are limited to the lab-scaled systems. It is of great interest to develop a large scale clathrate/semiclathrate hydrate process using a simulation study to investigate and estimate the performance of clathrate hydrates in cold storage and air- conditioning plants.

References

ABHAT, A. 1983. Low temperature latent heat thermal energy storage: heat storage materials. *Solar energy,* 30**,** 313-332.

AKBARI, H. & MERTOL, A. 1989. Thermal energy storage for cooling of commercial buildings. *Energy Storage Systems.* Springer.

AKIYA, T., SHIMAZAKI, T., OOWA, M., MATSUO, M. & YOSHIDA, Y. 1999. Formation Conditions of Clathrates Between HFC Alternative Refrigerants and Water. *International Journal of Thermophysics,* 20**,** 1753-1763.

AYA, I., YAMANE, K. & NARIAI, H. 1997. Solubility of CO_2 and density of CO_2 hydrate at 30 MPa. *Energy,* 22**,** 263-271.

AYEL, V., LOTTIN, O. & PEERHOSSAINI, H. 2003. Rheology, flow behaviour and heat transfer of ice slurries: a review of the state of the art. *International Journal of Refrigeration,* 26**,** 95-107.

BACHER, P. 2002. Meeting the energy challenges of the 21st century. *International journal of energy technology and policy,* 1**,** 1-26.

BELANDRIA, V., ESLAMIMANESH, A., MOHAMMADI, A. H. & RICHON, D. 2011. Gas hydrate formation in carbon dioxide+ nitrogen+ water system: Compositional analysis of equilibrium phases. *Industrial & Engineering Chemistry Research,* 50**,** 4722-4730.

BELANDRIA, V., MOHAMMADI, A. H., ESLAMIMANESH, A., RICHON, D., SANCHEZ-MORA, M. F. & GALICIA-LUNA, L. A. 2012. Phase equilibrium measurements for semi-clathrate hydrates of the (CO_2+ N_2+ tetra-n-butylammonium bromide) aqueous solution systems: Part 2. *Fluid Phase Equilibria,* 322**,** 105-112.

BELTRÁN, J. G. & SERVIO, P. 2010. Morphological Investigations of Methane−Hydrate Films Formed on a Glass Surface. *Crystal Growth & Design,* 10**,** 4339-4347.

BI, Y., GUO, T., ZHANG, L., CHEN, L. & SUN, F. 2010. Entropy generation minimization for charging and discharging processes in a gas-hydrate cool storage system. *Applied Energy,* 87**,** 1149-1157.

BI, Y., GUO, T., ZHANG, L., ZHANG, H. & CHEN, L. 2009. Experimental study on cool release process of gas-hydrate with additives. *Energy and Buildings,* 41**,** 120-124.

BI, Y., GUO, T., ZHU, T., FAN, S., LIANG, D. & ZHANG, L. 2004. Influence of volumetric-flow rate in the crystallizer on the gas-hydrate cool-storage process in a new gas-hydrate cool-storage system. *Applied Energy,* 78**,** 111-121.

BI, Y., GUO, T., ZHU, T., ZHANG, L. & CHEN, L. 2006. Influences of additives on the gas hydrate cool storage process in a new gas hydrate cool storage system. *Energy Conversion and Management,* 47**,** 2974-2982.

BIRCH, K. 2003. Estimating uncertainties in testing. *Measurement Good Practice Guide.*

BREWER, P. G., FRIEDERICH, G., PELTZER, E. T. & ORR, F. M. 1999. Direct experiments on the ocean disposal of fossil fuel CO2. *Science,* 284**,** 943-945.

BRIGGS, F., HU, Y. & BARDUHN, A. 1962. New agents for use in the hydrate process for demineralizing sea water. *Research and Development Progress Report no. 59.* United States Department of the Interior.

CARBAJO, J. J. 1983. Mixed Clathrates for Cool Storage Applications. United Siatcs of America: OAK RIDGE NATIONAL LABORATORY, Oak Ridge , Tennessee 37831.

CARBAJO, J. J. 1985. A direct-contact-charged direct-contact-discharged cool storage system using gas hydrate. *ASHRAE Trans.;(United States),* 91.

CARROLL, J. 2009. *Natural gas hydrates: a guide for engineers*, Gulf Professional Publishing.

CHRISTOV, M. & DOHRN, R. 2002. High-pressure fluid phase equilibria: experimental methods and systems investigated (1994–1999). *Fluid Phase Equilibria,* 202**,** 153-218.

CHUN, M.-K., LEE, H. & RYU, B.-J. 2000. Phase equilibria of R22 ($CHClF_2$) hydrate systems in the presence of NaCl, KCl, and $MgCl_2$. *Journal of Chemical & Engineering Data,* 45**,** 1150-1153.

CHUN, M.-K., YOON, J.-H. & LEE, H. 1996. Clathrate Phase Equilibria for the Water + Deuterium Oxide + Carbon Dioxide and Water + Deuterium Oxide + Chlorodifluoromethane (R22) Systems. *Journal of Chemical & Engineering Data,* 41**,** 1114-1116.

CIRCONE, S., STERN, L. A., KIRBY, S. H., DURHAM, W. B., CHAKOUMAKOS, B. C., RAWN, C. J., RONDINONE, A. J. & ISHII, Y. 2003. CO2 hydrate: synthesis, composition, structure, dissociation behavior, and a comparison to structure I CH4 hydrate. *The Journal of Physical Chemistry B,* 107**,** 5529-5539.

CLAIN, P., DELAHAYE, A., FOURNAISON, L., MAYOUFI, N., DALMAZZONE, D. & FÜRST, W. 2012. Rheological properties of tetra-n-butylphosphonium bromide hydrate slurry flow. *Chemical Engineering Journal,* 193**,** 112-122.

COLLETT, T. S. 2002. Energy resource potential of natural gas hydrates. *AAPG bulletin,* 86**,** 1971-1992.

COLLETT, T. S. & KUUSKRAA, V. A. 1998. Hydrates contain vast store of world gas resources. *Oil and Gas Journal,* 96**,** 90-94.

DAHL, S., FREDENSLUND, A. & RASMUSSEN, P. 1991. The MHV2 model: a UNIFAC-based equation of state model for prediction of gas solubility and vapor-liquid equilibria at low and high pressures. *Industrial & Engineering Chemistry Research,* 30**,** 1936-1945.

DAHL, S. & MICHELSEN, M. L. 1990. High-pressure vapor-liquid equilibrium with a UNIFAC-based equation of state. *AIChE journal,* 36**,** 1829-1836.

DAITOKU, T. & UTAKA, Y. 2007. An effect of scraper shapes on detachment of solid adhered to cooling surface for formation of clathrate hydrate slurry. *Heat Transfer—Asian Research,* 36**,** 489-500.

DALMAZZONE, D., KHARRAT, M., LACHET, V., FOUCONNIER, B. & CLAUSSE, D. 2002. DSC and PVT measurements. *Journal of thermal Analysis and Calorimetry,* 70**,** 493-505.

DARBOURET, M., COURNIL, M. & HERRI, J.-M. 2005. Rheological study of TBAB hydrate slurries as secondary two-phase refrigerants. *International Journal of Refrigeration,* 28**,** 663-671.

DEATON, W. M. & FROST, E. M. 1937. *Oil Gas J.,,* 36**,** 75 (cited in Sloan and Koh 2008).

DELAHAYE, A., FOURNAISON, L., JERBI, S. & MAYOUFI, N. 2011. Rheological properties of CO2 hydrate slurry flow in the presence of additives. *Industrial & Engineering Chemistry Research,* 50**,** 8344-8353.

DELAHAYE, A., FOURNAISON, L., MARINHAS, S., CHATTI, I., PETITET, J.-P., DALMAZZONE, D. & FÜRST, W. 2006. Effect of THF on equilibrium pressure and dissociation enthalpy of CO2 hydrates applied to secondary refrigeration. *Industrial & engineering chemistry research,* 45**,** 391-397.

DELAHAYE, A., FOURNAISON, L., MARINHAS, S. & MARTÍNEZ, M. C. 2008. Rheological study of hydrate slurry in a dynamic loop applied to secondary refrigeration. *Chemical Engineering Science,* 63**,** 3551-3559.

DESCHAMPS, J. & DALMAZZONE, D. 2010. Hydrogen storage in semiclathrate hydrates of tetrabutyl ammonium chloride and tetrabutyl phosphonium bromide. *Journal of Chemical & Engineering Data,* 55**,** 3395-3399.

DOHRN, R. & BRUNNER, G. 1995. High-pressure fluid-phase equilibria: experimental methods and systems investigated (1988–1993). *Fluid Phase Equilibria,* 106**,** 213-282.

DOHRN, R., PEPER, S. & FONSECA, J. 2010. High-pressure fluid-phase equilibria: experimental methods and systems investigated (2000–2004). *Fluid Phase Equilibria,* 288**,** 1-54.

DQ, L. & XG, Y. 2008. Experimental study on flow characters of CH_3CCl_2F hydrate slurry. *International Journal of Refrigeration,* 31**,** 371-378.

DUARTE-GARZA, H. A., HWANG, C.-A., KELLERMAN, S. A., MILLER, R. C., HALL, K. R., HOLSTE, J. C., MARSH, K. N. & GAMMON, B. E. 1997a. Vapor Pressure, Vapor Density, and Liquid Density for 1,1-Dichloro-1-fluoroethane (R-141b). *Journal of Chemical & Engineering Data,* 42**,** 497-501.

DUARTE-GARZA, H. A., STOUFFER, C. E., HALL, K. R., HOLSTE, J. C., MARSH, K. N. & GAMMON, B. E. 1997b. Experimental Critical Constants, Vapor Pressures, and Vapor and Liquid Densities for Pentafluoroethane (R-125). *Journal of Chemical & Engineering Data,* 42**,** 745-753.

DYADIN, Y. A. & UDACHIN, K. 1984. Clathrate Formation in Wateer-Peralkylonium Salts Systems. *Clathrate Compounds, Molecular Inclusion Phenomena, and Cyclodextrins.* Springer.

ENGLEZOS, P. 1993. Clathrate hydrates. *Industrial & Engineering Chemistry Research,* 32**,** 1251-1274.

ENGLEZOS, P., KALOGERAKIS, N., DHOLABHAI, P. & BISHNOI, P. 1987. Kinetics of formation of methane and ethane gas hydrates. *Chemical Engineering Science,* 42**,** 2647-2658.

ESLAMIMANESH, A. 2012. Thermodynamic studies on semi-clathrate hydrates of TBAB+ gases containing carbon dioxide.

ESLAMIMANESH, A., MOHAMMADI, A. H., RICHON, D., NAIDOO, P. & RAMJUGERNATH, D. 2012. Application of gas hydrate formation in separation processes: A review of experimental studies. *The Journal of Chemical Thermodynamics,* 46**,** 62-71.

FAN, S.-S., CHEN, G.-J., MA, Q.-L. & GUO, T.-M. 2000. Experimental and modeling studies on the hydrate formation of CO_2 and CO_2 rich gas mixtures. *Chemical Engineering Journal,* 78**,** 173-178.

FAN, S.-S. & GUO, T.-M. 1999. Hydrate formation of CO2-rich binary and quaternary gas mixtures in aqueous sodium chloride solutions. *Journal of Chemical & Engineering Data,* 44**,** 829-832.

FAN, S., LI, S., WANG, J., LANG, X. & WANG, Y. 2009. Efficient capture of CO2 from simulated flue gas by formation of TBAB or TBAF semiclathrate hydrates. *Energy & Fuels,* 23**,** 4202-4208.

FONSECA, J., DOHRN, R. & PEPER, S. 2011. High-pressure fluid-phase equilibria: experimental methods and systems investigated (2005–2008). *Fluid Phase Equilibria,* 300**,** 1-69.

FOURNAISON, L., DELAHAYE, A., CHATTI, I. & PETITET, J.-P. 2004. CO_2 hydrates in refrigeration processes. *Industrial & engineering chemistry research,* 43**,** 6521-6526.

FOWLER, D., LOEBENSTEIN, W., PALL, D. & KRAUS, C. A. 1940. Some unusual hydrates of quaternary ammonium salts. *Journal of the American Chemical Society,* 62**,** 1140-1142.

FUKUSHIMA, S., MATSUMOTO, S., OGOSHI, H. & TAKAO, S. 2002. Thermal storge medium using a hydrate and apparatus thereof, and method for producing the thermal storage medium. Google Patents.

FUKUSHIMA, S., TAKAO, S., OGOSHI, H., IDA, H., AKIYAMA, T. & OTSUKA, T. 1999. Development of high-density cold latent heat with clathrate hydrate. *NKK TECHNICAL REPORT-JAPANESE EDITION-***,** 65-70.

GANJI, H., MANTEGHIAN, M., OMIDKHAH, M. & RAHIMI MOFRAD, H. 2007a. Effect of different surfactants on methane hydrate formation rate, stability and storage capacity. *Fuel,* 86**,** 434-441.

GANJI, H., MANTEGHIAN, M. & RAHIMI MOFRAD, H. 2007b. Effect of mixed compounds on methane hydrate formation and dissociation rates and storage capacity. *Fuel Processing Technology,* 88**,** 891-895.

GLEW, D. N. 1962. *Solution treatment*.

GOODWIN, A., DEFIBAUGH, D. & WEBER, L. 1992. The vapor pressure of 1, 1, 1, 2-tetrafluoroethane (R134a) and chlorodifluoromethane (R22). *International journal of thermophysics,* 13**,** 837-854.

GRAULS, D. 2001. Gas hydrates: importance and applications in petroleum exploration. *Marine and Petroleum Geology,* 18**,** 519-523.

GUILPART, J., STAMATIOU, E., DELAHAYE, A. & FOURNAISON, L. 2006. Comparison of the performance of different ice slurry types depending on the application temperature. *International journal of refrigeration,* 29**,** 781-788.

GUO, K., SHU, B. & YANG, W. Advances and applications of gas hydrate thermal energy storage technology. Proceedings of the first Trabzon international energy and environment symposium, 1996. 381-386.

HALL, C., THARAKAN, P., HALLOCK, J., CLEVELAND, C. & JEFFERSON, M. 2003. Hydrocarbons and the evolution of human culture. *Nature,* 426**,** 318-322.

HAMMERSCHMIDT, E. 1934. Formation of gas hydrates in natural gas transmission lines. *Industrial & Engineering Chemistry,* 26**,** 851-855.

HASHEMI, H., BABAEE, S., MOHAMMADI, A. H., NAIDOO, P. & RAMJUGERNATH, D. 2015a. Clathrate Hydrate Dissociation Conditions of Refrigerants R404A, R406A, R408A and R427A: Experimental Measurements and Thermodynamic Modeling. *The Journal of Chemical Thermodynamics*.

HASHEMI, H., BABAEE, S., MOHAMMADI, A. H., NAIDOO, P. & RAMJUGERNATH, D. 2015b. Experimental measurements and thermodynamic modeling of refrigerant hydrates dissociation conditions. *The Journal of Chemical Thermodynamics,* 80**,** 30-40.

HASHEMI, H., BABAEE, S., NAIDOO, P., MOHAMMADI, A. H. & RAMJUGERNATH, D. 2014. Experimental Measurements and Thermodynamic Modeling of Clathrate Hydrate Dissociation Conditions for Refrigerants R116, R23, and Their Mixture R508B. *Journal of Chemical & Engineering Data*.

HASHIMOTO, S., KAWAMURA, K., ITO, H., NOBEOKA, M., OHGAKI, K. & INOUE, Y. Rheological study on tetra-n-butyl ammonium salt semi-clathrate hydrate slurries. Proceedings of Seventh International Conference on Gas Hydrates, Edinburgh, Scotland, United Kingdom, 2011.

HASHIMOTO, S., MAKINO, T., INOUE, Y. & OHGAKI, K. 2010a. Three-Phase Equilibrium Relations and Hydrate Dissociation Enthalpies for Hydrofluorocarbon Hydrate Systems: HFC-134a, -125, and -143a Hydrates. *Journal of Chemical & Engineering Data,* 55**,** 4951-4955.

HASHIMOTO, S., MIYAUCHI, H., INOUE, Y. & OHGAKI, K. 2010b. Thermodynamic and Raman Spectroscopic Studies on Difluoromethane (HFC-32) + Water Binary System. *Journal of Chemical & Engineering Data,* 55**,** 2764-2768.

HENDRIKS, E. & MEIJER, H. 2004. *computer Aided Property Estimation for Process and Product Design, 1st Ed., Chptr. 11*.

HERSLUND, P. J. 2013. Thermodynamic and Process Modelling of Gas Hydrate Systems in CO2 Capture Processes. *Graduate Schools Yearbook 2012***,** 95.

HOLDER, G. D., CUGINI, A. V. & WARZINSKI, R. P. 1995. Modeling clathrate hydrate formation during carbon dioxide injection into the ocean. *Environmental science & technology,* 29**,** 276-278.

HUANG, C., FENNEMA, O. & POWRIE, W. 1965. Gas hydrates in aqueous-organic systems: I. Preliminary studies. *Cryobiology,* 2**,** 109-115.

HUANG, C., FENNEMA, O. & POWRIE, W. 1966. Gas hydrates in aqueous-organic systems: II. Concentration by gas hydrate formation. *Cryobiology,* 2**,** 240-245.

HURON, M.-J. & VIDAL, J. 1979. New mixing rules in simple equations of state for representing vapour-liquid equilibria of strongly non-ideal mixtures. *Fluid Phase Equilibria,* 3**,** 255-271.

ISOBE, F. & MORI, Y. H. 1992. Formation of gas hydrate or ice by direct-contact evaporation of CFC alternatives. *International Journal of Refrigeration,* 15**,** 137-142.

JAVANMARDI, J., AYATOLLAHI, S., MOTEALLEH, R. & MOSHFEGHIAN, M. 2004. Experimental Measurement and Modeling of R22 (CHClF2) Hydrates in Mixtures of Acetone + Water. *Journal of Chemical & Engineering Data,* 49**,** 886-889.

JAVANMARDI, J. & MOSHFEGHIAN, M. 2003. Energy consumption and economic evaluation of water desalination by hydrate phenomenon. *Applied thermal engineering,* 23**,** 845-857.

JERBI, S., DELAHAYE, A., OIGNET, J., FOURNAISON, L. & HABERSCHILL, P. 2013. Rheological properties of CO2 hydrate slurry produced in a stirred tank reactor and a secondary refrigeration loop. *International Journal of Refrigeration,* 36**,** 1294-1301.

KAI-HUA, L. Y.-H. Q. & SHUAN-SHI, L. D.-Q. F. 2003. STUDY ON REFRIGERANT HYDRATE CRYSTALLIZATION PROCESS IN THE ACTION OF ULTRASONIC. *Journal of Engineering Thermophysics,* 3**,** 006.

KAKIUCHI, H., YABE, M. & YAMAZAKI, M. 2003. A Study of Trimethylolethane Hydrate as a Phase Change Material. *Journal of chemical engineering of Japan,* 36**,** 788-793.

KAMATA, Y., OYAMA, H., SHIMADA, W., EBINUMA, T., TAKEYA, S., UCHIDA, T., NAGAO, J. & NARITA, H. 2004. Gas separation method using tetra-n-butyl ammonium bromide semi-clathrate hydrate. *Japanese journal of applied physics,* 43**,** 362.

KANG, S.-P., LEE, H. & RYU, B.-J. 2001. Enthalpies of dissociation of clathrate hydrates of carbon dioxide, nitrogen,(carbon dioxide+ nitrogen), and (carbon

dioxide+ nitrogen+ tetrahydrofuran). *The Journal of Chemical Thermodynamics,* 33**,** 513-521.
KIM, S. M., LEE, J. D., LEE, H. J., LEE, E. K. & KIM, Y. 2011. Gas hydrate formation method to capture the carbon dioxide for pre-combustion process in IGCC plant. *International Journal of Hydrogen Energy,* 36**,** 1115-1121.
KING JR, A. 2001. The solubility of gases in aqueous solutions of poly (propylene glycol). *Journal of colloid and interface science,* 243**,** 457-462.
KLAUDA, J. B. & SANDLER, S. I. 2000. A fugacity model for gas hydrate phase equilibria. *Industrial & engineering chemistry research,* 39**,** 3377-3386.
KLEIBER, M. 1995. An extension to the UNIFAC group assignment for prediction of vapor-liquid equilibria of mixtures containing refrigerants. *Fluid phase equilibria,* 107**,** 161-188.
KOJIMA, R., YAMANE, K. & AYA, I. Dual nature of CO2 solubility in hydrate forming region. Fourth international conference on gas hydrates, 2002. 286-9.
KUBOTA, H., SHIMIZU, K., TANAKA, Y. & MAKITA, T. 1984. THERMODYNAMIC PROPERTIES OF R13 ($CClF_3$), R23 (CHF_3), R152a ($C_2H_4F_2$), AND PROPANE HYDRATES FOR DESALINATION OF SEA WATER. *Journal of Chemical Engineering of Japan,* 17**,** 423-429.
KUBOTA, H., YAMASHITA, T., TANAKA, Y. & MAKITA, T. 1989. Vapor pressures of new fluorocarbons. *International Journal of Thermophysics,* 10**,** 629-637.
KUMANO, H., HIRATA, T. & KUDOH, T. 2011. Experimental study on the flow and heat transfer characteristics of a tetra-n-butyl ammonium bromide hydrate slurry (second report: heat transfer characteristics). *International Journal of Refrigeration,* 34**,** 1963-1971.
KVENVOLDEN, K. A. 1988. Methane hydrate—a major reservoir of carbon in the shallow geosphere? *Chemical Geology,* 71**,** 41-51.
LE PARLOUËR, P., DALMAZZONE, C., HERZHAFT, B., ROUSSEAU, L. & MATHONAT, C. 2004. Characterisation of gas hydrates formation using a new high pressure Micro-DSC. *Journal of Thermal Analysis and Calorimetry,* 78**,** 165-172.
LEE, S., LIANG, L., RIESTENBERG, D., WEST, O. R., TSOURIS, C. & ADAMS, E. 2003. CO2 hydrate composite for ocean carbon sequestration. *Environmental science & technology,* 37**,** 3701-3708.
LI, G., HWANG, Y. & RADERMACHER, R. 2012. Review of cold storage materials for air conditioning application. *International Journal of Refrigeration,* 35**,** 2053-2077.
LI, J., GUO, K., LIANG, D. & WANG, R. 2004. Experiments on fast nucleation and growth of HCFC141b gas hydrate in static water columns. *International Journal of Refrigeration,* 27**,** 932-939.
LI, S., FAN, S., WANG, J., LANG, X. & WANG, Y. 2010a. Clathrate Hydrate Capture of CO_2 from Simulated Flue Gas with Cyclopentane/Water Emulsion. *Chinese Journal of Chemical Engineering,* 18**,** 202-206.
LI, X.-S., XIA, Z.-M., CHEN, Z.-Y., YAN, K.-F., LI, G. & WU, H.-J. 2010b. Equilibrium hydrate formation conditions for the mixtures of CO_2+ H_2+ tetrabutyl ammonium bromide. *Journal of Chemical & Engineering Data,* 55**,** 2180-2184.
LI, X.-S., XU, C.-G., CHEN, Z.-Y. & WU, H.-J. 2010c. Tetra-n-butyl ammonium bromide semi-clathrate hydrate process for post-combustion capture of carbon

dioxide in the presence of dodecyl trimethyl ammonium chloride. *Energy,* 35**,** 3902-3908.

LIANG, D., GUO, K., WANG, R. & FAN, S. 2001. Hydrate equilibrium data of 1,1,1,2-tetrafluoroethane (HFC-134a), 1,1-dichloro-1-fluoroethane (HCFC-141b) and 1,1-difluoroethane (HFC-152a). *Fluid Phase Equilibria,* 187–188**,** 61-70.

LIN, W., DELAHAYE, A. & FOURNAISON, L. 2008. Phase equilibrium and dissociation enthalpy for semi-clathrate hydrate of CO_2+ TBAB. *Fluid Phase Equilibria,* 264**,** 220-227.

LINGA, P., ADEYEMO, A. & ENGLEZOS, P. 2007. Medium-pressure clathrate hydrate/membrane hybrid process for postcombustion capture of carbon dioxide. *Environmental science & technology,* 42**,** 315-320.

LINGA, P., KUMAR, R., LEE, J. D., RIPMEESTER, J. & ENGLEZOS, P. 2010. A new apparatus to enhance the rate of gas hydrate formation: Application to capture of carbon dioxide. *International Journal of Greenhouse Gas Control,* 4**,** 630-637.

LIPKOWSKI, J., KOMAROV, V. Y., RODIONOVA, T. V., DYADIN, Y. A. & ALADKO, L. S. 2002. The Structure of Tetrabutylammonium Bromide Hydrate $(C_4H_9)_4NBr.2\ 1/3H_2O$. *Journal of Supramolecular Chemistry,* 2**,** 435-439.

LIU, Y., GUO, K., LIANG, D. & FAN, S. 2003. Effects of magnetic fields on HCFC-141b refrigerant gas hydrate formation. *Science in China Series B: Chemistry,* 46**,** 407-415.

LU, T., ZHANG, Y., LI, X., CHEN, Z.-Y. & YAN, K.-F. 2009. Equilibrium conditions of hydrate formation in the systems of CO_2-N_2-TBAB and CO_2-N_2-THF. *Chin. J. Process Eng,* 9**,** 541-544.

MA, Z., ZHANG, P., WANG, R., FURUI, S. & XI, G. 2010. Forced flow and convective melting heat transfer of clathrate hydrate slurry in tubes. *International Journal of Heat and Mass Transfer,* 53**,** 3745-3757.

MAGNUSSEN, T., RASMUSSEN, P. & FREDENSLUND, A. 1981. UNIFAC parameter table for prediction of liquid-liquid equilibriums. *Industrial & Engineering Chemistry Process Design and Development,* 20**,** 331-339.

MAKOGON, T. Y., MEHTA, A. P. & SLOAN, E. D. 1996. Structure H and Structure I Hydrate Equilibrium Data for 2,2-Dimethylbutane with Methane and Xenon. *Journal of Chemical & Engineering Data,* 41**,** 315-318.

MAKOGON, Y., HOLDITCH, S. & MAKOGON, T. 2007. Natural gas-hydrates—A potential energy source for the 21st Century. *Journal of Petroleum Science and Engineering,* 56**,** 14-31.

MAKOGON, Y. F. Natural gas hydrates: the state of study in the USSR and perspectives for its use. Third Chemical Congress of North America, Toronto, Canada, 1988. 5-10.

MANTEGHIAN, M., MOUSAVI SAFAVI, S. M. & MOHAMMADI, A. 2013. The equilibrium conditions, hydrate formation and dissociation rate and storage capacity of ethylene hydrate in presence of 1, 4-dioxane. *Chemical Engineering Journal,* 217**,** 379-384.

MARINHAS, S., DELAHAYE, A., FOURNAISON, L., DALMAZZONE, D., FÜRST, W. & PETITET, J.-P. 2006. Modelling of the available latent heat of a CO_2 hydrate slurry in an experimental loop applied to secondary refrigeration. *Chemical Engineering and Processing: Process Intensification,* 45**,** 184-192.

MARSHALL, D. R., SAITO, S. & KOBAYASHI, R. 1964. Hydrates at high pressures: Part I. Methane-water, argon-water, and nitrogen-water systems. *AIChE Journal,* 10**,** 202-205.
MARTINEZ, M., DALMAZZONE, D., FÜRST, W., DELAHAYE, A. & FOURNAISON, L. 2008. Thermodynamic properties of THF+ CO_2 hydrates in relation with refrigeration applications. *AIChE journal,* 54**,** 1088-1095.
MAX, M. D. & PELLENBARG, R. E. 2000. Desalination through gas hydrate. Google Patents.
MAYOUFI, N., DALMAZZONE, D., DELAHAYE, A., CLAIN, P., FOURNAISON, L. & FUR T, W. 2011. Experimental data on phase behavior of simple tetrabutylphosphonium bromide (TBPB) and mixed CO_2+ TBPB semiclathrate hydrates. *Journal of Chemical & Engineering Data,* 56**,** 2987-2993.
MAYOUFI, N., DALMAZZONE, D., FUR T, W., DELAHAYE, A. & FOURNAISON, L. 2010. CO_2 Enclathration in Hydrates of Peralkyl-(Ammonium/Phosphonium) Salts: Stability Conditions and Dissociation Enthalpies. *Journal of Chemical & Engineering Data,* 55**,** 1271-1275.
MAYOUFI, N., DALMAZZONE, D., FÜRST, W., ELGHOUL, L., SEGUATNI, A., DELAHAYE, A. & FOURNAISON, L. 2012. Phase behaviour of tri-n-butylmethylammonium chloride hydrates in the presence of carbon dioxide. *Journal of thermal analysis and calorimetry,* 109**,** 481-486.
MCKOY, V. & SINANOĞLU, O. 1963. Theory of dissociation pressures of some gas hydrates. *The Journal of Chemical Physics,* 38**,** 2946-2956.
MCLINDEN, M., KLEIN, S., LEMMON, E. & PESKIN, A. 1998. Thermodynamic properties of refrigerants and refrigerant mixtures database (REFPROP). *O1 r R]. Gaithersburg, MD: NIST.*
MEYSEL, P., OELLRICH, L., RAJ BISHNOI, P. & CLARKE, M. A. 2011. Experimental investigation of incipient equilibrium conditions for the formation of semi-clathrate hydrates from quaternary mixtures of (CO_2+N_2+TBAB&+H_2O). *The Journal of Chemical Thermodynamics,* 43**,** 1475-1479.
MICHELSEN, M. L. 1990. A modified Huron-Vidal mixing rule for cubic equations of state. *Fluid Phase Equilibria,* 60**,** 213-219.
MIGUEL, A. A., FERREIRA, A. G. & FONSECA, I. 2000. Solubilities of some new refrigerants in water. *Fluid phase equilibria,* 173**,** 97-107.
MOHAMMADI, A., MANTEGHIAN, M., HAGHTALAB, A., MOHAMMADI, A. H. & RAHMATI-ABKENAR, M. 2014. Kinetic study of carbon dioxide hydrate formation in presence of silver nanoparticles and SDS. *Chemical Engineering Journal,* 237**,** 387-395.
MOHAMMADI, A. H., ANDERSON, R. & TOHIDI, B. 2005. Carbon monoxide clathrate hydrates: equilibrium data and thermodynamic modeling. *AIChE journal,* 51**,** 2825-2833.
MOHAMMADI, A. H., ESLAMIMANESH, A., BELANDRIA, V. & RICHON, D. 2011. Phase equilibria of semiclathrate hydrates of CO2, N2, CH4, or H_2+ Tetra-n-butylammonium bromide aqueous solution. *Journal of Chemical & Engineering Data,* 56**,** 3855-3865.
MOHAMMADI, A. H., ESLAMIMANESH, A., BELANDRIA, V., RICHON, D., NAIDOO, P. & RAMJUGERNATH, D. 2012. Phase equilibrium measurements for semi-clathrate hydrates of the (CO_2+ N_2+ tetra-n-butylammonium bromide) aqueous solution system. *The Journal of Chemical Thermodynamics,* 46**,** 57-61.

MOHAMMADI, A. H. & RICHON, D. Pressure–temperaturephasediagramsof clathrate hydratesofHFC-134a,HFC-152aandHFC-32. AIChE Annual Meeting, Proceeding, 2010 SaltLakeCity,UT.

MOHAMMADI, A. H., TOHIDI, B. & BURGASS, R. W. 2003. Equilibrium data and thermodynamic modeling of nitrogen, oxygen, and air clathrate hydrates. *Journal of Chemical & Engineering Data,* 48**,** 612-616.

MOLLERUP, J. 1986. A note on the derivation of mixing rules from excess Gibbs energy models. *Fluid Phase Equilibria,* 25**,** 323-327.

MOOIJER-VAN DEN HEUVEL, M., WITTEMAN, R. & PETERS, C. 2001. Phase behaviour of gas hydrates of carbon dioxide in the presence of tetrahydropyran, cyclobutanone, cyclohexane and methylcyclohexane. *Fluid phase equilibria,* 182**,** 97-110.

MOOIJER-VAN DEN HEUVEL, M. M., SAWIRJO, N. M. & PETERS, C. J. 2006. Influence of fluoroalkanes on the phase behaviour of methane gas hydrate systems. *Fluid Phase Equilibria,* 241**,** 124-137.

MORI, T. & MORI, Y. H. 1989a. Characterization of gas hydrate formation in direct-contact cool storage process. *International Journal of Refrigeration,* 12**,** 259-265.

MORI, Y. H. & MORI, T. 1989b. Formation of gas hydrate with CFC alternative R-134a. *AIChE Journal,* 35**,** 1227-1228.

NAJAFI, M. & SCHAETZLE, W. J. 1991. Cooling and heating with clathrate thermal energy storage system. *ASHRAE Trans.;(United States),* 97**,** 177-183.

NAKAYAMA, H. 1987. Hydrates of organic compounds. XI: Determination of the melting point and hydration numbers of the clathrate-like hydrate of tetrabutylammonium chloride by differential scanning calorimetry. *Bulletin of the Chemical Society of Japan,* 60**,** 839-843.

NGEMA, P., NELSON, W., NAIDOO, P., RAMJUGERNATH, D. & RICHON, D. 2014a. Isothermal method for hydrate studies using a transparent variable volume cell. *Review of Scientific Instruments,* 85**,** 045123.

NGEMA, P. T., PETTICREW, C., NAIDOO, P., MOHAMMADI, A. H. & RAMJUGERNATH, D. 2014b. Experimental Measurements and Thermodynamic Modeling of the Dissociation Conditions of Clathrate Hydrates for (Refrigerant + NaCl + Water) Systems. *Journal of Chemical & Engineering Data,* 59**,** 466-475.

OBARA, S. Y. 2010. Development of a hybrid compressed gas engine/PEFC power system using the dissociation expansion characteristics of gas hydrate. *International Journal of Hydrogen Energy,* 35**,** 10604-10612.

OBARA, S. Y., YAMADA, T., MATSUMURA, K., TAKAHASHI, S., KAWAI, M. & RENGARAJAN, B. 2011a. Operational planning of an engine generator using a high pressure working fluid composed of CO2 hydrate. *Applied Energy,* 88**,** 4733-4741.

OBARA, S. Y., YAMADA, T., MATSUMURA, K., TAKAHASHI, S., KAWAI, M. & RENGARAJAN, B. 2011b. Operational planning of an engine generator using a high pressure working fluid composed of CO_2 hydrate. *Applied Energy,* 88**,** 4733-4741.

OELLRICH, L. Natural gas hydrates and their potential for future energy supply. Proceedings of the 6th ISHMT/ASME Heat and Mass Transfer Conference, 2004. 5-7.

OGAWA, T., ITO, T., WATANABE, K., TAHARA, K.-I., HIRAOKA, R., OCHIAI, J.-I., OHMURA, R. & MORI, Y. H. 2006. Development of a novel hydrate-based refrigeration system: a preliminary overview. *Applied thermal engineering,* 26**,** 2157-2167.

OGOSHI, H. & TAKAO, S. 2004. Air-conditioning system using clathrate hydrate slurry. *JFE Tech. Rep,* 3**,** 1-5.

OHGAKI, K., MAKIHARA, Y. & TAKANO, K. 1993. Formation of CO2 Hydrate in Pure and Sea Waters. *Journal of chemical engineering of Japan,* 26**,** 558-564.

OHMURA, R., TAKEYA, S., UCHIDA, T. & EBINUMA, T. 2004. Clathrate hydrate formed with methane and 2-Propanol: Confirmation of structure II hydrate formation. *Industrial & engineering chemistry research,* 43**,** 4964-4966.

OOWA, M., NAKAIWA, M., AKIYA, T., FUKUURA, H., SUZUKI, K. & OHSUKA, M. Formation Of CFC Alternative R134a Gas Hydrate. Energy Conversion Engineering Conference, 1990. IECEC-90. Proceedings of the 25th Intersociety, 12-17 Aug 1990 1990. 269-274.

ORBEY, H. & SANDLER, S. I. 1995. Equation of state modeling of refrigerant mixtures. *Industrial & engineering chemistry research,* 34**,** 2520-2525.

OYAMA, H., EBINUMA, T., NAGAO, J., NARITA, H. & SHIMADA, W. Phase behavior of TBAB semiclathrate hydrate crystal under several vapor components. Proceedings of the 6th International Conference on Gas Hydrates (ICGH), Vancouver, Canada, 2008.

OYAMA, H., EBINUMA, T., SHIMADA, W., TAKEYA, S., NAGAO, J., UCHIDA, T. & NARITA, H. 2002. Viscosity Increase Before Nucleation of CO2 Gas Hydrate. *4th Int. Conf. on Gas Hydrates,*

. Yokohama, Japan.

OYAMA, H., SHIMADA, W., EBINUMA, T., KAMATA, Y., TAKEYA, S., UCHIDA, T., NAGAO, J. & NARITA, H. 2005. Phase diagram, latent heat, and specific heat of TBAB semiclathrate hydrate crystals. *Fluid Phase Equilibria,* 234**,** 131-135.

PAPADIMITRIOU, N. I., TSIMPANOGIANNIS, I. N., STUBOS, A. K., MARTÍN, A., ROVETTO, L. J., FLORUSSE, L. J. & PETERS, C. J. 2011. Experimental and Computational Investigation of the sII Binary He− THF Hydrate. *The Journal of Physical Chemistry B,* 115**,** 1411-1415.

PARK, K.-N., HONG, S. Y., LEE, J. W., KANG, K. C., LEE, Y. C., HA, M.-G. & LEE, J. D. 2011. A new apparatus for seawater desalination by gas hydrate process and removal characteristics of dissolved minerals (Na^+, Mg^{2+}, Ca^{2+}, K^+, B^{3+}). *Desalination,* 274**,** 91-96.

PARKER, A. 1942. Potable water from sea water. *Nature,* 149**,** 184-186.

PARRISH, W. R. & PRAUSNITZ, J. M. 1972. Dissociation Pressures of Gas Hydrates Formed by Gas Mixtures. *Industrial & Engineering Chemistry Process Design and Development,* 11**,** 26-35.

PENG, P. & ZHUANG, Y. 2012. The evaluation and comparison of carbon dioxide capture technologies applied to FCC flue gas. *Advanced Materials Research,* 347**,** 1479-1482.

PIRINGER, A. L. & BANER, O. G. 2007. Appendix II. *Plastic Packaging Materials for Food.* Wiley-VCH Verlag GmbH.

PROUST, P. & VERA, J. 1989. PRSV: The stryjek-vera modification of the peng-robinson equation of state. Parameters for other pure compounds of industrial interest. *The Canadian Journal of Chemical Engineering,* 67**,** 170-173.

RAAL, J. D. & MUHLBAUER, A. L. 1997. *The Measurement and Computation of Phase Equilibria*, Taylor & Francis.

RICHON, D. 1996. New experimental developments for phase equilibrium measurements. *Fluid phase equilibria,* 116**,** 421-428.
RICHON, D. 2009. Experimental techniques for the determination of thermophysical properties to enhance chemical processes. *Pure and Applied Chemistry,* 81**,** 1769-1782.
RICHON, D. & DE LOOS, T. W. 2005. *Vapour-liquid equilibrium at high pressure," Measurement of the Thermodynamic Properties of Multiple Phases*, Experimental Thermodynamics, Vol VII, R.D. Weir and T.W. de Loos, eds., Elsevier, 90-136.
SCHAETZLE, W., GADALLA, M. & NAJAFI, M. Experimental results of cooling cycles with clathrate energy storage. Proceedings of the 22nd Intersociety Energy Conversion Engineering Conference, Philadelphia, PA, USA, 1987. 1317-1323.
SCHROETER, J., KOBAYASHI, R. & HILDEBRAND, M. 1983. Hydrate decomposition conditions in the system hydrogen sulfide-methane-propane. *Industrial & engineering chemistry fundamentals,* 22**,** 361-364.
SEO, Y.-T., LEE, H. & YOON, J.-H. 2001. Hydrate phase equilibria of the carbon dioxide, methane, and water system. *Journal of Chemical & Engineering Data,* 46**,** 381-384.
SERVIO, P. & ENGLEZOS, P. 2001. Effect of temperature and pressure on the solubility of carbon dioxide in water in the presence of gas hydrate. *Fluid phase equilibria,* 190**,** 127-134.
SFAXI, I. B. A., DURAND, I., LUGO, R., MOHAMMADI, A. H. & RICHON, D. 2014. Hydrate phase equilibria of CO_2 + N_2 + aqueous solution of THF, TBAB or TBAF system. *International Journal of Greenhouse Gas Control,* 26**,** 185-192.
SHIMADA, W., EBINUMA, T., OYAMA, H., KAMATA, Y., TAKEYA, S., UCHIDA, T., NAGAO, J. & NARITA, H. 2003. Separation of gas molecule using tetra-n-butyl ammonium bromide semi-clathrate hydrate crystals. *Japanese journal of applied physics,* 42**,** L129.
SHIMADA, W., SHIRO, M., KONDO, H., TAKEYA, S., OYAMA, H., EBINUMA, T. & NARITA, H. 2005. Tetra-n-butylammonium bromide-water (1/38). *Acta Crystallographica Section C: Crystal Structure Communications,* 61**,** o65-o66.
SHIN, K., KIM, Y., STROBEL, T. A., PRASAD, P., SUGAHARA, T., LEE, H., SLOAN, E. D., SUM, A. K. & KOH, C. A. 2009. Tetra-n-butylammonium borohydride semiclathrate: a hybrid material for hydrogen storage. *The Journal of Physical Chemistry A,* 113**,** 6415-6418.
SLOAN, E. D. & KOH, C. A. 2008. *Clathrate hydrates of natural gases*, CRC PressTaylor &FrancisGroup,BocaRaton.
SMITH, J., VAN NESS, H. & ABBOTT, M. 1996. Chemical engineering thermodynamics. *Sat,* 18**,** 3.1-3.3.
SOAVE, G. 1972. Equilibrium constants from a modified Redlich-Kwong equation of state. *Chemical Engineering Science,* 27**,** 1197-1203.
STROBEL, T. A., TAYLOR, C. J., HESTER, K. C., DEC, S. F., KOH, C. A., MILLER, K. T. & SLOAN, E. 2006. Molecular hydrogen storage in binary THF-H2 clathrate hydrates. *The Journal of Physical Chemistry B,* 110**,** 17121-17125.
STRYJEK, R. & VERA, J. 1986. PRSV: An improved Peng—Robinson equation of state for pure compounds and mixtures. *The Canadian journal of chemical engineering,* 64**,** 323-333.

SUGINAKA, T., SAKAMOTO, H., IINO, K., TAKEYA, S., NAKAJIMA, M. & OHMURA, R. 2012. Thermodynamic properties of ionic semiclathrate hydrate formed with tetrabutylphosphonium bromide. *Fluid Phase Equilibria,* 317**,** 25-28.

SUN, Q., GUO, X., LIU, A., LIU, B., HUO, Y. & CHEN, G. 2010. Experimental study on the separation of CH4 and N2 via hydrate formation in TBAB solution. *Industrial & Engineering Chemistry Research,* 50**,** 2284-2288.

SUN, Z., WANG, R., MA, R., GUO, K. & FAN, S. 2003. Effect of surfactants and liquid hydrocarbons on gas hydrate formation rate and storage capacity. *International journal of energy research,* 27**,** 747-756.

TAKAO, S., OGOSHI, H., MATSUMOTO, S., TAKASHI, K., SUGIYAMA, M., AKIYAMA, T. & FUKUSHIMA, S. 2001. New air conditioning systems using hydrate slurry. *NKK TECHNICAL REPORT-JAPANESE EDITION-***,** 6-11.

TANII, T., MINEMOTO, M., NAKAZAWA, K. & ANDO, Y. 1997. Study on a cool storage system using HCFC (Hydro-Chloro-Fluoro-Carbon)-141B (CCI2 FCH3) (1, 1-dichloro-1-fluoro-ethane) clathrate. *The Canadian Journal of Chemical Engineering,* 75**,** 353-361.

TAYLOR, B. N. 2009. *Guidelines for Evaluating and Expressing the Uncertainty of NIST Measurement Results (rev*, DIANE Publishing.

TAYLOR, M., DAWE, R. A. & THOMAS, S. Fire and Ice: Gas hydrate transportation-A possibility for the Caribbean region. SPE Latin American and Caribbean Petroleum Engineering Conference, 2003. Society of Petroleum Engineers.

TERNES, M. P. 1984. *Characterization of refrigerant - 12 gas hydrate formation for heat pump cool storage applications*.

THOMAS, S. & DAWE, R. A. 2003. Review of ways to transport natural gas energy from countries which do not need the gas for domestic use. *Energy,* 28**,** 1461-1477.

TOMLINSON, J. J. 1982. Heat-pump cool storage in a clathrate of freon. Oak Ridge National Lab., TN (USA).

TOMLINSON, J. J., OLSZEWSKI M. & GEIST, G. A. A Comparative Study of Cool Storage Systems Based on Ice and Clathrates. in Proceedings of the 19th Intersociety Energy Conversion Erlgineering Conference, San Francisco, August 29-24,, August 29-24 1984 American Nuclear Society, La Grange Park. 1201-06.

UCHIDA, T., TAKAGI, A., MAE, S. & KAWABATA, J. 1997. Dissolution mechanisms of CO $_2$ molecules in water containing CO_2 hydrates. *Energy Conversion and Management,* 38**,** S307-S312.

WAALS, J. H. V. D. & PLATTEEUW, J. C. 2007. Clathrate Solutions. *Advances in Chemical Physics.* John Wiley & Sons, Inc.

WANG, X., DENNIS, M. & HOU, L. 2014. Clathrate hydrate technology for cold storage in air conditioning systems. *Renewable and Sustainable Energy Reviews,* 36**,** 34-51.

WENJI, S., RUI, X., CHONG, H., SHIHUI, H., KAIJUN, D. & ZIPING, F. 2009. Experimental investigation on TBAB clathrate hydrate slurry flows in a horizontal tube: Forced convective heat transfer behaviors. *international journal of refrigeration,* 32**,** 1801-1807.

WITTSTRUCK, T. A., BREY, W. S., BUSWELL, A. M. & RODEBUSH, W. H. 1961. Solid Hydrates of Some Halomethanes. *Journal of Chemical & Engineering Data,* 6**,** 343-346.

WU, J. & WANG, S. 2012. Research on cool storage and release characteristics of R134a gas hydrate with additive. *Energy and Buildings,* 45**,** 99-105.

XIAO, R., WU, S., TANG, L., HUANG, C. & FENG, Z. Experimental investigation of the pressure-drop of clathrate hydrate slurry (CHS) flow of tetra butyl ammonium bromide (TBAB) in straight pipe. Proceedings of the 10th International Conference on Thermal Energy Storage. the Richard Stockton College of New Jersey, USA, 2006.

XIE, Y., LI, G., LIU, D., LIU, N., QI, Y., LIANG, D., GUO, K. & FAN, S. 2010. Experimental study on a small scale of gas hydrate cold storage apparatus. *Applied Energy,* 87**,** 3340-3346.

XIE, Y., LIANG, D., GUO, K., FAN, S., GU, J. & CHEN, J. 2004. Advances of gas hydrate cool storage technology. *HV& AC (China),* 34**,** 25-8.

YAMAZAKI, M., SASAKI, C., KAKIUCHI, H., OSANO, Y. & SUGA, H. 2002. Thermal and structural characterization of trimethylolethane trihydrate. *Thermochimica acta,* 387**,** 39-45.

YANG, H., XU, Z., FAN, M., GUPTA, R., SLIMANE, R. B., BLAND, A. E. & WRIGHT, I. 2008. Progress in carbon dioxide separation and capture: A review. *Journal of Environmental Sciences,* 20**,** 14-27.

YANG, S., YANG, I., KIM, Y. & LEE, C. 2000. Measurement and prediction of phase equilibria for water+ CO_2 in hydrate forming conditions. *Fluid Phase Equilibria,* 175**,** 75-89.

YINGMING, X., DEQING, L. & KAIHUA, G. 2004. Advance of gas hydrate cool storage technology. *Heating Ventilating & Air Conditoning,* 34**,** 25-28.

YOUSSEF, Z., DELAHAYE, A., HUANG, L., TRINQUET, F., FOURNAISON, L., POLLERBERG, C. & DOETSCH, C. 2013. State of the art on phase change material slurries. *Energy Conversion and Management,* 65**,** 120-132.

ZHANG, J. & LEE, J. W. 2008. Equilibrium of Hydrogen+ Cyclopentane and Carbon Dioxide+ Cyclopentane Binary Hydrates†. *Journal of Chemical & Engineering Data,* 54**,** 659-661.

ZHANG, J., LEE, S. & LEE, J. W. 2007. Kinetics of methane hydrate formation from SDS solution. *Industrial & Engineering Chemistry Research,* 46**,** 6353-6359.

ZHANG, P. & MA, Z. 2012. An overview of fundamental studies and applications of phase change material slurries to secondary loop refrigeration and air conditioning systems. *Renewable and Sustainable Energy Reviews,* 16**,** 5021-5058.

ZHANG, P., MA, Z. & WANG, R. 2010. An overview of phase change material slurries: MPCS and CHS. *Renewable and Sustainable Energy Reviews,* 14**,** 598-614.

ZHENG, D.-Q., GUO, T.-M. & KNAPP, H. 1997. Experimental and modeling studies on the solubility of CO_2, $CHClF_2$, CHF_3, $C_2H_2F_4$ and $C_2H_4F_2$ in water and aqueous NaCl solutions under low pressures. *Fluid phase equilibria,* 129**,** 197-209.

ZHONG, Y. & ROGERS, R. 2000. Surfactant effects on gas hydrate formation. *Chemical Engineering Science,* 55**,** 4175-4187.

Appendix A: Application of Gas hydrate Technology

A.1. Gas hydrates as a source of energy

Gas hydrates can also form in deep ocean sediments and permafrost layers in which the hydrate formation requirements (high pressure and low temperature) are met. The discovery of enormous amounts of gas hydrates in the nature in 1960s, intensified this idea that gas hydrates can be considered as a new source of sustainable energy (Sloan and Koh, 2008). The estimations of the quantity of these hydrate reservoirs is highly uncertain however, Kvenvolden and Makogon showed that the amount of gas hydrate resources in 1988 was at least twice as much as the energy in the total fossil deposits (Kvenvolden, 1988, Makogon, 1988). Later, Collett and Kuuskraa estimated the range of 1.4×10^{1} to 3.4×10^{4} and 3.1×10^{3} to 7.6×10^{6} trillion cubic meter (tcm) for permafrost layers and oceanic sediments respectively (Collett and Kuuskraa, 1998). Though, fossil fuel reserves are currently adequate to meet worldwide energy requirements, gas production from natural gas hydrates reserves is being looked up on as a far alternative, particularly for offshore hydrate reserves (Grauls, 2001). However in the gas production from these reservoirs the environment impact is a significant issue.

The reader is refered to the following literature for further information (Collett, 2002, Seo et al., 2001).

A.2. Marine carbon dioxide sequestration

The enhanced greenhouse gas effect is mainly contributed to the worldwide emissions of carbon dioxide. Hence many studies have been carried out in order to moderate the amount of CO_2 in the atmosphere and several techniques have been proposed to date. One solution is the injection of the CO_2 in deep oceans (Brewer et al., 1999, Kojima et al., 2002, Lee et al., 2003). The CO_2 hydrate would form at the depth of approximately 500 to 900 meters and owing to the density of the hydrate it would sink to the bottom and stabilize. The project is still under experimental analysis and many studies focus the solubility of CO_2 in sea water, kinetics of the CO_2 hydrate formation and CO_2 hydrate stability zone (Kojima et al., 2002, Aya et al., 1997, Yang et al., 2000, Holder et al., 1995, Uchida et al., 1997, Circone et al., 2003, Lee et al., 2003).

A.3. Gas storage

Since a single volume of gas hydrate can hold up 184 volume of gas per one volume of water at standard conditions, they have been considered to be a decent media in gas storage and transportation applications. The main advantage of storage and transportation of gas using gas hydrate over conventional approaches such as liquefaction is their safety and lower process volume. The proposed process includes three steps: (1) hydrate formation (2) shipping of the gas hydrate (3) dissociation of the gas hydrate and recovery of the gas (Thomas and Dawe, 2003).

The first step is usually achieved by mixing of gas and water at an appropriate temperature. In order to promote the hydrate formation nucleation the application of surfactants has been proposed (Zhong and Rogers, 2000). In the second step the temperature of the system is set to approximately 258 K at atmospheric pressure in order to stabilize the gas hydrate during transportation (Taylor et al., 2003). Finally in the third step the hydrate is dissociated and the gas is released. The lower working pressures and higher working temperatures than those of the liquefaction and compression processes make this novel method tas practical as conventional processes.

A.4. Gas separation

Many studies reveal the fact that huge amounts of carbon dioxide, carbon monoxide, and hydrogen sulfide which are known as greenhouse gases are released every year into the atmosphere by combustion of fossil and fossil-based fuels (Hall et al., 2003, Yang et al., 2008, Peng and Zhuang, 2012, Bacher, 2002). The ever increasing concentration of these gases in the atmosphere is the main concern of the human being regarding the climate change. One solution to this problem is to separate these gases from their flue gas streams in industrial processes. A novel approach which has been considered recently is separation of gases through hydrate formation. The process has shown to be quite promising thanks to the difference in the tendency of CO_2 and other gases to be captured in the hydrate cages. After formation of gas hydrate crystals from the considered gas mixture, the hydrate phase can be enriched in CO_2 while the concentration of other gases can be increased in the gas phase. The hydrate will be dissociated afterwards to recover the CO_2 by depressurization and/or heating (Belandria et al., 2011).

The major problems of using the gas hydrates in any gas hydrate-based process is their high pressures and low temperatures of formation as well as their slow rate of formation. One solution to these problems is using gas hydrate promoters which can be categorized into two groups of thermodynamic and kinetic promoters (Sloan and Koh, 2008, Eslamimanesh et al., 2012). Thermodynamic promoters which can reduce the hydrate formation pressure and/ or increase the hydrate formation temperature are typically classified into two groups:

1. Chemical additives which do not participate in hydrogen bonded water molecules of the hydrate structure such as tetrahydrofuran (THF), cyclopentane, acetone etc. (Papadimitriou et al., 2011, Mooijer-Van Den Heuvel et al., 2001, Strobel et al., 2006)
2. Promoters that participate in the structures of the ordinary water cages in the traditional clathrates networks such as tetra-n-butylammonium salts such as TBAB and tetra-n-butylammonium borohydride (Shimada et al., 2003, Shin et al., 2009, Sun et al., 2010). 27,184,237–266

Kinetics additives which have no effect on the thermodynamics (pressure and temperature) of the hydrate formation, promote the hydrate nucleation rate by decreasing of the water surface tension consequently increasing the diffusivity of the gas molecules in water to initiate the hydrate nucleation. The kinetic additives which are used are including anionic surfactants sodium dodecyl sulfate (SDS) and linear alkyl benzene sulfonate (LABS), cationic surfactant cetyl trimethyl ammonium bromide (CTAB) and non-ionic surfactant ethoxylated nonylphenol (ENP) (Sun et al., 2010, Sloan and Koh, 2008). THF and TBAB are well-known thermodynamic promoters that have been used in non-industrial scale to date. The second category of thermodynamic promoters (semi-clathrate hydrates) comprises generally of environmental friendly tetra-n-butylammonium salts in which a part of the cage structure is broken in order to accommodate the large tetra-n-butyl ammonium molecule. This property of the semi-clathrate hydrates resulting in the more storage capacity comparing to that of promoters such as THF. Even though promoters such as THF can considerably promote the hydrate formation process, however, during their high volatility significant amount of the promoter would be lost during the corresponding storage/separation/transportation processes (Eslamimanesh et al., 2012).

A.5. Desalination of sea water

The cyclic formation and dissociation of refrigerant hydrate can be utilized as an alternative method for the purification of saline water instead of conventional approaches such as multistage flash (MSF) distillation and reverse osmosis (RO) (Max and Pellenbarg, 2000, Park et al., 2011, Javanmardi and Moshfeghian, 2003, Akiya et al., 1999). The process has been shown to be quite promising because water and an appropriate refrigerant can form hydrate at moderate temperatures and atmospheric pressure. The resultant hydrate can be dissociated later to obtain pure water and refrigerant which can be recycled into the system. Nemours studies have been carried out in the aim of designing an efficient and economic desalination process using gas hydrates (Parker, 1942, Briggs et al., 1962, Javanmardi and Moshfeghian, 2003, Ngema et al., 2014b). Although, the results indicate that the process may not be economically viable comparing to the conventional methods (Englezos, 1993, Chun et al., 2000) however, it was found that the application of hydrate promoters can reduce the energy cost of the process significantly.

A.6. Food industry

The food industry also use the gas hydrates favourably for producing of fluid concentrates. The process appears to be more efficient than freeze concentration since the gas hydrates can form at the temperatures above ice point. The process has been applied for different aqueous solutions including carbohydrates, proteins, or lipids and the concentration of apple, orange, and tomato juices (Glew, 1962, Huang et al., 1965, Huang et al., 1966).

Appendix B: G^E-EOS mixing rule

B.1. PRSV equation of state

In 1976 a cubic equation of state proposed by Peng and Robinson as follows:

$$P = \frac{RT}{V-b} - \frac{a}{V^2 - 2bV - b} \tag{B.1}$$

where

$$a_i(T) = 0.457235(\frac{R^2 T_c^2}{P_c})\alpha(T) \tag{B.2}$$

$$b_i = 0.077796(\frac{RT_C}{P_C}) \tag{B.3}$$

The expression proposed by Soave (Soave, 1972) is used for the α:

$$\alpha(T) = (1 + k(1 - T_r)^{0.5})^2 \tag{B.4}$$

in which k is assumed to be a function of acentric factor. Later, more accurate expression for parameter k was proposed by Stryjek and Vera (Stryjek and Vera, 1986) as a function of reduce temperature (T_r) and acentric factor (ω) as below:

$$k = k_0 + k_1(1 - T_r^{0.5})(0.7 - T_r) \tag{B.5}$$

$$k_0 = 0.378893 + 1.489715\ \omega - 0.17131\ \omega^2 + 0.01965\ \omega^3 \tag{B.6}$$

B.2. Huron and Vidal and (HV) Mixing Rules

Huron and Vidal (Huron and Vidal, 1979) established that the conventional van der Waals mixing rules are consistent with the usual solution theory and has restricted ability in fitting excess Gibbs energy data for polar classes over a wide pressure range. They developed a method that effectively incorporated the excess Gibbs energy, G^E, created from an equation of state with that from an activity coefficient model at infinite pressure. Their technique produced a mixing rule with the parameters a and b in a cubic EoS:

$$a = b\left[\sum x_i\left(\frac{a_i}{b_i}\right) + \frac{G^E}{C^*}\right] \tag{B.7}$$

b is formulated in a simple van der Waals form. C^* is an EoS-dependent parameter. For the PRSV EoS, this parameter equals to -0.62323. In incorporating G^E, Huron and Vidal also assumed that $V = b$, and $V^E = 0$.

The originality of the Huron and Vidal's grouping of an EoS and an activity (excess Gibbs model) has encouraged a family of matching methods over the last two decades. Of superior advantage is the use of predictive G^E models in these EoS-G^E models, such as the UNIFAC style, as it makes the EoS-G^E algorithm completely predictive.

B.3. Mixing Rules of Modified Huron-Vidal (MHV)

Since the low-pressure group interaction parameters have been continuously updated for UNIFAC, the conventional UNIFAC may not be suitable for a predictive EoS-G^E algorithm that was derived by matching G^E at infinite pressure. As a solution, Mollerup (Mollerup, 1986) suggested a procedure that incorporates excess free energies at zero pressure. This method, however, involves solving the molar volume of liquid species from an EoS, which is not always viable, as the isotherms of a cubic EoS do not necessary cross the molar volume axis at high temperatures. To solve this problem, Michelsen (Michelsen, 1990) proposed an extrapolation method to estimate the molar volume at zero pressure. The mixing rules developed from the matching at zero pressure contain the parameters a, b a solution of the following equations:

$$q(\alpha_m) = \sum_i z_i q(\alpha_i) + \frac{G_0^E}{RT} + \sum_i z_i \ln\left(\frac{b}{b_i}\right) \tag{B.8}$$

$$b = \sum z_i b_i \tag{B.9}$$

where

$$q(\alpha) = -\ln\left(\frac{V^0}{b} - 1\right) + \frac{a}{bRT}C^* \qquad \text{(B.10)}$$

In equation (B.8), z_i stands for the mole fraction of component i. The superscript 0 for molar volume and free Gibbs energy G_0^E defines their value at $P=0$. Michelsen et al. estimated q by a polynomial function of $\alpha = a/bRT$, a dimensionless energy parameter (Michelsen, 1990). Specially, in the so-called MHV1 model, Michelsen et al. selected a linear approximation for $q(\alpha)$ as bellows:

$$q(\alpha) = q_0 + q_1\alpha \qquad \text{(B.11)}$$

Later, in the so-called MHV2 model, a quadratic correlation was suggested for $q(\alpha)$ for better flexibility (Dahl et al., 1991):

$$q(\alpha) = q_0 + q_1\alpha + q_2\alpha^2 \qquad \text{(B.12)}$$

where the parameters q_1 and q_2 in the above equations are selected to ensure continuity of $q(\alpha)$ and its derivatives. The recommended values of q_1 and q_2 are -0.4347 and −0.003654, respectively for the PRSV EOS (Mollerup, 1986). Substituting Eq. (B.8) into Eq. (B.12) gives:

$$q_1(\alpha_m - \sum_{i=1}^{C} z_i\alpha_i) + q_2(\alpha_i^2 - \sum_{i=1}^{C} z_i\alpha_i^2) = \frac{G_0^E}{RT} + \sum_{i=1}^{C} z_i \ln(\frac{b_m}{b_i}) \qquad \text{(B.13)}$$

Where,

$$\frac{G_0^E}{RT} = \sum_i z_i \ln\gamma_i \qquad \text{(B.14)}$$

B.4. UNIFAC Activity model

In equation (B14), the activity coefficient of components can be obtained using UNIFAC group contribution activity model as bellows (Magnussen et al., 1981, Hashemi et al., 2015b):

$$\ln\gamma_i = \ln\gamma_i^C + \ln\gamma_i^R \tag{B.15}$$

where, $\ln\gamma_i^C$, is the combinatorial term defined by:

$$\ln\gamma_i^C = \left(\ln\frac{\Phi_i}{z_i} + 1 - \frac{\Phi_i}{z_i}\right) - 5q_i\left(\ln\frac{\Phi_i}{\theta_i} + 1 - \frac{\Phi_i}{\theta_i}\right) \tag{B.16}$$

in which z_i stands for the mole fraction of component i, θ_i presents the area function and Φ_i shows the segment function which is defined as bellow:

$$\theta_i = \frac{q_i z_i}{\sum_j q_j z_j} \tag{B.17}$$

$$\Phi_i = \frac{r_i z_i}{\sum_j r_j z_j} \tag{B.18}$$

$$r_i = \sum_k v_{ki} R_k \tag{B.19}$$

$$q_i = \sum_k v_{ki} Q_k \tag{B.20}$$

In the above equations, v_{ki} defines the number of groups of type k in molecule i, R_k and Q_k are UNIFAC volume and surface area parameters respectively. The residual term, $\ln\gamma_i^R$, defines the interaction between the molecules and can be presented by (Magnussen et al., 1981):

$$\ln\gamma_i^R = \sum_k v_{ki}\left(\ln\Gamma_k - \ln\Gamma_k^i\right) \tag{B.21}$$

where,

$$\ln \Gamma_k = Q_k \left[1 - \ln\left(\sum_m \theta_m \Psi_{mk} \right) - \sum_m \left(\frac{\theta_m \Psi_{km}}{\sum_n \theta_n \Psi_{nm}} \right) \right] \tag{B.22}$$

In this study the following expression has been used for evaluation of the interaction parameters, ψ, of the UNIFAC activity model:

$$\Psi_{mn} = \exp\left[-\left(\frac{a_{mn}}{T} \right) \right] \tag{B.23}$$

where *a* and *b* are the temperature-independent group interaction parameters.

Appendix C: Results

C. 1. Kinetic results

C.1.1. Initial conditions

Temperature difference between the initial refrigerant hydrate formation condition and equilibrium hydrate dissociation points ($\Delta T = T\text{-}T_{equilibrium}$) for refrigerants investigated in this study are depicted in Figures C.1 and C.2. The degree of subcooling is playing an important role in kinetic studies and this study is trying to present the kinetics of the hydrate formation of different refrigerants at different degree of subcooling.

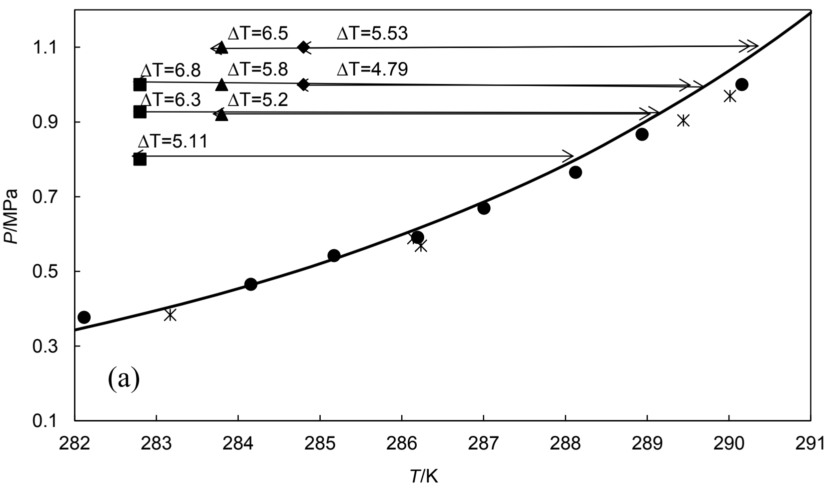

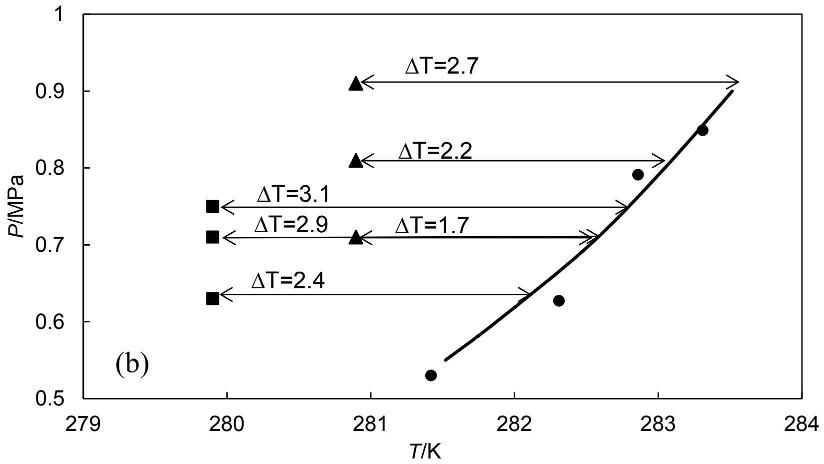

Figure C.1. Temperature differences between the initial refrigerant hydrate formation condition and equilibrium hydrate dissociation points. **(a)** R410A; ■, 282.8 K; ▲, 283.8 K; ♦, 284.8 K; ●, gas hydrate equilibrium conditions; **(b)** R507C, ■, 279.9K; ▲, 280.9K; gas hydrate equilibrium conditions:●, this work; Solid lines, model predictions.

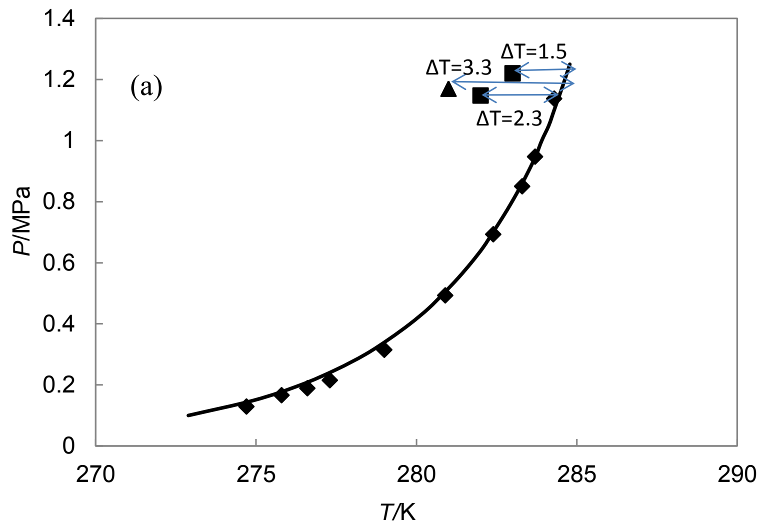

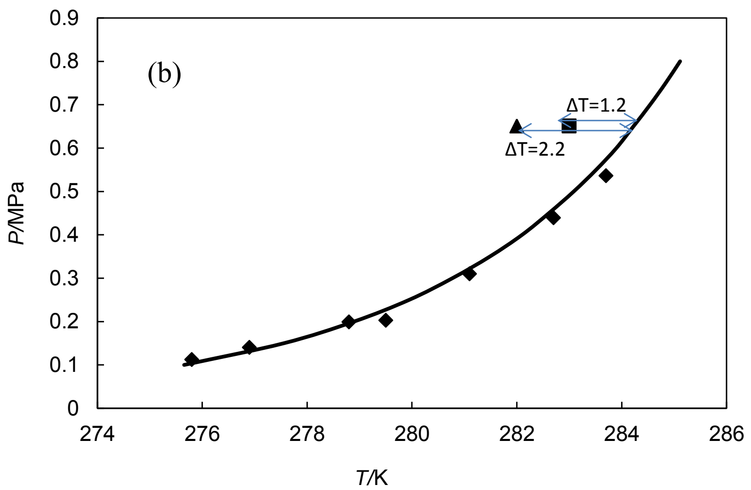

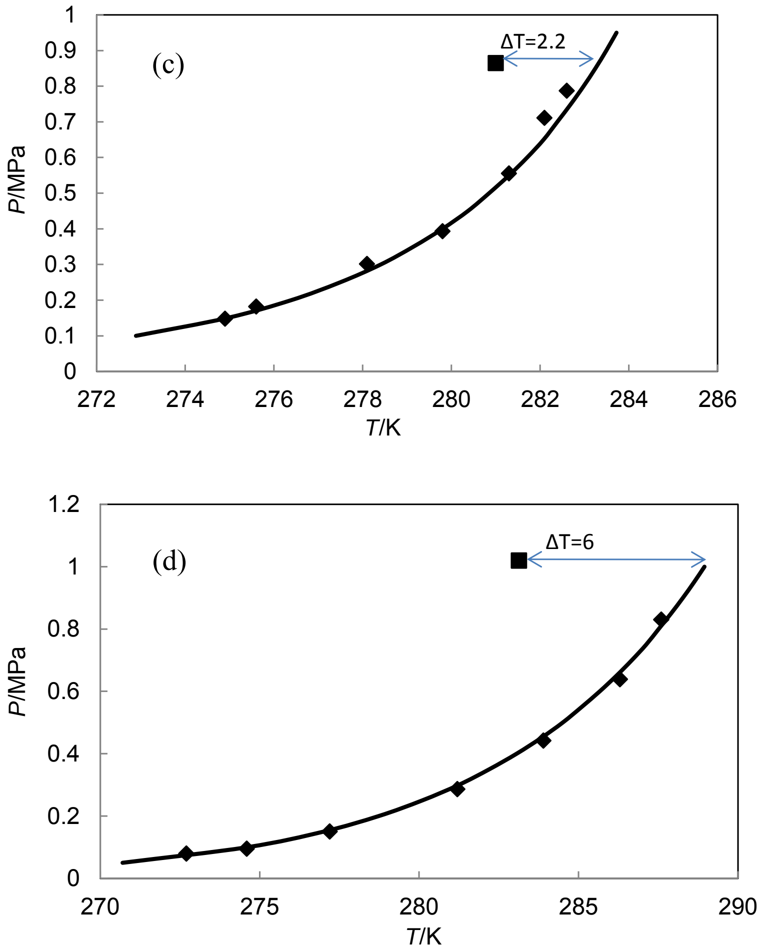

Figure C.2. Temperature difference between the initial refrigerant hydrate formation condition and equilibrium hydrate dissociation points. **(a)** R404A; ▲, 281 K; ■, 282K; **(b)** R406A, ▲, 282 K; ■, 283K; **(c)** R408A, ■, 281K; **(d)** R427A, ■, 283.14K; ♦, gas hydrate equilibrium conditions; solid lines, model predictions.

C.1.2. Pressure change and induction time

The pressure change before and during the gas hydrate formation is depicted in this section. The effect of the initial pressure as well as addition of SDS solutions on the induction time of gas hydrate formation are studied and shown in Figures C.3 to C.16. The results show that the induction time decreases with increasing pressure. The effect of SDS solution is different for different refrigerants.

C.1.2.1. Effect of SDS solution on the induction time

The effects of SDS solution on refrigerant nucleation rate are summarized as bellow:

- SDS solution inhibited the gas hydrate formation and nucleation rate for three refrigerants R410A, R407C and R 507C (Figures C.9 to C.11).
- The hydrate formation rate of R404A was promoted using 400 ppm SDS solution (Figures C12).
- The hydrate formation rate of R406A increased in the presence of 400 ppm SDS solution and decreased in the presence of 600 ppm SDS solution (Figures C13 and C14).
- No effect of SDS solution with concentration of 400 ppm observed for 408A and a promotion effect was observed in the presence of 600 ppm SDS solution (Figure C.15).
- The hydrate nucleation rate for R427A was increased in the presence of 400 ppm SDS solution (Figure 16).

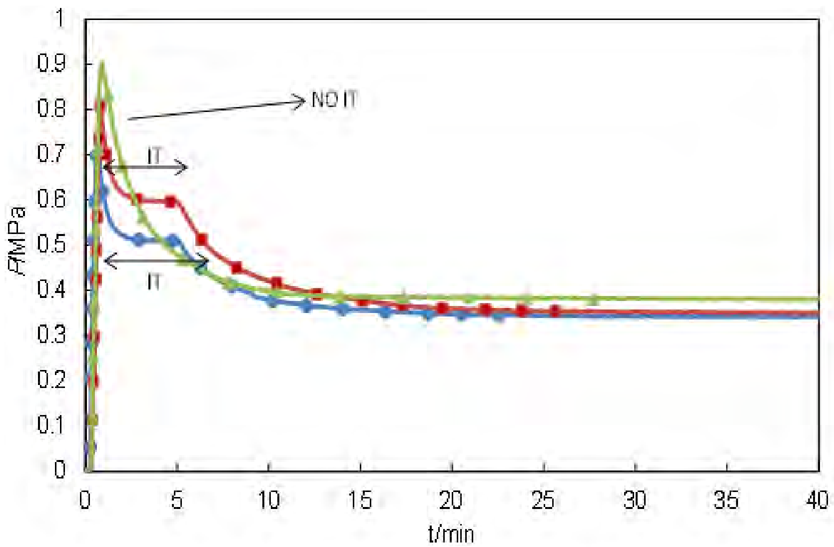

Figure C.3. Pressure change during R407C hydrate formation at a constant temperature of 281.8 K and varying pressures with a stirrer speed at 620 rpm, ●, 0.73 MPa; ■, 0. 81 MPa; ▲, 0.9 MPa. IT, induction time; solid lines, trend lines.

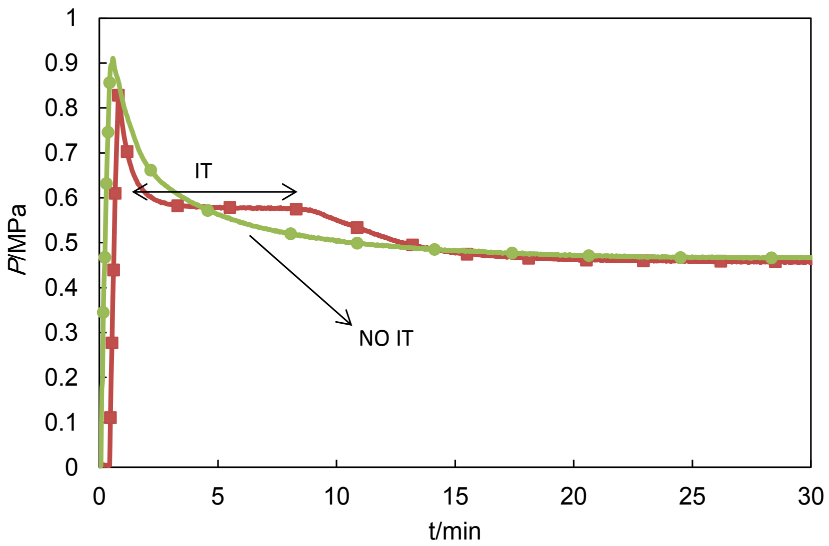

Figure C.4. Pressure change during R407C hydrate formation at a constant temperature of 283.8 K and varying pressures with a stirrer speed at 620 rpm: ■, 0. 82 MPa; ●, 0.91MPa; IT, induction time; solid lines, trend lines.

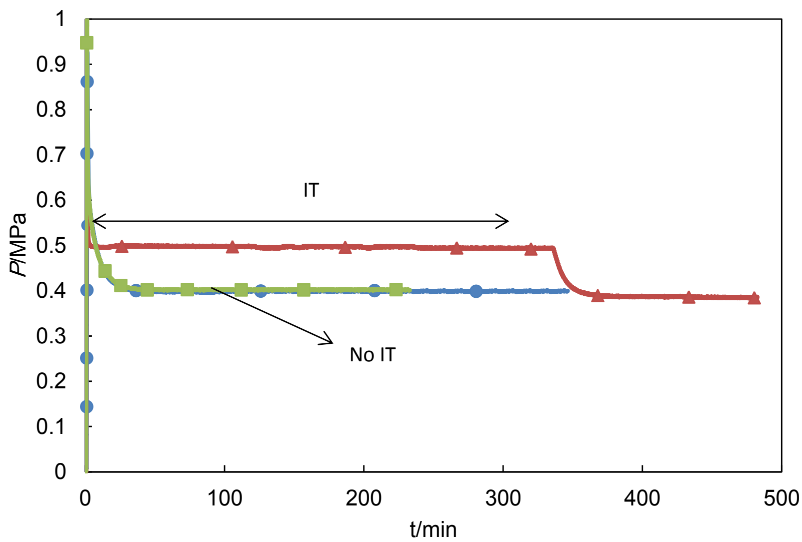

Figure C.5. Pressure change during R410A hydrate formation at a constant temperature of 282.8 K and varying pressures with a stirrer speed 620 rpm: ▲, 0.83 MPa; ●, 0.93 MPa; ■, 1 MPa; IT, induction time; solid lines, trend lines.

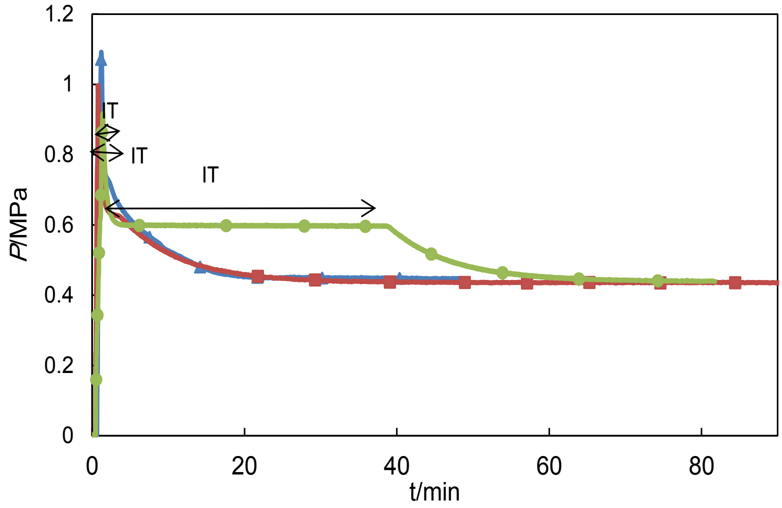

Figure C.6. Pressure change during R410A hydrate formation at a constant temperature of 283.8 K and varying pressures with a stirrer speed 620 rpm: ●, 0.92 MPa; ■, 1MPa; ▲, 1.1 MPa; IT, induction time; solid lines, trend lines.

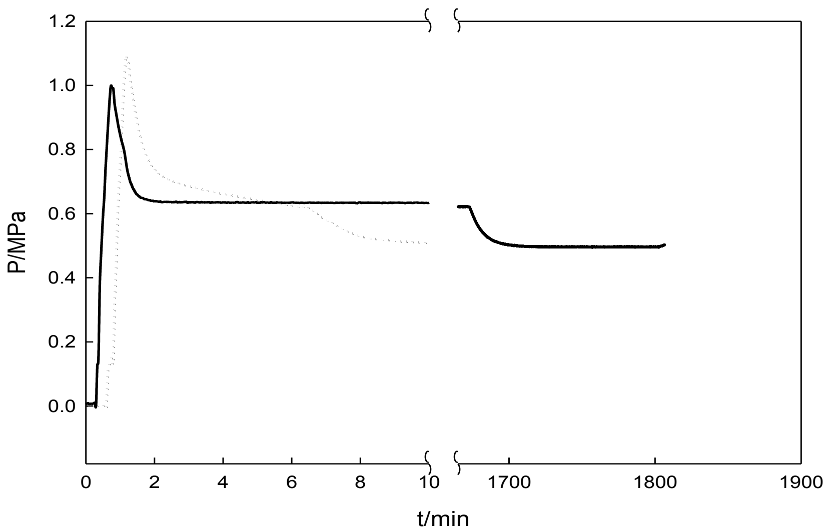

Figure C.7. Pressure change during R410A hydrate formation at a constant temperature of 284.8 K and varying pressures with a stirrer speed 620 rpm: (▬), 1 MPa; (-----), 1.1MP. IT, induction time.

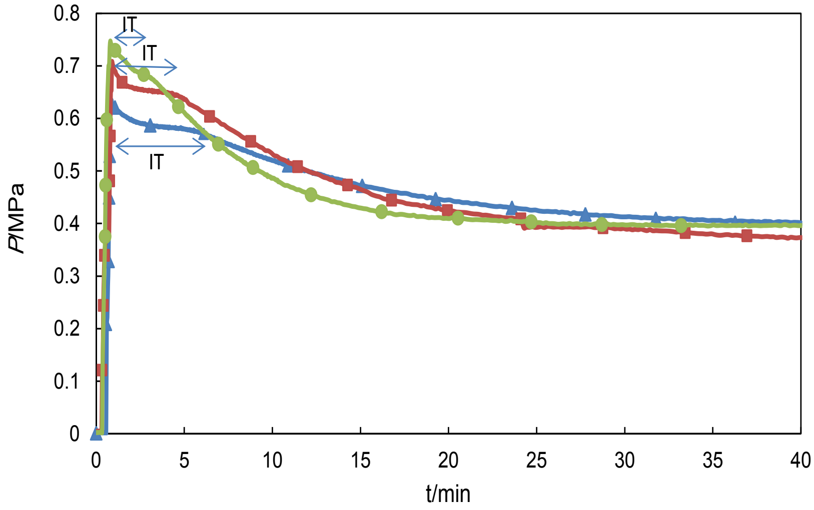

Figure C.8. Pressure change during R507C hydrate formation at a constant temperature of 279.9 K and varying pressures with a stirrer speed 620 rpm: ▲, 0.63 MPa; ■, 0.71MPa; ●, 0.75 MPa; IT, induction time; solid lines, trend lines.

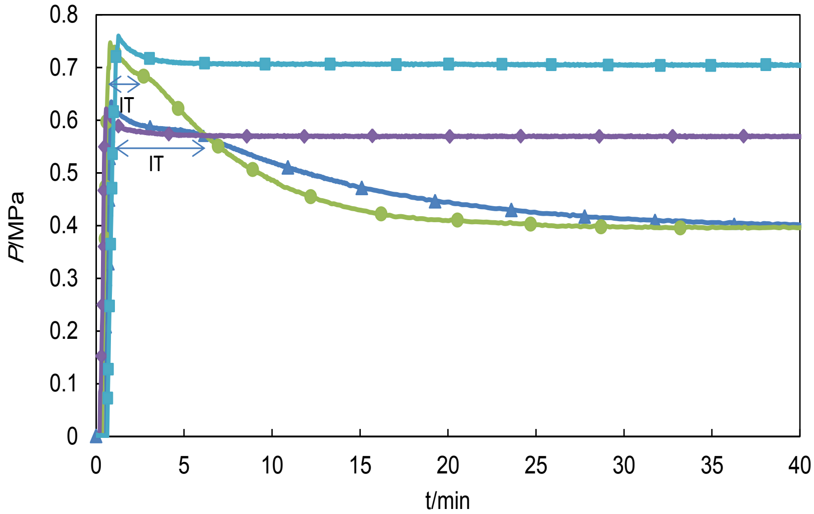

Figure C.9. Pressure change during R507C hydrate formation at a constant temperature of 279.9 K and varying pressures with a stirrer speed at 620 rpm: ▲, 0.63 MPa (pure water); ●, 0.75 MPa (pure water); ♦, 0.62 MPa (400 ppm SDS); ■, 0.76 MPa (100 ppm SDS); IT, induction time; solid lines, trend lines.

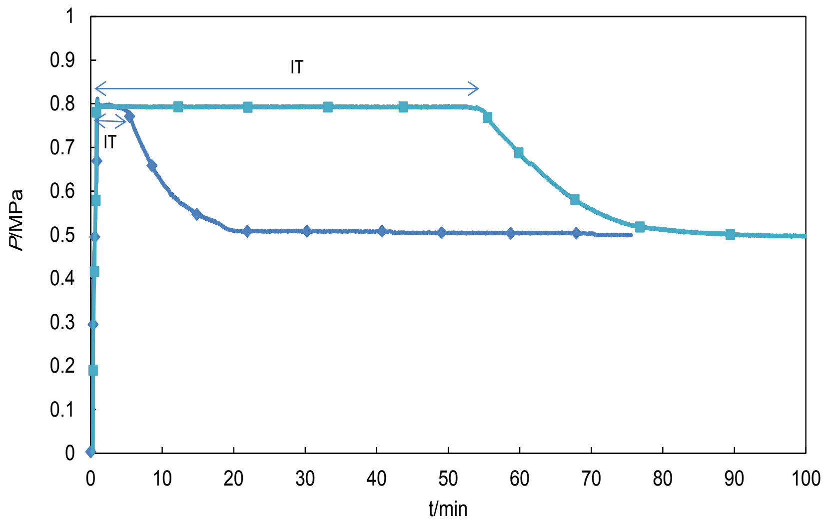

Figure C.10. Pressure change during R507C hydrate formation at a constant temperature of 280.9 K and pressure of 0.81 MPa and 620 rpm stirrer speed; ■, 400 ppm SDS; ♦, pure water; IT, induction time; solid lines, trend lines.

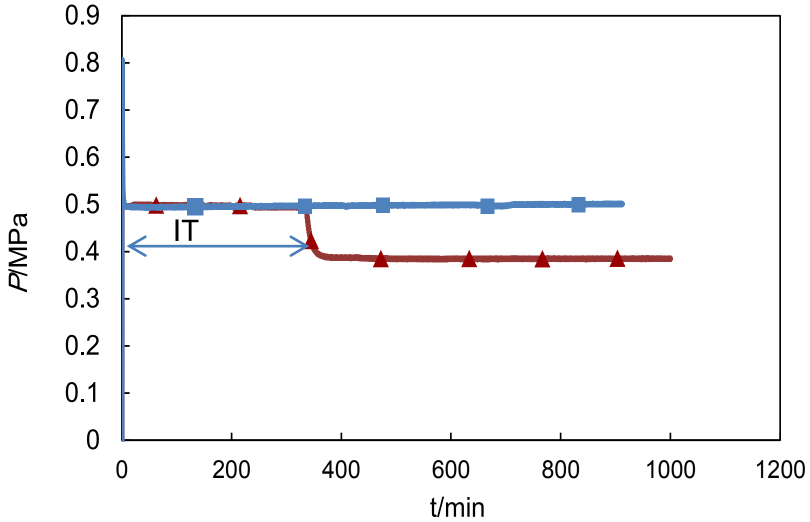

Figure C.11. Pressure change during R410A hydrate formation at a constant temperature of 282.8 K and pressure of 0.8 MPa and 620 rpm stirrer speed ; ■, 400 ppm SDS; ▲, pure water; IT, induction time; solid lines, trend lines.

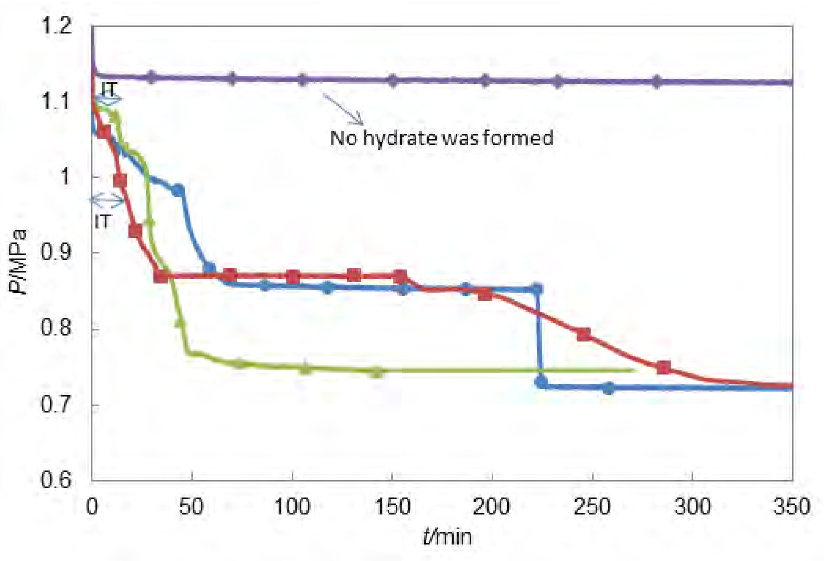

Figure C.12. Pressure change during R404A hydrate formation at different initial conditions of ●, 282 K and 1.147 MPa pure water ;▲, 282 K and 1.147 MPa 400 ppm SDS; ■, 281 K and 1.17MPa pure water; ♦, 283 K and 1.22 MPa pure water, with a stirrer speed 620 rpm; IT, induction time; solid lines, trend lines..

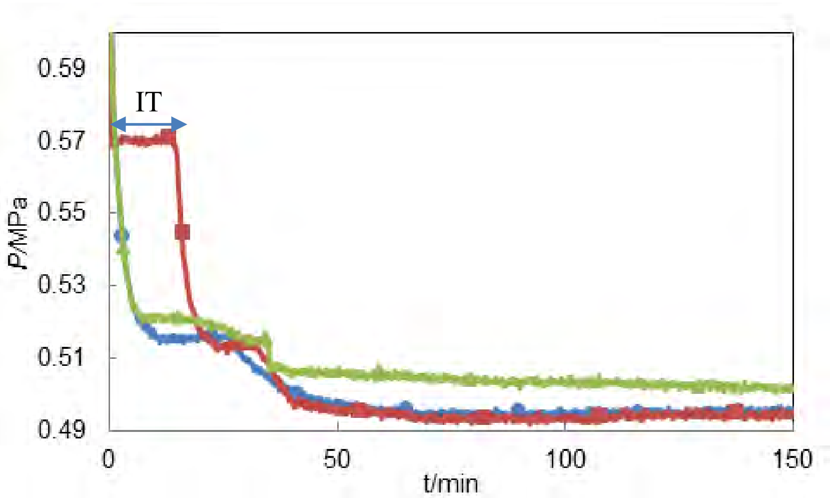

Figure C.13. Pressure change during R406A hydrate formation at a constant temperature and pressure of 282 K and 0.651 MPa respectively with a stirrer speed 620 rpm: ●, pure water; ▲, 400 ppm SDS; ■, 600 ppm SDS; IT, induction time; solid lines, trend lines.

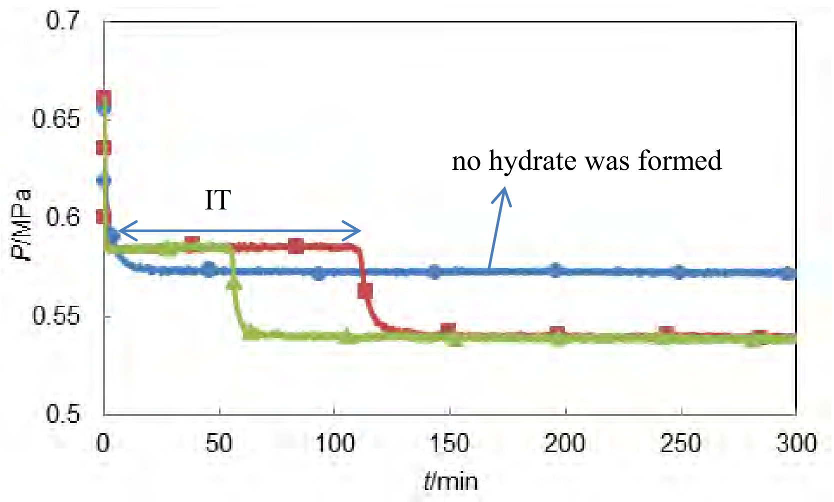

Figure C.14. Pressure change during R406A hydrate formation at a constant temperature and pressure of 283 K and 0.651 MPa respectively with a stirrer speed 620 rpm: ■, 400 ppm SDS; ▲, 500 ppm SDS; ●, pure water; IT, induction time; solid lines, trend lines.

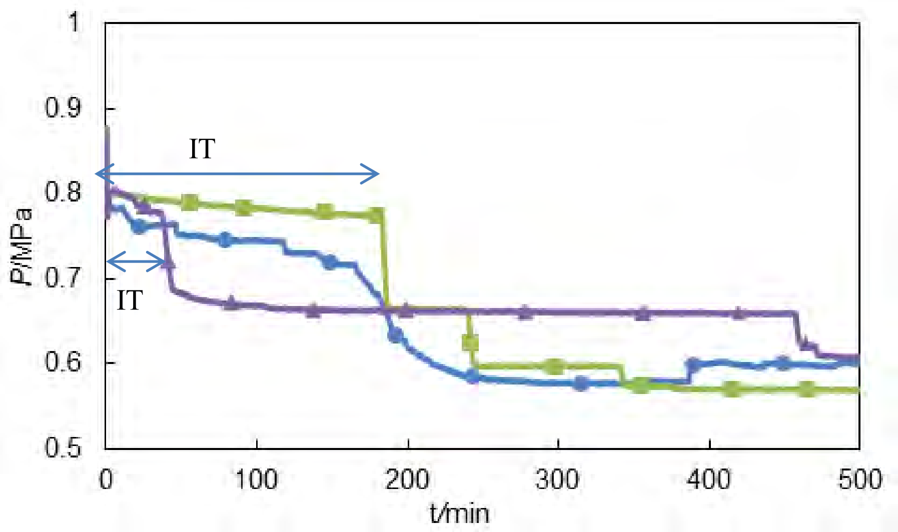

Figure C.15. Pressure change during R408A hydrate formation at a constant temperature and pressure of 281 K and 0.864 MPa respectively with a stirrer speed 620 rpm: ●, pure water; ■, 400 ppm SDS; ▲, 600 ppm SDS; IT, induction time; solid lines, trend lines.

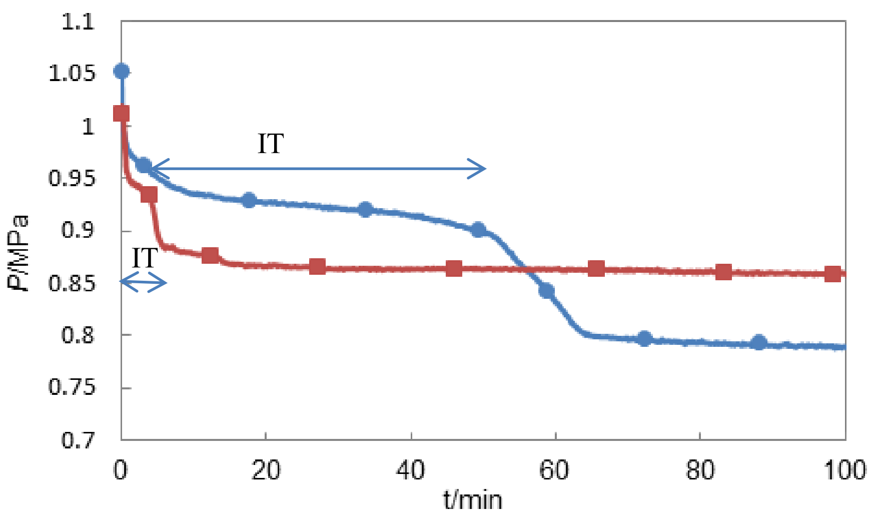

Figure C.16. Pressure change during R427A hydrate formation at constant temperature of 283.1 K and varying pressures with a stirrer speed 620 rpm: ●, 1.051MPa pure water; ■, 1.109 MPa 400 ppm SDS; IT, induction time; solid lines, trend lines.

C.1.3. Storage capacity (SC)

The storage capacity as a function of time is depicted in Figures C.17 to C.26. The results indicate that the storage capacity increases with increasing pressure. The effect of SDS solution is different for different refrigerants.

C.1.3.1. Effect of SDS solution

The effects of SDS solution on the refrigerant hydrates storage capacity are summarized as bellow:

- For R507C the SDS solution decreased the storage capacity (Figure C.23).
- The storage capacity of R404A increased using 400 ppm SDS solution (Figures C.24).
- The storage capacity of R406A increased in the presence of 400 ppm SDS solution and decreased in the presence of 600 ppm SDS solution (Figures C.25).
- For R408A the storage capacity increased in the presence of SDS solution with concentration of 400 ppm and decreased in the presence of 600 ppm SDS solution (Figure C.26).

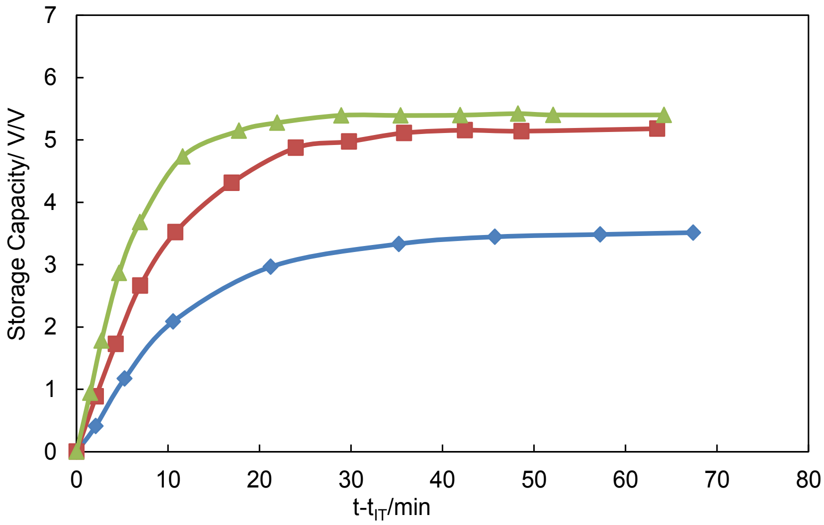

Figure C.17. Storage Capacity during R507C hydrate growth at an initial temperature of 279.9 K and different pressures. ♦, 0.64 MPa; ■, 0.71 MPa; ▲, 0.75 MPa; solid lines, trend lines.

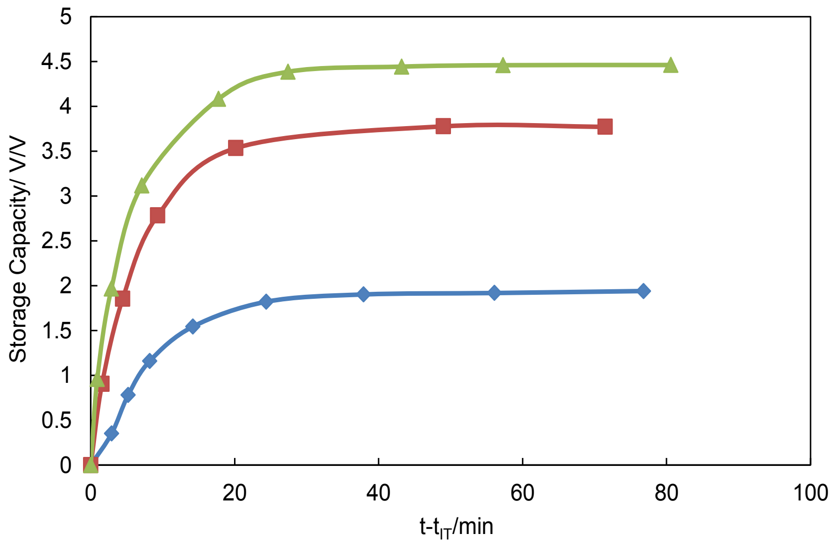

Figure C.18. Storage Capacity during R410A hydrate growth at an initial temperature of 282.8 K and pressures of: ♦, 0.81 MPa; ■, 0.93 MPa; ▲, 1 MPa in the presence of pure water; solid lines, trend lines.

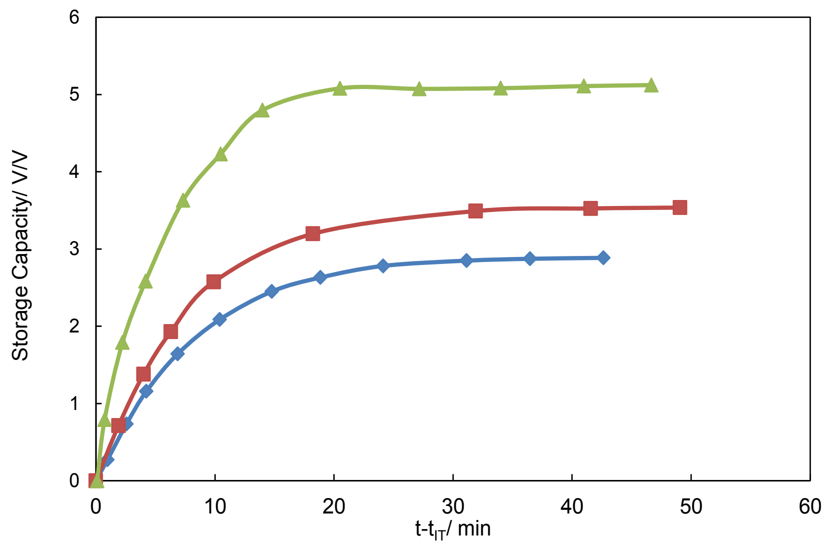

Figure C.19. Storage Capacity during the R410A hydrate growth at an initial temperature of 283.8 K and the pressures of: ♦, 0.92 MPa; ■, 1 MPa ; ▲, 1.1 MPa in the presence of pure water; solid lines, trend lines..

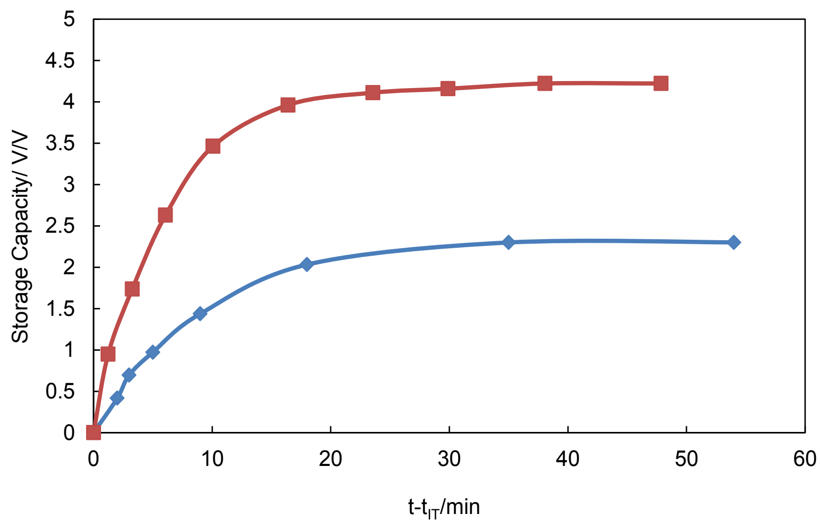

Figure C.20. Storage Capacity during the R410A hydrate growth at an initial temperature of 284.8 K and the pressures: ♦, 1 MPa; ■, 1.1 MPa in the presence of pure water; solid lines, trend lines.

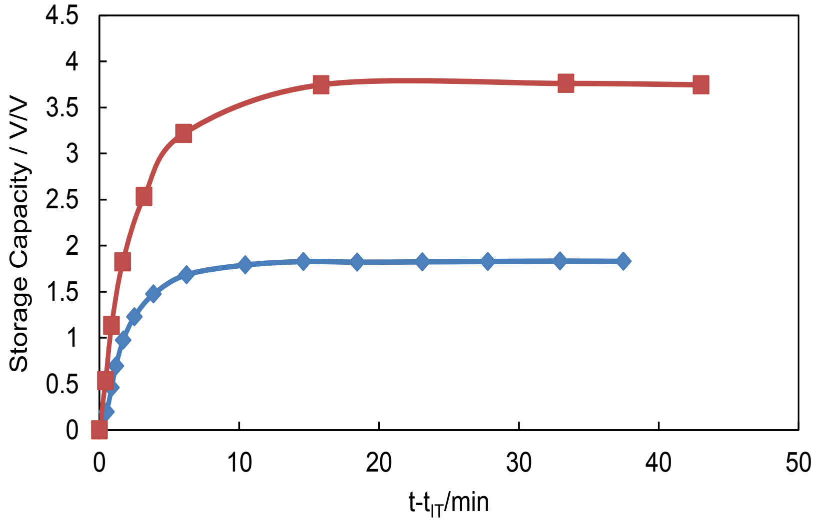

Figure C.21. Storage Capacity during R407C hydrate growth at an initial temperature of 282.8 K and the pressures: ♦, 0.71 MPa; ■, 0.82 MPa in the presence of pure water; solid lines, trend lines.

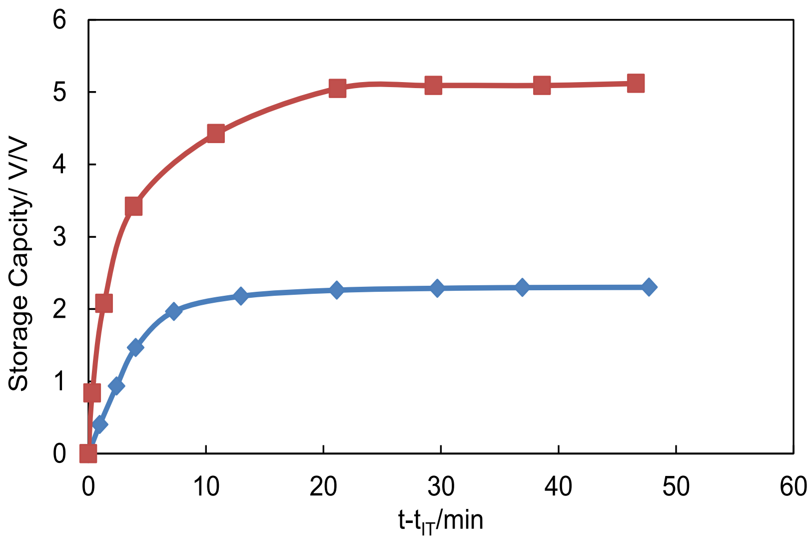

Figure C.22. Storage Capacity during R407C hydrate growth at an initial temperature of 283.8 K and the pressures: ♦, 0.82 MPa; ■, 0.91 MPa in the presence of pure water; solid lines, trend lines.

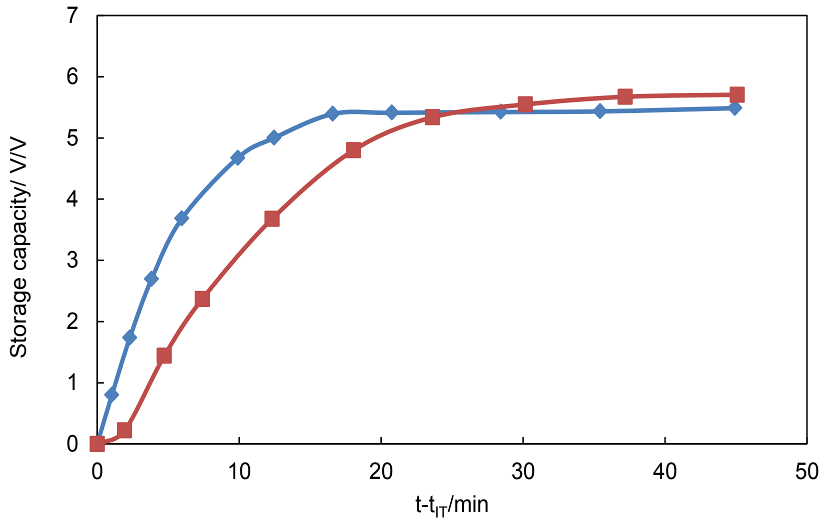

Figure C.23. Storage Capacity during the R507C hydrate growth at an initial temperature and pressure of 279.9 K and 0.81 MPa, ♦, pure water; ■, 400 ppm SDS; solid lines, trend lines.

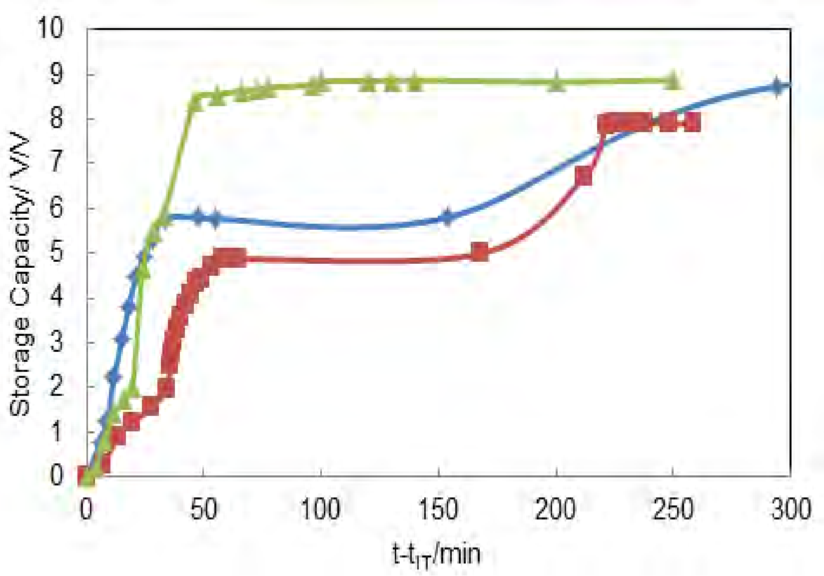

Figure C.24. Storage Capacity during R404A hydrate growth at initial conditions of: ♦, 281 K, 1.147 MPa, pure water; ■, 282 K, 1.17, MPa, pure water; ▲, 282 K, 1.147 MPa 400 ppm SDS; solid lines, trend lines..

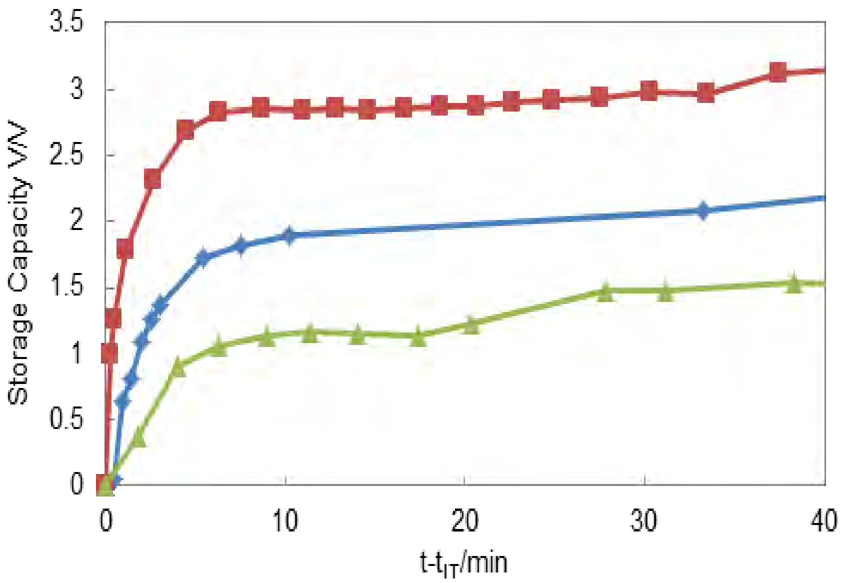

Figure C.25. Storage Capacity during R406A hydrate growth at initial condition of 282 K and 0.651 MPa: ♦, pure water; ■, 400 ppm SDS; ▲, 600 ppm SDS; solid lines, trend lines..

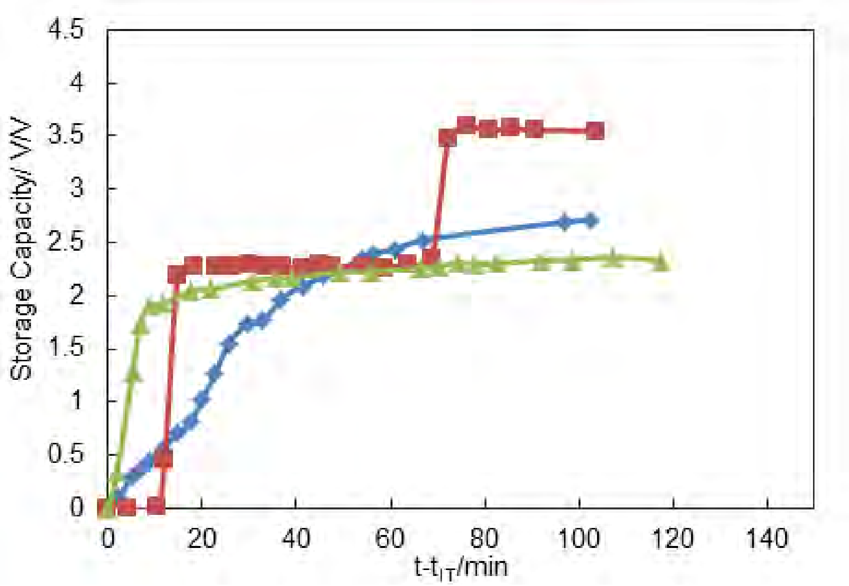

Figure C.26. Storage Capacity during R408A hydrate growth at initial condition of 281 K and 0.864 MPa: ♦, pure water; ■, 400 ppm SDS; ▲, 600 ppm SDS; solid lines, trend lines..

C.1.4. Apparent rate constant

Apparent rate constant (K_{app}) of the hydrate formation as a function of time is depicted in Figures C.27 to C.35 for the refrigerants studied. The results indicate that the apparent rate constant increases with increasing pressure. The effect of SDS solution is different for different refrigerants.

C.1.4.1. Effect of SDS solution

The effects of SDS solution on the apparent rate constant of the refrigerant hydrates formation are summarized as bellow:

- Apparent rate constant of R507C hydrate formation decreased in the presence of the SDS solution (Figure C.30).
- There were no significant change in the apparent rate constant of R404A in the presence of 400 ppm SDS solution (Figures C.33).
- Apparent rate constant of R406A hydrate formation increased in the presence of 400 ppm SDS solution and decreased in the presence of 600 ppm SDS solution (Figures C.34).
- For R408A the apparent rate constant of hydrate formation increased in the presence of both 400 and 600 ppm SDS solutions. However, the effect of 400 ppm SDS solution was higher than that of 600 ppm (Figure C.35).

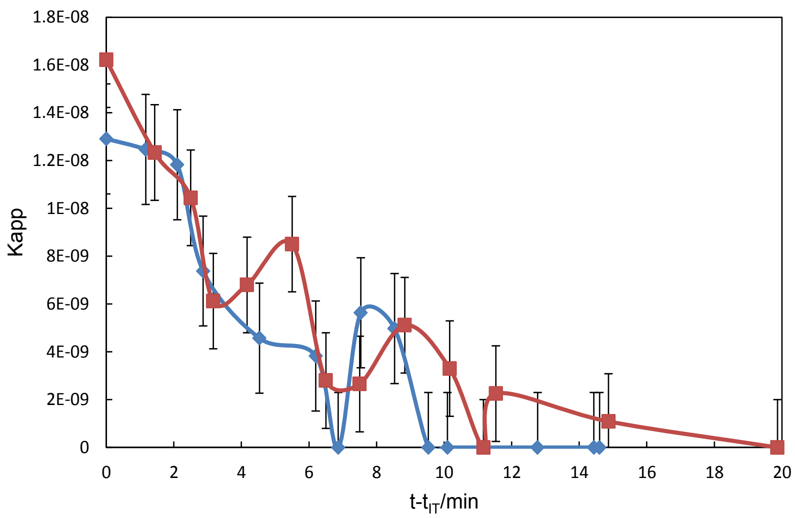

Figure C.27. Apparent rate constant as a function of time during R407C hydrate growth at an initial temperature of 282.8 K and initial pressures of ♦,0.71MPa and ■, 0.82MPa.

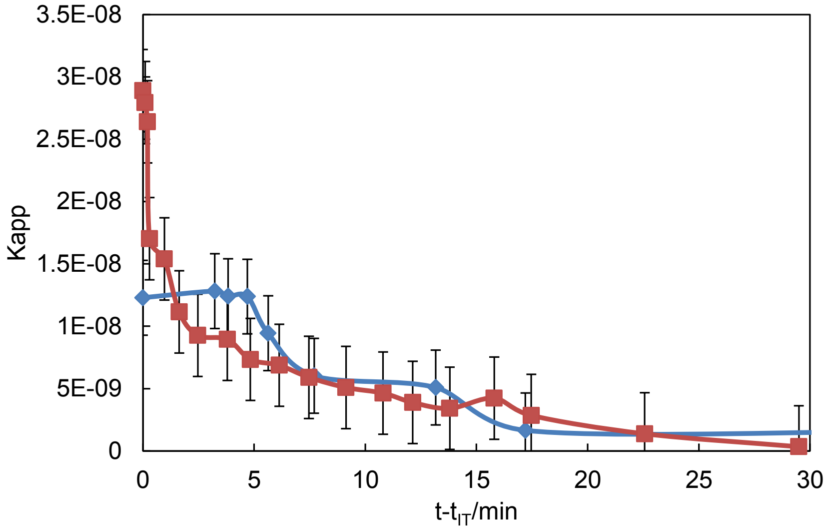

Figure C.28. Apparent rate constant as a function of time during R407C hydrate growth at an initial temperature of 283.8 K and initial pressures of ♦, 0.82MPa; ■, 0.91MPa.

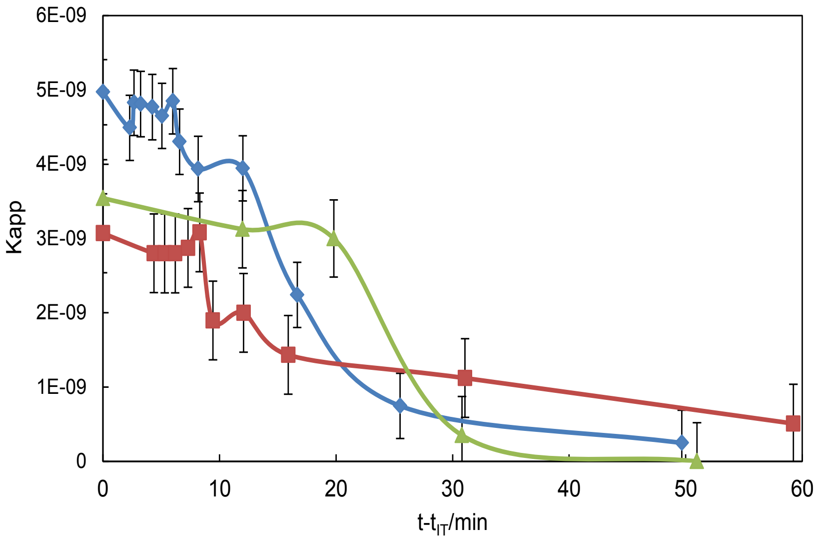

Figure C.29. Apparent rate constant as a function of time during R507C hydrate growth at an initial temperature of 279.9 K and initial pressures of ■, 0.64MPa; ▲, 0.71MPa; ♦, 0.75MPa.

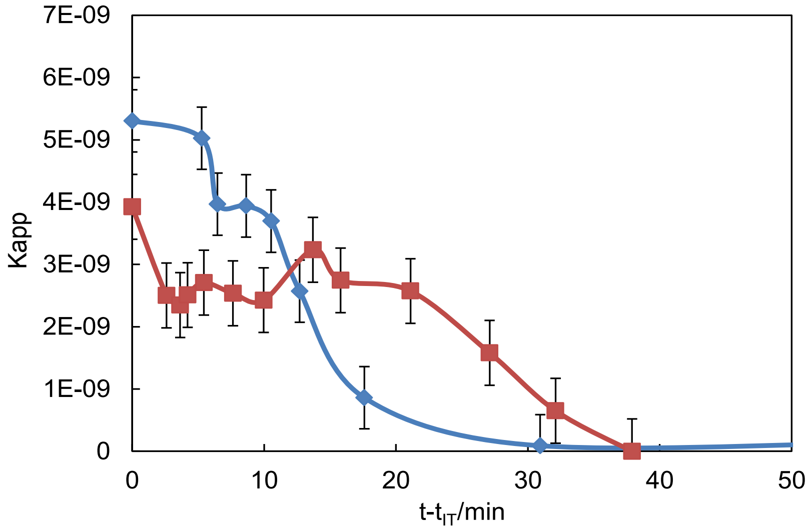

Figure C.30. Apparent rate constant as a function of time during R507C hydrate growth at an initial temperature of 280.9 K and an initial pressure of 0.81 MPa; ♦, pure water; ■, 400 ppm SDS.

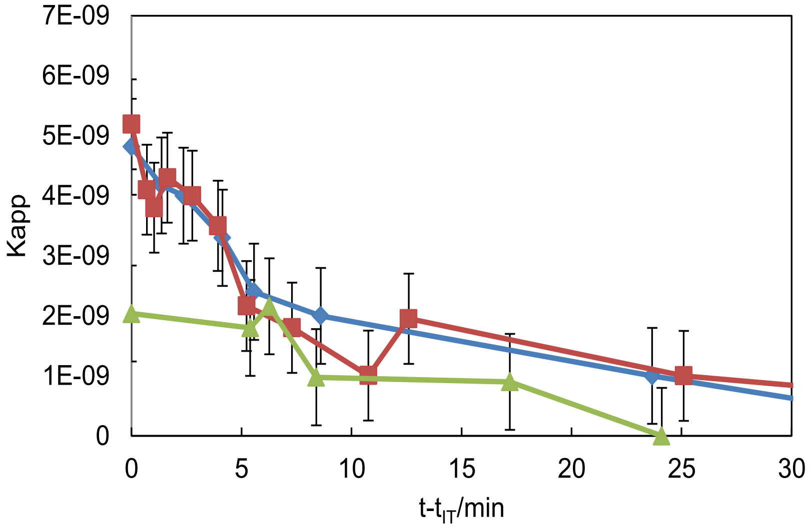

Figure C.31. Apparent rate constant as a function of time during R410 hydrate growth at an initial temperature of 282.8 K and an initial pressures of ▲, 0.81MPa; ♦, 0.93MPa; ■, 1 MPa.

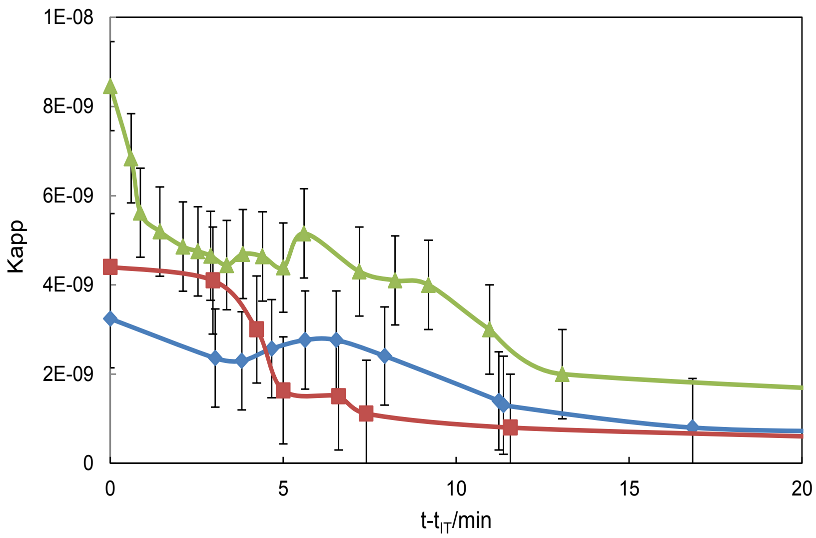

Figure C.32. Apparent rate constant as a function of time during R410 hydrate growth at an initial temperature of 283.8 K and an initial pressures of ♦, 0.92MPa; ■,1 MPa; ▲, 1.1 MPa.

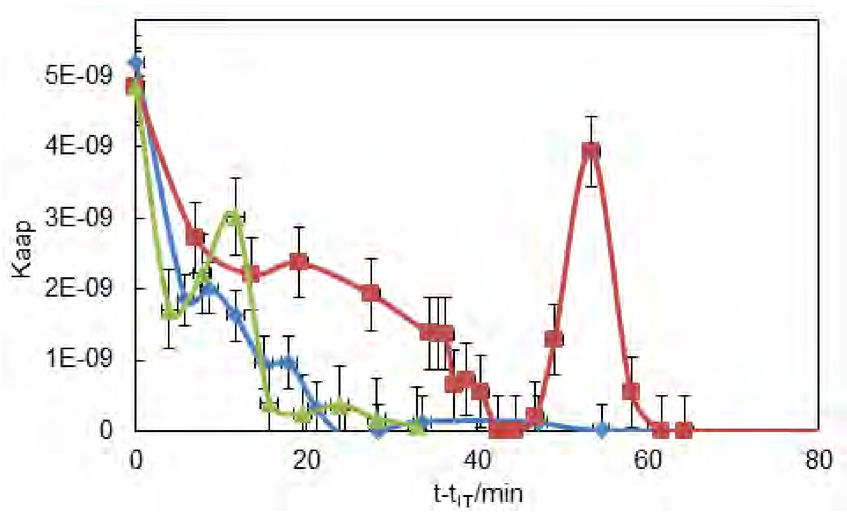

Figure C.33. Apparent rate constant as a function of time during R404A hydrate growth at initial conditions of : ♦, 281 K 1.147 MPa, pure water; ■, 282 K, 1.17, MPa, pure water; ▲, 282 K, 1.147 MPa 400 ppm SDS.

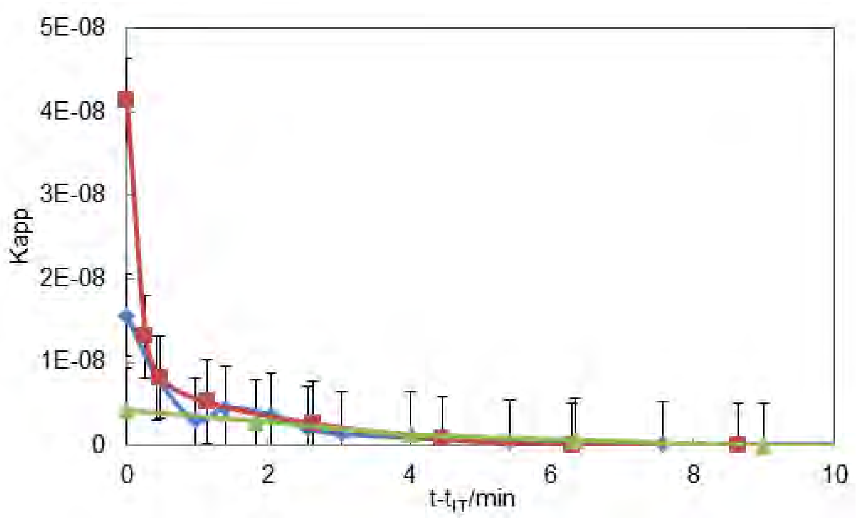

Figure C.34. Apparent rate constant as a function of time during R406A hydrate growth at initial condition of 282 K and 0.651 MPa: ♦, pure water; ■, 400 ppm SDS; ▲, 600 ppm SDS.

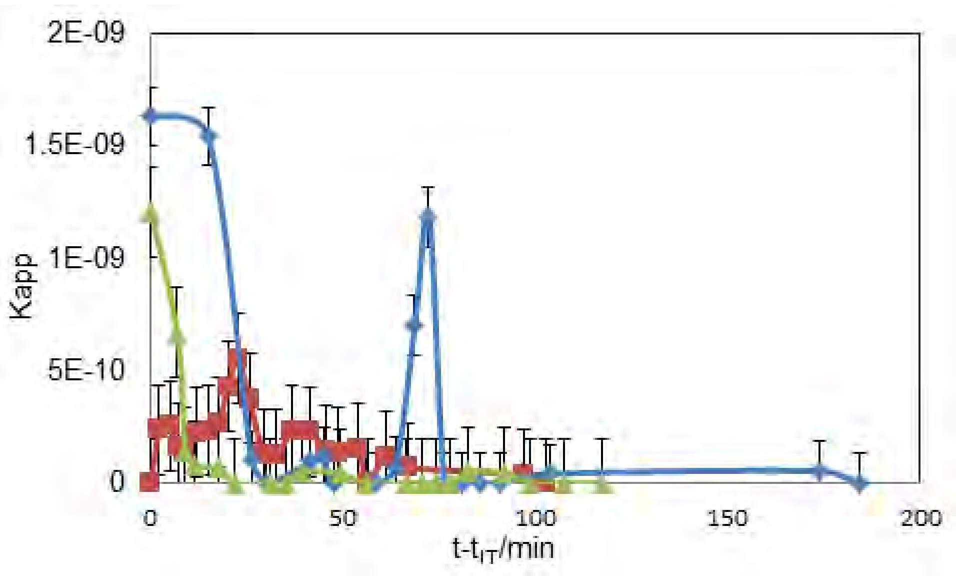

Figure C.35. Apparent rate constant as a function of time during R408A hydrate growth at initial condition of 281 K and 0.864 MPa: ■, pure water; ♦, 400 ppm SDS; ▲, 600 ppm SDS.

C.2. Modeling results

The results obtained from the developed models are presented in this section. The parameters of the hydrate model as well as fluid phase model is reported. The modeling results are compared with experimental data measured in this study and those of the literature in Figures C.36 to C.52.

C.2.1. Modeling parameters

The model specific parameters for both hydrate model as well as fluid phase model are reported in this section.

C.2.1.1. Hydrate model

The hydrate model used in this study contains some specific model parameters such as the thermodynamic properties of the reference hydrate which are reported in Table C.1.

Table C.1. Phase transition parameters for different hydrate structures (Mohammadi et al., 2005)

Structure	$\Delta\mu_w^0$ /Jmol^{-1}	Δh_w^0 /Jmol^{-1}	Δv_w^0 /cm^3.mol^{-1}
I	1297	-4620.5	4.6
II	937	-5201	5.0

$\Delta\mu_w^0$: Chemical potential difference between empty hydrate lattice and pure water

Δh_w^0: Molar enthalpy difference between empty hydrate lattice and ice at the ice point and zero pressure

Δv_w^0: Volume difference between empty hydrate lattice and pure water

C.2.1.2. Fluid phase model

The pure component parameters used in PRSV EoS (Stryjek and Vera, 1986), the UNIFAC volume and surface area parameters and the interaction parameters used in the UNIFAC model are reported in Tables C.2 to C.4.

Table C.2. PRSV EoS parameters used in this study

Refrigerant	T_C/K	P_C/MPa	ω	k_1	Ref
R11(CCl_3F)	471.20	4.409	0.18749	0.03708	(Proust and Vera, 1989)
R12(CCl2F_2)	385.00	4.131	0.17875	0.04722	(Proust and Vera, 1989)
R13($CClF_3$)	302.00	3.870	0.17135	0.05054	(Proust and Vera, 1989)
R14(CF_4)	227.50	3.742	0.17977	0.02136	(Proust and Vera, 1989)
R22($CHClF_2$)	369.30	4.989	0.21974	0.04513	(Proust and Vera, 1989)
R23(CHF3)	299.07	4.836	0.26537	0.00535	(Proust and Vera, 1989)
R32(CH_2F_2)	351.55	5.830	0.27704	-0.02874	(Proust and Vera, 1989)
R600a(C_4H_{10})	408.1	3.655	0.18466	0.00238	(Proust and Vera, 1989)
R134a($C_2H_2F_4$)	374.26	4.068	0.32610	0.00000	(Orbey and Sandler, 1995)
R142b($C_2H_2F_4$)	409.6	4.330	0.25100	n.a	(McLinden et al., 1998)
R143a($C_2H_3F_3$)	346.04	3.776	0.26110	n.a	(McLinden et al., 1998)
R152a($C_2H_4F_2$)	386.41	4.517	0.27520	n.a	(McLinden et al., 1998)
R141b($C_2H_2F_4$)	477.50	4.194	0.21780	n.a	(Duarte-Garza et al., 1997a)
R125a(C_2HF_5)	339.41	3.639	0.30380	n.a	(Duarte-Garza et al., 1997b)

Table C.3. UNIFAC volume and surface area parameters used in this study (Kleiber, 1995, Piringer and Baner, 2007)

Main	group	Subgroup	R_k	Q_k
7	H_2O	H_2O	0.9200	1.400
1	CH_2	CH_3	0.9011	0.848
54	CClF	CCl_3F	3.0356	2.644
		CCl_2F	2.2446	1.920
55	$CC1F_2$	CCl_2F_2	2.5926	2.368
56	$CClF_3$	$CClF_3$	2.1971	2.104
45	CF_4	CF_4	1.8016	1.840
40	CF_2	CF_3	1.4060	1.380
57	CHClF	$CHClF_2$	2.0290	1.872
53	CHF_3	CHF_3	1.6335	1.608
52	CHF_2	CH_2F_2	1.4654	1.460
		(CF_3-) CH_2F	1.0699	1.000
		CHF_2	1.2380	1.232

Table C.4. Temperature-independent group interaction parameters for various refrigerant main groups and water (Kleiber, 1995, Piringer and Baner, 2007)

	7 H_2O	1 CH_2	54 CClF	55 $CC1F_2$	56 $CClF_3$	45 CF_4	40 CF_2	57 CHClF	53 CHF_3	52 CHF_2
7 H_2O	0.00	300	0.00	n.a.	n.a.	n.a.	0.00	n.a.	203.54	*640.92
1 CH_2	1318	0.00	-47.33	33.490	-68.51	182.56	33.510	257.30	156.08	134.38
54 CClF	0.00	74.33	0.00	124.21	97.41	n.a.	n.a.	122.89	192.28	n.a.
55$CC1F_2$	n.a.	441.66	-80.930	0.0000	2.730	220.12	110.370	60.700	73.570	165.97
56 $CClF_3$	*677.90	203.28	-0.5400	52.660	0.000	28.830	2666.62	323.32	157.25	156.77
40 CF_2	n.a.	87.260	n.a.	-54.69	-321.67	n.a.	0.0000	65.100	118.65	245.25
57CHClF	n.a.	-63.82	-34.210	4.6500	-144.56	102.90	55.500	0.0000	202.79	-168.85
53 CHF_3	-109.52	96.280	-132.28	83.200	-14.910	37.100	36.99	-113.88	0.0000	-131.47
52 CHF_2	*640.92	35.650	n.a.	-44.17	-16.78	154.22	-11.44	207.50	224.25	0.0000

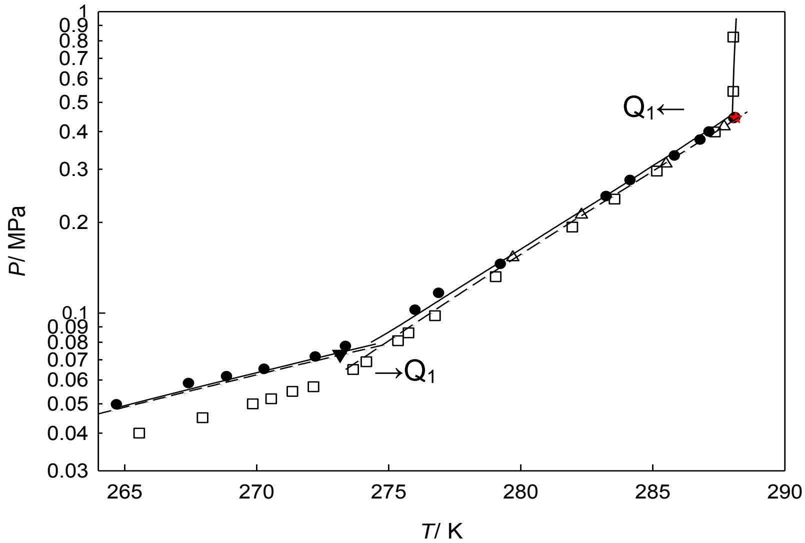

Figure C.36. Hydrate phase diagram of R152a ($C_2H_4F_2$) Hydrate; Experimental data: Δ, (Mohammadi and Richon, 2010); ●,(Liang et al., 2001); □, (Kubota et al., 1984); ▼, lower quadruple point, (Liang et al., 2001) ; ★ ,upper quadruple point (Liang et al., 2001); solid lines, model predictions using the Kihara approach, dash lines model predictions using the Parrish and Prausnitz (1972) approach.

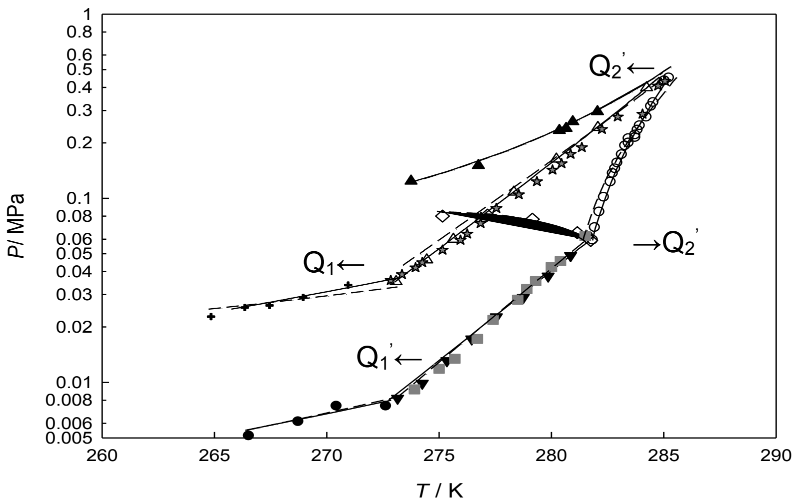

Figure C.37. Hydrate phase diagram of pure R12 (CCl_2F_2), pure R11 (CCl_3F), mixture of R12 + R11, mixture of R11 + R114 and mixture of R12+R114. Experimental data: Δ, (Carbajo, 1983), ★, (Wittstruck et al., 1961), R12 Hydrate + Aqueous solution + Vapor (L_w-H-V); ▼,(Carbajo, 1983); ■, (Wittstruck et al., 1961), R11 Hydrate + Aqueous solution + Vapor (L_w-H-V); ●, (Wittstruck et al., 1961), R11 Hydrate + Ice + Vapor (H-I-V); ✚, (Wittstruck et al., 1961) R12, Hydrate + Ice + Vapor (H-I-V) ; ⬡ , (Carbajo, 1983), R12+R11 Hydrate + Aqueous solution + R11 liquid + Vapor (H-L_w-L_{R11}-V); ◊, (Carbajo, 1983), R11 Hydrate+R114 liquid + Aqueous solution + Vapor (L_w-L_{R114}-H-V) ;▲, (Carbajo, 1983), R12 Hydrate + R114 liquid + Aqueous solution + Vapor (L_w-L_{R114}-H-V); solid lines, model predictions, using the Kihara approach, dash lines model predictions using the Parrish and Prausnitz (1972) approach.

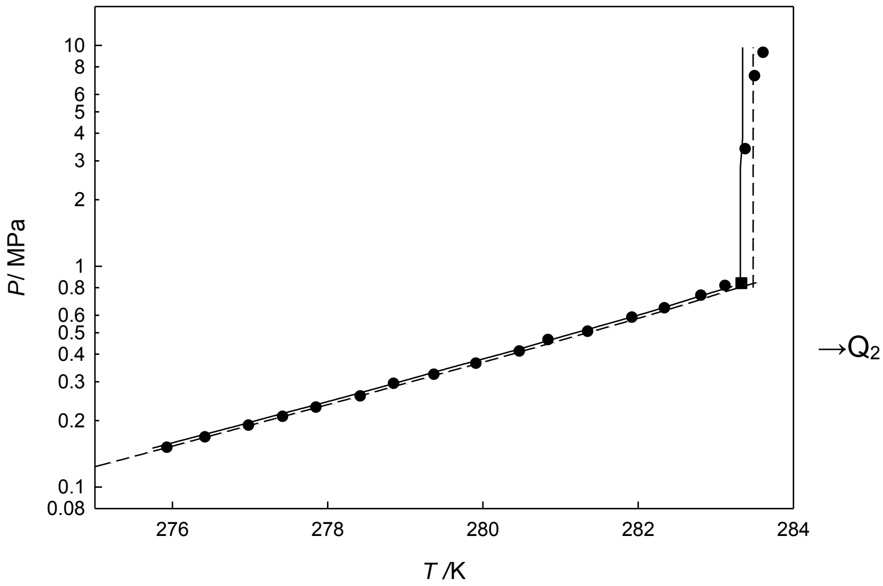

Figure C.38. Hydrate Phase diagram of R143a ($C_2H_3F_3$); Experimental data: ●, (Hashimoto et al., 2010a); ■, upper quadruple point, (Hashimoto et al., 2010a); Q_2, upper quadruple point; solid lines, model predictions using the Kihara approach, dash lines model predictions using the Parrish and Prausnitz (1972) approach.

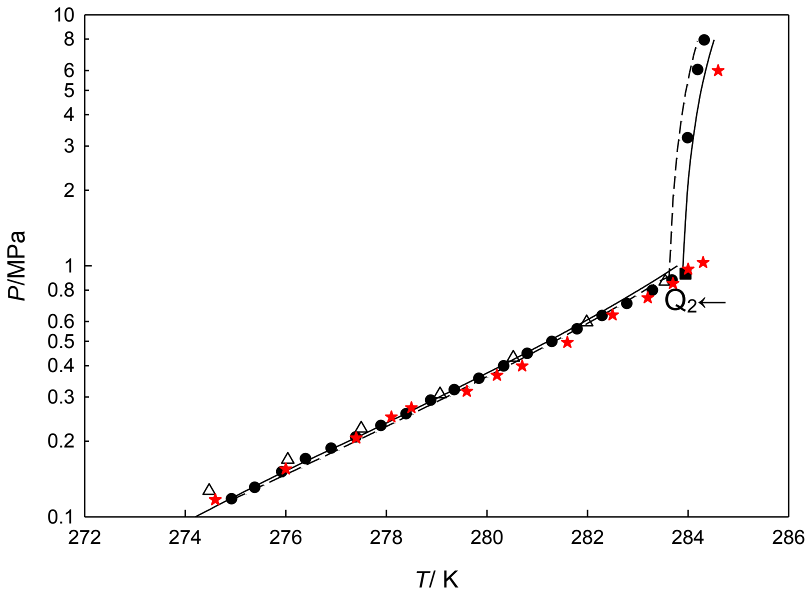

Figure C.39. Hydrate phase diagram of R125a (C_2HF_5); Experimental data: ★, this work; ●, (Hashimoto et al., 2010a); Δ, (Akiya et al., 1999); ■, upper quadruple point, (Hashimoto et al., 2010a); solid lines, model predictions using the Kihara approach, dash lines model predictions using the Parrish and Prausnitz (1972) approach.

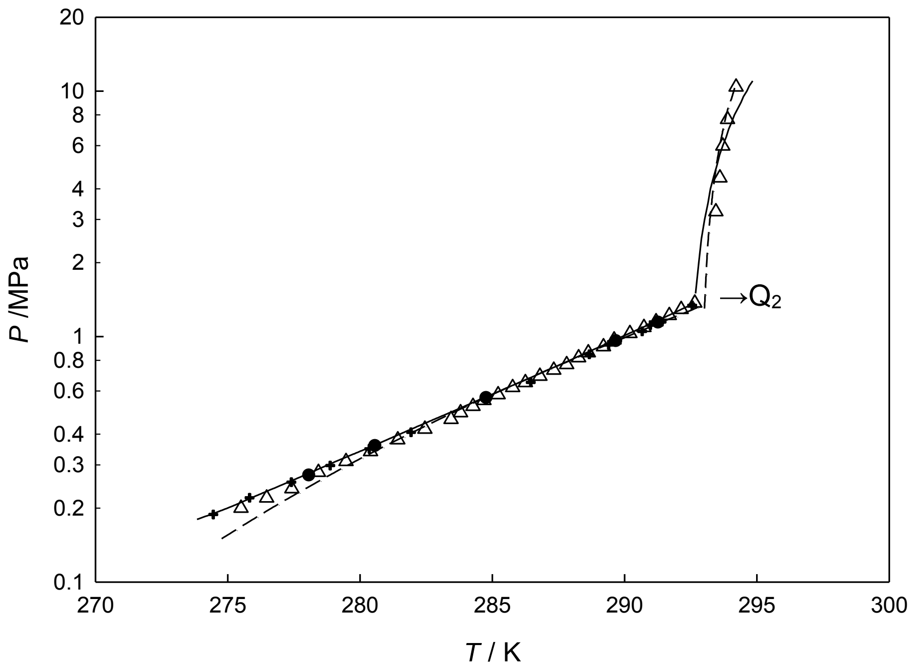

Figure C.40. Hydrate phase diagram of R32 (CH_2F_2); Experimental data: ●,(Mohammadi and Richon, 2010); Δ, (Hashimoto et al., 2010b); +, (Akiya et al., 1999); Q_2, upper quadruple point; Solid lines, model predictions using the Kihara approach, dash lines model predictions using the Parrish and Prausnitz (1972) approach.

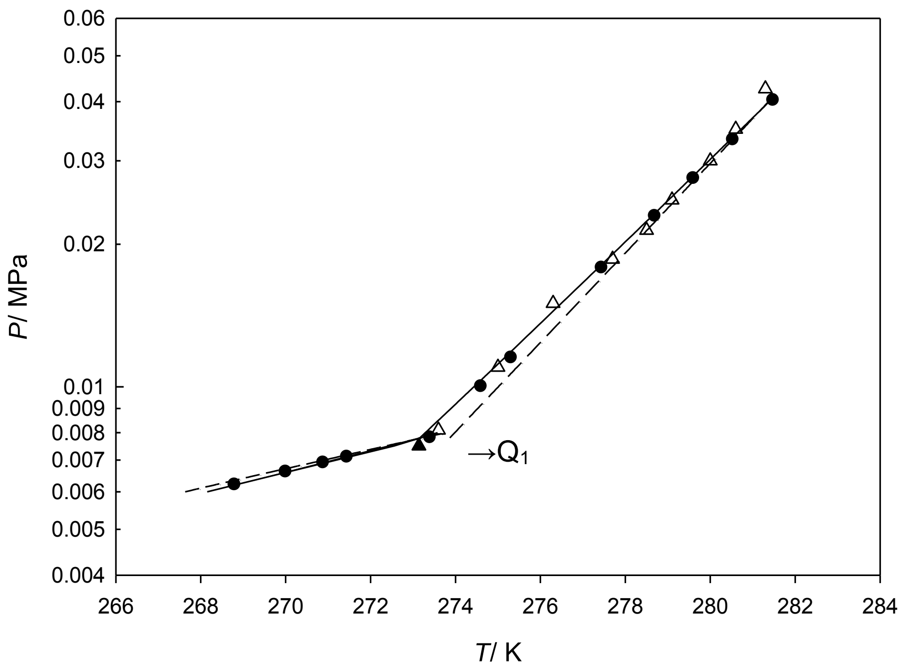

Figure C.41. Hydrate phase diagram of R141b ($C_2H_3Cl_2F$); Experimental data:●, (Liang et al., 2001);▲, lower quadruple point, (Liang et al., 2001);Q_1, lower quadruple point; Solid lines, model predictions using the Kihara approach, dash lines model predictions using the Parrish and Prausnitz (1972) approach.

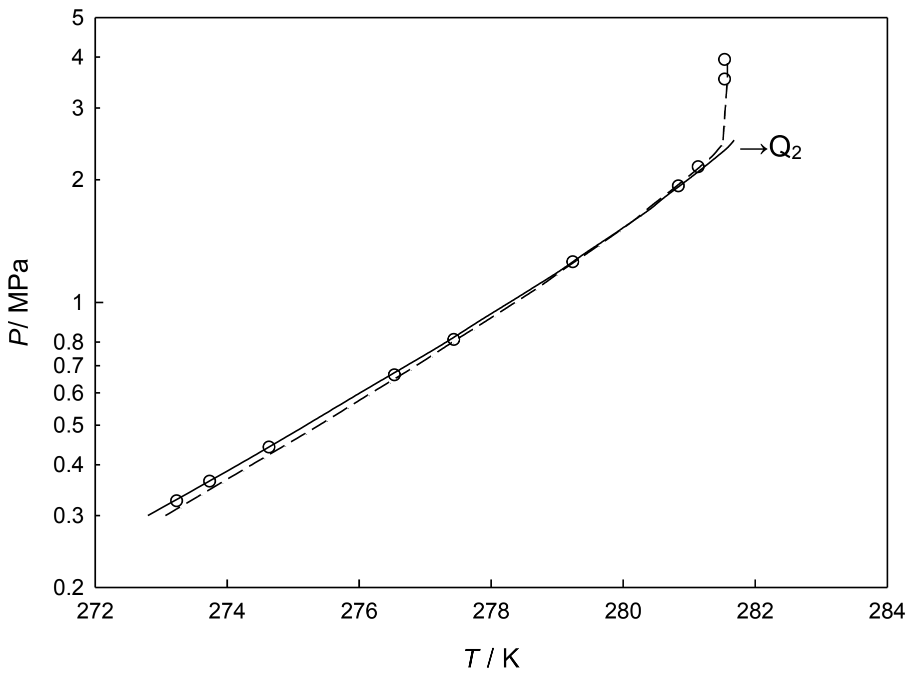

Figure C.42. Hydrate Phase diagram of R13 ($CClF_3$); Experimental data:○, (Kubota et al., 1984); Q_2, upper quadruple point; Solid lines, model predictions using the Kihara approach, dash lines model predictions using the Parrish and Prausnitz (1972) approach.

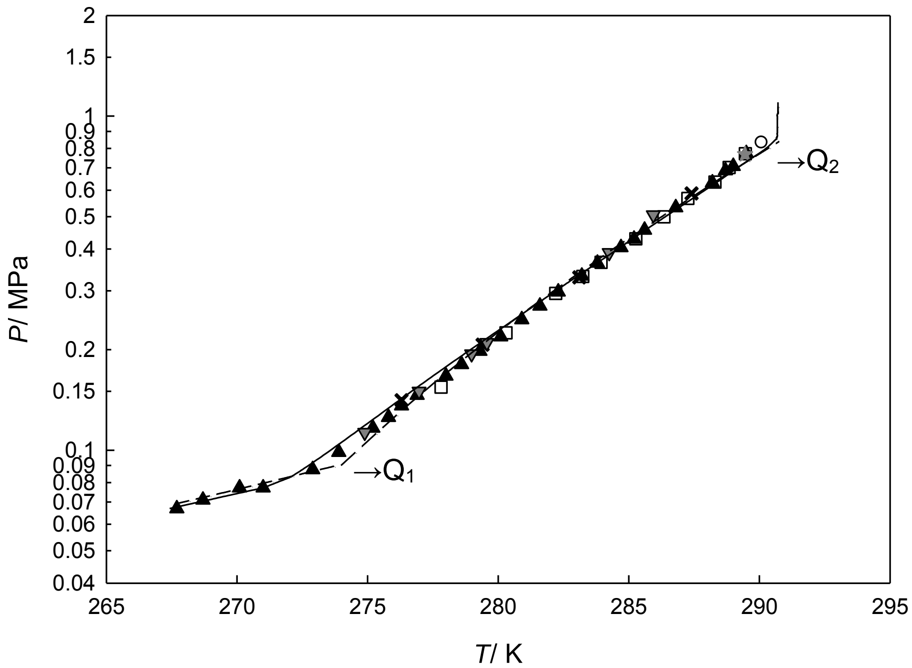

Figure C.43. Hydrate phase diagram of R22 ($CHClF_2$); Experimental data:▼, this work; ▲,(Wittstruck et al., 1961); □, (Javanmardi et al., 2004); ×, (Chun et al., 1996); ○, ★, upper quadruple points, (Carbajo, 1983), (Chun et al., 1996); Q_2, upper quadruple point; Q_1, lower quadruple point; Solid lines, model predictions using the Kihara approach, dash lines model predictions using the Parrish and Prausnitz (1972) approach.

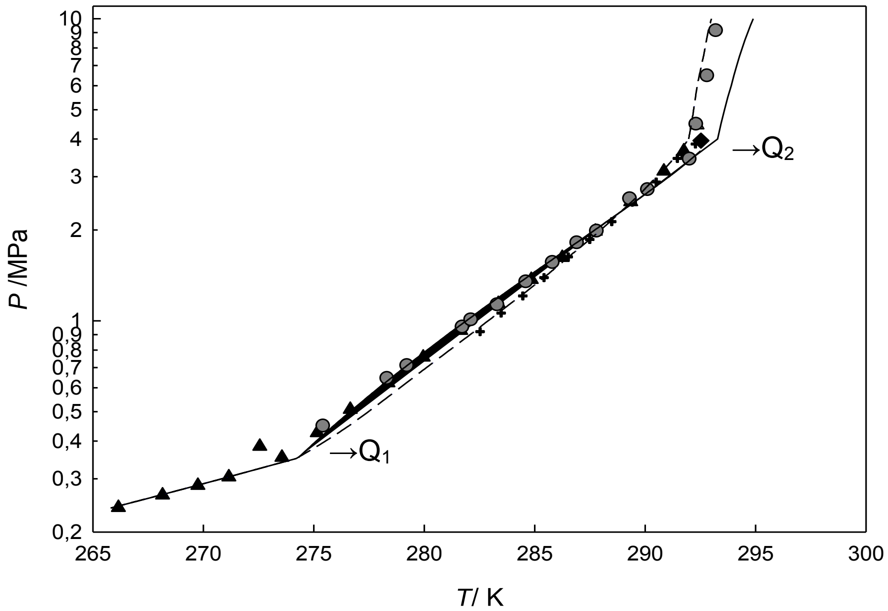

Figure C.44. Hydrate phase diagram of R23(CHF_3); Experimental data:●, this work; ▲, (Kubota et al., 1984); +, (Mooijer-van den Heuvel et al., 2006) ; ◆ , upper quadruple point, (Mooijer-van den Heuvel et al., 2006); △ , upper quadruple point, (Kubota et al., 1984); Q_2, upper quadruple point; Q_1, lower quadruple point ;Solid lines, model prediction using the Kihara approach, dash lines model predictions using the Parrish and Prausnitz (1972) approach.

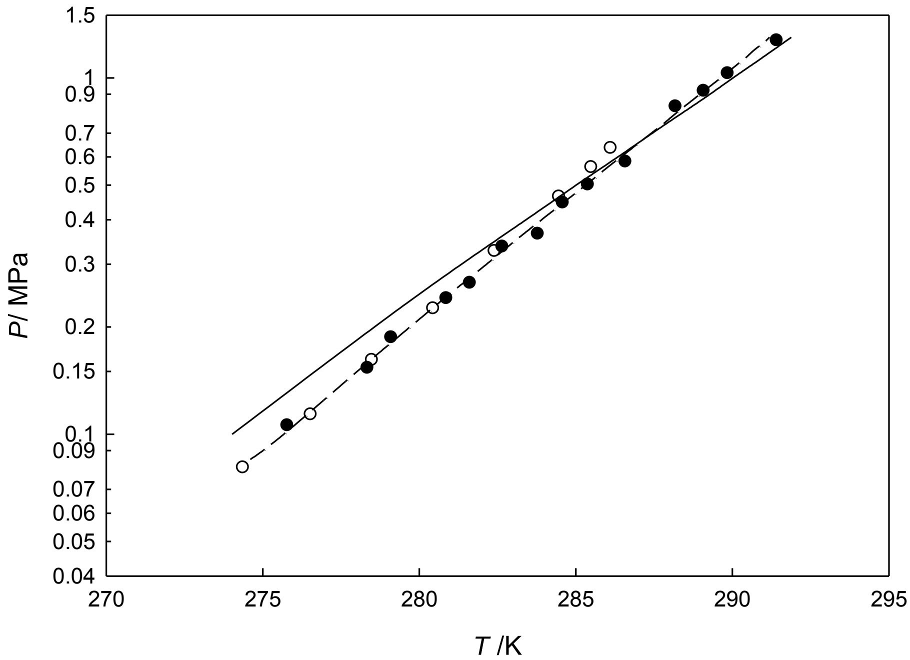

Figure C.45. Hydrate phase diagram of R407C (the mixture of R32/R125a/R134a, mole percent respectively:38.1/18/43.9); Experimental data:●, this work; ○, (Akiya et al., 1999); Solid lines, model predictions using the Kihara approach, dash lines model predictions using the Parrish and Prausnitz (1972) approach.

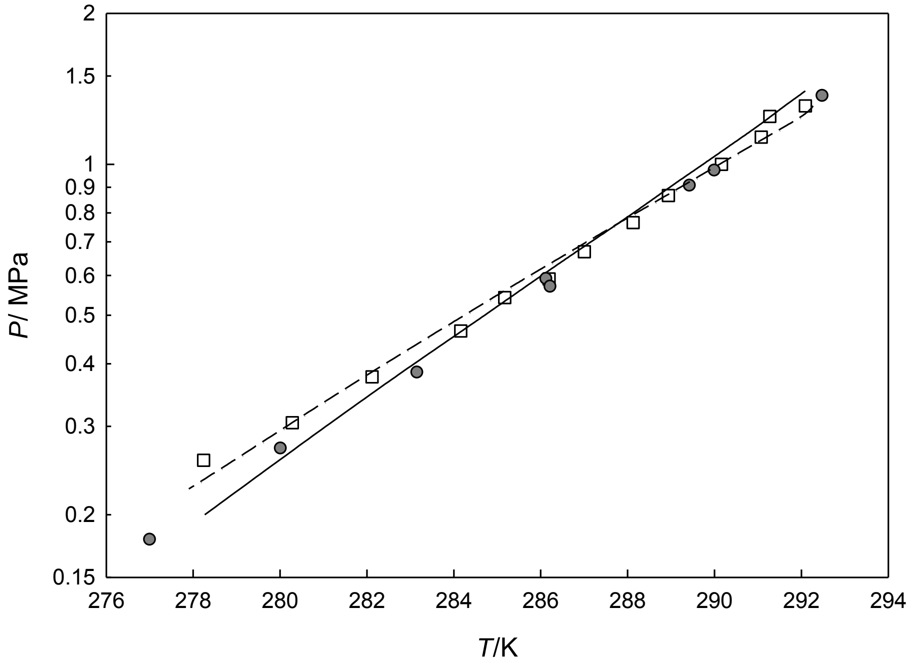

FigureC.46. Hydrate phase diagram of R410A (mixture of R32/R125a with mole percent respectively:69.76/30.24); Experimental data:●, this work; ●, (Akiya et al., 1999); solid lines, model predictions using the Kihara approach, dash lines model predictions using the Parrish and Prausnitz (1972) approach.

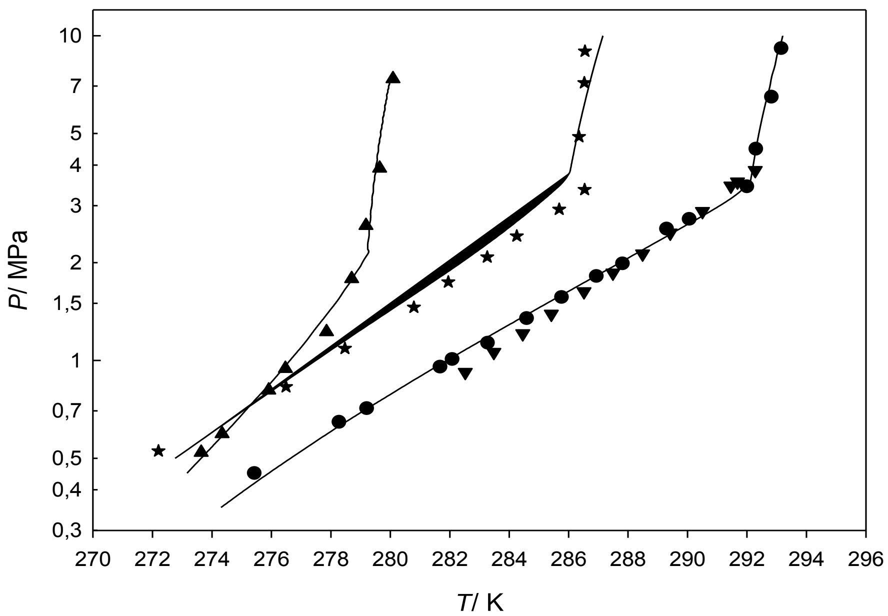

Figure C.47. Hydrate phase equilibrium for the refrigerants:●, R23 (this work); ▼,R23 (Mooijer-van den Heuvel et al., 2006); ▲, R116 (this work);★, R508B (this work); solid lines, model predictions.

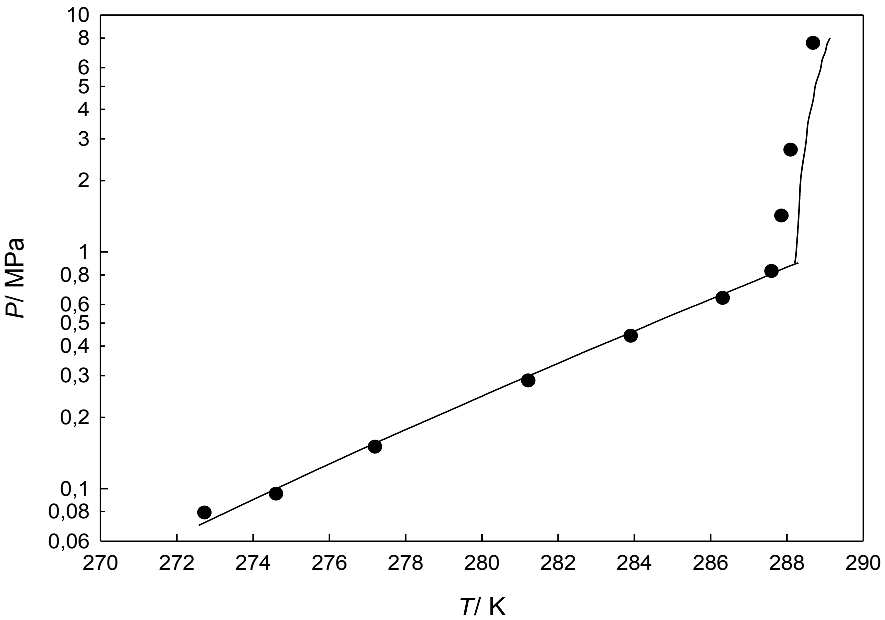

Figure C.48. Hydrate phase equilibrium of R427a, experimental data: ●, (this work); solid lines , model predictions using Kihara approach.

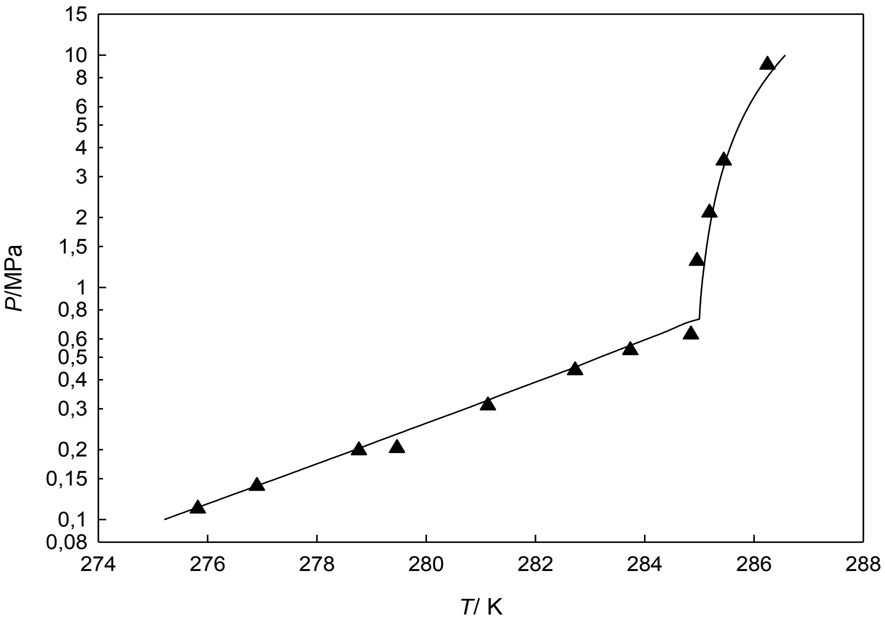

Figure C.49. Hydrate phase equilibrium of R406A, experimental data: ▲, (this work); solid lines, model predictions using Kihara approach.

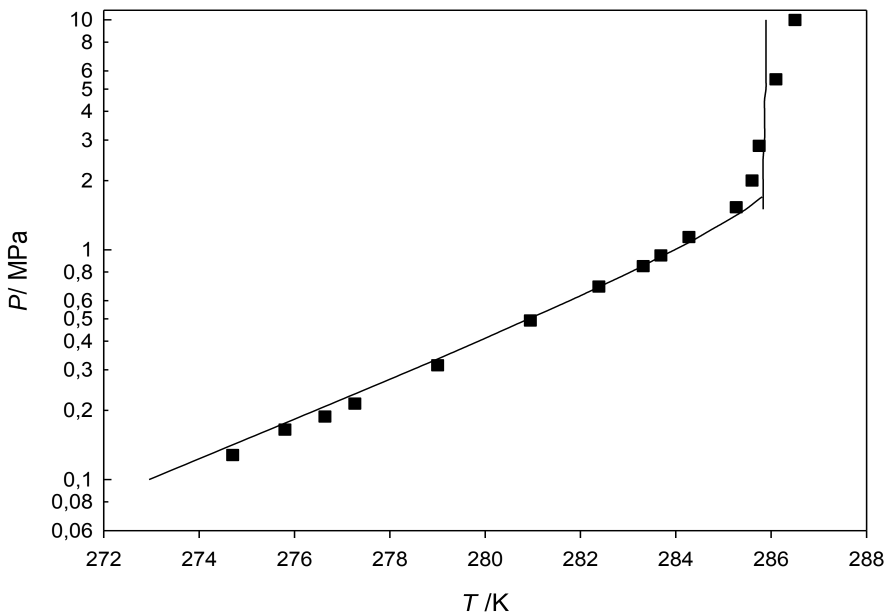

Figure C.50. Hydrate phase equilibrium of R404A, experimental data: ■, (this work); solid lines, model predictions using Kihara approach.

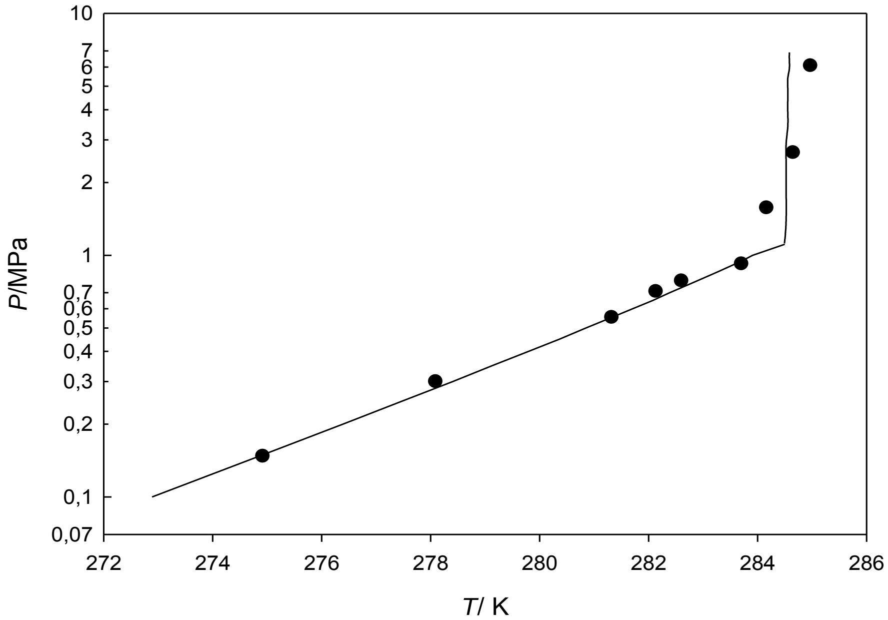

Figure C.51. Hydrate phase equilibrium of R408A, experimental data: ●, (this work); solid lines, model predictions using Kihara approach.